UNIVERSIDAD DE MURCIA

FACULTAD DE BIOLOGÍA

Identifying Components of the non-Canonical RNA Silencing Mechanism in Mucor circinelloides

Identificación de Componentes del Mecanismo no Canónico de Silenciamiento Mediado por RNA en Mucor circinelloides

D. Trung Anh Trieu

2015

Identifying components of the non-canonical RNA silencing mechanism in *Mucor circinelloides*

Trabajo realizado en el Departamento de Genética y Microbiología de la Universidad de Murcia, para optar al grado de Doctor en Biología, por el Licenciado **Trung Anh Trieu**,

Murcia, 20 de Mayo de 2015

D. **Mariano Gacto Fernández**, Catedrático de Universidad del Área de Microbiología y Director del Departamento de Genética y Microbiología, INFORMA:

Que la Tesis Doctoral titulada "**Identifying components of the non-canonical RNA silencing mechanism in *Mucor circinelloides***", ha sido realizada por D. **Trung Anh Trieu**, bajo la inmediata dirección y supervisión de Dª **Rosa Mª Ruiz Vázquez**, Catedrática del Área de Genética, y D. **Francisco E. Nicolás Molina**, Investigador contratado, y que el Departamento ha dado su conformidad para que sea presentada ante la Comisión de Doctorado.

En Murcia, a 20 de Mayo de 2015

Dª. **Rosa Mª Ruiz Vázquez**, Catedrática de Universidad del Área de Genética y D. **Francisco E. Nicolás Molina**, Investigador contratado, ambos en el Departamento de Genética y Microbiología, AUTORIZAN:

La presentación de la Tesis Doctoral titulada "**Identifying components of the non-canonical RNA silencing mechanism in *Mucor circinelloides***", realizada por D. **Trung Anh Trieu**, bajo nuestra inmediata dirección y supervisión, y que presenta para la obtención del grado de Doctor por la Universidad de Murcia.

En Murcia, a 20 de Mayo de 2015

This study has contributed to the following publications:

Journal Article

Trung Anh Trieu*, Silvia Calo*, Francisco E. Nicolás, Ana Vila, Simon Moxon, Tamas Dalmay, Santiago Torres-Martínez, Victoriano Garre, Rosa M. Ruiz-Vázquez (2015). A Non-Canonical RNA Silencing Pathway Promotes mRNA Degradation in Basal Fungi. ***PLoS Genetics*** 11(4): e1005168. DOI: 10.1371/journal.pgen.1005168

* The authors contributed equally to this work

Conference Abstracts and Posters

Trung Anh Trieu, Silvia Calo, Francisco E. Nicolás, Simon Moxon, Tamas Dalmay, Santiago Torres-Martínez, Victoriano Garre and Rosa M. Ruiz-Vázquez (2015). A novel RNase III-like protein participates in an RdRP-dependent Dicer-independent degradation mechanism of endogenous mRNAs in basal fungi. ***28th Fungal Genetics Conference***, USA, pp.183.

Trung Anh Trieu, Francisco E. Nicolás, Silvia Calo, Victoriano Garre, Santiago Torres-Martínez and Rosa M. Ruiz-Vázquez (2014). Identifying the RNase III involved in a dicer-independent non-canonical RNA silencing mechanism in *Mucor circinelloides*. ***12th European Conference on Fungal Genetics***, Spain, pp. 210.

This study was supported by the following research projects and grants:

Endogenous small RNAs in the regulation of responses to light, pathogenesis and other cellular processes in the basal fungus Mucor circinelloides. Organization: Ministry of Economic and Competitiveness. PI: Victoriano Garre. Reference: BFU2012-32246.

Endogenous functions of the RNA silencing mechanism in the fungus Mucor circinelloides. Organization: Ministry of Science and Innovation. PI: Rosa Mª Ruiz Vázquez. Reference: BFU2009-07220.

Erasmus Mundus Action 2 (MOVER program), Grant agreement number 2011-2595/001-001-EMA2.

To my grandparents and parents,

To my wife, and

To my children: Bảo Thư, Quỳnh Như
and Đức Vinh

ACKNOWLEDGEMENT

During almost three years of my study in University of Murcia, I have had a lot of unforgotten memories with all of you, my professors, my colleagues and my friends. As the first step in early career, my PhD research has been successfully finished with your kind assistances. I would like to express my special appreciation and thanks to my supervisors, Dr. Rosa and Dr. Curro, who are tremendous mentors to me. At the beginning, Dr. Rosa supported me to get the Erasmus Mundus scholarship hosted by European Union, which offered me a great opportunity to work with you in this beautiful country. As my direct supervisor, Dr. Curro has kindly instructed me how to perform all the experiments, step by step, in our labs and service centers. Many emerging problems with my experiments were solved with the great suggestions and recommendations from Dr. Curro, Dr. Rosa and other people during the study process. In addition, thanks to the strong supports of you, I would be able to finish this thesis and relative scientific publications. I would like to thank you for encouraging my research and supporting me in order to be a young scientist. Your advices on my research as well as career have been priceless.

I would like to special thank Dr. Victor, Dr. Santiago and Dr. Sebi for your all patience and support, as you always welcome my questions with a deep attention. There have been many times that I have interrupted you with my questions which relate to the research or simply just asking you where the bottle of agar is. I would also give a huge thank to all of you, my lab mates, who have been working here for a long time and who have just joined in. This lab is like my second home, and you are my dear family members. We have had interesting daily conservations together as well as good discussions in the seminars and learnt a lot from each other. I always remember all of you: Maribel, Carlos, Raquel, Joseto, Ana, Loles, Sonia, Jesús, Sergio, Adrián, Tauste, and Elena-"mother of birds", and etc. Being worked, collaborating and sharing ideas with our team are my wonderful experiences. Yingtong, Javi, Gábor and Lupita, who had visited the lab for a short time, also left me an impression. Specially, I still remember José Antonio, who is making our jobs easier to be done with already sterile solutions and equipment. María Jesús, the woman who always appears with a smile, have kindly assisted me whenever I am in need. I would like to thank the experts and officers in the Molecular Biology Service (SACE-CAID) and International Relation Office, at the University of Murcia,

because you always have been there to support me when I had to collect data for my thesis and process the documentary jobs.

I would like to thank you very much, the people in other groups: Juanma, who encouraged me to get involved in student group of our Department when I just arrived to the campus; Dr. Paco Murillo, Dr. Montse, Dr. Padhu, Dr. Carmen, Dr. Marta who also support me when I need. I would never forget you, Marisa, Aranza, Diego, Josepe, Dani, Pepe, Pablo, Jesús, Bego, Silvia, María Ruiz, Miguel, Sheriza, etc. We have enjoyed a lot of interesting activities together, including daily lunches, parties, playing sports, picnics and many other celebrations.

A warmly thank to you for your sharing moments, my flat mates, Josepe, Gínes, Nines and Lydia, and my Vietnamese friends: Huy, Tina, Danny, Quỳnh, Hải, Nhung, Hà, Táo Mều, Tình, Linh, Bốp, Ngân, Khánh, Vy, Huyền Trân, Trang, Dũng, Nghề, etc. You have brought the "Vietnamese air" to Murcia and it made me feel like home when I am outside of the lab. We have had wonderful moments together with interesting stories in our mother tongue language. My friends and colleagues even are living outside of Spain, who often contact with me via internet, Huyền, Hà, Tuyết Nguyễn, Ngọc Anh, Vân Anh, Huyền Phạm, Quyên, Lương, Bình, Gia Trang Tran, Hương, Tuấn, and many more. Your messages sent from Vietnam alleviated my homesickness. I would never forget you, who have always been by my side, heard my complaints and tried to cheer me up when I lose the strength to keep going. You have helped me a lot to enjoy my life. I am very lucky to have so many kind friends around me who love and support me.

At the end, a special thanks to my family. Words cannot express how grateful I am to my grandparents, my parents and my parents-in-law for all of the sacrifices that you have made on my behalf. I would like express appreciation to my beloved wife Thêu Phạm, who is looking after our children when I am away from home. And my children, Bảo Thư, Quỳnh Như and Đức Vinh, who always cheer me up with lovely voices and encourage me to overcome the challenges as well as soon finish this job regardless of a long geological distance. I can never take back everything you have given to me, but I keep trying all my best.

THANK YOU!

INDEX

INDEX OF FIGURES

INDEX OF TABLES

I. INTRODUCTION

I.1. *Mucor circinelloides*

Mucor circinelloides is a filamentous fungus with a wide distribution. It can be found in soil, manure and other decaying organic substrates. It belongs to the subdivision Mucoromycotina, characterized by having a sexual reproduction by gametangial fusion, presenting a generally coenocytic mycelium (in some species, septa may exist), and producing non-flagellated and immobile spores. *M. circinelloides* is listed in the *Mucorales* order since it produces vegetative spores endogenously developed in a structure known as sporangium, and in the *Mucoraceae* family because the sporangium appears separated from the rest of the sporangiophore by a septum called columella. The genus *Mucor*, which gives the name to the family and order, has branched sporangiophores and globose sporangia.

I.1.1. General characteristics and life cycle

M. circinelloides is a dimorphic fungus as it can grow as yeast or mycelium. Its dimorphic switch can be observed when changing the oxygen concentration in the environment. This fungus grows as filamentous fungus aerobically, and as budding yeast in anaerobic conditions (Orlowski, 1991; Lubbehusen et al., 2003). Genus *Mucor* is heterothallic, including two sexual types (+ and -) with identical morphology. There are two different kinds of life cycles in *M. circinelloides* (**Figure 1**):

1) **Vegetative (asexual) cycle**, characterized by the formation of vegetative spores or sporangiospores, which may contain one or more nuclei. These spores mature in the sporangium, which is located at the end of the sporangiophore. In a suitable medium, spores germinate and produce one or more germ tubes, giving rise to hyphae that grow and branch to form the mycelium.

2) **Sexual cycle**, which supports the recombination of genetic material of the strains involved in it, thus ensuring genetic variability of the species. Sexual cycle occurs when two mycelia of opposite mating type come together, which causes inhibition of the formation of sporangiophores, induction of β-carotene synthesis and production of zygophores that are sexually differentiated hyphae. The zygophores from (+) and (-) mating types are fused, usually at the apex, resulting in the progametangia, which are separated from the rest of the sexual hyphae by a septum.

Cell walls located in the fusion zone are degenerated, and cytoplasm are mixed (plasmogamia), while the rest of the wall thickens and accumulates compounds like sporopollein, a polymer of oxidized carotenoids, and melanin, which protect the zygospores (Gooday et al., 1973). The fusion of different mating type nuclei (karyogamy) occurs within the zygospore, although most of the nuclei are degraded. Only one of the four meiotic products survives. After a latency period, which varies according to species, zygospores containing the products of meiosis germinate to produce germospores.

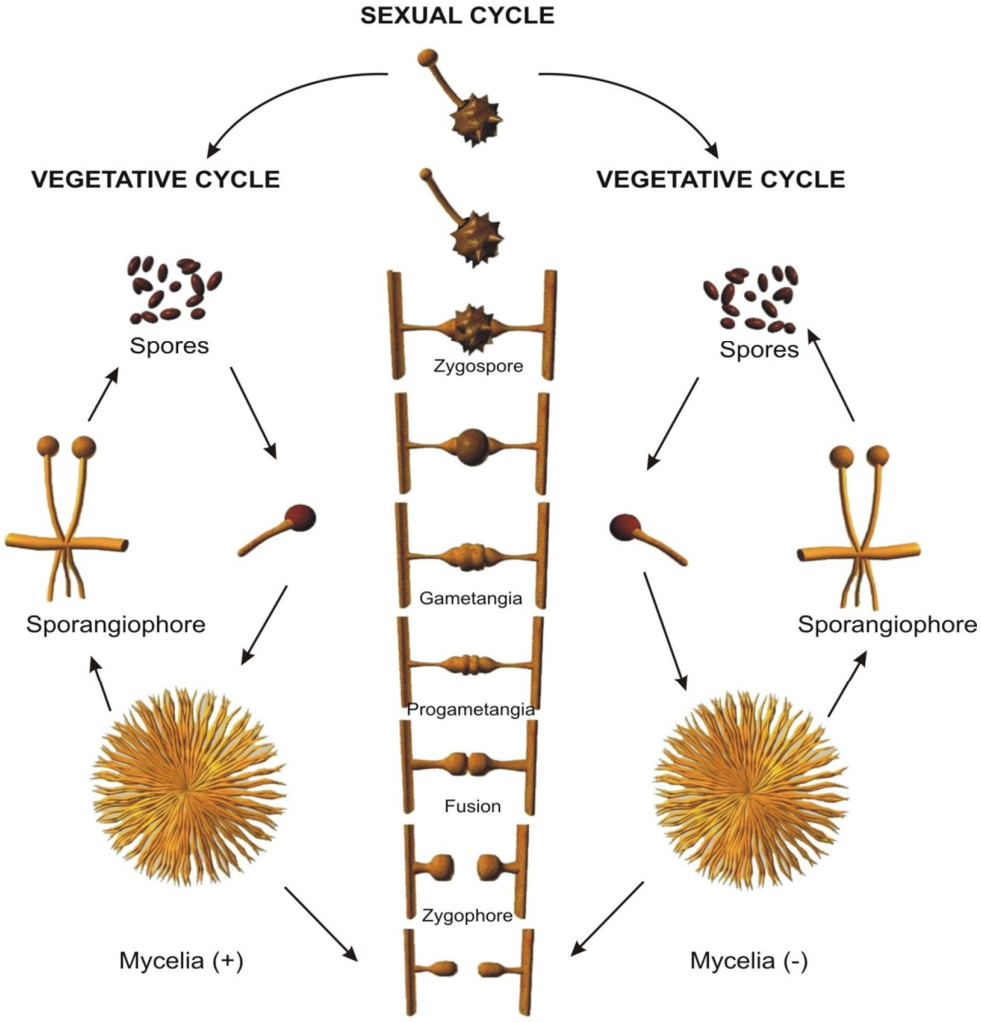

Figure 1. Life cycle of *Mucor circinelloides*

I.1.2. *M. circinelloides* is a study model organism

M. circinelloides has become an outstanding model organism for the study of different molecular processes in the fungal kingdom, such as dimorphism, light responses, accumulation of lipids, anaerobic and aerobic production of ethanol and gene silencing mechanisms (RNAi). Several molecular tools are available for this fungus, including transformation with self-replicative plasmids (van Heeswijk and Roncero, 1984) and integrative DNA fragments (Navarro et al., 2001), which has allowed the generation of unstable transformants or homologous stable recombinants, respectively. More recently, the discovery of the phenomenon of gene silencing in *M. circinelloides* (Nicolás et al., 2003) has led to the incorporation of a new molecular tool to study gene function without generating null mutants (Nicolás et al., 2008). Besides all the available molecular tools, its evolutionary distance from other fungal model organisms, such as *N. crassa*, has made *Mucor* an attractive model for studying gene function in the basal lineage of the fungal kingdom. This feature and its potential use for producing industrial biofuels (Vicente et al, 2009; Vicente et al, 2010) influenced the Joint Genome Institute, which depends on the Department of Energy of United States, to approve in 2007 a project led by our research group to sequence the genome of *M. circinelloides*. A database of the complete genome sequence containing 26 scaffolds and 36,6 megabases has been generated (*M. circinelloides* CBS277.49: http://genome.jgi-psf.org/Mucci2/Mucci2.home.html), which includes 11719 genes. The availability of the genome sequence has accelerated the molecular biology research in this fungus, opening up the possibility of new experimental approaches based on genomics, transcriptomics and proteomics.

One of the well-studied processes in *M. circinelloides* is its response to light. This fungus responds to light by inducing the synthesis of carotenoids (reviewed by Ruiz-Vázquez and Torres-Martínez, 2003), guiding the sporangiophore to light (Silva et al., 2006) and increasing production of spores (Nicolás et al., 2008). The best characterized response is the induction of β-carotene biosynthesis by blue light.

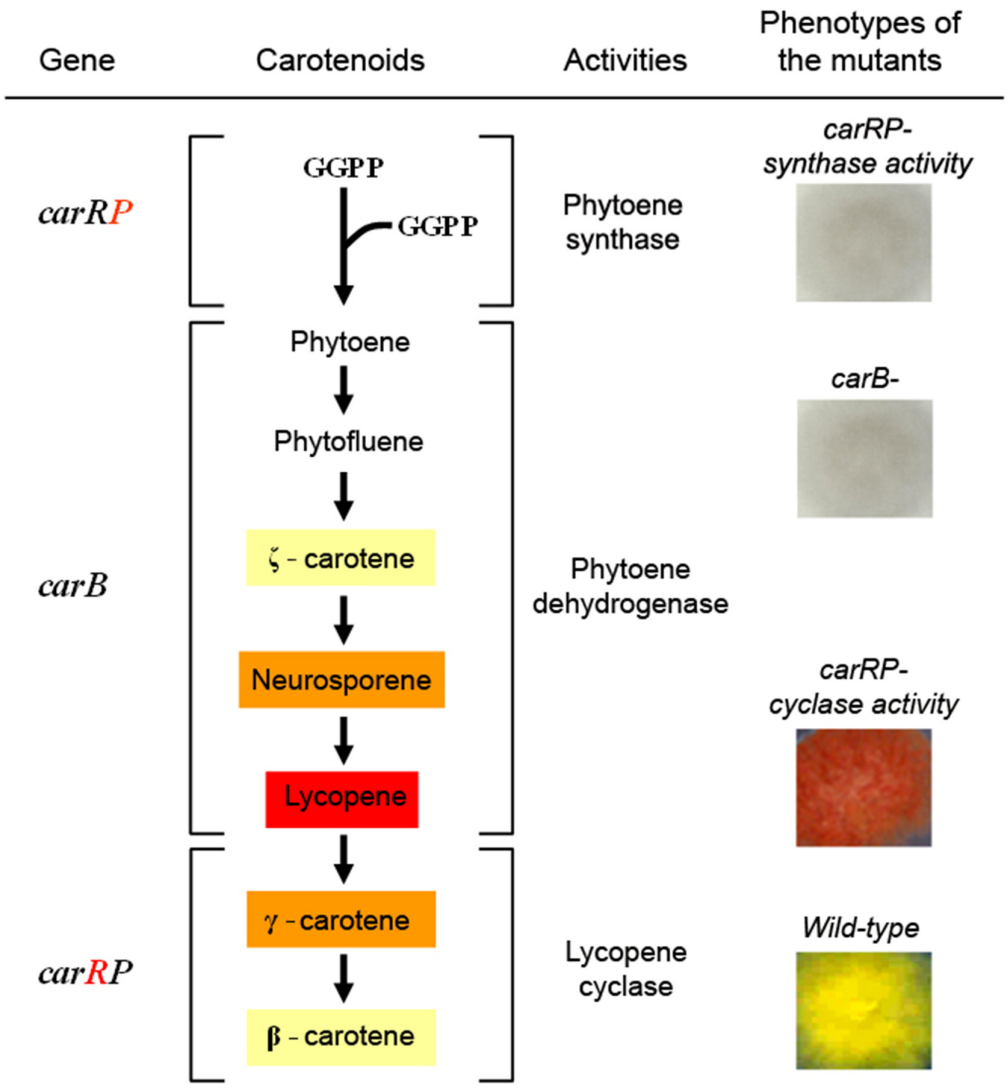

Figure 2. Carotenoid biosynthesis pathway in *M. circinelloides*. The bifunctional gene *carRP* is responsible for the phytoene synthase activity, which generates the first carotene of the pathway from the fusion of two geranylgeranylpyrophosphate (GGPP) molecules. Four dehydrogenations that convert phytoene to lycopene are carried out by the *carB* gene product. The synthesis of β-carotene is completed with the assistance of the lycopene cyclase activity of the bifunctional CarRP enzyme. On the right column, the color phenotypes of mutants affected in the various activities of the β-carotene biosynthesis pathway are shown.

Several genes have been involved in this response, such as the *crgA* gene, a repressor of the synthesis of carotenoids (Navarro et al., 2001), and white-collar -1c (*mcwc-1c*), which mediates the induction of the synthesis of carotenoids by light (Silva et al., 2006). The *crgA* effect on the synthesis of carotenoids is carried out by ubiquitylation of another member of the family of white-collar regulators, the product of *mcwc-1b* gene (Silva et al., 2008). In addition to these regulatory genes,

structural genes like *carB* and *carRP* have been cloned and characterized (Velayos et al., 2000a; Velayos et al., 2000b), allowing a detailed knowledge of the carotenoid biosynthesis pathway of *M. circinelloides* (**Figure 2**).

The wild-type strains of *M. circinelloides* show deep yellow color under light conditions due to the accumulation of β-carotene, while null mutants for the *carB* or *carRP* genes are unable to accumulate colored compounds. Therefore, they show an albino phenotype in both dark and light conditions (**Figure 2**). For this reason, the *carB* gene has been used as a reporter gene to analyze the gene silencing mechanism in *M. circinelloides* (Nicolás et al., 2003). In this mechanism, mRNA degradation of the *carB* gene is induced by the introduction of transgenic copies of *carB*, which leads to the lack of its function and an easily distinguishable albino phenotype (see below).

I.2. RNA-mediated gene silencing

For a long time, RNA was thought as only an intermediate molecule of genetic information flow from DNA to protein. Nowadays, many researchers have revealed that RNAs are not only templates for protein synthesis, but also regulators involved in the regulation of gene expression in eukaryote species via a homology-based repressing mechanism known as RNA-mediated gene silencing. In this mechanism, the transcription of the genes produces mRNAs, but these mRNAs will be destroyed or blocked by homologous sequences using specific machinery. As a consequence, the gene product is not produced, thus, gene expression is silenced.

I.2.1. General aspects

RNA mediated gene silencing is an evolutionary conserved mechanism that suppresses expression of endogenous genes and defends the integrity of host genome against exogenous nucleic acids, such as viruses, transposons and plasmids. It has received different names depending on the organism in which it was studied. In 1990, Napoli *et al* reported a phenomenon in which ectopic transgenes can inhibit the expression of endogenous homologous genes in plants, calling “co-suppression” (Napoli et al., 1990). The same phenomenon was described in the fungus *Neurospora crassa* by Romano and Macino, being called as “quelling”, (Romano

and Macino, 1992). In 1998, the phenomenon was described in *Caenorhabditis elegans* by the breakthrough research of Fire and Mello (Fire et al., 1998), being called as RNA interference (RNAi).

RNAi pathway is triggered by dsRNA (double-stranded RNA) molecules, which can be produced by RdRP enzymes (RNA-dependent RNA polymerases) using ssRNAs (single-stranded RNA) as a template, by stem-loop intramolecular base pairing or by other means. The dsRNAs are used as substrates by protein Dicer, a member of the RNase III family of endonucleases, to produce short RNA molecules (20-30 nucleotides). Those Dicer-dependent small RNAs (sRNAs) are classified into two different groups, siRNAs (small interfering RNAs) and miRNAs (micro RNAs), depending on their origins and biogenesis (**Figure 3**). There is another class of sRNAs, piRNAs (piwi-interacting RNAs), that are produced by a Dicer-independent mechanism (see below). The small RNA duplexes are loaded onto inactive RISC (RNA-induced Silencing Complex) containing the core Argonaute (AGO) protein, becoming active when the passenger strand of sRNAs is removed. The active RISC uses the guide strand of sRNAs to target homologous mRNAs. Targeting of the mRNA molecules can result in degradation or translation inhibition, both options conducing to the absence of protein production.

Each group of small RNA is distinguished from each other by its biogenesis and functions in the cells. The first group of small RNAs, siRNAs, mediates RNAi by down-regulating target RNAs through slicing by endonucleolytic cleavage (**Figure 3A**). These small RNAs are derived from long dsRNA molecules that result from RNA virus replication, convergent transcription of cellular genes or mobile genetic elements, self-annealing transcripts or experimental transfection. The siRNA molecules results from the activity of the Dicer protein to cleave the dsRNA at 21-25nt nucleotides. The guide strand of the siRNA duplex loaded onto an AGO protein is used to detect target mRNA molecules. The target mRNAs containing perfectly complementary sequences are sliced. After slicing, the cleaved target RNA is released, and the RISC is recycled for another round of slicing (reviewed by Jinek and Doudna, 2009). The second group, miRNAs, is genome-encoded. Whereas most plant miRNAs silence target mRNAs via degradation, similarly to siRNAs, animal miRNAs mediate gene silencing without mRNA slicing (**Figure 3B**). Transcription of endogenous miRNA loci produces primary transcripts (pri-miRNAs), containing

~65-70-nucleotide stem-loop structures. In animals, the hairpin structure is processed by the Drosha-DGCR8 complex to generate precursor miRNAs (pre-miRNAs) in the nucleus. Pre-miRNAs are exported into the cytoplasm and diced by a Dicer protein to generate mature miRNA duplex. Then, the guide strand of miRNAs is loaded onto an AGO protein. In mammals, miRNAs typically are only partly complementary to sequences in the 3' untranslated regions of their target mRNAs, and this prevents the target from being sliced by the AGO protein. The mechanism of miRNA-mediated gene silencing is not fully understood, but is thought to act by blocking translation of target mRNA and/or removing poly(A) tails, which leads to mRNA degradation (reviewed by Jinek and Doudna, 2009). The third group, piRNAs, corresponds to ~24-31nt long sRNAs that play a role in transposon silencing in animal germ cells. piRNAs compose the largest class of small non-coding RNA molecules expressed in animal cells (Seto et al., 2007). However, its biogenesis and mechanism of action is not completely understood. A model for its biogenesis in *D. melanogaster* is shown in **Figure 3C**. The biogenesis of piRNAs does not require the presence of Dicer, suggesting that precursors of piRNAs are single-stranded RNAs. A "Ping-Pong" mechanism involving reciprocal slicer-dependent cleavages of sense and antisense transposon transcripts has been proposed for piRNA biogenesis. This process is mediated by the PIWI clade of the Argonaute family, which includes PIWI, Aubergine (AUB) and AGO3 proteins in *D. melanogaster*. PIWI- or AUB-mediated slicing of sense transposon transcripts generates sense piRNAs, which are incorporated onto AGO3 to digest antisense transposon transcripts. The slicing product generates antisense piRNAs, which in turn bind to PIWI and AUB and guide the slicing of sense transposon transcripts to generate sense piRNAs (reviewed by Jinek and Doudna, 2009).

Based on the important functions of RNAi on genome protection and gene expression regulation, it has become an essential mechanism that has been evolutionarily conserved through all the kingdoms of the eukaryotic domain. However, the RNAi pathway is absent in some species, like *Saccharomyces cerevisiae* and other close relative yeasts, filamentous fungi such as *Ustilago maydis* and *Cryptococcus gattii,* and protozoan parasites such as *Leishmania major, Trypanosoma cruzi,* and *Plasmodium falciparum,* since they lack the main components of the RNAi machinery, such as Dicer and/or Argonaute proteins. The

loss of RNAi in these species raises the question of how they can survive during the evolutionary process without the defensive role of RNAi (Drinnenberg et al., 2011; Nicolás et al., 2013). This has led to the proposal that loss of the RNAi machinery may provide some evolutionary advantage that can somehow counteract the apparent disadvantage resulting from losing a mechanism that has been consolidated throughout evolution in the vast majority of eukaryotic organisms (Drinnenberg et al., 2011; Nicolás et al., 2013).

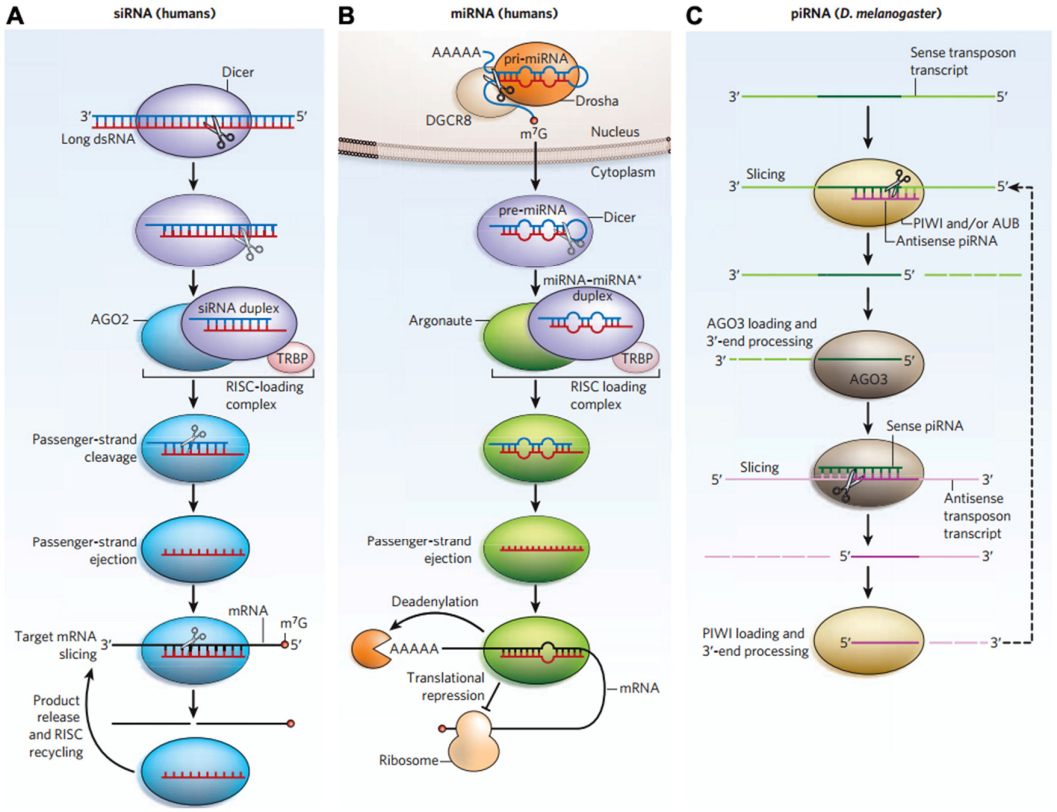

Figure 3. Biogenesis and mechanism of action of the three main groups of small regulatory RNAs, including siRNA, miRNA and piRNA in human (*Homo sapiens*) and fly (*Drosophila melanogaster*) (Jinek and Doudna, 2009).

I.2.2. RNA silencing in filamentous fungi

RNA silencing studies in filamentous fungi have revealed the diversity and important roles of sRNAs and RNA pathways in these organisms. Besides common features of the canonical RNA silencing pathway, these studies also show the enormous variability and peculiarities of RNAi in filamentous fungi. In the following session, we are going to discuss the characteristics and functions of the RNAi pathways in the main fungal models. The RNA silencing mechanism and the most important features of sRNAs in *M. circinelloides* will be discussed in a specific section.

I.2.2.1. RNAi in *Neurospora crassa*

In fungi, the first transgene-induced silencing phenomenon was discovered in the filamentous fungus *N. crassa* (Romano and Macino, 1992). *N. crassa* is one of the most important model systems for RNAi studies in the fungal kingdom. This fungus produces carotenoids through a biosynthetic pathway in which the structural genes *al-1*, *al-2* and *al-3* participate in the production of the final compound neurosporaxanthin, which is responsible for the light orange color of the wild-type mycelia. Mutations in one of these genes result in the albino phenotype. Quelling occurs when transforming exogenous *al-1* or *al-3* sequences into the wild-type strain, which triggers the silencing mechanism in some transformants that show an albino phenotype as a consequence of the repression of endogenous *al-1* or *al-3* genes. These albino transformants, however, were not stable since they spontaneously and progressively reverted to wild-type or intermediate phenotype after several vegetative cycles. Southern blot analysis of the albino transformants demonstrated the presence of the exogenous sequences, which were randomly integrated in ectopic locations into the host genome with a range from 2 to 20 copies. The analyses of the revertants showed that quelling efficiency seemed to be correlated with the number of integrative sequences in genomic DNA (Romano and Macino, 1992). Like “co-suppression” phenomenon in plants (Napoli et al., 1990), quelling also inhibits the expression of both the transgene and homologous endogenous sequences.

Three quelling-defective *(qde)* mutants, which mapped into three complementation groups, *qde-1, qde-2* and *qde-3*, were isolated and characterized

(Cogoni and Macino, 1997). The functional analysis of these *qde* genes significantly increased our understanding about the RNAi mechanism (Cogoni and Macino, 1997; Dang et al., 2011). The first component demonstrated to be involved in the RNAi machinery in *N. crassa* is a RdRP enzyme encoded by the *qde-1*gene (Cogoni and Macino, 1999a). Interestingly, *qde-1* gene product is a bifunctional enzyme, acting as a DdRP (DNA-dependent RNA polymerase) to produce ssRNA from DNA, and as an RdRP for generating dsRNA from ssRNA templates (Lee et al., 2010a). It has been suggested that QDE-1 protein produces RNAi-triggering dsRNA using as a template aberrant RNAs (aRNAs) that are transcribed from transgenes (**Figure 4A**). The *qde-3* gene was identified as a homologous gene of ReQ DNA helicase that is involved in both quelling and biogenesis of qiRNA, a type of small RNAs that is generated from rDNA after DNA damage (**Figure 4B**) (Cogoni and Macino, 1999b; Pickford et al., 2003; Lee et al., 2009). This suggested that *qde-3* protein participates in these mechanisms by facilitating the production by *qde-1* of aberrant RNAs from anomalous repetitive DNA structures. The dsRNAs are processed into siRNAs by the ribonuclease III Dicer. There are two Dicer proteins in *N. crassa*, Dicer 1 and Dicer 2, which have redundant functions in the production of siRNAs (Catalanotto et al., 2004). Biogenesis of sRNAs in *Neurospora* is *qde-1* and *qde-3* dependent, but *qde-2* independent, suggesting that *qde-2* acts downstream of sRNA production (Catalanotto et al., 2002). In fact, the gene *qde-2* encodes an Argonaute protein (Cogoni and Macino, 1997). The passenger strand of siRNAs is cleaved by the endonucleolytic activity of QDE-2 to produce nicked duplex siRNAs, and then is removed by the exonucleolytic activity of QIP (a QDE2-interacting protein), promoting the activation of RISC (Maiti et al., 2007). QIP protein is also required for meiotic silencing by unpaired DNA (MSUD) a mechanism found in *N. crassa* that silences unpaired DNA during meiotic cycle (Shiu et al., 2001).

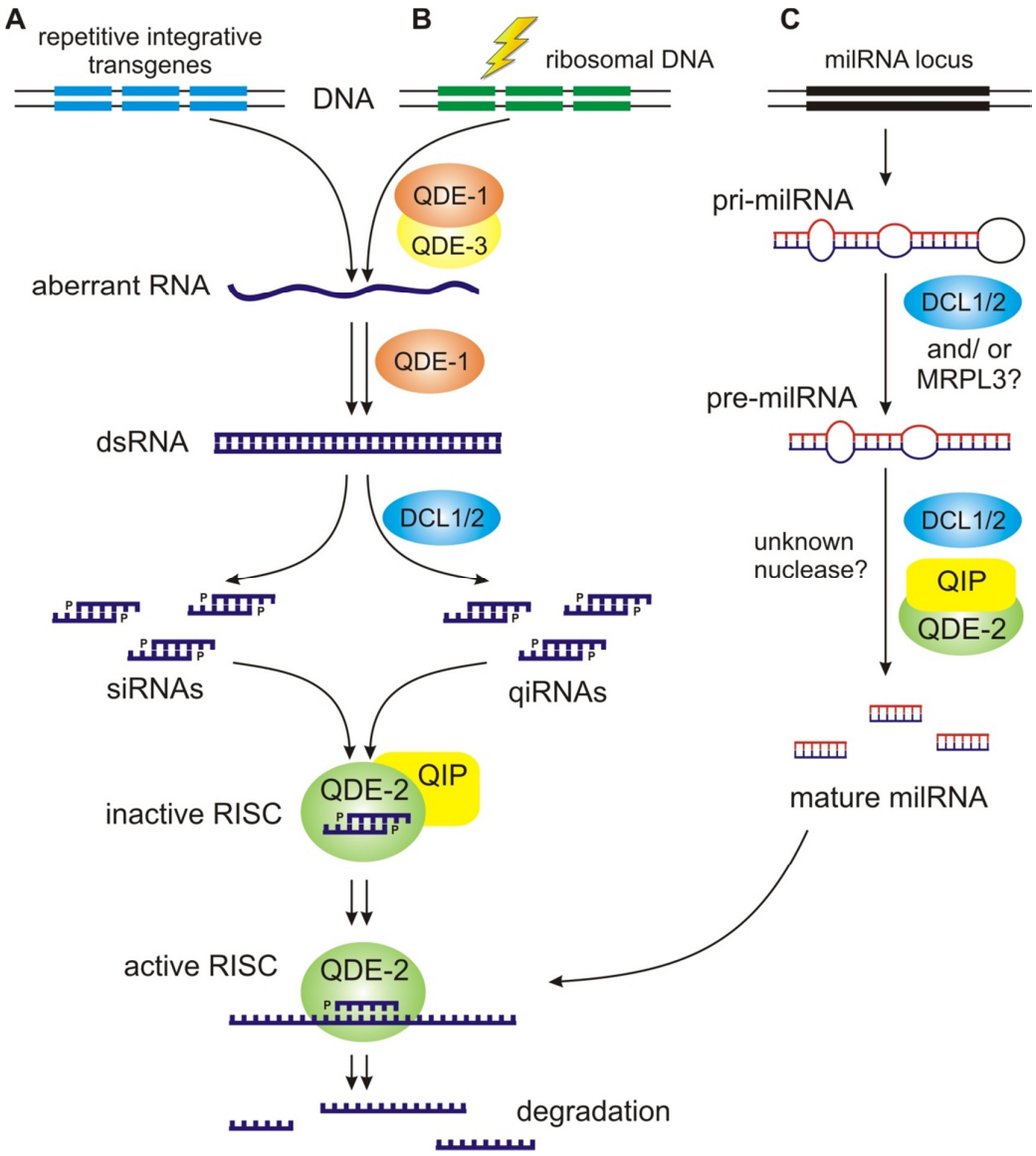

Figure 4. RNAi in *N. crassa*. The scheme shows biogenesis of siRNAs, qiRNAs and milRNAs in *N. crassa*. (**A** and **B**) Aberrant RNAs are generated by QDE-1 (acting as a DdRP enzyme) and QDE-3 from repetitive integrative transgenes or damaged ribosomal DNA regions in siRNA or qiRNA biogenesis, respectively. QDE-1 also uses its RdRP activity to convert aRNA to dsRNA, which is digested by DCL-1/2 into siRNAs or qiRNAs in quelling or qiRNAs biogenesis, respectively. These sRNAs are transferred onto QDE-2/QIP complex to assembly an active RISC that degrades the target mRNAs. **(C)** The pri-milRNAs with stem-loop structures, produced from the milRNA loci, are diced by DCL-1/2 and/or MRPL3 and/or an unidentified nuclease to generate pre-milRNAs. Those intermediated products are digested by Argonaute QDE-2 and/or QIP and/or an unknown nuclease to produce mature milRNAs, which are loaded onto QDE-2 RISC and used to identify and cleavage the target mRNAs.

I.2.2.2. RNAi in other filamentous fungi

Defensive roles against viruses, plasmids and transposable elements were the first associated functions of the RNAi mechanism within eukaryotic species (Chang et al., 2012). In the fungal kingdom, the defensive role of the RNAi machinery was demonstrated in the chestnut blight fungus *Cryphonectria parasitica* (Zhang et al., 2008). The RNAi-based viral response of this fungus requires the presence of only one Dicer-like protein, Dcl-2 and one Argonaute-like protein, Agl-2 (Zhang and Nuss, 2008; Zhang et al., 2008; Sun et al., 2009), suggesting that the anti-viral RNAi pathway in *C. parasitica* acts following the canonical mechanism. Interestingly, many animal, plant and fungal viruses have evolved by counteracting the antiviral immunity system within their hosts by encoding RNAi suppressors, such as papain-like protease p29, p21 and HC-Pro, which act in a promoter-dependent manner, mediating the repression of RNAi genes, and/or by binding to siRNAs to interfere the siRNA-RISC assembly (Suzuki et al., 2003; Lakatos et al., 2006; Segers et al., 2006; Sun et al., 2009). As a result of this neutralization, the antiviral silencing system is blocked, and host cells cannot detect and fight against the virus invasion. Similar results have been found in *Aspergillus nidulans*, indicating that infective viruses can be both targets and suppressors of RNAi pathway in fungi (Hammond et al., 2008).

RNAi triggered by the integration of exogenous sequences has been described in many other fungi (Chang et al., 2012; Nicolás et al., 2013). Particularly interesting is the silencing mechanism of the human fungal pathogen *Cryptococcus neoformans*. This fungus has the usual RNAi machinery with Argonaute, Dicer and RdRP as the central components, similarly to other fungi in which RNAi has been described. However, the induction of RNAi by tandem integration of transgenes in this fungus results in a special sex-induced silencing (SIS), as the repetitive transgene is silenced at an ~250-fold lower frequency during vegetative mitotic growth compared with sexual reproduction (Wang et al., 2010). Besides sense transgenes, gene silencing triggered by dsRNA-expressing transgenes, containing inverted repeats or two opposite promoters, has been described in many filamentous fungi including *Ascomycota, Basidiomycota* and *Zygomycota* (Li et al., 2010).

I.2.3. Functional diversity of RNAi-associated small RNAs in fungi

I.2.3.1. Host defense small RNAs

The RNAi mechanism can be triggered by a wide variety of exogenous nucleic acids that represent a threat for genome integrity. Thus, different exogenous nucleic acids such as integrative transgenes, viruses and transposons have been found to trigger the RNAi mechanism against whatever is transcribed from them. RNAi in fungi triggered by viruses and transgenes has been mentioned in the previous section. In this section, RNAi triggered by transposons and unpaired DNA will be discussed.

Short RNAs production triggered by transposons

"Co-suppression" in plant and "quelling" in *N. crassa* were discovered as gene silencing mechanisms triggered by integrative transgenes randomly inserted into the host genome (Napoli et al., 1990; Romano and Macino, 1992). The repetitive nature of transgene integration in silenced strains suggested that RNAi in *N. crassa* could be used as a defense mechanism against invasive repetitive sequences like transposons. In fact, the first example in fungi showing the important role of RNAi in the maintenance of genome integrity by silencing transposable elements was described in *N. crassa*. Genetic analysis with an African strain of this fungus that harbors a LINE-like transposon showed that the RNAi mechanism is required to suppress transposon replication (Nolan et al., 2005). This study revealed that, unlike quelling, Argonaute QDE2 and Dicer, but not the RdRP protein QDE1 or the RecQ DNA helicase QDE3, are essential for silencing the transposable elements. This analysis also suggested that dsRNAs derived from inverted repeat regions that are generated by the transposition mechanism can trigger the RNAi pathway. On the other hand, small RNAs derived from transposable sequences were detected by deep sequencing in other fungi, such as *M. circinelloides* (Nicolás et al., 2010) and *Magnaporthe oryzae* (Nunes et al., 2011), indicating that RNA silencing acts as an effective defense mechanism against transposable elements in diverse fungal species.

siRNAs triggered by unpaired DNA during meiotic phase

Meiotic silencing by unpaired DNA (MSUD) is an RNAi-related pathway that occurs only during the meiotic process and that has been described in *N. crassa* (Shiu et al., 2001) and *Gibberella zeae* (Son et al., 2011). Unpaired DNA refers to

genes lacking their pairing partner during prophase of meiosis I, as occurs when transposon or virus nucleic acids are inserted into host genome (Shiu et al., 2001; Shiu and Metzenberg, 2002; Son et al., 2011). MSUD protects the host genome by transiently silencing all copies of the DNA fragments that are unpaired during the pairing of homologous chromosomes.

The molecular mechanism of MSUD, like quelling, is also triggered by dsRNA molecules that are synthesized using aberrant RNA templates transcribed from unpaired DNA regions (Shiu et al., 2001) (**Figure 5**). MSUD-associated siRNAs (masiRNAs) are produced by processing of those dsRNAs (Hammond et al., 2013). MSUD requires the canonical RNAi components DCL-1 and QIP. However, there are some different components involved in this mechanism when compare with the canonical RNAi pathway. One of them are the *sad* genes *(suppressor of ascus dominance)*, which includes *sad-1* and *sad-2* (Shiu et al., 2001; Shiu et al., 2006; Son et al., 2011). *sad-1* is a homolog of *qde-1* and encodes an RdRP protein (Shiu et al., 2001; Shiu and Metzenberg, 2002). Although the *sad-2* protein product does not contain any conserved domain, it plays a role in the localization of SAD-1 (Shiu et al., 2006). SAD-3 is a putative helicase required for MSUD and sexual spore production. It is homologous to the *S. pombe* protein Hrr1, which is a member of the RNA-dependent RNA polymerase complex (RDRC) involved in RNAi-mediated heterochromatin formation (Motamedi et al., 2004), suggesting that the mechanism of MSUD could be related with heterochromatinization. Both *N. crassa* SAD-3 and *S. pombe* Hrr1 interact with an RdRP and an Argonaute protein, indicating that the silencing machinery may be conserved between these two fungi (Motamedi et al., 2004; Hammond et al., 2011). The *sms-2 (suppressor of meiotic silencing-2)* gene, encoding a homolog of the Argonaute protein, was identified and characterized from the *Neurospora* genome. Analysis of *sms-2* mutants demonstrated that this gene plays an important role in the MSUD pathway (Galagan et al., 2003; Lee et al., 2003). In the quelling pathway, both DCL-1 and DCL-2 are involved in the production of siRNAs. In contrast, only DCL-1 but not DCL-2 is required for MSUD, and only DCL-1 is expressed during meiosis (Alexander et al., 2008).

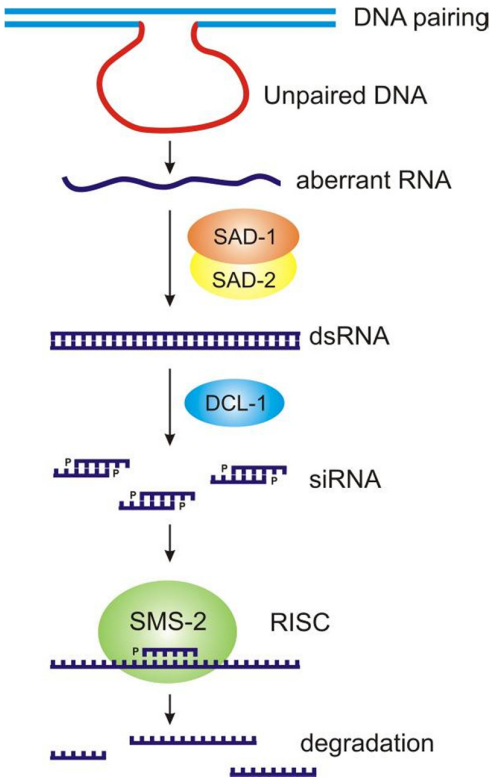

Figure 5. A simple model for MSUD in *N. crassa.* The unpaired DNA region could be produced by inserted DNA of viruses or transposons. Aberrant RNAs transcribed from unpaired DNA regions are converted into dsRNA by SAD-1 and processed by DCL-1 to produce siRNAs. These siRNAs are loaded into RISC in which the Argonaute SMS-2 protein is the main component. The activated RISC degrades homologous RNAs resulting in silencing of the unpaired DNA sequences. SAD-2 could function by recruiting SAD-1 to its proper location to perform its activity.

I.2.3.2. Regulatory endogenous small RNAs

Besides the genome defense function, RNAi plays important roles in the endogenous regulation of gene expression. RNAi is involved in cell differentiation and other biological processes through the production of diverse small non-coding RNAs. These endogenous small RNAs (esRNAs) are similar to siRNAs in their biogenesis, with the main difference based in the fact that they are directly produced from an endogenous precursor rather than an exogenous trigger molecule. In plants and animals, esRNA precursors are generated by various mechanisms (**Figure 6**). The unexpected diversity of esRNAs and their biogenesis pathways in fungi will be discussed along this section.

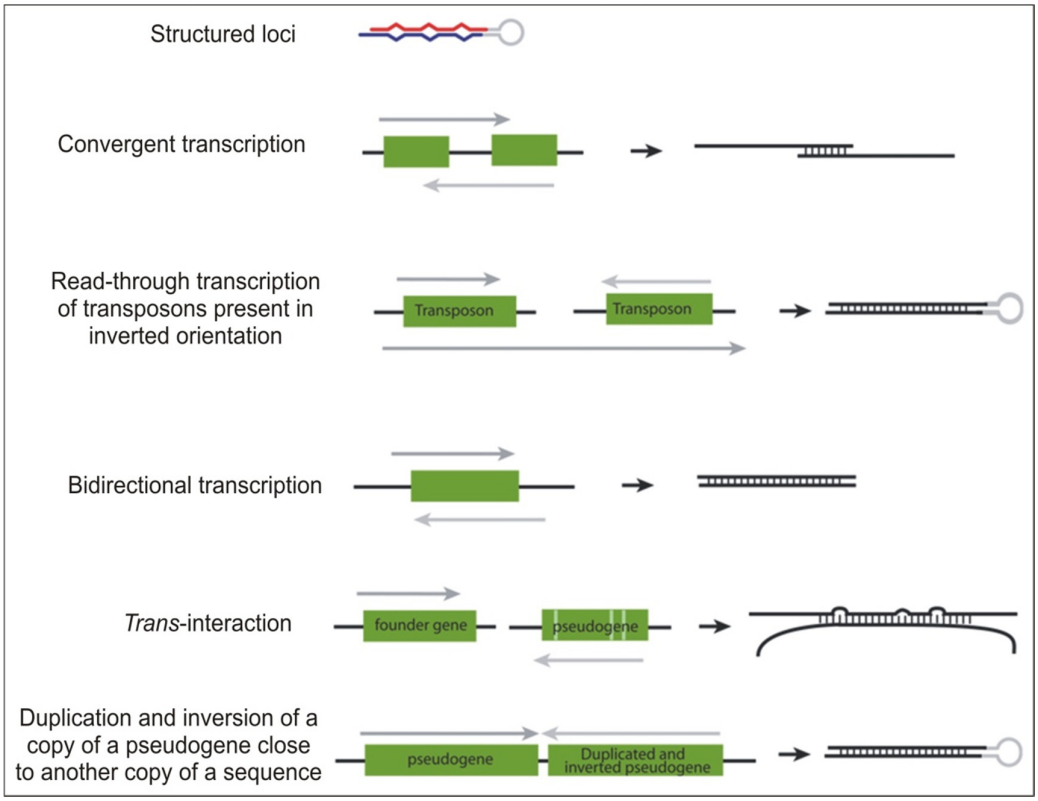

Figure 6. Genomic sources of dsRNA for generation of esRNAs in flies and animals (Ghildiyal and Zamore, 2009).

Micro RNA-like RNAs (milRNAs)

miRNAs belong to a group of esRNAs processed from stem-loop precursor transcripts (Bartel, 2004). They have been found and characterized in plants, animals and algae, but for a long time it was assumed that fungi lacked a miRNA biogenesis mechanism. However, Lee *et al* (2010b) found miRNA-like small RNAs (milRNAs) of four different classes in *N. crassa* by analyzing small RNAs species associated with Argonaute QDE-2 protein (**Figure 4C**) (Lee et al., 2010b). These milRNAs were encoded by 25 potential loci in the *Neurospora* genome and were mostly distributed into two different sizes, 19 and 25nt, with a very strong preference for U at their 5' termini. The most abundant milRNAs were generated from four loci located in intergenic regions, and were named *milR-1, milR-2, milR-3* and *milR-4*, which are distinguished by the components of the silencing machinery involved in their biogenesis (**Figure 7**) (Lee et al., 2010b). The generation of *milR-1* requires Dicer, QDE-2, QIP and MRPL3 (an RNase III domain-containing protein that could be involved in the Dicer-independent biogenesis of some milRNAs in *N. crassa*). Production of *milR-3* only requires Dicer1/2. The production of *milR-4* is partially

dependent on Dicer and requires MRPL3. In contrast, *milR-2* biogenesis requires QDE-2, but not Dicer (Lee et al., 2010b). The exact role of MRPL3 is still not clear, since there are no MRPL3 knockout strains for these studies. Although the *N. crassa* milRNAs have been demonstrated to be functional on reporter genes, their role in the regulation of endogenous functions is still unknown, since no target mRNAs have been found for these molecules.

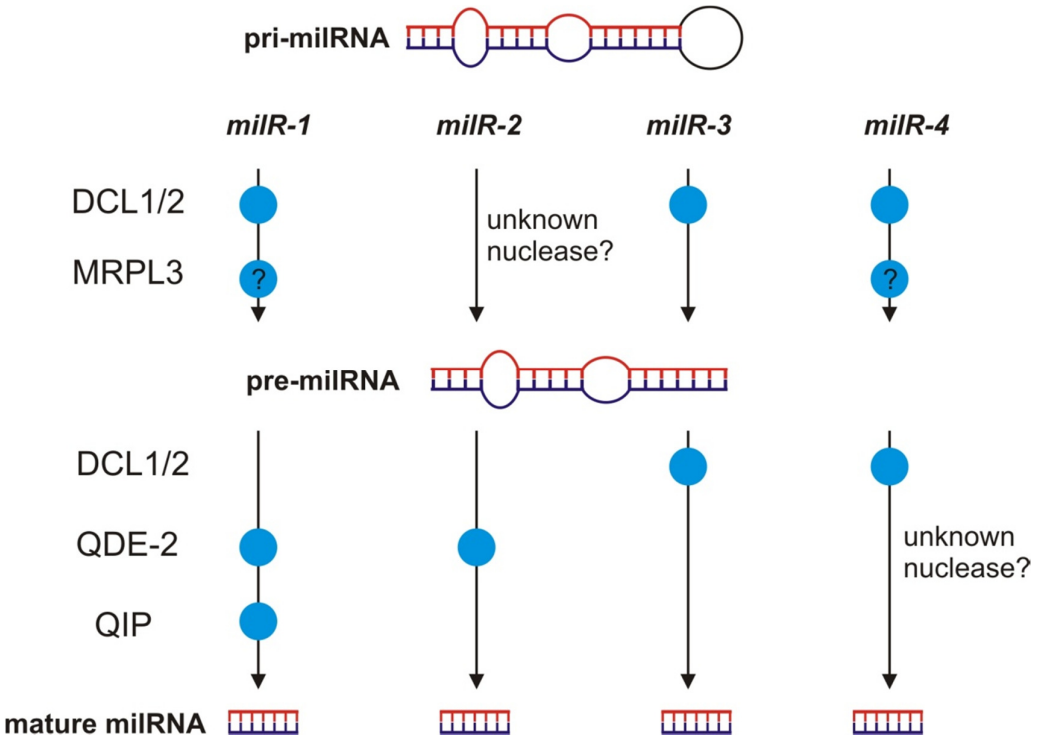

Figure 7. Four different biogenesis pathways for milRNAs in *Neurospora*. The blue circles indicate the involvement of each enzyme in the biogenesis of the different milRNAs. In most milRs, except *milR-2*, the pri-milRNAs with the stem-loop structure have around 170nt, and are digested by DCL-1/2 enzymes to produce pre-milRNAs. MRPL3 involvement in the biogenesis of milRNAs is still an open question. The production of mature *milR-3* is completely *dcl-1/2*-dependent while *milR-4* requires an unknown nuclease. Argonaute protein QDE-2 is involved in both *milR-1* and *milR-2* generation. Finally, *milR-1* also needs QIP for its biogenesis.

Dicer-independent small interfering RNAs (disiRNAs)

A novel group of small RNAs, termed Dicer-independent small interfering RNAs (disiRNAs) were also found in *N. crassa* by analyzing the QDE-2 associated small RNAs (Lee et al., 2010b). Fifty predicted disiRNA loci were identified in the *N. crassa* genome producing nearly equal amount of sRNAs from both DNA strands in a *dicer*-independent manner. Unlike qiRNAs (see below), disiRNA production is not triggered by DNA damage and neither they derive from repetitive DNA. Most

disiRNAs are 22 nt in length and have 5' uridine overhang (Lee et al., 2010b). Although the functions of disiRNAs are unclear, the association with the Argonaute QDE-2 protein suggests that they may function via the RNAi pathway.

Although disiRNAs are processed from natural occurring dsRNA precursors, their biogenesis is Dicer-independent. In addition, disiRNA levels are not affected in *qde-1*, *qde-2* and *qde-3* mutants. Further analyses showed that disiRNA production is also independent of SMS-2 and the RNAi component MRPL3 (Lee et al., 2010b). Thus, none of the known RNAi components is involved in the disiRNA biogenesis pathway, and how they are produced and how they work in the cell are still open questions.

The DNA damage-induced small RNAs (qiRNAs)

In *Neurospora*, DNA damage increases the expression levels of the Argonaute QDE-2 protein and induces the production of a small RNA class, called quelling induced RNAs (qiRNAs). These qiRNAs are 20-21nt in length with strong preference for uridine at the 5' end, and most of them are produced from repetitive regions of ribosomal DNA loci (Lee et al., 2009). The qiRNA biogenesis requires the presence of RdRP QDE-1, RecQ DNA helicase homolog QDE-3 and Dicer proteins (**Figure 4B**) (Pickford et al., 2003; Lee et al., 2009). Both siRNA and qiRNA biogenesis pathways require the same components, indicating that their mechanisms are similar (Lee et al., 2009; Lee et al., 2010a). Deep sequencing of qiRNAs showed that they correspond to both sense and antisense strands of rDNA loci, suggesting that dsRNA is also a requirement for qiRNA biogenesis. The special feature of qiRNAs is their production from repetitive sequences of rDNA as a response to DNA damage. The proposed model suggests that DNA damage promotes the formation of aberrant forms of recombination intermediates of repetitive DNA, which are recognized by QDE-3 and QDE-1 to produce aRNA and dsRNA (Xue et al., 2012). In this process, *Neurospora* QDE-1 acts as a DNA-dependent RNA polymerase (DdRP) to produce aRNAs and as an RdRP to convert aRNAs to dsRNAs (Lee et al., 2009; Lee et al., 2010a).

It has been suggested that qiRNAs are involved in repressing protein biosynthesis after DNA damage. A proposed model suggests that regulation of rRNA expression by qiRNAs would inhibit protein synthesis, which could help the cells to arrest the cell cycle and activate the DNA repair machineries (Lee et al., 2009).

Other fungal regulatory esRNAs

Endogenous siRNAs (esRNAs) have been also detected in some other fungal species, such as *M. oryzae* (Nunes et al., 2011) and *Trichoderma atroviride* (Carreras-Villasenor et al., 2013). In the filamentous rice blast fungal pathogen *M. oryzae*, esRNAs were identified from mycelia and appressorium tissues by deep sequencing (Nunes et al., 2011). Similar to *M. circinelloides* (see below), those esRNAs mapped to protein-coding genes, intergenic regions and repetitive DNA fragments. *M. oryzae* esRNAs differentially accumulate in vegetative and specialized-infection tissues. The mycelium sRNAs are 18-23nt long and derive from intergenic and repetitive regions. A large proportion of these sRNAs derived from LTR retrotransposons and they were classified as LTR retrotransposon-siRNAs (LTR-siRNAs). On the other hand, sRNAs produced from appressorium cells have 28-35nt and are mainly generated from tRNA loci, being classified as tRNA-derived RNA fragments (tRFs) (Nunes et al., 2011). Although the function of those esRNAs is still not fully understood, they could play a role in controlling genome integrity and regulating growth and development in *M. oryzae* (Nunes et al., 2011).

In *T. atroviride,* the RNAi mechanism plays a role in regulation of metabolism, development and mycelium morphology through the production of *dicer*-dependent esRNAs (Carreras-Villasenor et al., 2013). Transcriptomic analyses of wild type, Δ*dcr1*, Δ*dcr2* and Δ*dcr1*Δ*dcr2* demonstrated that each Dicer protein regulates different biological processes, such as development and metabolism. The esRNAs population of Δ*dcr2* is different to that of wild type and partly correlates with transcript expression, suggesting that the RNAi machinery of *T. atroviride* plays a role in controlling endogenous processes (Carreras-Villasenor et al., 2013). Together, those results underscore the significant roles of esRNAs in the regulation of endogenous gene expression and the control of developmental processes in the fungal kingdom (Nicolás et al., 2013).

I.2.4. RNAi in *Mucor circinelloides*

I.2.4.1. Characteristics

The filamentous fungus *M. circinelloides* has become an outstanding model organism for studies of carotenoid biosynthesis, RNA silencing and human fungal pathogenesis, mainly due to the availability of a large number of molecular tools and its evolutionary distance from other fungal model organisms, such as *N. crassa*. Particularly, *M. circinelloides* has notably contributed to the understanding of the RNA silencing mechanism in fungi. The existence of a gene silencing mechanism in *Mucor* was discovered by F.E. Nicolás (Nicolás et al., 2003) by using a simple visual reporter system to analyze transgene-induced gene silencing. Wild-type strains transformed with complete or truncated copies of the *carB* gene, coding for the phytoene dehydrogenase enzyme, presented an albino phenotype instead of the bright yellow color seen when the *carB* gene is expressed at the wild-type levels (**Figure 8A**). One peculiar characteristic of the silencing mechanism in this basal fungus is the presence of two different size classes of small antisense RNAs, 21 and 25nt in length, which are differentially accumulated during the vegetative cycle (**Figure 8B**) (Nicolás et al., 2003). In contrast, only one sense sRNA size class of 25nt was detected. Accumulation of the 21nt antisense siRNAs has been related with silencing efficiency and stability, suggesting that this siRNA class, instead of the longer one, could be the guide for mRNA degradation (Nicolás et al., 2009). Both antisense 21nt and sense 25nt siRNAs are transmitted into spores (**Figure 8B**) (Nicolás et al., 2003), explaining why the silencing effect can be inherited to the next generations. Genes involved in the biogenesis of these siRNAs have been identified and functionally characterized. Two dicer genes were identified, of which *dicer-2* (*dcl-2*), but not *dicer-1* (*dcl-1*), plays the major role in the biogenesis of the two size classes of siRNAs (Nicolás et al., 2007; de Haro et al., 2009). How a single enzyme can produce two different size classes of siRNAs is still unclear. It has been proposed that the spatial arrangement of PAZ and RNase III domains within Dicer protein (see below) and the interaction of this enzyme with other proteins, such as dsRNA-binding proteins, could explain the generation of different length siRNAs (Qi and Hannon, 2005; Macrae et al., 2006).

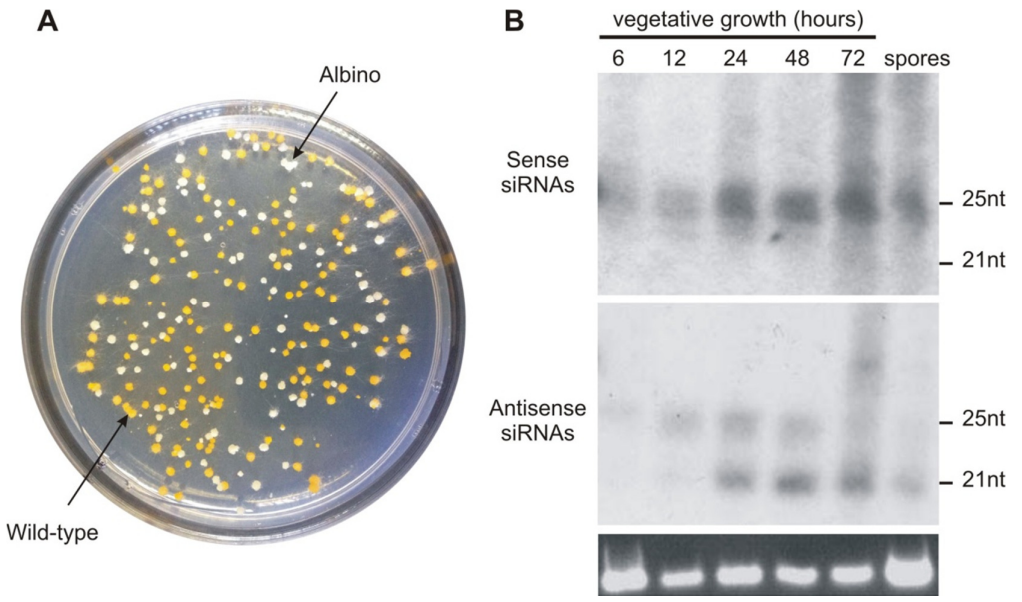

Figure 8. Transgene-induced RNA silencing in *M. circinelloides*. **(A)** Silencing of *carB* expression by introduction of non-integrative transgenes containing *carB* sequences results in albino phenotype. **(B)** Differential accumulation of sense and antisense siRNA classes during vegetative growth of the silenced strains (Nicolás et al., 2003).

Unlike *N. crassa* and many other fungi, transforming DNA in *M. circinelloides* does not integrate into the genome but is maintained in an episomal state. Thus, transgene constructs are easily recovered in multimeric forms from the transformant nuclei (Roncero et al., 1989; Navarro et al., 2001). The non-integrative nature of transgenes is an added value of *M. circinelloides* studies on gene silencing, since transgene expression is not affected by position effects or host regulatory sequences at insertion sites, both of which are thought to be involved in the production of abnormally processed RNAs. This allowed demonstrating that a high level of expression of transgenes is essential for silencing, since the silencing frequency increased from 3 to 90 % when the expression of the transgene was increased in different ways (Nicolás et al. 2009; de Haro et al. 2009; Calo et al. 2012). This could be explained if a high transgene expression results in the accumulation of enough aberrant RNA to activate RdRP-mediated copying.

I.2.4.2. Amplification of silencing

In plants and nematodes, the RNAi mechanism is supplemented through the action of an RdRP activity that expands the initial siRNA production (primary siRNAs) with the generation of secondary siRNAs. Secondary siRNAs, contrary to

primary siRNAs, do not derive from the initial triggering molecule but they come from the targeted mRNAs, which are used as templates by RdRP proteins. While primary siRNAs only correspond to sequences of the dsRNA molecules that initiate the silencing mechanism, secondary siRNAs may also correspond to sequences of the endogenous gene upstream and downstream of the initial inducer sequence (reviewed in Ghildiyal and Zamore 2009).

Secondary sense and antisense siRNA molecules corresponding to sequences of the endogenous gene downstream of the initial triggering molecule have been detected in *M. circinelloides*, supporting the existence of an amplification mechanism in this fungus (Nicolás et al., 2003). Although *rdrp* genes have been identified in several fungi, the role of those genes in amplification of the silencing signal through the production of secondary siRNAs has been scarcely analyzed. In *N. crassa* and *A. nidulans*, the *rdrp* genes are not required for gene silencing when using dsRNA as inducer and no secondary siRNAs have been detected, suggesting the absence of a siRNA amplification step mediated by RdRPs (Chang et al. 2012). Unlike those fungi, in *M. circinelloides* both size classes of siRNAs are present as secondary siRNA (Nicolás et al. 2003).

Two different *rdrp* genes (*rdrp-1* and *rdrp-2*) with different roles in the RNA silencing mechanism of *M. circinelloides* have been identified (Calo et al., 2012). Functional analysis of *rdrp* null mutants indicated that *rdrp-1* is essential for initiation of silencing by sense transgenes through the production of antisense RNA transcripts derived from the transgene, but it is not necessary for amplification of the silencing signal. On the other hand, *rdrp-2* is required for efficient accumulation of the two different classes of secondary siRNAs regardless the nature of the silencing trigger, suggesting a crucial role of this gene in amplification of the silencing signal (Calo et al., 2012).

I.2.4.3. Transgene-induced RNAi pathway in *M. circinelloides*

The RNA silencing pathway in *M. circinelloides* plays a role in both host genome defense and regulation of endogenous gene expression (see below). In the host genome defense system (**Figure 9**), the transgene-induced RNAi pathway is activated by aberrant RNAs (aRNAs) derived from invading exogenous nucleic acids (viruses, plasmids, transgenes and transposons), which are converted to dsRNAs by the polymerase activity of the RdRP-1 protein (Calo et al., 2012). Alternatively, it

can be also triggered by dsRNAs directly originated from hairpin RNA (hpRNA) expressing transgenes. These dsRNAs are digested by the dicing activity of Dcl-2 to produce two different classes of siRNAs, 21and 25 nt long. Even though Dcl-2 plays a main role in siRNA production, both *dcl* genes have a partially redundant function in the RNAi mechanism of *M. circinelloides* (Nicolás et al., 2007; de Haro et al., 2009). The siRNAs are transferred into Ago-1, the only functional Argonaute protein in this fungus. There are two other Ago proteins in *Mucor*, but they do not seem to play any role in RNA silencing during the vegetative growth (Cervantes et al., 2013).

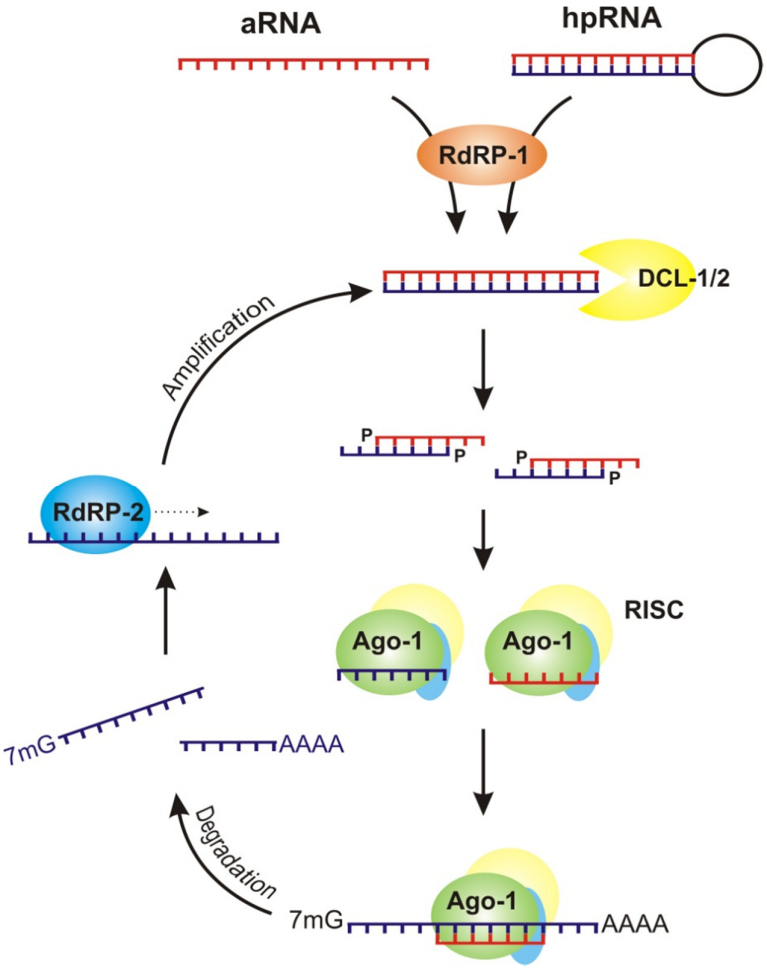

Figure 9. Transgene-induced RNAi pathway in *M. circinelloides*. Double-stranded RNA is directly transcribed from hairpin structures or generated from aberrant RNAs by the activity of RdRP-1 enzyme. Later, it is digested by the dicing activity of Dcl-1 and Dcl-2 to produce siRNAs. These siRNAs are loaded onto RISC complexes in which Ago-1 is the core component. The passenger strand of the siRNA duplex is removed and activated RISC uses the antisense siRNA strand as a guide to specifically recognize and degrade the target mRNAs, resulting in silencing of the target gene. The processed mRNAs can be used as templates by RdRP-2 to produce secondary siRNAs.

Target mRNAs are specifically recognized by antisense siRNAs associated with activated RISC complex, and are degraded by the endonuclease and exonuclease

activities of RISC, resulting in silencing of the expression of targeted gene. After targeting by primary siRNAs, a second RdRP encoded by the *rdrp-2* gene uses the processed target transcripts to generate new dsRNAs that are diced into secondary siRNAs, amplifying the silencing signal (Calo et al., 2012). The existence of this amplification mechanism can explain the strong and stable silencing found in *Mucor*, even though host cells were transformed by a small amount of transgenes.

I.2.4.4. The RNAi machinery in *Mucor*

The RNAi pathway consists of different steps which require specific proteins, such as Dicer, RdRP and Argonaute. Those proteins constitute the RNAi machinery, which has been widely conserved during evolution. Those elements have been identified and characterized in the filamentous fungus *M. circinelloides*.

I.2.4.4.1. The Dicer enzyme

The Dicer enzyme is a member of the RNase III family of ribonucleases that specifically digests dsRNA to produce short dsRNAs with a monophosphate group at the 5' end and two nucleotide overhangs on their 3' end. Dicer proteins display a complex structure, including two RNase III domains and a single dsRNA-binding domain (dsRBD) at the C-terminus, an amino-terminal ATP-dependent RNA helicase domain (DEXD/H-box domain), an DUF283 domain of unknown function proposed to fold as a dsRNA binding domain (Dlakic, 2006), and a Piwi-Argonaute-Zwille (PAZ) domain, which binds specifically to the 3' end of ssRNA (**Figure 10A**). The Dicer enzymes of lower eukaryote species have a less complex domain structures (Jaskiewicz and Filipowicz, 2008). The distance between the PAZ domain and the catalytic RNase III domains controls the length of the Dicer products.

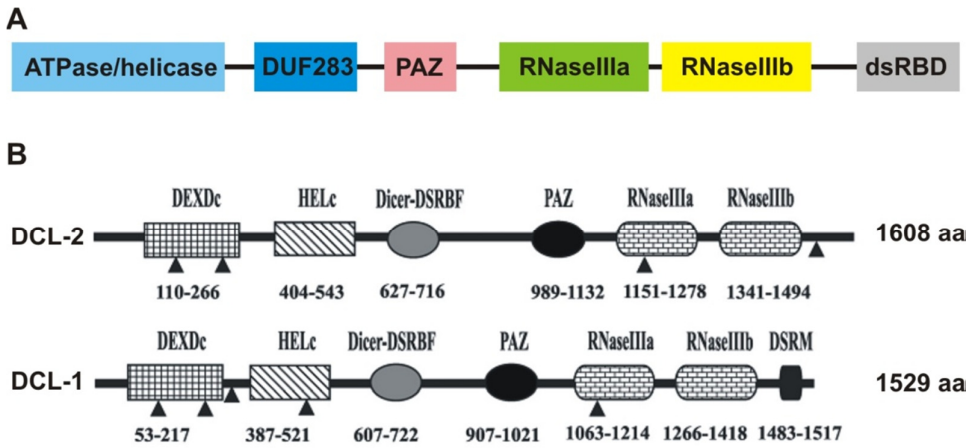

Figure 10. Structure of Dicer protein. **(A)** Domain structure of Dicer proteins, including the helicase domain; DUF283 domain; PAZ (Piwi/Argonaut/Zwille) domain; RNase III a and b and dsRBD (dsRNA-binding domain). **(B)** Domain organization of the two Dcl proteins identified in *M. circinelloides*, with the starting and stopping amino acid) of each domain indicated. The black bars correspond to the full protein sequences. DEXDc, DEAD-like helicase superfamily domain; HELc, helicase C domain; Dicer-DSRBF, a dsRNA-binding domain found in members of the Dicer family (DUF283 domain); PAZ domain; RNase III a and b; and DSRM (dsRNA binding motif). The arrowheads indicate the positions of introns (de Haro et al., 2009).

In *M. circinelloides*, the first RNAi machinery element that was identified and characterized was the *dicer-like* 1 (*dcl-1*) gene, which produces an enzyme containing all the structural domains normally found in other eukaryotic Dicer proteins, including two RNase III domains, RNA helicase DEXD/H-box domain, PAZ domain and a dsRBD domain (**Figure 10B**) (Nicolás et al., 2007). However, *dcl-1* gene does not play a significant role in transgene-induced RNA silencing, since there was no differences in the silencing frequencies between wild-type and *dcl-1* null mutant strains when silencing was triggered by both sense and inverted-repeat transgenes. On the other hand, *dcl-1* null mutant did not affect the accumulation of any class of antisense siRNAs, suggesting that the *dcl-1* gene is not essential for the production of any of the two classes of siRNAs associated with transgene-induced silencing in *M. circinelloides* and implying that, at least, one additional *dicer* gene would have to exist in this fungus to produce the siRNA molecules. (Nicolás et al., 2007). However, *dcl-1* gene seems to be involved in the regulation of endogenous cellular processes, since *dcl-1* mutant strains showed a reduction in their vegetative growth rate and presented an altered hyphal morphology (Nicolás et al., 2007).

The *dcl-2* gene plays a pivotal role in the production of siRNAs triggered by both sense transgene and dsRNA-expressing constructs, as gene silencing is severely

impaired in the *dcl-2*$^{-}$ mutant. The *M. circinelloides* null *dcl-2* mutant does not accumulate any of the two classes of antisense siRNAs, suggesting that both are generated by the same Dcl-2 activity (de Haro et al. 2009). Despite the main role of *dcl-2* in the RNAi pathway, gene silencing was only completely abolished in the *dcl-1/dcl-2* double null mutant, suggesting that *dcl-1* has a partially redundant role in transgene-induced gene silencing in *M. circinelloides*. Both *dcl-2* and the double *dcl-1/dcl-2* mutants are affected in vegetative development since they showed a strong reduction in the production of asexual spores (de Haro et al., 2009). They also exhibited an accelerated autolytic response to nutritional stress (Cervantes et al., 2013), a well-regulated process where many enzymatic activities are involved (Emri et al., 2008). These results point to a crucial role for *dcl-2* in an endogenous gene regulation mechanism in *M. circinelloides*.

I.2.4.4.2. The Argonaute protein

Argonaute proteins (AGO) are the core components of RISC, the final effector in the silencing mechanism by targeting mRNAs through complementarity with the single-stranded siRNA. The AGO protein digests these siRNA-bound targets using its endonuclease activity. The domain structure of the AGO protein family includes PAZ, MID (Middle), and PIWI domains (Wei et al., 2012). Within these domains, PIWI is the catalytic center of AGO, which has a cleaving activity similar to RNaseH (**Figure 11A**).

AGO proteins are widely conserved during evolution, even though they show high diversification in structure and function (Wei et al., 2012). The number of *ago* genes identified in filamentous fungal genomes also varies from zero to eight (Nakayashiki et al., 2006). In *M. circinelloides*, three *ago* genes were identified and were named *ago-1*, *ago-2* and *ago-3*. Their protein products contain all the regular domains found in AGO proteins (**Figure 11B**). However, functional analyses of the corresponding mutants revealed that only *ago-1* gene plays an essential role in the RNAi mechanism, at least during vegetative growth (Cervantes et al., 2013). Neither *ago-2* nor *ago-3* are involved in vegetative gene silencing and the corresponding null mutants do not have recognizable phenotypes, although a possible role for these genes cannot be discarded at different growth conditions or specialized structures.

The *ago-1* null mutant completely abolished gene silencing when induced by both sense and inverted-repeat transgenes. Interestingly, *ago-1* gene was also required for the production and/or stability of siRNAs, since no siRNAs were detected in the *ago-1* null mutant (Cervantes et al., 2013). This suggests that Ago-1 could have a role in the biogenesis of siRNAs, although lack of siRNA accumulation in *ago-1* mutants could also indicate that these small RNAs are stabilized by binding to Ago-1, so that in its absence the siRNAs would be rapidly degraded (Cervantes et al., 2013).

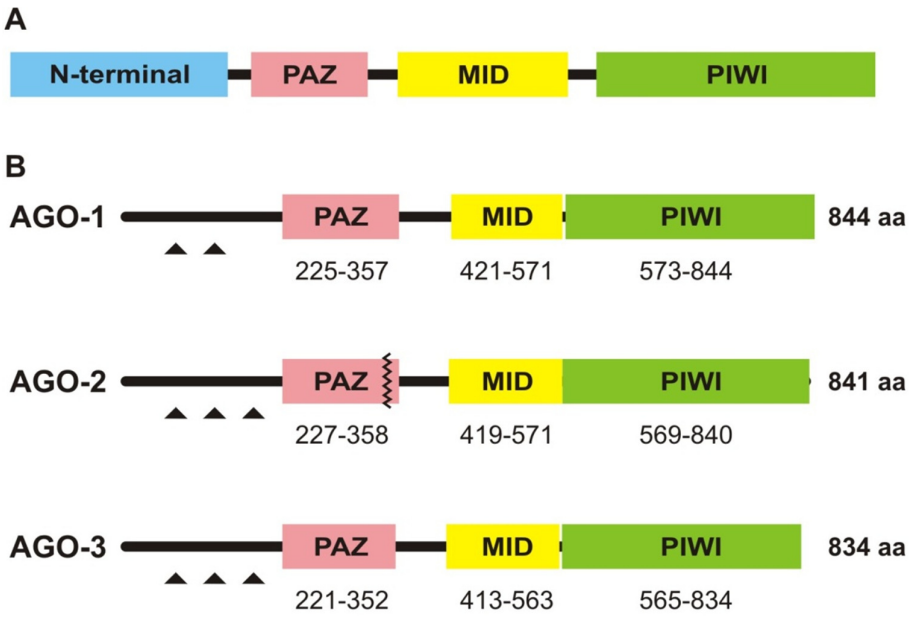

Figure 11. Structure of AGO protein. **(A)** Domain structure of AGO protein. **(B)** Structure of the three *M. circinelloides* Ago proteins. Intron positions are indicated by arrowheads; an in-frame stop codon in Ago-2, which is probably a pseudogene, is indicated by a zigzag line (Cervantes et al., 2013).

The essential role of the *ago-1* gene in the RNAi pathway explains the phenotype observed in the *ago-1*$^-$ mutant. Like *dcl-2*$^-$ mutant, *ago-1*$^-$ mutant exhibits a strong reduction in the production of asexual spores and an accelerated autolytic response to nutrient starvation (Cervantes et al., 2013). These observations reveal the importance of the RNAi machinery in the endogenous regulation of cellular and differentiation processes in *M. circinelloides*.

I.2.4.4.3. The RNA-dependent RNA polymerases

Within the RNAi machinery elements, Dicer and Argonaute proteins are found in the vast majority of eukaryotic species. However, RNA-dependent RNA polymerases (RdRP) are not highly conserved, since they only have been found in plants, nematodes and some fungal species. In those organisms, RdRPs function in the initiation of silencing by sense transgenes, through the production of the triggering dsRNA molecules from single-stranded transcripts derived from the transgenes. Besides this initiation step, RdRPs may also amplify siRNA signals by producing dsRNA from the degraded mRNAs fragments, which generate secondary siRNAs molecules (Sijen et al., 2001). In most organisms, the same enzyme participates in both processes, being absolutely required to initiate silencing by sense transgenes but affecting only the stability of the silenced phenotype when silencing is induced by dsRNA molecules. As indicated above, a third function has been proposed for RdRPs in the RNAi mechanism, namely the direct production of aberrant RNA from a DNA template (Lee et al., 2010a), as has been demonstrated for the *N. crassa* QDE-1 protein.

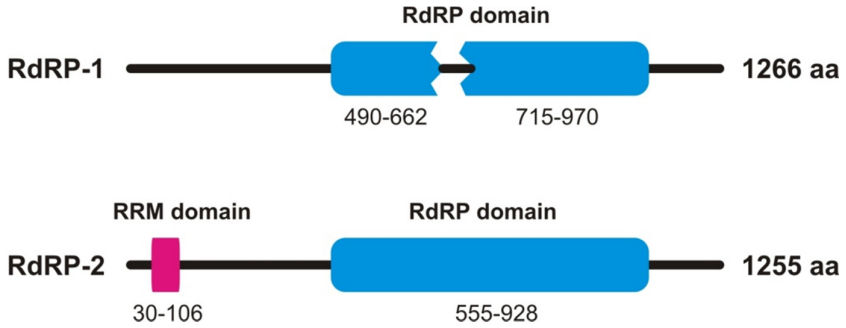

Figure 12. Structure of RdRP proteins in *M. circinelloides*. Domain structure of the two RdRP proteins in *M. circinelloides* with the starting and stopping amino acid of each domain indicated. The black bars correspond to the full protein sequences. RdRP, RNA-dependent RNA polymerase domain; RRM, RNA recognition motif. Insertion of a track of acidic residues into the RdRP domain of RdRP-1 protein is indicated as a disrupted domain (Calo et al., 2012).

There are three *rdrp* genes identified in *M. circinelloides*. Whereas *rdrp-3* does not have any role in the transgene-induced silencing mechanism during the vegetative growth (our unpublished data), RdRP-1 and RdRP-2 enzymes control the initiation and amplification steps of RNAi, respectively (Calo et al., 2012). The domain organization of these two proteins is similar. However, the RdRP domain of RdRP-1 protein is interrupted by an insertion of 53 amino acids rich in acidic

residues (**Figure 12**). Notably, this inserted fragment was also found in the RdRP-like sequences of two other zygomycetes, *Rhizopus oryzae* and *Phycomyces blakesleeanus*. Despite the insertion into the RdRP domain, the zygomycete RdRP-1 proteins maintain all the conserved residues found in other RdRPs (Ng et al., 2008). Contrary to other organisms, where only one RdRP is involved in the initiation and amplification processes, *Mucor* RdRPs show functional diversification. As indicated above, RdRP-1 protein is required for initiation of silencing by sense transgene but not for accumulation of secondary siRNAs when silencing is triggered by dsRNA-expressing constructs. Antisense RNA transcripts derived from sense transgenes were not detected in *rdrp-1*$^-$ mutant, which confirms the role of RdRP-1 for converting ssRNA transcripts into dsRNA molecules (Calo et al., 2012). The function of RdRP-1 in *M. circinelloides* is similar to QDE-1 in *N. crassa*, which also initiates silencing by generating dsRNA molecules from template ssRNAs, but which is not required when silencing is triggered by inverted repeat transgenes (Chang et al., 2012). On the other hand, *M. circinelloides* RdRP-2 is involved in the amplification step of the silencing mechanism, and it is responsible for the production of the two size classes of secondary siRNAs (Calo et al., 2012). The *rdrp-2*$^-$ mutants showed a very low silencing frequency and unstable silenced phenotype when silencing was triggered by both sense and inverted repeat transgenes. But these mutants are perfectly able to produce antisense RNA molecules from sense transgenes, suggesting that RdRP-2 is not involved in initiation of silencing by sense transgenes. The differentiated roles of RdRP-1 and RdRP-2 in the silencing mechanism indicate a functional diversification of these proteins, which have evolved to participate in different steps of the same RNA silencing pathway.

As expected from the relevant and differential roles of *rdrp-1* and *rdrp-2* in the RNAi pathway, mutants affected in those genes showed different phenotypic defects. Thus, while *rdrp-2*$^-$ mutants are affected in vegetative spore production and response to nutritional stress, the *rdrp-1*$^-$ mutant showed differential response to environmental signals (Nicolás et al., 2015; Trieu et al., 2015), supporting the role of those genes in the regulation of different endogenous functions.

I.2.4.5. Regulatory small RNAs in *Mucor*

I.2.4.5.1. The *dicer*-dependent ex-siRNA classes

Endogenous regulation is one of the main functions of the RNAi pathways in eukaryotes. *M. circinelloides* mutants affected in the silencing mechanism showed phenotypic changes relative to the wild-type strain (see above), which suggested a role for the silencing machinery in the regulation of endogenous genes through the production of esRNAs. In fact, deep sequencing analysis of small RNAs in *M. circinelloides* wild type and silencing mutant strains revealed a plethora of regulatory esRNA molecules, which were *dicer*-dependent (Nicolás et al. 2010; Cervantes et al. 2013).

Genomic mapping of the identified esRNA revealed that they corresponded to repetitive sequences and transposons, intergenic regions and exons. Interestingly, the majority of *M. circinelloides* esRNAs were generated from exons and they were called exonic-small interfering RNAs (ex-siRNAs). Hundreds of ex-siRNAs-producing exons were identified, which corresponded to a total of 276 genes, since some genes contained more than one exon producing these ex-siRNAs. Northern blot analyses confirmed that those ex-siRNAs play a significant role in the regulation of the protein-coding genes from which they were produced by guiding degradation of the corresponding mRNAs. Thus, the mRNAs of the target genes accumulated at a high level in those silencing mutants that are unable to produce the corresponding ex-siRNAs. The ex-siRNAs were classified into four different classes based on the proteins of the silencing machinery required for their biogenesis (**Figure 13** and **Table 1**) (Nicolás et al., 2010).

Classes 1 and 2 include the ex-siRNAs that are *dcl-2* and *ago-1*-dependent. They show a strong preference for uracil at the 5' end of the molecule and present a defined size of 23-24 nt. Class 2 is the largest one, representing 68,5% of the detected ex-siRNA-producing loci. Classes 1 and 2 ex-siRNAs are generated from both sense and antisense strands, since they do not show strong strand bias, and they act *in cis* because the accumulation of ex-siRNAs correlates with a decrease in the corresponding mRNA levels. The isolation of Ago-1-bound esRNAs from wild-type *M. circinelloides* confirmed that ex-siRNAs of classes 1 and 2 bind specifically to

Class	Nº of exons	Dependent of					ex-siRNA (%)	5' U (%)
		dcl-1	*dcl-2*	*rdrp-1*	*rdrp-2*	-		
1	9	-	+	-	+	+	13,42	**92,18**
2	222	-	+	+	-	+	58,74	**92,12**
3	88	+	+	+	+	+	27,36	**8,39**
4	5	+	-	+	+	+	0,48	**28,28**

Table 1. Characteristics of the four classes of ex-siRNAs in *M. circinelloides*. The number of exons belonging to each class and the genes required for their biogenesis (marked with +) are indicated. The percentage of ex-siRNA reads corresponding to each class is indicated. The percentage of reads that contain Uracil at the 5' end of the molecule is also shown.

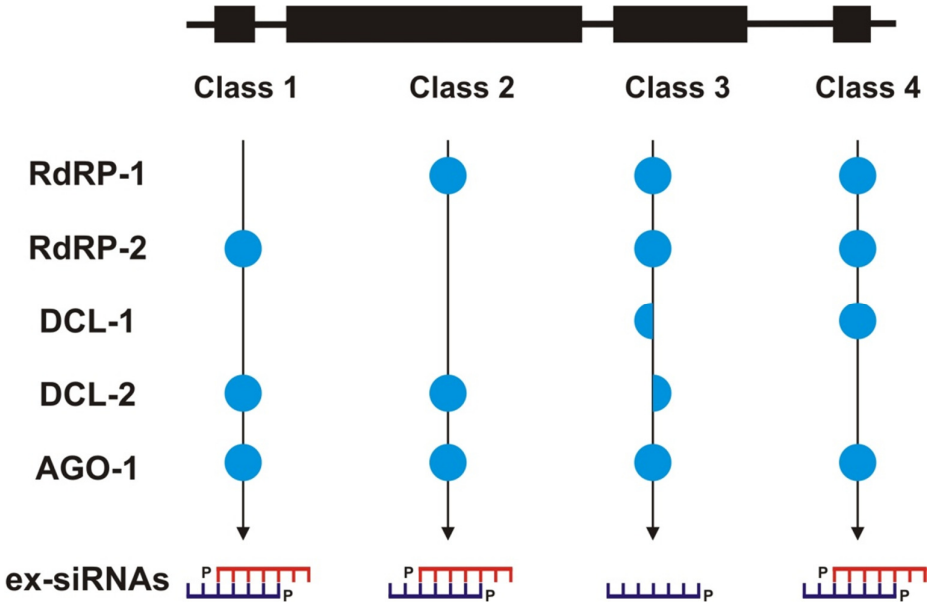

Figure 13. Proteins involved in the biogenesis of the four different classes of ex-siRNAs in *M. circinelloides*. Black boxes show ex-siRNA-producing exons. The proportion of each ex-siRNA class is indicated by the length of boxes. The whole blue circles located in the arrows show the involvement of the enzyme at the left side in the biogenesis of each ex-siRNA class. Halves blue circles in class 3 ex-siRNA biogenesis pathway indicate the redundant roles of both Dcl-1 and Dcl-2.

Ago-1, which indicates that they are functional siRNAs produced by a canonical RNAi pathway to suppress the expression of the corresponding target genes (Cervantes et al. 2013). Class 2 ex-siRNAs require RdRP-1 but not RdRP-2 for their biogenesis. The requirement of Dcl-2 and RdRP-1 for the biogenesis of class 2 ex-siRNAs suggests that RdRP-1 converts mRNAs from those loci into dsRNAs, which are then processed by Dcl-2. These two enzymes have also a prominent role in the

biogenesis of siRNAs generated from transposons and intergenic regions (**Figure 14**) (Nicolás et al., 2010).

An important ex-siRNA group is class 3, which represent around 27,2% of ex-siRNA-producing exons in *M. circinelloides*. Class 3 ex-siRNAs are processed either by Dcl-1 or Dcl-2, since they are only down-regulated in the double *dcl-1/dcl-2* mutant, but not in *dcl-1* or *dcl-2* single mutants. On the other hand, both RdRP-1 and RdRP-2 proteins, as well as Ago-1, are involved in class 3 ex-siRNA production, since levels of these ex-siRNAs are significantly reduced in the corresponding single mutant strains. This class of ex-siRNAs shows several peculiar characteristics. Most of them are exclusively sense to the mRNAs and they do not present a preference for uracil at the 5' end of the molecules. Besides that, they show a random spread of size distribution instead of the defined size of 23-24nt showed by class 2 ex-siRNAs. Together, these results suggested that class 3 ex-siRNAs are not generated by a canonical RNAi pathway, and how they are produced is still unclear. This non canonical biogenesis pathway would also require the Ago-1 protein, as down-regulation of class 3 ex-siRNAs in the *ago-1*$^-$ mutant cannot be explained by stabilization of these ex-siRNAs by Ago binding, since they are not detected among the Ago-1-bound ex-siRNAs (Cervantes et al. 2013). The preference for 5' uracil of *M. circinelloides* Ago-1 may explain lack of binding of class 3 ex-siRNAs, which show a preference for adenine at the 5' end. Although these ex-siRNAs could bind to a different *M. circinelloides* Ago protein, the unusual structural characteristics of class 3 ex-siRNAs point to a non-canonical biogenesis mechanism, a frequent situation in filamentous fungi (Lee et al. 2010b).

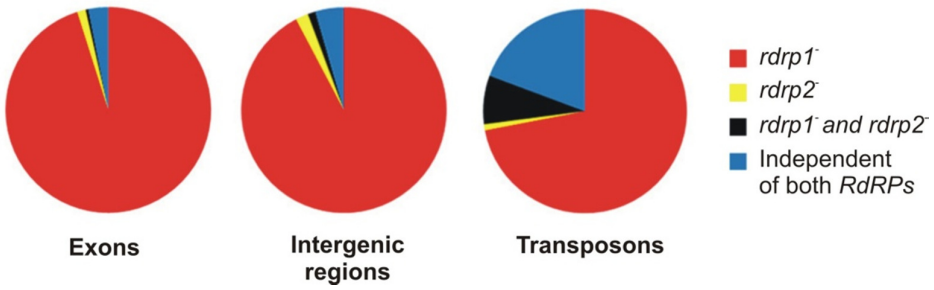

Figure 14. Genes involved in the biogenesis of esRNAs derived from different genomic regions. The pie charts show the percentage of *dcl-2*-dependent loci that also show reduced level of esRNAs in *rdrp-1*$^-$ and *rdrp-2*$^-$ mutants strains (Nicolás et al., 2010).

Classes 1 and 4 are small groups that include ex-siRNAs produced from 9 and 5 exons, respectively. Class 1 production requires the presence of Dcl-2 and RdRP-2, but not RdRP-1. The two RdRP enzymes seem to compete during biogenesis of class 1 ex-siRNAs, since their production highly increased when RdRP-1 was absent, suggesting that both RdRP enzymes can bind to the target mRNA, but only RdRP-2 can direct it into the RNAi pathway. Class 1 ex-siRNAs have structural characteristics similar to that of class 2. Finally, class 4 ex-siRNAs corresponds to a tiny group of ex-siRNAs that requires Dcl-1, Ago-1 and the two RdRPs for their biogenesis. Interestingly, one of these ex-siRNA-producing exons encode a conserved protein that was demonstrated to be involved in polarized growth in yeast and other fungi (Bi et al., 2000; Chesneau et al., 2004; Prigent et al., 2011). Some other exons code for proteins involved in mitochondria metabolism and ribosome function. Taken together, these results could explain the abnormal hyphal morphology and decreased growth rate of *dcl-1* null mutants (Nicolás et al., 2007; Nicolás et al., 2010). Comparing biogenesis of the above ex-siRNAs with the RNAi pathways in plants and animals reveals that the ex-siRNA biogenesis pathways in *Mucor* use all the known RNAi components but in a new and unique combination and highlights the complexity of the small RNA production in this basal fungus. An overview of the *M. circinelloides* RNAi pathways involved in the biogenesis of host defense siRNAs and regulatory esRNAs is shown in **Figure 15**.

The role of the *dicer*-dependent ex-siRNAs in the regulation of endogenous genes has been confirmed by RNA-seq analysis of *M. circinelloides* RNAi mutants (Nicolás et al., 2015). This analysis identified hundreds of genes that showed differential mRNA expression compared to the wild type strain. Detailed analysis of the differentially expressed genes allowed the identification of candidate genes that could be responsible for the phenotypes shown by mutants affected in the RNAi machinery, such as defects in vegetative growth, hyphal morphology and sporulation efficiency, or even differential response to nutritional stress (see above). Most of these phenotypes are related to developmental responses to endogenous and environmental signals, suggesting that the RNAi machinery modulates the expression of genes involved in these responses. This is supported by the ability of *M. circinelloides* to adapt to the environment through a new epigenetic mechanism based on an RNAi-mediated pathway (Calo et al., 2014), pointing out the relevance of the RNAi mechanism in the control of phenotypic plasticity.

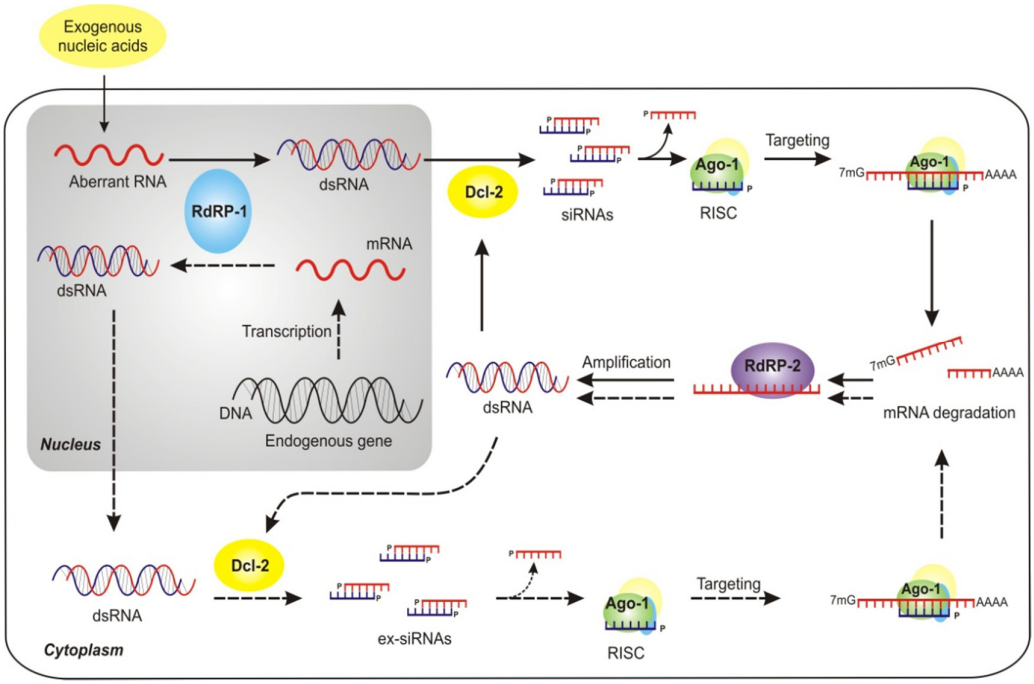

Figure 15. Two different RNAi pathways in *M. circinelloides*. The transgene-induced RNAi pathway (*solid line*) is a mechanism to defend the integrity of the host genome. The endogenous regulatory RNAi pathways (*dashed line*) play a main role in the control of gene expression in this fungus. Only biogenesis of classes 1 and 2 ex-siRNAs are indicated (RdRP-2 and RdRP-1-dependent, respectively).

I.2.4.5.2. A new class of *rdrp*-dependent *dicer*-independent sRNAs

Previous analyses of *M. circinelloides* esRNAs were exclusively focused on those produced through *dicer*-dependent pathways, since only esRNAs that showed a significant reduction in normalized reads in any of the *dcl*$^-$ mutants compared to wild type were considered (Nicolás et al., 2010; Cervantes et al., 2013). On the other hand, comparisons of the phenotypes shown by the different RNAi mutants revealed that several phenotypes were shared by the *rdrp-1*$^-$ and *rdrp-2*$^-$ mutants but not the *dcl*$^-$ mutants (Nicolás et al., 2015). This suggested that a new esRNA class should have to exist that were produced in a *dcl*-independent manner. In fact, analysis of the complete esRNA content of the wild type, *dcl*$^-$ and *rdrp*$^-$ strains identified a new *rdrp*-dependent *dicer*-independent esRNA class derived from exons. The *rdrp*-dependent *dicer*-independent sRNA loci were identified as those that showed at least a fourfold decrease in normalized sRNA reads in *rdrp-1*$^-$ and/or *rdrp-2*$^-$ mutants compared to wild type, with no significant change between wild-type and any of the *dicer*$^-$ mutants. A total of 1523 *rdrp*-dependent loci were identified, among which

611 were *dicer*-independent, and they were grouped based on the annotation of the locus as intergenic, transposon or exonic loci (**Table 2**). Whereas none or a small number of transposon and intergenic loci were *rdrp*-dependent *dicer*-independent, as many as 531 exonic loci corresponded to this category (Trieu et al., 2015). These loci produced sRNAs that showed a very strong strand bias, almost all of them being exclusively sense to the mRNAs (**Figure 16A**; Trieu et al., 2015), and they did not show enrichment for a specific size but they showed a random spread of size distribution (**Figure 16C**). This suggested that these sRNAs are not produced by a canonical RNA silencing mechanism, since the majority of the known *M. circinelloides* ex-siRNAs are *dicer*-dependent and derive from exons producing a mixed sense and antisense ex-siRNAs mainly 23-24 nt long (Nicolás et al., 2010). The *rdrp*-dependent sRNAs were either not detectable in Northern blot hybridization or the probes detected a smear between 15-2000-nt but not discrete bands with sizes between 20-25nt (**Figure 16B**), suggesting that these sRNAs are small degradation products of mRNAs.

Type of loci	**Down-regulated in**[a]			
	rdrp-1$^-$	***rdrp-2***$^-$	***rdrp-1***$^-$ **and** ***rdrp-2***$^-$	**Total**
Transposons	151 (0)	2 (0)	16 (0)	169 (0)
Intergenic regions	424 (29)	12 (4)	71 (47)	507 (80)
Exons	448 (223)	23 (20)	376 (288)	847 (531)
Total	1023 (252)	37 (24)	463 (335)	1523 (611)

Table 2. Number of loci down-regulated at sRNA level in *rdrp-1*$^-$ and *rdrp-2*$^-$ mutants. Total number of loci showing a fourfold or higher reduction in the *rdrp*$^-$ mutant strains compared to the wild type is shown.[a]Loci that show the reduction only in the *rdrp-1*$^-$ or *rdrp-2*$^-$ mutants are considered separated from those with reduced levels of sRNAs in both *rdrp-1*$^-$ and *rdrp-2*$^-$ strains (Trieu et al., 2015). Numbers in parentheses show the number of loci of each category that are *dicer*-independent.

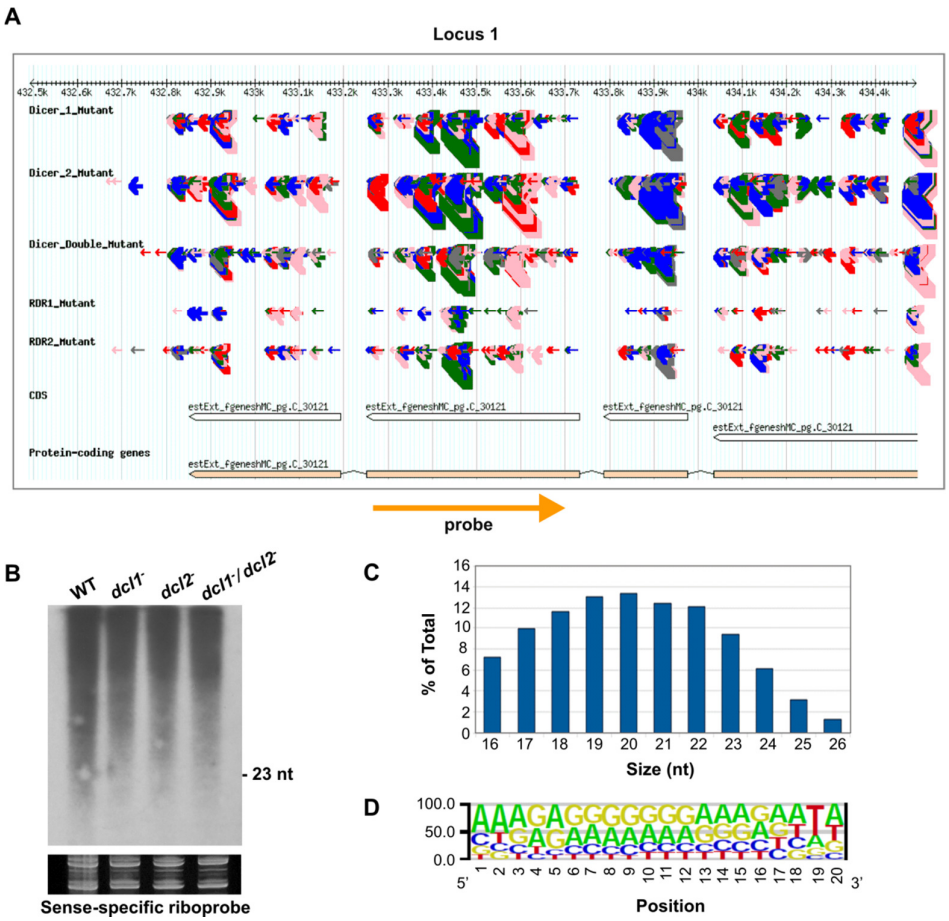

Figure 16. A new class of *dicer*-independent sRNAs in *M. circinelloides*. **(A)** Genome browser shot of a representative *rdrp*-dependent *dicer*-independent sRNA-producing locus showing sRNA accumulation in different mutant strains. Arrows represent sRNA sequence reads, which are exclusively sense to the mRNA. Thickness of the arrows indicates the abundance of read on a log scale. Color of arrows refers to the length of the sequence (between 19-25 nt). Orange arrow represents the position and orientation of the probe used for sRNA detection by Northern blots. **(B)** Northern blot analysis of sRNAs from locus 1 using the sense-specific riboprobe shown in (A) (Trieu et al., 2015). No signal was detected with an antisense-specific riboprobe. **(C)** Size distribution of *rdrp*-dependent *dicer*-independent sRNAs in the wild type strain. The graph represents the percentage of raw reads corresponding to different length of sequenced sRNAs in the wild type strain. **(D)** Sequence logo of the 20 nt size class of *rdrp*-dependent *dicer*-independent sRNAs.

Nevertheless, the generation of this class of sRNAs is not random, since the analyses of the nucleotide distribution in each position of the *rdrp*-dependent *dicer*-independent sRNA degradation products revealed a very strong bias for uracil at the penultimate position for all sizes of sRNAs (18-24 nt; **Figure 16 D**), whereas it is under-represented in the rest of the sRNAs. Taken together, these results suggested that the *rdrp*-dependent *dicer*-independent sRNAs were produced by a degradation pathway in which the RdRP-1 and/or RdRP-2 proteins mark specific transcripts to be

degraded by an unknown RNase that preferentially cleaves mRNAs two nucleotides downstream of any uracil (Trieu et al., 2015).

I.3. Objectives of this study

As mentioned in previous sections, our research group has been studying to unveil the secrets of the gene silencing mechanisms in the basal fungus *M. circinelloides*. We have identified several genes which are involved in RNAi and control different cellular and differentiation processes in this organism. These genes include *dcl-1* (Nicolás et al., 2007), *dcl-2* (de Haro et al., 2009), *ago-1* (Cervantes et al., 2013), *rdrp-1* and *rdrp-2* (Calo et al., 2012). Different combinations of these genes participate in the biogenesis of esRNAs.

Besides the four classes of *dicer*-dependent ex-siRNAs identified previously (Nicolás et al., 2010; Cervantes et al., 2013), a new class of *rdrp*-dependent *dicer*-independent sRNAs was recently identified and characterized (Trieu at al., 2015). These esRNAs were suggested to be produced by a degradation pathway in which the RdRP proteins mark specific transcripts to be degraded by an unknown RNase. One of the objectives of this thesis is the identification of the RNase involved in this degradation pathway and the demonstration of its role in regulation of gene expression.

On the other hand, *M. circinelloides* has recently been identified as an emerging opportunistic human pathogen and a causal agent of the rare but lethal infection mucormycosis (also known as zygomycosis) (Brown, 2005; Chayakulkeeree et al., 2006). Mucormycosis mainly affects immunocompromised patients, such as those affected by diabetes, hematologic malignancies, hematopoietic stem cell/solid organ transplantation, trauma or AIDS (Ribes et al., 2000; Roden et al., 2005). The high virulence and mortality rate of this infection, which can reach up to 90% in disseminated infections (Kontoyiannis and Lewis, 2006), makes an ongoing need to identify new targets and to develop new therapeutic treatments. However, our understanding about genetics of pathogenesis in mucorales is scarce (Rogers, 2008). Recently, our research group, in collaboration with the group of Joseph Heitman (Duke University, USA), has shown the first clue to understand the pathological processes caused by several *Mucor* subspecies, linking

the size of the sporangiospores to the degree of virulence (Li et al., 2011). To identify new genes involved in pathogenesis, a functional genomics analysis based on RNAi has been developed. Other broad objective of this work has been the construction of genomic libraries for functional studies, characterization of these libraries and identification of *M. circinelloides* candidate genes with possible roles in pathogenesis.

The general objectives stated above are specified in the following objectives of this thesis:

1. Functional analysis of the *rdrp*-dependent *dicer*-independent pathway in the regulation of gene expression.
2. *In silico* identification of *M. circinelloides* candidate RNases to be involved in the *rdrp*-dependent *dicer*-independent degradation pathway.
3. Functional studies of the candidate genes by generation of the corresponding null mutants and analysis of their role in the production of *rdrp*-dependent *dicer*-independent esRNAs.
4. Construction of genomic libraries for functional analysis by knocking-down genes using silencing vectors to identify *M. circinelloides* sequences with putative roles in pathogenesis.
5. Generation of null mutants for each candidate gene to confirm the phenotype and for further investigation of their roles in *Mucor* pathogenesis.

II. MATERIALS AND METHODS

II.1. Strains and plasmids used in this work

The *M. circinelloides* strains used in this study and their main characteristics are listed in **Table 3**. All strains with prefix MU were obtained at the University of Murcia and derived from the R7B strain, which is wild-type for carotenogenesis, auxotrophic for leucine and was obtained by chemical mutagenesis from the (-) mating type *M. circinelloides f. lusitanicus* wild-type strain CBS 277.49 (ATCC 1216b *Mucor racemosus*; Schipper, 1976).

Strain MU402 (Nicolás et al., 2007) is a uracil and leucine auxotroph derived from R7B that was used as recipient strain to knock out RNase candidate genes. Strains MU411 (*dcl-1*$^-$*/dcl-2*$^-$) (de Haro et al., 2009), MU413 (*ago-1*$^-$) (Cervantes et al., 2013), MU419 (*rdrp-1*$^-$) and MU420 (*rdrp-2*$^-$) (Calo et al., 2012) were all derived from MU402. The *M. circinelloides f. lusitanicus* strain of the (+) mating type NRRL3631 was used in sexual interaction analysis. The MU450 and MU451 strains derive from MU402 and were generated by replacing the gene ID136157 by a copy of the *pyrG* gene of *M. circinelloides*. The MU455 to MU461 strains derive from MU412 (*r3b2*$^-$), and were produced by integration of a wild-type copy of the *r3b2* gene (MU455 to MU457), or a mutated copy of *r3b2* gene (MU458 to MU461) into the *carRP* locus.

The MU464 strain derives from MU402 and was generated by replacing the *mcclasp* gene (ID 84675, v1.0) by the *pyrG* gene. Similarly, MU465 was obtained by disruption of the *mcmyo5* locus (ID 51513).

The strain DH5α of *Escherichia coli (F*$^-$*, recA1, endA1, gyrA96, hsdR17 (*r_k^-*,* m_k^-*), supE44, thi-1, relA1, lacZ,* λ^-) was used to prepare the competent cells for cloning experiments (Hanahan, 1983). The plasmids used in this study and their descriptions are listed in **Table 4.**

Strains	Genotype	Phenotype	References
CBS277.49	Wild-type strain (mating type -)	Wild-type	*Mucor racemosus* ATCC1216b; Schipper, 1976
NRRL3631	Wild-type strain (mating type +)	Wild-type	NRRL collection
MU239	*pyrG*$^{+}$, *leuA*$^{+}$	Wild-type	This laboratory
R7B	*pyrG*$^{+}$, *leuA*$^{-}$	Leu^{-}, Ura^{+}	Prof. M.I.G. Roncero, Univ. of Córdoba
MU402	*pyrG*$^{-}$, *leuA*$^{-}$	Leu^{-}, Ura^{-}	(Nicolás et al., 2007)
MU411	*dcl-1::leuA, dcl-2::pyrG*	Leu^{+}, Ura^{+}	(de Haro et al., 2009)
MU412	*leuA*$^{-}$, *r3b2::pyrG*	Leu^{-}, Ura^{+}	Calo, 2010
MU413	*leuA*$^{-}$, *ago-1::pyrG*	Leu^{-}, Ura^{+}	(Cervantes et al., 2013)
MU419	*leuA*$^{-}$, *rdrp-1::pyrG*	Leu^{-}, Ura^{+}	(Calo et al., 2012)
MU420	*leuA*$^{-}$, *rdrp-2::pyrG*	Leu^{-}, Ura^{+}	(Calo et al., 2012)
MU450 & MU451	*leuA*$^{-}$, *ID 136157:: pyrG*	Leu^{-}, Ura^{+}	This study
MU455 to MU457	*r3b2::pyrG, carRP::(leuA + r3b2*^{wt}*)*	Leu^{+}, Ura^{+}	This study
MU458 to MU461	*r3b2::pyrG, carRP::(leuA + r3b2*)*	Leu^{+}, Ura^{+}	This study
MU464	*mcclasp (84675)::pyrG, leuA*$^{-}$	Leu^{-}, Ura^{+}	This study
MU465	*mcmyo5(51513)::pyrG (heterokaryon), leuA*$^{-}$	Leu^{-}, Ura^{+}	This study

Table 3. *Mucor circinelloides* strains used in this work. *r3b2** is a mutant allele of *r3b2* gene containing mutations at its catalytic RNase III-like domain obtained by site-directed mutagenesis.

Plasmids	Characteristics	References
pGEM-T Easy	Amp^R, used for TA cloning	Promega
pBluescript II SK+/- (pBS)	Amp^R	Stratagene
pLEU4	Amp^R, *leuA*	(Roncero et al., 1989)
pEPM1	Amp^R, *pyrG*	(Benito et al., 1992)
pPATA5	Amp^R, *pyrG*	Dr. Silvia Calo, Duke University
pMAT1253	Amp^R, *leuA, carB* inverted repeat	(Calo et al., 2012)
pMAT1279	Amp^R, *carB, leuA* (1,5 kb fragment of *carB* gene)	(Calo et al., 2012)
pMAT761	Amp^R, gene ID110239 (2,5 kb) cloned in pGEM-T Easy	This study
pMAT762	Amp^R, gene ID 110239 (2,5 kb) sub-cloned in pBS	This study
pMAT763	Amp^R, gene 110239::*pyrG* (disruption of gene ID 110239)	This study
pMAT765	Amp^R, gene ID 77996 (2,5kb)	This study
pMAT766	Amp^R, gene 77996::*pyrG* (disruption of gene ID 77996)	This study
pMAT767	Amp^R, gene ID 136157 (3,4kb)	This study
pMAT768	Amp^R, gene 136157::*pyrG* (disruption of gene ID 136157)	This study
pMAT770	Amp^R, gene 77996::*pyrG* (2kb) (disruption of gene ID 77996)	This study
pMAT771	Amp^R, *leuA*, *carB* inverted repeat, *r3b2* ^{wt} (for complementation experiments)	This study
pMAT772	Amp^R, *leuA*, *carB* inverted repeat, *r3b2** (for complementation experiments)	This study

Plasmids	Characteristics	References
pMAT1476	Amp^R, *leuA* flanked by *carRP* adjacent regions	(Rodriguez-Frometa et al., 2013)
pMAT787	Amp^R, *carRP:: leuA+r3b2^{wt}* (for integrative complementation experiments)	This study
pMAT788	Amp^R, *carRP:: leuA+r3b2** (for integrative complementation experiments)	This study
pMAT1812	Amp^R, *leuA, carB*	This laboratory
pMAT798	Amp^R, *leuA, carB*, 0,3 kb fragment of gene 166338 (for silencing experiments)	This study
pMAT822	Amp^R, *leuA, carB*, 0,8 kb fragment of gene 119711 (for silencing experiments)	This study
pMAT823	Amp^R, *leuA, carB*, 1 kb of gene 84675_v1.0 (for silencing experiments)	This study
pMAT824	Amp^R, *leuA, carB*, 0,8 kb fragment of gene 156742 (for silencing experiments)	This study
pMAT825	Amp^R, *leuA, carB*, 0,4 kb fragment of gene 145873 (for silencing experiments)	This study
pMAT828	Amp^R, *leuA, carB*, 2 kb of gene 51513 (for silencing experiments)	This study
pMAT831	Amp^R, *leuA, carB*, 1,2 kb of gene 111232 (for silencing experiments)	This study
pMAT832	Amp^R, *mcmyo5*::*pyrG* (2kb) for disruption of gene 51513	This study
pMAT833	Amp^R, *mcclasp*::*pyrG* (2kb) for disruption of gene 84675 (ver.1)	This study

Table 4. Plasmids used in this work. *r3b2** is a mutant allele of *r3b2* gene containing mutations at its catalytic RNase III-like domain obtained by site-directed mutagenesis.

II.2. Media and growth conditions

II.2.1. *Escherichia coli*

E. coli was grown at 37°C with shaking (250 rpm) in Luria Broth medium (LB) (Miller, 1972). The medium was adjusted to pH 7,2~7,4 and sterilized by autoclaving before use. For preparing solid media, 15 g/l agar was added. When necessary, the antibiotic ampicillin was added after autoclaving at a final concentration of 100 µg/ml.

II.2.2. *Mucor circinelloides*

The fungus *M. circinelloides* was cultivated at 26°C under continuous light. The media for growing this fungus include minimal media YNB (Lasker and Borgia, 1980) and MMC (Nicolás et al., 2007) and rich media YPG (Bartnicki-Garcia and Nickerson, 1962) and YPD (Difco). When necessary, after autoclaving, YNB minimal medium was supplemented with leucine (20 µg/ml) and YNB, MMC, YPG media with uridine (0,2 mg/ml). In transformation experiments, sorbitol was added to a final concentration of 0,5 M to prevent that osmotic pressure difference would make protoplasts busted. In all cases, agar solid media was autoclaved separately to prevent the hydrolysis of agar. The pH was adjusted to 4,5 for normal mycelial growth and 2,8 to 3,2 for colony growth. Spores of different strains were stored in sterile distilled water at 4°C for daily use, and at -20°C for storing permanently.

II.3. Buffers and reagents

a) Nucleic acids isolation from *M. circinelloides*

Genomic DNA isolation:

Lysis buffer

- Tris-HCl pH 8,0 — 200 mM
- EDTA pH 8,0 — 100 mM
- SDS — 1 %

RNA isolation:

TRI reagent solution (Sigma)

b) Plasmid isolation from *E. coli*

STET buffer

Sucrose	8%
Triton X-100	0,5%
EDTA pH 8,0	50 mM
Tris-HCl pH 8,0	50 mM

c) DNA manipulation

TE

• Tris-HCl (pH 8,0)	10 mM
• EDTA (pH 8,0)	1 mM

Sodium acetate pH 5,0

CH_3COONa	3 M

50x TAE

• Tris	2 M
• Acetic acid	5,71 %
• EDTA	0,05 M

10x loading buffer (for electrophoresis)

• Bromophenol blue	0,25 %
• Sucrose	40 %

d) RNA manipulation

MOPS buffer

• MOPS pH 7,0	20 mM
• Sodium acetate	5 mM
• EDTA	1 mM

Ribonuclease buffer

• Tris-HCl pH 7,5	20 mM
• NaCl	60 mM
• EDTA pH 8,0	5 mM

Alkaline buffer

- $NaHCO_3$ (sodium bicarbonate) 80 mM
- Na_2CO_3 (sodium carbonate) 120 mM

The buffers used in the experiments with RNA were prepared using diethyl pyrocarbonate (DEPC)-treated water 0,1%. DEPC-treated water 0,1% was obtained by mixing water and DEPC and incubating at room temperature for at least 1 hour to destroy the ribonucleases. DEPC was subsequently removed by autoclaving for 20 minutes.

e) Polyacrylamide gel electrophoresis

2x Formamide loading buffer

- Formamide 95 %
- Bromophenol blue 0,1 %
- Xylene cyanol 0,1 %
- EDTA pH 8 5 mM

10x TBE

- Tris base 0,9 M
- Boric acid 0,9 M
- EDTA 20 mM

f) Transformation of *M. circinelloides*

Phosphate sorbitol buffer (PS)

- Sorbitol 0,5 M
- Sodium phosphate buffer (NaH_2PO_4-Na_2HPO_4) pH 6,5 10 mM

Sorbitol solution 0,5 M

YPGS pH 4,5

YPG liquid medium supplemented with 0,5 M sorbitol.

YNBS pH 4,5

YNB liquid medium supplemented with 0,5 M sorbitol.

g) Transferring nucleic acid to membranes

NaOH (for DNA transferring) 0,4 N

20x SSC pH 7,0 (for RNA transferring)

- NaCl 3 M
- Sodium citrate 300 mM

h) Hybridization buffers

Buffers for DNA and mRNA detection

Prehybridization buffer

- NaCl 0,9 M
- SDS 1 %

Hybridization buffer

This buffer is obtained by supplying 0,1 g/ml of dextran sulfate to the prehybridization solution.

As a blocking agent, denatured salmon sperm DNA was added to those buffers at a final concentration of 50 µg/ml.

50x Denhardt´s solution

- Bovine serum albumin (BSA) 1 % (w/v)
- Ficoll 400 1 % (w/v)
- Polyvinylpyrollidone (PVP) 1 % (w/v)

Buffers for small RNA detection

Buffers for prehybridization/ hybridization with formamide

- Formamide 40 %
- Denhardt´s 1x
- SDS 7 %
- Phosphate buffer pH 7 0,05 M
- NaCl 0,3 M

The denatured salmon sperm DNA was added to this buffer at a final concentration of 100 μg/ml.

h) Buffers for washing membranes

Buffer 1: 2x SSC; 0,1% SDS

Buffer 2: 1x SSC; 0,1% SDS

Buffer 3: 0,1x SSC; 0,1% SDS

Buffer 4: 0,1% SDS (for cleaning membranes before hybridization with a new probe).

II.4. Transformation of *E. coli*

The heat shock method (Green and Sambrook, 2012) was used for transformation of *E. coli*. Competent DH5α cells were obtained by calcium chloride procedure (Green and Sambrook, 2012). These cells were slowly defrosted, mixed with DNA and incubated in ice for 20 minutes. The heat shock was performed by incubating cell mixtures at 42°C for 50 seconds, and then chilling them immediately in ice for 2 minutes. After transformation, 1 ml of LB liquid medium was added and cells were incubated at 37°C for 1 hour before plating them in LB solid medium containing suitable antibiotic compounds.

II.5. Transformation of *M. circinelloides*

The transformation was performed by electroporation of protoplasts (Gutierrez et al., 2011), which were generated essentially following the protocol described by van Heeswijck and Roncero (1984). Protoplasts were obtained from germinated spores by removing cell wall, which allows the incorporation of exogenous DNA into the protoplast, in this case by electroporation.

Fresh spores of the recipient strain were harvested and stored in sterile distilled water at 4°C. The spore concentration was calculated by using a 0,1 mm counting chamber (Hirschmann EM Techcolor). Spores were inoculated into 25 ml of YPG liquid medium pH 4,5 at 10^7 spores/ml. This culture was supplied, when required, with 0,2 mg/ml of uridine. Cultures were incubated overnight at 4°C

without shaking. Then, they were incubated at 26°C in 500ml-flask, covered by aluminum foil to avoid light, with vigorous shaking (250 rpm) for a period of 3 to 4 hours, until most of spores' germ tube length becomes about four times the swollen spore diameter.

Then the spores were precipitated by centrifugation for 5 minutes at 1000 rpm, washed twice in phosphate-sorbitol buffer, and finally resuspended in the same buffer at 5×10^7 spores/ml. For digestion of the cell walls, two digestive enzymes were added: 1 mg/ml of a commercial preparation of lytic enzymes rich in chitinase (Lysing Enzymes from *Trichoderma harzianum*; Sigma); and 0,15 mg/ml of commercial chitosanase (Chitosanase-RD, US Biologicals). The germinated spores were incubated at 30°C with gentle shaking (60 rpm) for 90 minutes. To stop the digestion, protoplasts were washed twice with 5 ml of cold 0,5 M sorbitol, centrifuging for 5 minutes at 1000 rpm. Finally, the protoplasts were resuspended in a final volume of 800 µl of cold 0,5 M sorbitol and kept in ice.

For transformation, 10 µl of DNA in double distilled water (1 µg/µl of circular DNA or 3 µg/µl of linear DNA) were mixed with 200 µl of protoplasts, and transferred to a precooled electroporation cuvette of 2 mm. The electrical pulses were conducted in the electroporator Bio-Rad GenePulser XCell following electroporation parameters: 800 V; 25 µF capacitance and a constant resistance of 400 Ω. After applying the electric pulse, 1 ml of cold YPGS pH 4,5 was immediately added and transferred to a clean 2 ml eppendorf tube. The transformation mixtures were incubated for 1 hour at 26°C with shaking at 150 rpm to allow recovery of the protoplasts. Subsequently, protoplasts were collected by centrifugation for 5 minutes at 800 rpm and resuspended in 600 µl of YNBS pH 4,5. This solution was carefully inoculated in appropriate medium for selection of transformants.

II.6. Integration of exogenous DNA into the genome of *M. circinelloides*

Integrative transformation was performed in *M. circinelloides* using linearized DNA in the transformation protocol described above. Transformed protoplasts were plated on MMC solid medium pH 3,2 with 0,5 M sorbitol. To identify transformants that had integrated the exogenous DNA harboring *pyrG* gene as selectable marker, the proportion of Ura^+ spores was determined after three cycles

of growth in selective medium. For this, the number of colonies growing in selective (MMC pH 3,2) and non-selective (MMC pH 3,2 with uridine) media was compared. Transformants with the higher percentage of Ura^+ spores were selected as putative carriers of the integrated DNA. Up to 5 or 6 cycles of vegetative growth in selective medium were performed to ensure the integration of the foreign DNA in all nuclei (homokaryons).

For integration into the *carRP* gene, the *leuA* gene was used as selective marker (in the generation of *r3b2* strains for integrative complementation experiments). Therefore, the selective and non-selective media were YNB pH 3,2 and YNB pH 3,2 with leucine, respectively. Besides the albino phenotype selection, Leu^+ nuclei proportion was determined like above.

II.7. DNA manipulation

II.7.1. *M. circinelloides* DNA isolation

The DNA of *M. circinelloides* was isolated basically following the protocol described by van Heeswijck and Roncero (1984), with slight modifications (de Haro, 2010). Genomic DNA was extracted from mycelia grown in liquid or solid medium at pH 4,5.

An amount of 200 mg of fungal mycelia was collected to isolate genomic DNA. The mycelium was grinded to fine pounder with liquid nitrogen to destroy the cell structures. Then it was resuspended in 800 µl of lysis buffer and mixed vigorously. To destroy protein molecules, 30 µl of proteinase K in TE buffer (2 mg/ml) was added and the reaction was incubated for 1 hour at 56°C. To remove RNA molecules, 30 µl of RNase A (10 mg/ml) was added and the mixture was incubated 10 minutes at 37° C. To purify DNA and remove protein, the mixture was mixed with a volume of saturated phenol equilibrated with 0,1 M Tris-HCl pH 8,0 and centrifuged to collect the aqueous phase. Cleaning steps were continued several times with ½ volume of saturated phenol equilibrated with 0,1 M Tris-HCl pH 8,0 and ½ volume of a 24:1 chloroform:isoamyl alcohol solution, until the surface between two phases become clean. To remove phenol, a volume of 24:1 chloroform:isoamyl alcohol solution was added, mixed and removed by centrifugation at 12000 rpm for 5 minutes. To precipitate DNA, a volume of

isopropanol and 0,1 volume of 3 M AcNa, pH 5,2 were added and then incubated at -20°C for 30 minutes. The mixture was centrifuged at 12000 rpm for 10 minutes and the DNA pellet was washed with 1 ml of 75% ethanol. The dried DNA pellet was dissolve in 50 µl of sterile double distilled H_2O and stored at -20°C.

II.7.2. Plasmid DNA isolation

Plasmid DNA from *E. coli* was routinely isolated by the rapid boiling method (Holmes and Quigley, 1981). However, plasmids obtained by this method do not have the required purity for sequencing, PCR, transformation of *M. circinelloides*, etc. When highly pure plasmid preparations were required, they were isolated by commercial plasmid purification columns (GeneJET Plasmid Miniprep Kit, Thermo Scientific; or StrataPrep Plasmid Miniprep Kit, Agilent Technologies).

II.7.3. Treatment of DNA with enzymes

The most common enzymatic reactions used in this study included:

i) **Digestion** of DNA to generate linear vectors, to check plasmid size, orientation of inserts, etc. These reactions were performed with restriction enzymes (Fermentas or Amersham Biosciences), following the provider's instructions.

ii) **Dephosphorylation** with shrimp alkaline phosphatase enzyme (Fermentas) to remove 5' phosphate group and prevent vector self-ligation. All treatments were performed according to the supplier's specifications.

iii) **Ligation** of DNA vectors and inserts. Ligation reactions were carried out in small volumes (10~20 µl) with ligation buffer and a unit of T4 DNA ligase enzyme (Fermentas). The ligation mixtures were incubated at 22°C for a minimum of 4 hours. In general, the molar ratio of vector:insert was 1:3 or 1:10. When it was required, the enzymes were inactivated by heat (70°C, 5 minutes), as specified by the provider.

II.7.4. Electrophoresis techniques

In this study, electrophoresis was applied to characterize plasmids, to separate different size DNA fragments, to check PCR products, etc. DNA was electrophoresed on horizontal agarose gel using 1x TAE buffer. The agarose concentration varied between 0,7% and 1,5% depending on the size of fragments to be separated. To visualize the DNA fragments under ultraviolet light, ethidium bromide was added to the gel to a final concentration of 0,5 μg/ml. After separation by electrophoresis, if necessary, DNA fragments were purified using GeneJET Gel Extraction Kit (Thermo Scientific) according to the supplier's instructions. The concentration and size of the DNA fragments were calculated using the linear reference markers λ DNA/HindIII (Fermentas) and GeneRuler DNA Ladder Mix (Fermentas), respectively.

II.7.5. Polymerase Chain Reaction (PCR), primers and fusion PCR

Polymerase Chain Reaction (PCR) is a technique to amplify nucleic acid fragments limited by a primer pair. The DNA amplification process was carried out using 20 pmol of each oligonucleotide (60 pmol in the case of degenerated primers) and Herculase II Fusion DNA Polymerase (Agilent Technologies), Taq DNA polymerase (Sigma-Aldrich) or BIOTAQ DNA Polymerase (Bioline), following the recommendations of the suppliers. The samples were subjected to a cycle of 5 min at 95°C and 30~35 cycles of denaturalization (30 sec at 95°C), alignment (30 sec at the Tm of the primers) and polymerization (1 minute per kb of amplified product at 72°C) (de Haro, 2010). The sequences of the primers used in PCR experiments are shown in **Table 5**.

Fusion PCR, or overlap PCR, is a technique used in this study to generate the constructions used for gene replacement without restriction enzyme reactions. In this method, the upstream and downstream fragments (about 1kb per each) of the target genes were amplified using primers containing a complementary tail to the gene marker *pyrG* (**Figure 17**).

Loci	Name	Sequence (5' - 3')[1]
General	**PU**	GTTGTAAAACGACGGCCAGT
	PUR	CAGGAAACAGCTATGAC
	PEUKASalI	TCCCCAAGTCGACTTGGGCCCAAGCTTTCAAATG
	peuka-1	CATGAAGTGTGAGACATTGCG
pyrG	**pyrG-R2**	ATCCCACCAGAAGGAGTACATGG
	pyrG-F2	GGCAAGTAACACCACATTCAGAGC
	pyrG10	GGCAGAAGGGAGGAGGCACACGC
	pyrGZ	GGCATTGGGATGCTGTTGTC
	F-pyrG	TGCCTCAGCATTGGTACTTG
	R-pyrG	GTACACTGGCCATGCTATCG
leuA	**leuA P1**	GATGTAGTTAGAGTATTTCGC
	leuA P2	GTACATTCTGGTCAACTCG
	LeuAFowSalI	AAGAATGTCGACATACTCTAACTACATCAAATGC
carB	**carbsal-1**	TTCGTCGACAGCGAACTCGGTGTACTGCAAC
	carB-7	GCTGGGAGGATCCCACAGCACCTGAAGCACATCATG
carRP	**carRP-F1**	TAATCGCATGCCCGGGCGCATTGTAGATAAACTCG
	carRP-R1	TCGCTGGTACCCGGGCATGTGTAACAGTGCATTGG
	carRP-R2	AGGACCTGCAGCCATATTGAGTCATCCTGC
136157	**F1**	ACATCCATTTGTTTACAGCAGCAAAG
	F2	GTAACATGCACTCAGAAGCACATGGCGTCA
	F3	ATCTGCAGAGATCTCCGAGGACTTTGTCAGAAATCTCCAGCA
	R1	GGAACCACTCACTAAAACCTCCTA
	R2	ACATGCTGAGCCTGATGTTTAGAAAGCACGA
	R3	ATCTGCAGAGATCTTTCTCCGTGTATAGAAACACCACTGGCAAG
110239	**F4**	CAGTTTCTGGATAGTGGAAGCAGCAG
	F5	GGGTAACGAGATGATACAATACTGGCAGGA

Loci	Name	Sequence (5' - 3')[1]
77996	**F6**	TAGGATCCATGAGGTCACGAACATGTACAATGCATC
	R4	ATACATTGGCATCCTCCACATCCGA
	R5	GATAATCCAGCCATGTATTCCTGGTAGCTC
	R6	AAGGATCCAATCAAGGTGCAGGAACCCAAGCGTCA
	F7	TGCTTGTGACTCATATGTGTGCTG
	F8	CCTGTAGGTGAGGAACGCTGTATCGCTT
	F9-pyrG	CGATAGCATGGCCAGTGTACAAATGACGCTCAACATCTCGCATTCGACA
	R7	TGCTCTTTGCTGATGATTCTCCAG
	R8	GTCCAAGGCAGCTTCCTCGTTGTAGAC
	R9-pyrG	CAAGTACCAATGCTGAGGCAAACTGTCTTCGGCCTTGTTGGTGCTG
80729 (*r3b2*)	**F11**	GGGGGCTCGAGTTGCTGAGGGAACATTGGACCTGGATGAGC
	R11	GGGGGCTCGAGCGTACTACTGCAAAACATAGCCTGAGCGGG
	MutFow	GAG**GC**CAAGTTCAACTACATTG**C**AG**C**GTCTGCAGTGC
	MutRev	AGAC**G**CT**G**CAATGTAGTTGAACTTG**GC**CTCTGCCACCTC
51513	**FYL1**	TCGCGGCCGCACCACGGTGAAAGCGCTGTTGGAG
	RYL1	CTCTCGAGCTTCAGGAGTAGCACAAGCTGTTCAAG
	FYL1U	AAGCCGACGAGCCTGTGGCAGATG
	RYL1D	CTCACCATCCTCACATTCAACGAAACAAGG
	FYL1N	GTGCTTGGATTGAACCCGCTGCCCTT
	RYL1N	GGCATTGGAAGAGCAACTAGCTTTTGGAG
	RYL1-pyrG	CAAGTACCAATGCTGAGGCAGACCATCTTACACATCCAAGTGCCTGA
	FYL1-pyrG	CGATAGCATGGCCAGTGTACGACACCCAAGCCTCGTCTTCGTCTT
166 338	**FYL1.2**	TAGCGGCCGCAGCATTCTCGTTAATGGCATAAGCAATGGG

Loci	Name	Sequence (5' - 3')[1]
	RYL1.2	ATCTCGAGGATGATCAATTGGTACATCTCACGTCAAAG
111232	**FYL2**	AAGCGGCCGCAAGCCCTACCTGGAAACATCTGTGCTAAG
	RYL2	CGAAACGATGCTCGTACCATGGAGTTC
119711	**F.YL8**	TAGCGGCCGCATCCCAAACTCACTAAAGACGTTCAGACT
	R.YL8	GGCTCGAGTTATCAGCTTGAGATCGGCCCCATGAT
84675	**FYL10.1**	ATGCGGCCGCCAAAGATGAATCCACAGACGTAGATCCTGT
	RYL10.1	GTGTTCCTGCTGCATCTGAGACGAG
	FYL10U	TACCGACGGGCCATGCCTTTGAG
	RYL10D	GACGAGGATCTTTCTTCTGCCCAGC
	FYL10	ATCCCTTGCGCGAACCATTGTCTCACG
	RYL10	TTGATGGGGTGAAAGAGAGGTGGAGATG
	RYL10-pyrG	CAAGTACCAATGCTGAGGCAGTGTGTTGGTACCTGAAGGGTGCCT
	FYL10-pyrG	CGATAGCATGGCCAGTGTACGCCTTGGTCGCCTTTCACGAAGTTC
156742	**FYL10.2**	TTGCGGCCGCTCCAGCTATGAGCAAGACTTTACATCCATC
	RYL10.2	TTCTCGAGCCATGCCTTTGAGCGTCTTAGATGCC
145873	**FYL10.3**	ATGCGGCCGCCGTCATTAGCGTCCTTGATACCTTCTTCAG
	RYL10.3	ATCTCGAGCACAGTGGAACTCAGTGATAAACACACTG

Table 5. Primers used in this study. [1]The sequences marked in red or green color indicate the restriction sites used for cloning. The underlined sequences correspond to *pyrG* sequences used for fusion PCR reactions. The bold and underlined nucleotides indicate changes relative to the wild type sequence.

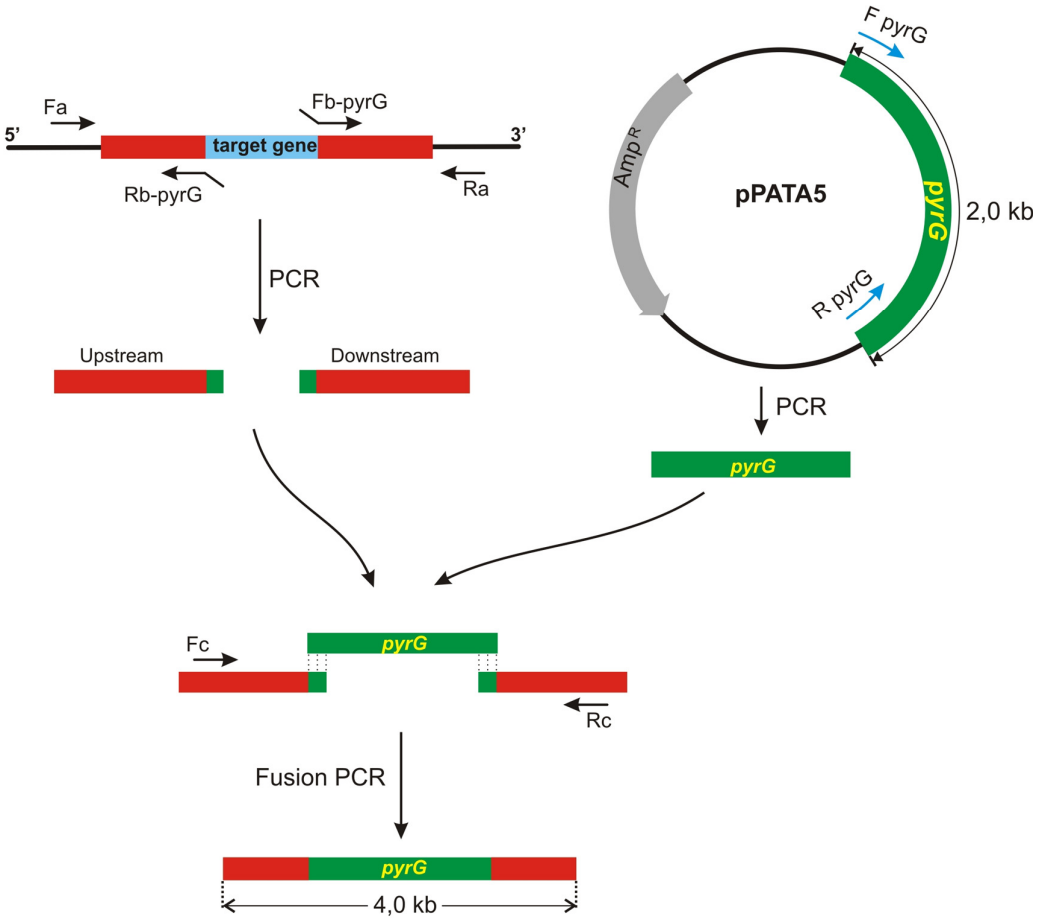

Figure 17. Fusion PCR to generate the gene replacement fragments. The selective marker *pyrG* gene with 2 kb in length was fused with upstream and downstream fragments of the target gene (around 1 kb per each) by overlap PCR. Subsequently, the fusion fragment can be cloned into pGEMT-easy vector.

The *pyrG* marker gene was amplified using the primer pair F-pyrG and R-pyrG (**Table 5**). The upstream and downstream fragments were amplified by two primer pairs Fa/Rb-pyrG and Fb-pyrG/Ra, respectively (**Figure 17**). In a second PCR, templates were added in a ratio of 1:3:1 upstream:marker:downstream. The PCR program was used with several modification to reduce the rate of temperature changing (Mastercycler® personal, Eppendorf): 3 min at 95°C, 10 cycles of denaturation (30s at 95°C), 1 sec at 70°C, alignment (30s at 55°C, ramp down 0,3°C/s) and polymerization (1 minute per kb of amplified product at 68°C, ramp up 0,3°C/s). Then 25 cycles of denaturation (30s at 95°C), 1 sec at 70°C, alignment (30s at 55°C, ramp down 0,3°C/s) and polymerization (2 minutes for 4kb products, at 68°C, ramp up 0,3°C/s, +10s). The fusion PCR products were purified from gel and cloned into pGEMT-easy vectors by TA cloning method.

II.7.6. Southern blots

II.7.6.1. Radioactive labeling of DNA fragments

Gene replacement techniques used in *M. circinelloides* usually generate transformant colonies containing different kinds of nuclei (wild-type and mutant), called heterokaryons. To increase the proportion of transformed (mutant) nuclei, those transformants must be grown in selective medium for several vegetative cycles. Southern blot hybridization was used to confirm the homokaryon state of the transformants. The DNA used as a probe in Southern hybridization experiments was labeled introducing dCTP radioactively labeled with phosphor 32 (^{32}P) in the position α (Easytides® Deoxycitydine 5'-triphosphate, [α-^{32}P], Perkin Elmer) (Feinberg and Vogelstein, 1983, 1984). A volume of 6 µl of solution containing 50 ng of DNA probe, 1 ng of DNA ladder and 25 ng of random hexanucleotides was denatured by incubating at 95°C for 5 minutes, and then chilled in ice immediately for 5 minutes. For labeling reaction, a nucleotide mix (3,3 mM per each, without dCTP), 20 uCi of dCTP ^{32}P and 0,1 U/µl of Klenow enzyme in appropriate buffer (Thermo Scientific) was added to the denatured DNA probe. This mixture was incubated at 37°C for 1 h for complete labeling. A more simple method of DNA labeling was performed using the Ready-To-Go^{TM} DNA Labeling Beads kit (dCTP) (Amersham) following the supplier's instructions. To stop the labeling reactions and remove unincorporated nucleotides, 50 µl of the reaction was passed through a column of Sephadex G-50 Fine DNA Grade (Amersham Pharmacia). The purified labeled probe was denatured by heating before hybridization steps.

II.7.6.2. DNA hybridization

One microgram of genomic DNA was digested with appropriate restriction enzymes and separated by agarose gel electrophoresis. To denature DNA molecules, the gel was incubated for 20-25 minutes in a solution of 0,4 N hydrochloric acid after electrophoresis, washed with double distilled water and incubated for 20-25 minutes in a 0,4 N NaOH solution. Finally, DNA was transferred to a nylon membrane (Hybond-N^{+}, Amersham Biosciences) by capillarity transferring with 0,4 N NaOH solution for at least 2 hours (Green and Sambrook, 2012). Once transferred, the filter was dried at room temperature. Hybridization method includes two steps:

prehybridization and hybridization, using the appropriate buffers (see Section II.3) supplemented with denatured salmon sperm DNA (final concentration of 0,1 mg/ml). Both steps were performed at 65°C, the first one for at least 2h, and the second one hybridizing with labeled DNA probes overnight.

After hybridization, the membranes were washed to remove the unincorporated probes with the following conditions: 20 min at 65°C with 2x SSC; 0,1% SDS; 20 minutes at 65°C with 1x SSC, 0,1 % SDS; 20 minutes at 65°C with 0,5x SSC, 0,1% SDS and 20 minutes at 65°C with 0,1x SSC, 0,1% SDS (de Haro, 2010). These washing steps are not fixed, since they depend on the signals strength.

II.7.7. DNA sequencing

PCR products or plasmids carrying various DNA fragments were purified with columns GeneJET PCR Purification Kit or GeneJET Plasmid Miniprep Kit (Thermo Scientific), respectively. The sequencing was carried out by the Molecular Biology Service (SACE-CAID), at the University of Murcia.

II.8. RNA Manipulation

II.8.1. Isolation of total RNA from *M. circinelloides*

Total RNA was isolated from *M. circinelloides* using monophasic lysis reagent described by Green and Sambrook (2012) (Trizol method) with a few modifications. In brief, an amount of 150 mg of *M. circinelloides* mycelium was collected, freeze and grinded as fine powder in liquid nitrogen. These powder was quickly mixed with 1,5 ml of Tri-reagent (Sigma) in a cold 50 ml tube. The mixture was transferred to a 2 ml eppendorf tube and centrifuged at 10000 rpm, 4°C for 10 minutes. The supernatant was collected and incubated at room temperature for 5 minutes. Three hundred microliters of chloroform was added to the solution and mixed for 15 seconds, then incubated at room temperature for five minutes. After centrifugation at 10000 rpm, during 15 minutes at 4ºC, the aqueous phase which contains the RNAs was collected. RNAs were precipitated adding a volume of isopropanol and incubating 10 minutes in ice. After centrifugation as above, the aqueous phase was discarded and the RNA pellet washed in 75% ethanol and dried

on the bench during 10 minutes at room temperature. The RNA pellet was resuspended in DEPC-treated H_2O. RNA concentration was quantified using a biophotometer (Eppendorf).

When higher quality was required, RNA samples were purified using Direct-zol™ RNA MiniPrep (Zymo Research), which directly purifies RNAs from the Tri-reagent mixtures, following the instructions of the supplier.

II.8.2. Isolation of low molecular weight RNA from *M. circinelloides*

The protocol for extraction of short RNAs is similar to the one for isolating total RNAs with some modified and extended steps as bellow (Nicolás et al., 2003).

At the step of precipitation of RNAs with isopropanol, it was incubated at -20°C during 2 h. And then, after the washing and drying steps, total RNA pellet was resuspended in 300 µl DEPC-treated H_2O. For the separation of short RNAs, 40 µl of 50% PEG8000 and 50 µl of 4M NaCl were added, and after mixing and incubating in ice for 30 minutes, the solution was centrifuged at 10000 rpm at 4°C for 10 minutes to collect the aqueous phase, which contains the low molecular weight RNAs. The small RNAs were precipitated using 3 volume of 100% ethanol. This solution was incubated at -20°C overnight. The RNA pellet was collected by centrifugation at 10000 rpm for 10 minutes at 4ºC, then washed with 80% ethanol, dried on the bench during 10 minutes and resuspended in 15-20 µl of DEPC-treated H_2O. All RNA samples were stored frozen at -80°C.

II.8.3. Hybridization of total RNA

For Northern blot hybridization, total RNA must be separated in an agarose gel containing formaldehyde. RNA samples were prepared in a total volume of 25 µl containing 30-50 µg of RNA; 2,5 µl of 10x MOPS; 4,4 µl of formaldehyde and 12,5 µl of formamide. The mixture was heated at 65°C for 10 minutes to remove RNA secondary structures and then chilled for 5 minutes on ice. After adding 2,5 µl of loading buffer, samples were loaded onto a 1,2% agarose gel containing 2,2 M formaldehyde and electrophoresed in 1x MOPS buffer. After electrophoresis, the gel was washed for 30 minutes in water to remove formaldehyde and capillarity

transferred overnight to positively charged nylon membrane (Hybond-N^+, Amersham Biosciences) using 20x SSC buffer. After transferring, cross-linking was carried out to fix RNA molecules to the membrane by ultraviolet light (120000 µJ/cm^2) using a UV-Crosslinker (Hoefer). The DNA fragments used as probes in Northern experiments (P1 to P3), which correspond to the reporter genes of the *rdrp*-dependent pathway, were PCR-amplified by specific primers (**Table 6**). These probes were labeled as the DNA probes used for Southern blot experiments (Section II.7.6.1), but without DNA ladder. RNA hybridization with labeled probes was performed exactly as in the case of hybridization of DNA membranes (see Section II.7.6.2).

Name	Sequence (5'-3')	Use[1]
P1 forward	AATGCCAACGAATTGAACGCCTCTTATGCT	Primer for DNA probe for mRNA from gene ID 155412
P1 reverse	ACGAGGCATGATGACTTCGATAAAGTGC	Primer for DNA probe for mRNA from gene ID 155412
P2 forward	AGACCGAGATTCCCAACATTGCTGCCAT	Primer for DNA probe for mRNA from gene ID 164785
P2 reverse	CAAACTTGAGAACGCCTTGGTTTTCCAGAA	Primer for DNA probe for mRNA from gene ID 164785
P3 forward	ATGAGTACAGGATTCTCGAGCGCACA	Primer for DNA probe for mRNA from gene ID 156561
P3 reverse	CTCATCACACACTTAAATAGAGGAGGCAG	Primer for DNA probe for mRNA from gene ID 156561

Table 6. Oligonucleotides used in Northern blot experiments. [1] Primers for DNA probes for mRNA analysis amplified 1479 bp (P1), 761 bp (P2) and 309 bp (P3) fragments. These primers were also used to amplify sense and antisense-specific riboprobes for sRNA validations of the different loci. Those fragments were cloned, in different orientations relative to the T7 promoter, into pGEM-T easy (Promega).

II.8.4. Hybridization of low molecular weight RNA

Each RNA sample was prepared in a total volume of 7 µl containing 20-30 µg of low molecular weight RNA and 7 µl of 2x formamide loading buffer. The mixture was heated at 90°C for 30 seconds to remove RNA secondary structures and then chilled in ice for 5 minutes immediately. Samples were loaded onto a denaturing gel of 15% polyacrylamide (19 acrylamide: 1 bisacrylamide) containing 7 M urea and 0,5x TBE and electrophoresed in 0,5x TBE buffer. After electrophoresis,

RNA was transferred to a positively charged nylon membrane (Hybond-N^+, Amersham Biosciences) by electroblotting at 250 mA for 45 minutes (Semi-Dry Electroblotting Unit, Sigma), using 0,5x TBE as transferring buffer. RNA was fixed to the membrane by ultraviolet light (120000 $\mu J/cm^2$). The membrane was prehybridized during 2-3 hours and then hybridized with the labeled riboprobe overnight in the same prehybridization/hybridization buffer (Section II.3). Both prehybridization and hybridization steps were performed at 30°C. After hybridization, the membranes were washed three times at 50°C with 2x SSC solution containing 0,2% SDS for 20 minutes.

In order to increase the signal intensity, an alternative crosslinking protocol was used. The RNA was crosslinked to a non-charged membrane (Hybond-NX®, Amersham Biosciences) using l-ethyl-3-(3-dimethylaminopropyl) carbodiimide (EDC) (Sigma), which increases the sensitivity of sRNAs detection about 25-50 folds regarding UV fixation (Pall et al., 2007). Briefly, a 0,24 M EDC solution was prepared in 0,15 M 1-methylimidazole at pH 8,0. The membrane was placed on Whatmann paper saturated with this solution, wrapped with transparent film and incubated at 60°C for 1 to 2 hours. Finally, the membrane was washed with double distilled water to remove excessive EDC before the hybridization steps. Hybridization was carried out in ULTRAhyb®-Oligo buffer (Ambion) at 37ºC overnight. Membranes were washed as above except that the temperature was 37°C. In both protocols, an additional washing step was performed when the background signal was excessive. The membrane was incubated with 0,81 kunits/ml of bovine pancreatic ribonuclease A and 20 U/ml of ribonuclease T1 from *Aspergillus oryzae* in a volume of 20 ml of ribonuclease buffer at 37°C for 20 minutes. Finally, ribonucleases were removed by washing the membranes with 2x SSC and 0,1% SDS for 2 or 3 minutes at room temperature. Subsequently, the membranes were exposed to Kodak® Biomax MS film (high sensitivity) at -70°C, or to phosphorimager screens BAS-MP2040 (Fujifilm) that were scanned in the reader Molecular Imager FX system (Bio-Rad). The exposing time depended on the signal strength. The images were densitometry adjusted and densities were calculated using Quantity One application (Bio-Rad) or ImageJ (National Institutes of Health, NIH) softwares.

II.8.5. Radioactive synthesis of riboprobes

RNA probes used in hybridization experiments of low molecular weight RNA were labeled by introducing UTP nucleotide labeled with phosphorus-32 (Easytides® Uridine 5'-triphosphate, [α-32P], Perkin Elmer). RNA sense or antisense specific riboprobes were synthesized by *in vitro* transcription from linear plasmids carrying the appropriate fragments for each locus, using T7 MAXIscript® in vitro Transcription Kit (Ambion), following the supplier's recommendations.

After *in vitro* transcription, riboprobes were treated with RNase-free DNase to remove the DNA used as template for transcription. Subsequently, the labeled probes were cleaved into small molecules of about 50 nt to facilitate hybridization with the small RNA molecules. This process was performed by mixing 20 µl of riboprobe with 300 µl of alkaline buffer, incubating for 3 hours at 60°C and stopping the hydrolysis reaction with 20 µl of 3M sodium acetate pH 5,0. The solution was passed through a column of Sephadex G-50 Fine DNA Grade (GE Healhcare) to remove unincorporated nucleotides by centrifuging for 2 minutes at 2000 rpm.

II.9. Functional genomic analysis

II.9.1. Construction of RNAi-based genomic DNA libraries

A DNA library is a population of identical vectors each containing a different DNA insert. To construct a DNA library, the target DNA is digested with a restriction enzyme that generates various DNA fragments. Then cleaved DNA is ligated into a vector digested with the appropriate enzyme, generating a large collection of vectors with different DNA inserts (Watson et al., 2008). In this study, we constructed RNAi-based genomic libraries to investigate gene functions through the gene silencing mechanism. In order to produce RNAi-triggering dsRNA molecules from the inserted fragments, the vector pMAT1812 was constructed with two opposite promoters that flank the multi cloning site and a fragment of the *carB* gene. This vector was kindly provided by Sonia Reverte Ródenas (this laboratory). The *carB* gene fragment was used as a silencing marker (**Figure 18**). In theory, once this vector containing an inserted fragment is transformed into *Mucor* cells, it will generate sense and antisense transcripts of the fragment flanked by the two

promoters. The resulting dsRNAs will trigger the RNAi pathway to silence endogenous homologous sequences (Nicolás et al., 2003).

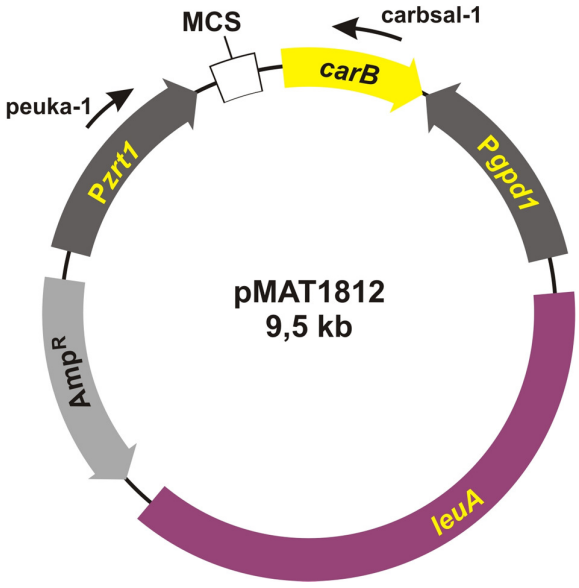

Figure 18. Structure of the silencing vector pMAT1812. Plasmid pMAT1812 contains two opposite promoters, P*zrt1* and P*gpd1* flanking a MCS region (multi cloning site) and a reporter gene *carB*. The *leuA* gene was used as a selective marker. The positions of the primers peuka-1 and carbsal-1, used to amply the cloned fragment, are indicated.

In order to generate the fragmented pool of genomic DNA (gDNA) , twenty microgram of gDNA extracted from wild type strain R7B was digested by three restriction enzymes *Nhe*I, *Spe*I and *Xba*I in 7 different combinations (*Nhe*I, *Spe*I, *Xba*I, *Nhe*I-*Spe*I, *Nhe*I-*Xba*I, *Spe*I-*Xba*I and *Nhe*I-*Spe*I-*Xba*I). Those enzymes were selected because they produce compatible sticky ends. Plasmid pMAT1812 (3 µg) was digested with the enzyme *Nhe*I. Linear plasmids were treated with Shrimp Alkaline Phosphatase (SAP, Thermo Scientific) to reduce the frequency of auto-ligation. The digested DNA fragments with the size range from 0,5 to 8 kb were purified from agarose gel by using GeneJET Gel Extraction Kit (Thermo Scientific) according to the instructions of the provider. The cleaved gDNA and linear plasmid were incubated for ligation and heat-shocked transformed into *E. coli* DH5α (see section II.4). The populations of *E. coli* transformants were grown on solid LB medium supplemented with ampicillin. The collection of *E. coli* transformants was directly used to extract the plasmidic DNA that contained the genomic library. It was extracted using commercial plasmid purification columns (GeneJET Plasmid Miniprep Kit, Thermo Scientific; or StrataPrep Plasmid Miniprep Kit, Agilent

Technologies) according to recommendation of the supplier. Then, the gDNA library was transformed into *M. circinelloides* R7B strain to start the screenings of new phenotypes triggered by the silencing of the gene fragments cloned in the library (**Figure 19**). This strategy to construct gDNA library was two-times repeated to obtain two different libraries, in order to increase representativeness.

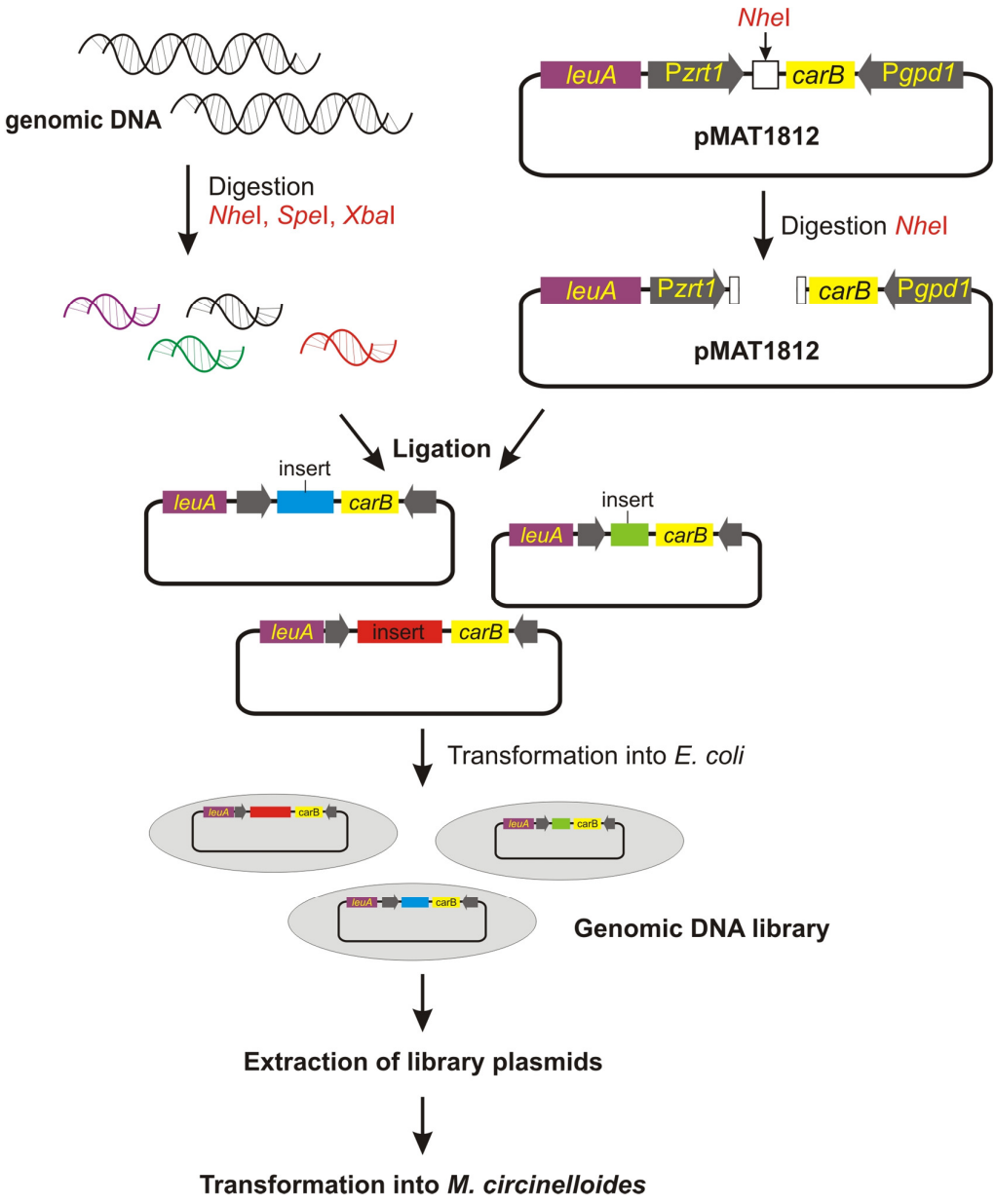

Figure 19. Genomic DNA library construction. Genomic DNA extracted from R7B strain was digested by *Nhe*I, *Spe*I and *Xba*I using 7 different combinations. These digested DNA fragments were cloned into pMAT1812 digested with *Nhe*I. The population of recombinant plasmids was transformed into *E. coli* DH5α. The obtained genomic libraries were used to transform *M. circinelloides* R7B strain.

II.9.2. Identification of candidate genes involved in *M. circinelloides* morphogenesis

The leucine auxotroph strain R7B was used as recipient strain for transformation with the RNAi-based genomic libraries (see section II.5). After transformation, spores of all transformants collected from the original plates were grown on YNB pH 2,8 solid medium. The low pH allowed screening up to 200 colonies per plate. In order to identify candidate genes that are involved in *Mucor* pathogenesis, we focused the screening in transformants with phenotypes such as increased or reduced growth rate, different sporulation efficiency, or any other morphological change that could affect the regular morphogenesis of *Mucor*. Once transformants with those phenotypes were isolated, we proceed to identify the DNA fragments that could be behind of the phenotypes observed. Total DNA (20 µg) from the transformants (gDNA and plasmidic DNA) was separated in agarose gel electrophoresis (see section II.7.4). In order to isolate the plasmidic DNA, an agarose gel piece was cut from right below the gDNA band to the 10 kb running position delimitated by the size marker (the size of the empty vector is 9,5 kb). The DNA purified from these gel pieces was used as template (250 ng) for PCR reactions with primer pair peuka-1 and carbsal-1 (**Table 5, Figure 18**). The PCR programs were applied with annealing temperature at 55°C and elongation at 72°C during 4 minutes, using Herculase II Fusion DNA Polymerase (Agilent Technologies) following the instructions of the provider. The PCR products containing the inserted fragments and a small piece of *carB* gene were purified from agarose gel using GeneJET Gel Extraction Kit (Thermo Scientific) according to the instructions of the supplier, and then sequenced. After removing the sequence of *carB* fragment, the remaining sequences were used for searching the candidate genes using the BLAST application that is available on the JGI server (http://genome.jgi-psf.org/pages/blast-query.jsf?db=Mucci2).

II.10. Phenotypic analyses

II.10.1. Quantification of the production of vegetative spores

For quantification of spore production of the different strains, small pieces of mycelium (1 mm diameter, n = 15) were pick up and transplanted to an appropriate

medium. After incubation at 26°C for 72 hours under continuous light or dark conditions, the diameter of each colony was measured to calculate its area. The colony was placed in an eppendorf tube with 1 ml of distilled water and stirred vigorously for 1 minute to ensure complete release of the spores. Finally, the spores were quantified with a 0,1 mm counting chamber (Hirschmann EM Techcolor). Spore production of each strain was calculated relative to the area of the colonies.

II.10.2. Determination of the growth rate

To measure growth rate of *M. circinelloides* strains, small pieces of mycelium (1 mm diameter, n = 15) were pick up and transplanted to an appropriate medium. The different strains to test were grown in the same solid plates to reduce variability of the growth conditions. They were incubated at 26°C under continuous light. The growth rate of each strain was calculated by measuring the diameter of colonies during three time periods: 24 h, 48 h and 72 h.

II.11. Sequence analyses

The genome sequence of *M. circinelloides* and its annotations are available at Joint Genome Institute (JGI, http://jgi.doe.gov/), which has provided a strong analytical tool for gene structures and functions. Computational sequence analysis was carried out using European Bioinformatics Institute Server softwares (EMBL Outstation, Hinxton, U.K., http://www.ebi.ac.uk/), the National Center for Biotechnology Information Server (NCBI, Bethesda, MD, USA, http://www.ncbi.nlm.nih.gov/) and ExPASy (http://www.expasy.org/).

For the analysis of endogenous sRNAs, raw reads were processed and normalized as previously described (Nicolás et al., 2010; Cervantes et al., 2013). sRNAs were mapped to annotated exons, transposons and intergenic regions of the *M. circinelloides* genome (http://genome.jgi-psf.org/Mucci1/Mucci1.home.html) (v 1.0) using PatMaN (Prufer et al., 2008). sRNA loci were said to be down-regulated in a given sample if the normalized locus abundance showed at least a fourfold decrease in comparison to the wild type sample ($\log_2$ fold change $\leq$ -2). This arbitrary fourfold difference was used as a cut-off to increase the stringency of the analysis. sRNAs were said to be bound to Ago-1 if the normalized abundance in the

Ago-1 fractions purified from the wild type strain showed at least a fourfold increase relative to the *ago-1*$^-$ sample ($\log_2$ fold change ≥ 2). To increase the stringency of the analysis and avoid lowly expressed regions, any loci with a normalized abundance count of less than 50 in the wild type were excluded from the analysis.

For finding homologous sequences of an specific protein, we used BLASTp program of NCBI (Altschul et al., 1997). Predictions of conserved domains were performed with the "InterProScan" (EMBL-EBI), "Conserve Domain Database" (NCBI) and "Pfam" (Sanger Institute) programs. The sequence comparison analyses were carried out using the program ClustalW2 EMBL-EBI (Larkin et al., 2007). The molecular weight and isoelectric point of the proteins were determined with the "Compute pI/Mw" (ExPASy) program (Wilkins et al., 1999). Phylogenetic analyses between different sequences were performed with ClustalW2 (EMBL-EBI) and MABL Phylogeny.fr server program (http://www.phylogeny.fr/).

II.12. Nucleotide sequence accession number

The accession numbers of the sRNAs cloned in the wild type and *rdrp-1*$^-$ and *rdrp-2*$^-$ mutants are GSM469403, GSM469406 and GSM469407, respectively; all accessions are under GEO accession GSE18958 (Nicolás et al., 2010). The raw reads of *M. circinelloides* Ago-1-bound small RNAs in wild type and *ago-1*$^-$ mutant are deposited in the Sequence Read Archive (SRA) database under the accession number SRR835448 (Cervantes et al., 2013). The raw reads of *M. circinelloides* small RNAs in the *r3b2*$^-$ mutant have been deposited in the SRA database under the accession number SRR1576768.

III. RESULTS. CHAPTER I

III.1. A new *rdrp*-dependent RNA degradation pathway in *M. circinelloides*

We have previously demonstrated the existence of different classes of endogenous siRNAs (esRNAs) in *M. circinelloides* produced with the involvement of a Dicer activity. The *ago-1*, *rdrp-1* and, at a minor extent, *rdrp-2* genes are also required, in different combinations, for the production of those esRNAs. Many of these esRNAs derive from exons (ex-siRNAs) and regulate the expression of the protein coding genes from which they are produced (Nicolás et al., 2010; Cervantes et al., 2013). Besides the mentioned *dicer*-dependent esRNAs, sequencing of the 18-25nt sRNA libraries identified 531 new loci that produced exon-derived esRNAs by a *dicer*-independent but *rdrp-1*- and/or *rdrp-2*-dependent mechanism (Trieu et al., 2015). The structural characteristics of those esRNAs suggested that they are more likely small degradation products of mRNAs that are produced by an RNase that preferentially cleaves mRNAs two nucleotides downstream of any uracil (see section I.2.4.5.2). This cleavage preference would produce fragments of various sizes resulting in the smears observed in the Northern blot analyses. However, when the distance between two uracils is 18-25 nucleotides, the cleavage products would be present in the sRNA library, as the libraries were generated from any 18-25-mer RNA molecules that can be ligated to adapters. In this study, we have confirmed these results by repeating the Northern blot experiments to detect those *dicer*-independent *rdrp*-dependent sRNAs. As previously demonstrated, these sRNAs were either not detectable or the probes detected a smear, but not discrete bands with sizes between 20-25nt.

In agreement with the non-canonical nature of the *rdrp*-dependent *dicer*-independent sRNAs, they do not show the strong bias for uracil at the 5' end shown by the canonical ex-siRNAs bound by *M. circinelloides* Ago-1 (**Figure 20**) (Nicolás et al., 2010; Cervantes et al., 2013). In fact, only eleven out of 531 sRNAs of the *rdrp*-dependent *dicer*-independent class were detected among those specifically bound to *M. circinelloides* Ago-1 (**Supplementary Table S1**), suggesting that this sRNA class does not act through the canonical RNAi pathway. According to the nature of the *rdrp*-dependent *dicer*-independent RNA class, which was identified through sequencing small RNAs but corresponds to non-random degradation products of mRNAs that can have any size and are generated by an *rdrp*-dependent

mechanism, we named those RNA molecules as ***r**drp*-dependent **d**egraded RNA (**rdRNA**).

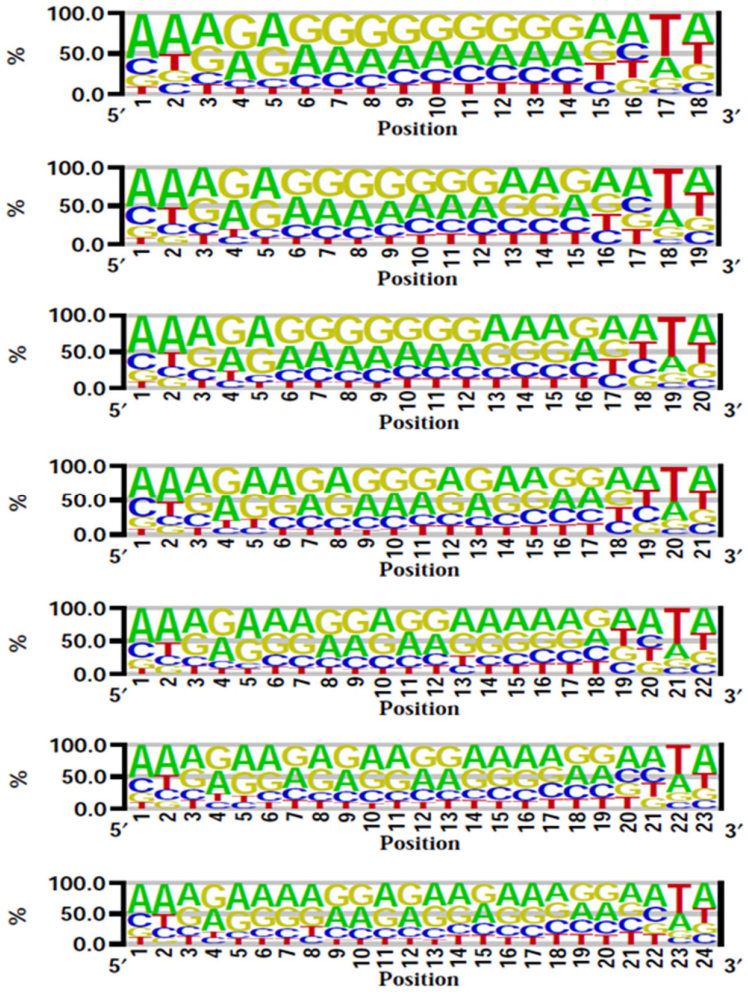

Figure 20. Sequence logo of *rdrp*-dependent *dicer*-independent sRNAs. The frequency of each of the four bases was calculated in *rdrp*-dependent *dicer*-independent exonic sRNAs. The result is shown for separate sizes of 18-24 nt. The numbers on the x-axis refer to the position in the sRNAs and the y-axis shows the percentage distribution. The top to bottom order of bases in each position is determined by their frequency (highest on top). The figure shows that uracil (T in the cDNA sequences) is under-represented in the most 5' position and highly enriched at the penultimate position.

III.2. The *rdrp*-dependent *dicer*-independent RNA degradation pathway regulates gene expression

Although previous results indicated that the *rdrp*-dependent *dicer*-independent rdRNAs are not "classical sRNAs" (i.e. they are not 20-24-mer RNA molecules generated by *dicer*), the sequencing data suggested that they are specific degradation products, since accumulation of these rdRNAs was significantly reduced in the *rdrp*$^{-}$ mutants relative to the wild type and *dicer*$^{-}$ strains (**Supplementary**

Table S1). This fact raised the possibility that this new pathway could also regulate the level of mRNAs. Therefore, we analyzed mRNA accumulation during the exponential growth from representative loci in the wild type, *rdrp*⁻ and *dicer*⁻ mutants. For that, we performed Northern blot analysis of RNA samples isolated from cultures grown 24 hours in liquid MMC medium. Three different *rdrp*-dependent *dicer*-independent rdRNA-producing exons (P1 to P3) were selected based on their different numbers of normalized sRNA reads in the wild type strain, thus representing the variability found in the sRNA transcriptomic analysis (**Table 7**). The accumulation of all tested mRNAs increased two fold, as an average, in the *rdrp*⁻ mutant strains compared to the wild type and *dicer*⁻ mutants when growing exponentially (**Figures 21A** and **21B**, lanes 1-4). This demonstrated a clear trend of the reverse relationship between mRNAs and small RNAs accumulation of the selected reporter genes, the increase in mRNA levels being associated with the reduction in the normalized sRNA reads in the *rdrp*⁻ mutants relative to the wild type and *dicer*⁻ mutant strains (**Figure 21C**). A strict linear correlation between sRNA decrease and mRNA increase is not expected, given the different methods used for detection of mRNAs and sRNAs. Short RNA read numbers are affected by the length of the mRNA, uracil content and distribution, and the ligation bias (Sorefan et al., 2012), since only degradation fragments with a distance between two uracil of 18-24 nt would be able to be included in the sRNA libraries. However, if transcript accumulation of different genes is regulated by the same mechanism, it is expected that alteration of this mechanism by mutation provokes a comparable effect in all those genes. And in fact, the three analyzed genes showed a similar two fold increase in mRNA accumulation in the *rdrp*⁻ mutants relative to the wild type.

To confirm that the effect of *rdrp*⁻ mutation on gene expression operates throughout the complete vegetative cycle, mRNA accumulation of the reporter genes was analyzed at a different growth phase. Similar results were obtained at stationary growth conditions, when cultures were grown for 48 hours in liquid MMC medium (**Figures 21D** and **21E**, lanes 1-4). These results confirm the existence of a degradation pathway in *M. circinelloides* that regulates mRNA levels and requires RdRP-1 and/or RdRP-2 proteins but not Dcl-1 and Dcl-2.

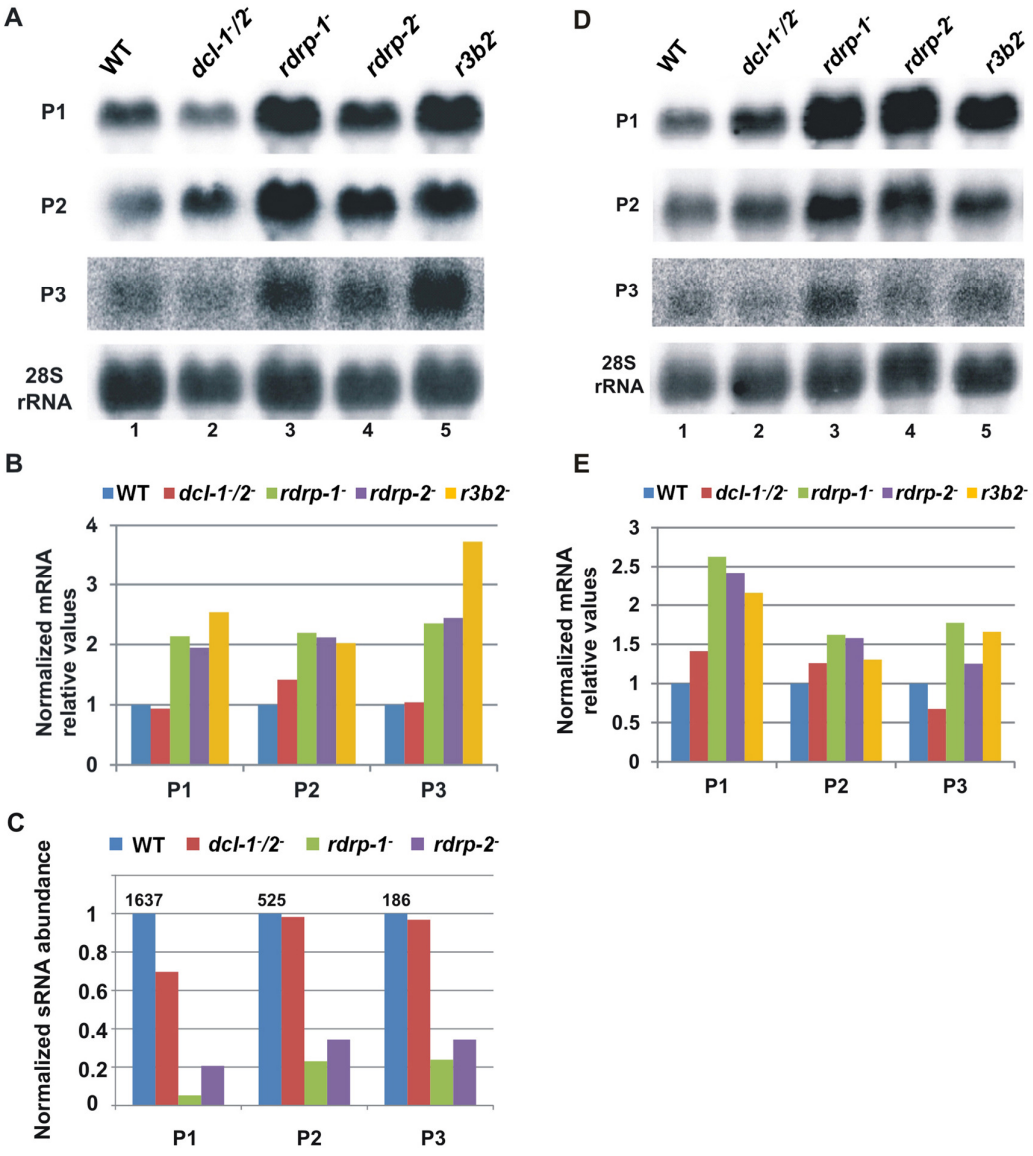

Figure 21. The *rdrp*-dependent *dicer*-independent RNA degradation pathway regulates gene expression. **(A)** Accumulation of mRNAs in wild type and silencing mutants. Northern blots of high molecular weight RNAs corresponding to rdRNA-producing exons (genes P1 to P3) were carried out using total RNA (50 µg) extracted from wild type, *dcl*$^-$ and *rdrp*$^-$ mutant strains (lanes 1-4) and a mutant affected in the ribonuclease gene *r3b2* (lane 5) grown 24 hours in liquid MMC medium pH4,5. Samples were separated in 1,2% denaturing agarose gel, transferred to membranes and hybridized with gene specific probes (**Table 6**). The rdRNA-producing exon loci correspond to the following gene products: P1: ID 155412, piruvate decarboxylase, P2: ID 164785, actin binding protein, P3: ID 156561, transmembrane protein similar to the B-cell receptor-associated protein Bap31 (**Table 7** and **Supplementary Table S1**). The membranes were reprobed with a 28S rRNA probe as loading control. Images are representative of three independent experiments. **(B)** Densitometric analysis of expression data shown in (A). Signal intensities were quantified and normalized to rRNA levels. All data were again normalized with respect to the expression value of the wild type strain (R7B) for each gene. **(C)** Normalized reads (abundance) in the *dcl*$^-$ and *rdrp*$^-$ mutant strains of rdRNAs corresponding to the exon loci P1 to P3 compared to wild type (R7B). All data were again normalized with respect to the abundance values of the wild type strain for each gene. Absolute normalized reads for each gene in the wild type strain are indicated. **(D)** Accumulation of mRNAs in wild type and silencing mutants during stationary growth. The experimental conditions are the same as in (A), except that RNA samples were isolated from cultures grown for 48 hours in MMC medium. **(E)** Densitometric analysis of expression data shown in (D) with the same quantification methods indicated in (B).

rdRNA-producing exons	Protein ID (v1)	Protein ID (v2)	Exon coordinates	WT	*dcl-1*$^{-}$*/2*$^{-}$	*rdrp-1*$^{-}$	*rdrp-2*$^{-}$
P1	26072	155412	scaffold_2/1367350-1369052	1637,07	1141,64	66,47	339,41
P2	92956	164785	scaffold_8/1301699-1302454	524,87	516,09	121,53	180,4
P3	92251	156561	scaffold_5/2811886-2812243	186,2	180,27	44,44	64,08

Table 7. Normalized sRNA reads of three different *rdrp*-dependent *dicer*-independent rdRNA-producing exons. The genomic position of these exons and the ID of the corresponding proteins in the 1 (v1.0) and 2 (v2.0) versions of the *M. circinelloides* genomic sequence is indicated.

III.3. Processes regulated by the *rdrp*-dependent *dicer*-independent RNA degradation pathway

To identify the processes regulated by this new pathway, we performed a Eukaryotic Orthologous Group (KOG) enrichment analysis of the *rdrp*-dependent *dicer*-independent rdRNA-producing exons, according to the whole-genome annotation of *M. circinelloides*, whose version 2.0 is now available (http://genome.jgi-psf.org/Mucci2/Mucci2.home.html) (**Figures 22** and **23** and **Supplementary Table S1**). Although most of the KOG classes were similarly represented both among genes regulated by the non-canonical pathway and the total genome (**Figure 22**), we observed a significant enrichment in the regulated genes for those involved in coenzyme transport and metabolism, cytoskeleton, inorganic ion transport and metabolism, intracellular trafficking and secretion, and secondary metabolites biosynthesis, transport and catabolism. The most highly enriched class was the coenzyme transport and metabolism category, with 21 genes that account for 3,95% of the total number of regulated genes, compared to the 0,87% of these genes in the total genome (**Figure 22**). Twelve out of 21 genes of this class participate in heme B biosynthesis pathway or metabolism (**Figure 23**). Besides haemoglobin and myoglobin, hemes are also found in a number of other biological relevant hemoproteins, such as catalase, which is an essential enzyme for protecting the cell from oxidative damage. Also the gene coding for gamma-glutamylcysteine synthetase (now glutamate cysteine-ligase, ID87510), which controls the first and rate-limiting step in the biosynthesis of the cellular antioxidant glutathione, is included in this class, accumulating a significantly lesser amount of rdRNAs in the *rdrp*$^{-}$ mutants relative to the wild type (**Figure 23**). The differential expression of

those genes in the *rdrp*$^{-}$ mutants could be responsible for the specific phenotypic alterations shown by those strains. In fact, the *rdrp-1*$^{-}$ and, at a lesser extent, *rdrp-2*$^{-}$ mutants are more resistant to oxidative stress than the wild type strain, as indicated by their ability to germinate in the presence of different concentrations of hydrogen peroxide (Trieu et al., 2015).

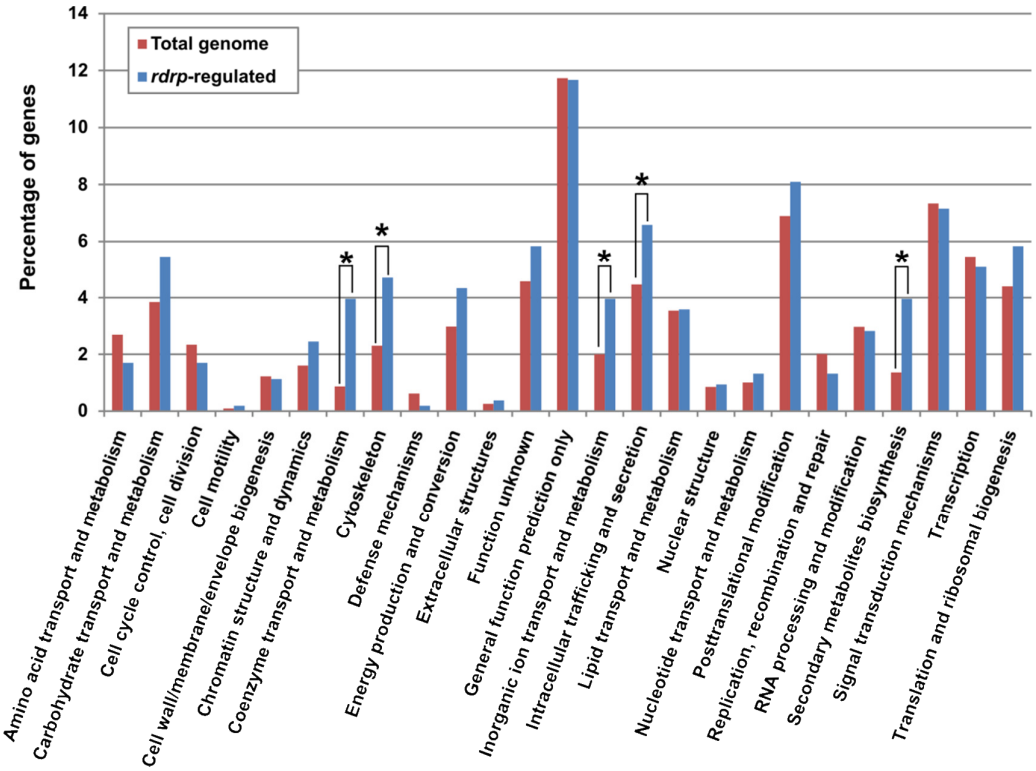

Figure 22. KOG classification of genes regulated by the *rdrp*-dependent *dicer*-independent rdRNAs. The distribution of genes regulated by the non-canonical *rdrp*-dependent *dicer*-independent RNA degradation pathway among the different Eukaryotic Orthologous Groups (KOG) classes (*rdrp*-regulated) is compared to the proportion of each class in the *M. circinelloides* whole genome (total genome). Asterisks indicate KOG classes showing significant enrichment in the *rdrp*-regulated genes relative to the total genome (Pearson's chi-squared test with Yates' continuity correction).

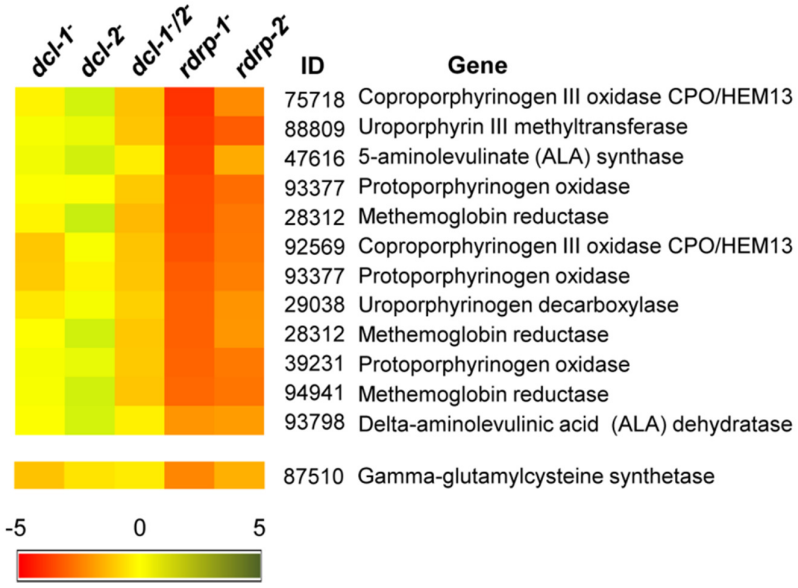

Figure 23. Differential regulation of genes involved in heme B biosynthesis or metabolism in *rdrp*⁻ mutants. The heat map shows the accumulation of *rdrp*-dependent *dicer*-independent rdRNAs from genes involved in heme B biosynthesis or metabolism. Accumulation of rdRNAs derived from the glutamate cysteine-ligase coding gene involved in the synthesis of the antioxidant glutathione is also shown. Each colored cell in the heat map represents the $\log_2$ fold change of rdRNAs in *dicer*⁻ and *rdrp*⁻ mutants compared to wild type strain. Expression levels above 0 represent up-accumulation, whereas those below 0 represent down-accumulation. Data were taken from **Supplementary Table S1**.

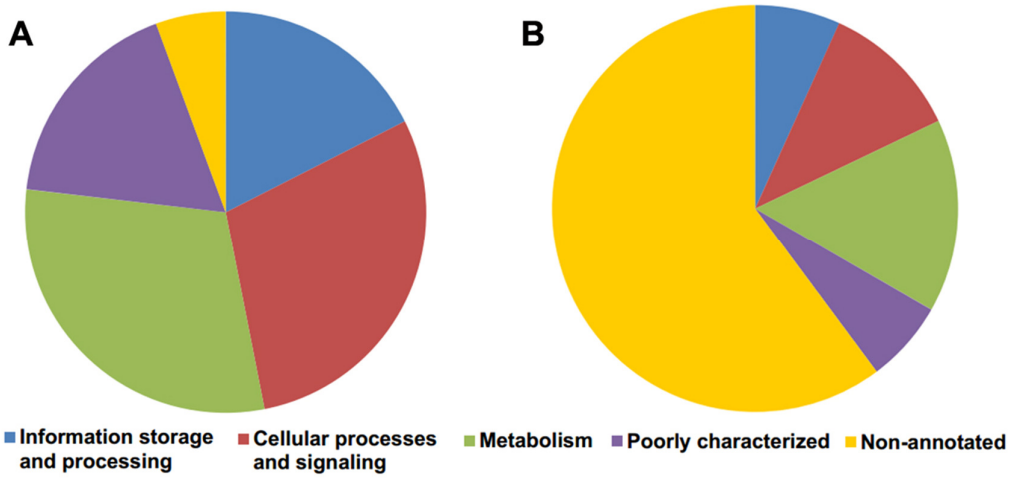

Figure 24. Biological process categories of genes regulated by the *rdrp*-dependent *dicer*-independent RNA degradation pathway. **(A)** The proportion of genes regulated by the *rdrp*-dependent *dicer*-independent non-canonical pathway within the different KOG biological process categories is shown. Data were taken from Supplementary Table S1. **(B)** Similar analysis of genes regulated by canonical *dicer*-dependent ex-siRNAs is shown for comparison. Data were taken from Nicolás et al (2010).

It is also worth noting the significant reduction in non-annotated genes among those regulated by the non-canonical pathway, with only 5,65% of non-

annotated genes compared to 22,57% in the total genome (**Supplementary Table S1**). In fact, almost 60% of the rdRNA-producing loci correspond to conserved genes involved in metabolism and cellular processes and signaling (**Figure 24A** and **Supplementary Table S1**), which is significantly different to the functional annotation of genes regulated by the canonical *dicer*-dependent ex-siRNAs (**Figure 24B**, Nicolás et al., 2010). Thus, the canonical and non-canonical RNA pathways seem to regulate different groups of genes.

III.4. Searching for candidate RNases in the *Mucor* genome

The proposed pathway for the production of the rdRNAs involves the participation of an RNase that degrades target mRNAs. To identify the implicated RNase, we attempted to knock out four genes for putative RNases: 80729, 136157, 110239, and 77996. Those proteins were identified by performing an *in silico* analysis of the *M. circinelloides* genome (v2.0) looking for annotated proteins containing RNase domains. Twenty-four proteins annotated under the endoribonuclease activity GO term (GO 0004521) were identified. A careful analysis of those proteins allowed us to select several candidates to be investigated for their participation in the non-canonical silencing pathway. Briefly, we selected putative RNases without precise information on their molecular role or those with functional annotation that could be related with the non-canonical pathway (**Table 8**), discarding proteins with well-described ribonuclease activities, such as Dcl-1, Dcl-2, RNase P, RNase T2, RNase A, RNase H and others. Thus, the four putative RNases mentioned above were investigated. Three of these proteins contain dsRNA-specific RNase III domains, since it was argued that participation of RdRP proteins in the degradation pathway should involve the production of dsRNA stretches at some point of the process. The other RNase protein, 131157, belongs to the RNase L family, which are proteins involved in the control of mRNA stability. Because protein 80729 contains an RNase III domain (*r3*), and two dsRNA binding domain (*b2*), we named the corresponding gene *r3b2*. The selected genes and their adjacent sequences were amplified from genomic DNA and knockout vectors were designed to disrupt each candidate gene by gene replacement.

Protein ID	Scaffold	Number of residues	Domains[1]
77996	scaffold_02:4034471-4035091	166	RNase III
80729	scaffold_03:4859492-4861037	494	RNase III-like 2 x dsRBD
110239	scaffold_04:2084271-2085274	297	RNase III dsRBD
136157	scaffold_01:4095479-4096928	425	PKc RNase_Ire1

Table 8. Candidate RNase proteins in the *Mucor* genome v2.0. [1]RNase III: double-stranded RNA-specific ribonuclease; dsRBD: double stranded RNA binding domain; RNase_Ire1, endoribonuclease domain of *Saccharomyces cerevisiae* Ire1, a multifunctional protein essential for the endoplasmic reticulum unfolded protein response (UPR); PKc: catalytic domain of protein kinases.

III.5. Generation of knock-out mutants for candidate RNases

The *r3b2* null mutant strain, MU412, was generated and kindly provided by Dra. Silvia Calo (this laboratory). The mutant allele in MU412 has replaced 1,3 kb of the *r3b2* coding region by the *pyrG* gene. Knockout vectors pMAT768, pMAT763 and pMAT766 were designed to disrupt 136157, 110239 and 77996 genes, respectively (see below). Restriction fragments from each knockout vector containing the *pyrG* gene flanked by sufficient sequences of the candidate RNase genes to allow homologous recombination were used to transform the MU402 strain (Ura^-, Leu^-). Ura^+ transformants were grown in selective medium for several vegetative cycles to increase the proportion of transformed nuclei, as primary transformants are heterokaryons due to the presence of several nuclei in the protoplasts. Homokaryotic transformants were PCR analyzed to distinguish homologous from ectopic integrations, and the disruption of each gene was confirmed by Southern analysis.

III.5.1. Disruption of candidate gene 136157

To disrupt candidate RNase 136157, plasmid pMAT768 was constructed. This plasmid derives from pMAT767, which harbors a 3,4 kb genomic fragment containing the complete 136157 gene and adjacent regions. This fragment was PCR-

amplified from genomic DNA using primer pairs F2 and R2 (**Table 5,**) and cloned into pBluescript vector (**Figure 25**). Plasmid pMAT767 was then used as a template for inverse PCR amplification with primers F3 and R3 (**Table 5**), which contain *Bgl*II restriction sites. The amplified 5,1 kb fragment was *Bgl*II digested and ligated with the 3,4 kb *pyrG* fragment from pEPM1 to give plasmid pMAT768 (**Figure 25**). A 5,5 kb replacement fragment harboring the *pyrG* gene flanked by 1,1 kb and 1,0 kb of sequences adjacent to 136157 was released from plasmid pMAT768 by *Pvu*II digestion, amplified with primers F2 and R2 (**Table 5**) and introduced into MU402 by transformation.

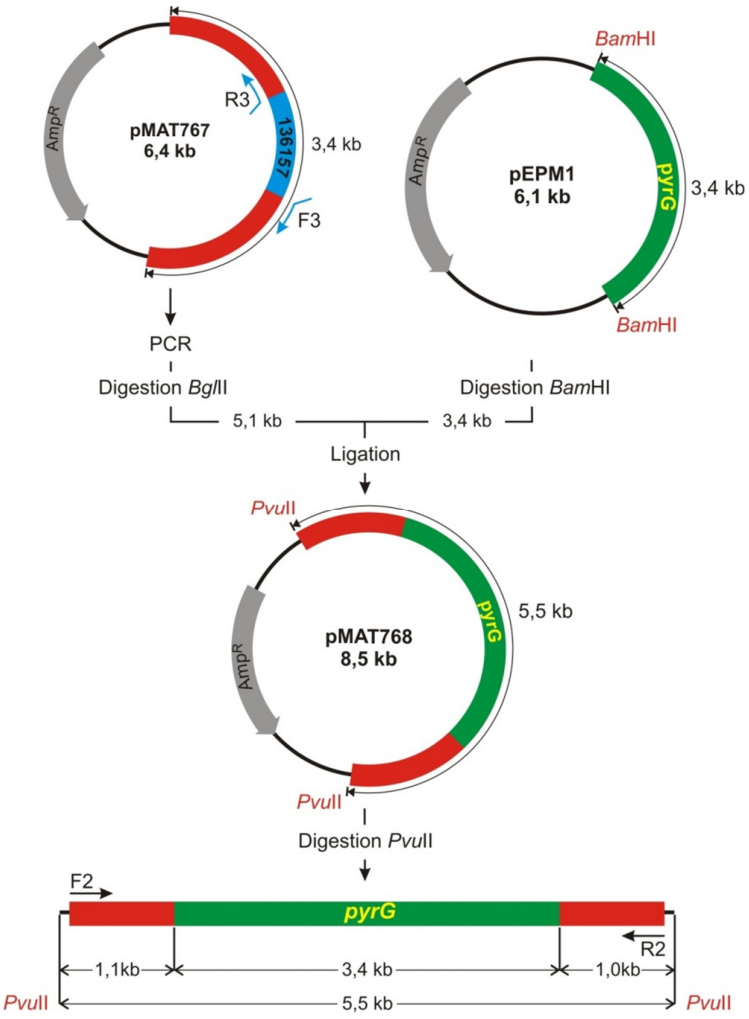

Figure 25. Construction of the replacement fragment used to disrupt 136157 gene. The red boxes indicate adjacent regions of the target gene, which is shown in dark blue. The selective marker *pyrG* gene is shown in dark green. The positions of restriction sites and primers used for cloning are indicated.

After transformation of MU402, the original Ura$^+$ transformants were grown for three vegetative cycles in selective medium to increase the proportion of transformed nuclei. Transformants with more than 90% of Ura$^+$ nuclei were selected to check if they contain the disruption fragment correctly integrated into the target gene using PCR analysis. For candidate gene 136157, three different PCR reactions with different primers were performed (**Figure 26A**). Only disruption strains generated by homologous recombination would amplify an specific size fragment with primer pair pyrg-R2/F1 (**Figure 26A**). Four out of five transformants analyzed (numbers 2-5) amplified the expected fragment (**Figure 26B**), indicating that those transformants had integrated the disruption fragment into the 136157 locus.

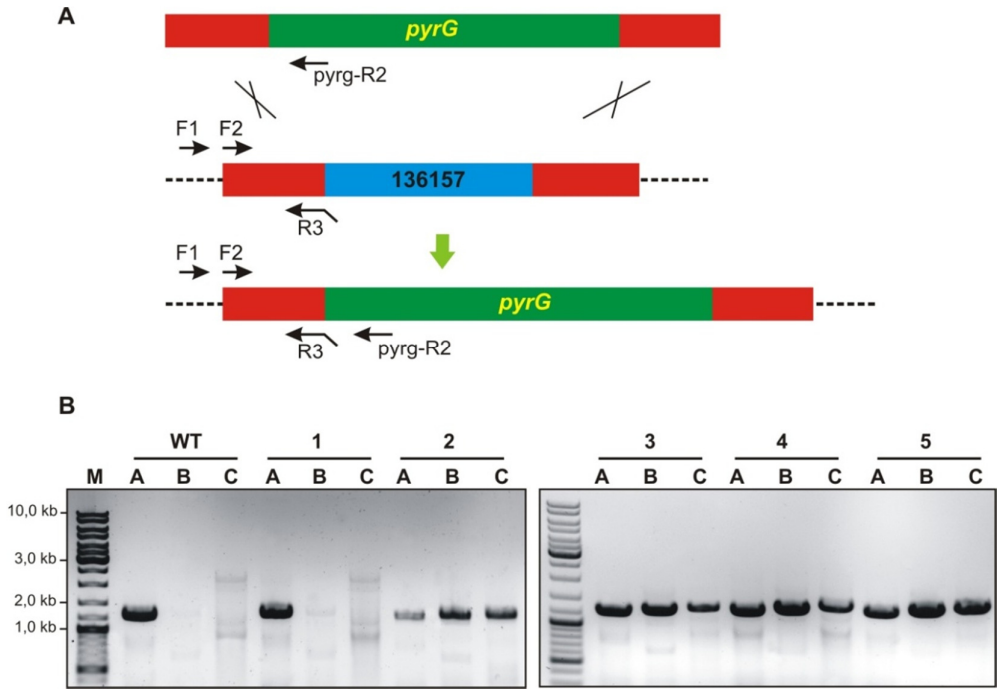

Figure 26. PCR analyses of transformants obtained to disrupt the 136157 gene. **(A)** Schematic representation of the wild type 136157 locus (middle) and after homologous recombination with the disruption fragment (below). Dark blue and red boxes represent genomic 136157 locus and adjacent sequences, respectively; dark green boxes, *pyrG* selectable marker; dashed lines, sequences not included in the disruption fragment. The positions of the primers used for PCR reactions (**Table 5**) are indicated. Three PCR reactions were performed for each transformant with different primer pairs. Reaction A (F2/R3) is an internal control of the DNA quality, reaction B (F2/pyrg-R2) detects the presence of the disruption fragment in the transformant and reaction C (F1/pyrg-R2) identifies disruption mutants. **(B)** PCR results of the wild-type strain R7B and five 136157 transformants (numbers 1 to 5). M, GeneRuler DNA ladder mixture (Fermentas).

After several vegetative cycles on selective media to increase the proportion of transformed nuclei, putative homokaryotic transformants were isolated and analyzed by Southern blot. *Eco*RI-digested DNA from each transformant was

hybridized with specific probes that recognized both wild type and mutant alleles but could discriminate between them (probe b, **Figure 27**), or corresponded to a DNA region deleted in the knockout vector (probe c, **Figure 27**). Probes *b* and *c* correspond to a 1,1 kb *Hinc*II and 0,6 kb *Nco*I/*Sac*I fragments isolated from plasmid pMAT767, respectively. Two homokaryotic transformants obtained with the 136157 disruption fragment were confirmed as replacement mutants and were named MU450 and MU451 (**Figure 27**).

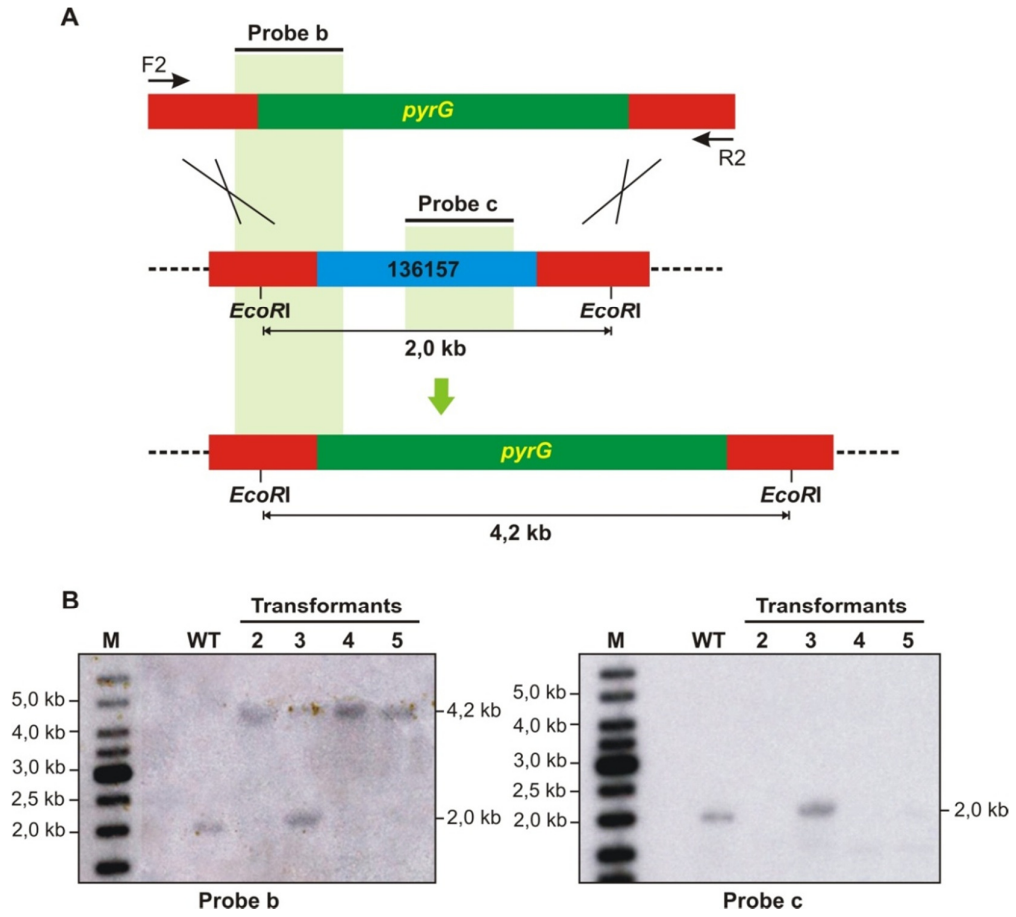

Figure 27. Disruption of the 136157 gene. **(A)** Schematic representation of the wild type 136157 locus (middle) and after homologous recombination with the disruption fragment (below). The color code is the same as **Figure 26**. The positions of the probes used (probes b and c) and the expected sizes of the *EcoR*I restriction fragments are indicated. The primers used to amplify the disruption fragment from the knockout vector pMAT768 (F2 and R2) are shown (**Table 5**). **(B)** Southern blot analysis of the wild type strain R7B and four 136157 transformants. Genomic DNA (1 µg) was digested with *EcoR*I and hybridized with probe b (left) and with probe c (right). M, GeneRuler DNA ladder mixture (Fermentas). Only transformants 2 and 4 are homokaryotic disruption mutants.

III.5.2. Disruption of candidate genes 110239 and 77996

A similar strategy to that mentioned above was used to disrupt candidate gene 110239. A 2,5 kb genomic fragment that includes the entire 110239 locus and flanking regions was PCR-amplified using genomic DNA and primers F5 and R5 (**Table 5**) and it was cloned into pBluescript vector to give plasmid pMAT762 (**Figure 28**). This plasmid was used as a template for inverse PCR amplification with primers F6 and R6 (**Table 5**), which include *BamH*I restriction sites. The 4,6 kb amplified fragment was digested with *BamH*I and ligated with the 3,4 kb *pyrG*

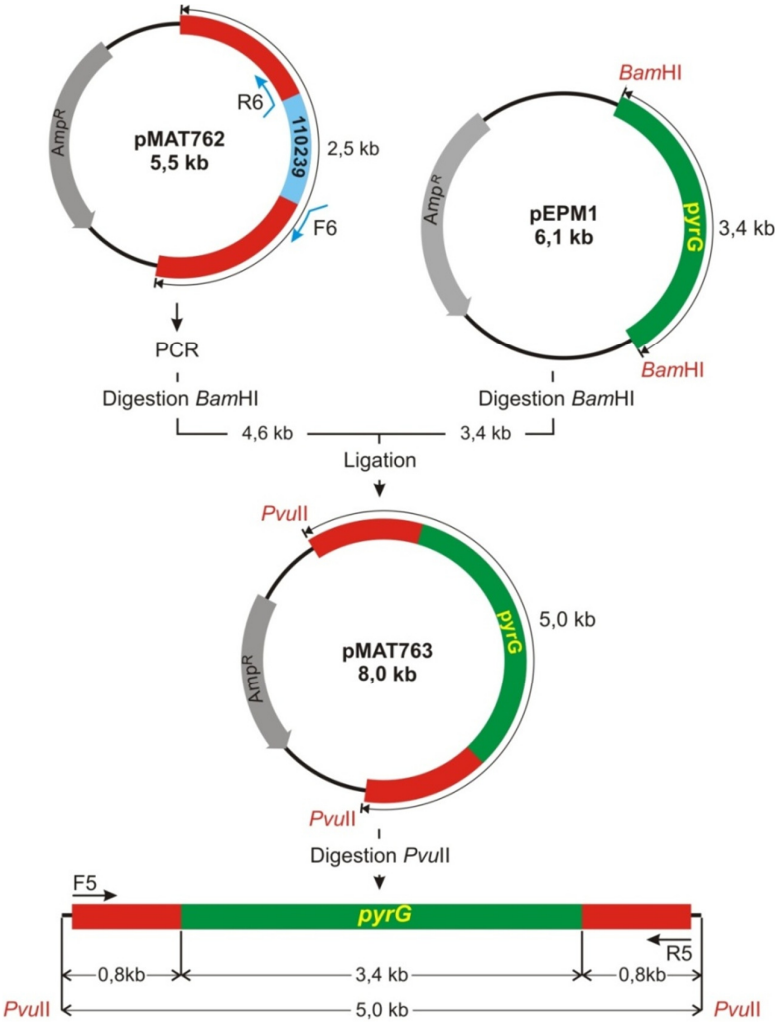

Figure 28. Construction of the replacement fragment used to disrupt 110239 gene. The red boxes indicate adjacent regions of the target gene, which is shown in light blue. The selective marker *pyrG* gene is shown in dark green. The positions of restriction sites and primers used for cloning are indicated.

fragment to give plasmid pMAT763. A 5,0 kb replacement fragment harboring the *pyrG* gene flanked by 0,8 kb of upstream and downstream sequences of 110239 was released from plasmid pMAT763 by *Pvu*II digestion, amplified with primers F5 and R5 (**Table 5, Figure 28**) and introduced into MU402 by transformation.

To disrupt the 77996 gene a different strategy based in overlapping PCR was used. The knockout vector pMAT770 contains a 4,0 kb fragment that includes the *pyrG* gene flanked by upstream and downstream sequences of the 77996 gene. It was constructed by fusion PCR using primer pairs F7/R9-pyrG (**Table 5**), and F9-pyrG/R7 (**Table 5**) to amplify 1,0 kb of upstream and downstream sequences of the 77996 locus, respectively (see II.7.5 and Figure 16 of Materials and Methods). Those fragments were used in a fusion PCR together with a 2,0 kb *pyrG* fragment amplified from plasmid pEMP1 using primers F-pyrG and R-pyrG (**Table 5**). The 4,0 kb fusion fragment was amplified with internal primers F8 and R8 (**Table 5**) and cloned into pGEM-T easy vector to give plasmid pMAT770 (**Figure 29**). The 4,0 kb replacement fragment was released from plasmid pMAT770 by *Pvu*II digestion, amplified with primers F8 and R8 and introduced into MU402 by transformation.

MU402 transformants with high proportion of Ura^+ nuclei were PCR analyzed to distinguish homologous from ectopic integrations. For both RNase candidate genes, 110239 and 77996, PCR reactions with primers located at the 5'-end and 3'-end of the target sequences were used to identify homologous integration events at the corresponding loci (**Figures 30 and 31**). As the results, six transformant strains for 110239 gene and four strains for 77996 gene, were identified as containing correctly integrated mutant alleles. However, it was impossible to obtain homokaryotic knockout mutants for those genes, as transformants containing the mutant alleles maintained wild type nuclei even after more than ten vegetative cycles on selective media (**Figure 32**). This suggests that genes 110239 and 77996 may play essential roles for the viability of *M. circinelloides* and hampers a functional analysis of those two genes.

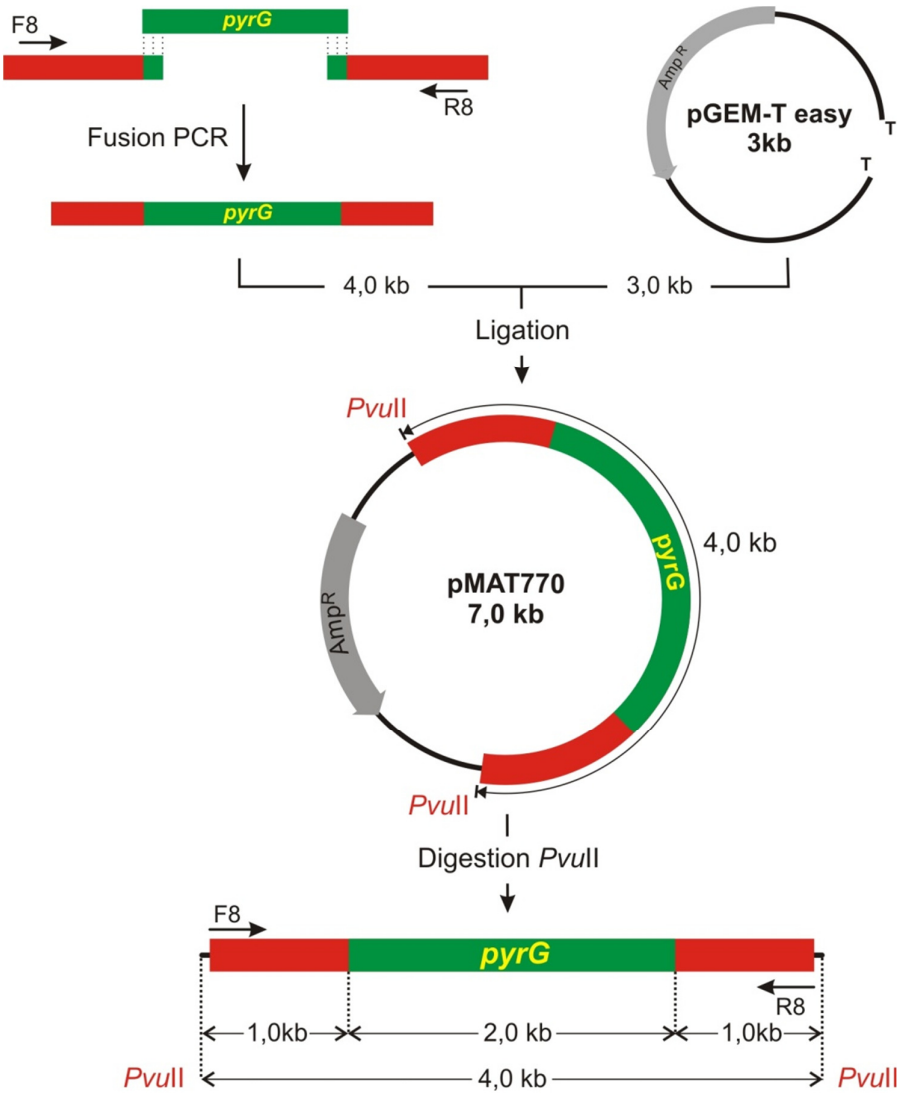

Figure 29. Construction of the replacement fragment used to disrupt 77996 gene. Overlap PCR reaction was used to fuse three fragments and generate the replacement fragment, which includes flanking sequences (red boxes) of the 77996 gene and the selective marker *pyrG* (dark green boxes). This fragment was cloned into vector pGEMT-easy to generate plasmid pMAT770. The positions of restriction sites and primers used for cloning are indicated.

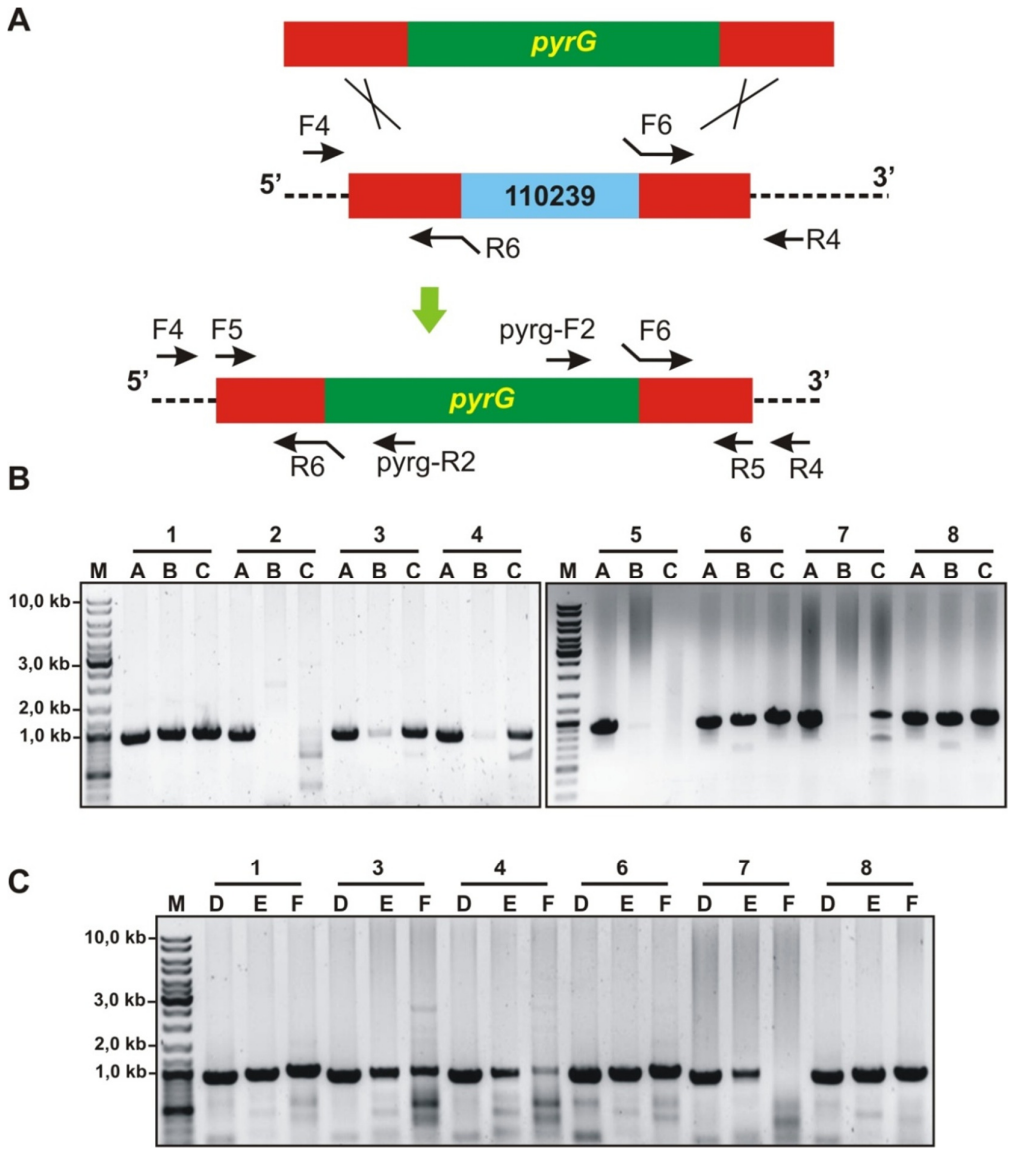

Figure 30. PCR analyses of transformants obtained to disrupt the 110239 gene. **(A)** Schematic representation of the wild type 110239 locus (middle) and after homologous recombination with the disruption fragment (below). Light blue and red boxes represent genomic 110239 locus and adjacent sequences, respectively; dark green boxes, *pyrG* selectable marker; dashed lines, sequences not included in the disruption fragment. The positions of the primers used for PCR reactions (**Table 5**) are indicated. **(B)** PCR analyses at the 5' end of eight 110239 transformants (numbers 1 to 8). Three PCR reactions were performed for each transformant with different primer pairs. Reaction A (F5/R6) is an internal control of the DNA quality, reaction B (F5/pyrg-R2) detects the presence of the disruption fragment in the transformants and reaction C (F4/pyrg-R2) identifies disruption mutants. Transformants 1, 3, 4, 6, 7 and 8 have the disruption fragment correctly integrated at its 5' end. M, GeneRuler DNA ladder mixture (Fermentas). **(C)** Similar PCR analyses at the 3' end of the six 110239 transformants which gave positive results in the 5' end PCRs. The control reactions D (primers F6/R5) and E (primers pyrg-F2/R5) and the informative reaction F (primers pyrg-F2/R4) confirmed that at least 5 out of the 6 transformants have a correctly integrated mutant allele into the 110239 locus. M, GeneRuler DNA ladder mixture (Fermentas).

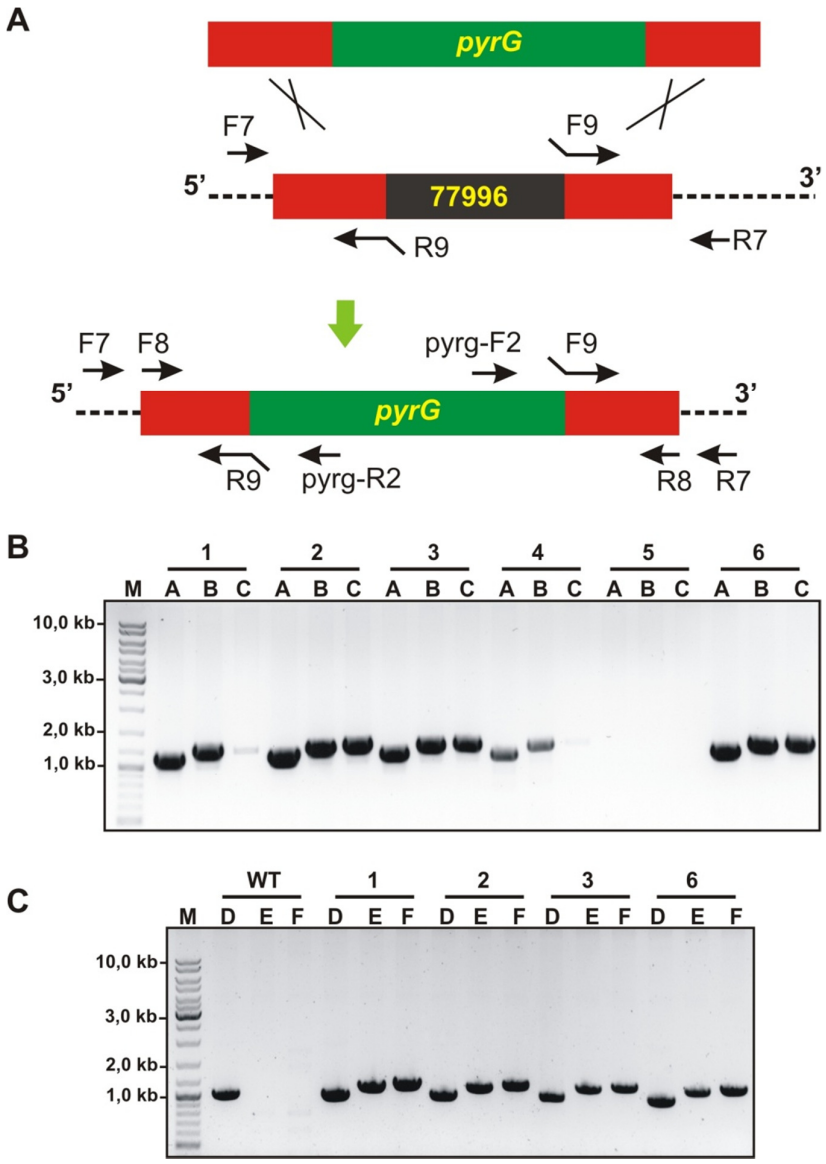

Figure 31. PCR analyses of transformants obtained to disrupt the 77996 gene**. (A).** Schematic representation of the wild-type 77996 locus (middle) and after homologous recombination with the disruption fragment (below). Black and red boxes represent genomic 77996 locus and adjacent sequences, respectively; dark green boxes, *pyrG* selectable marker; dashed lines, sequences not included in the disruption fragment. The positions of the primers used for PCR reactions (**Table 5**) are indicated. **(B)** PCR analyses at the 5' end of six 77996 transformants (numbers 1 to 6). Reaction A (primers F8/R9), reaction B (primers F8/pyrg-R2) and reaction C (primers F7/pyrg-R2) showed that the transformants 1, 2, 3 and 6 have the disruption fragment correctly integrated at its 5' end. M, GeneRuler DNA ladder mixture (Fermentas). **(C)** Similar PCR analyses at the 3' end of the four 77996 transformants which gave positive results in the 5' end PCRs. Reactions D (primers F9/R8), E (primers pyrg-F2/R8) and F (primers pyrg-F2/R7) confirmed that all of those transformants have a correctly integrated mutant allele into the 77996 locus. M, GeneRuler DNA ladder mixture (Fermentas).

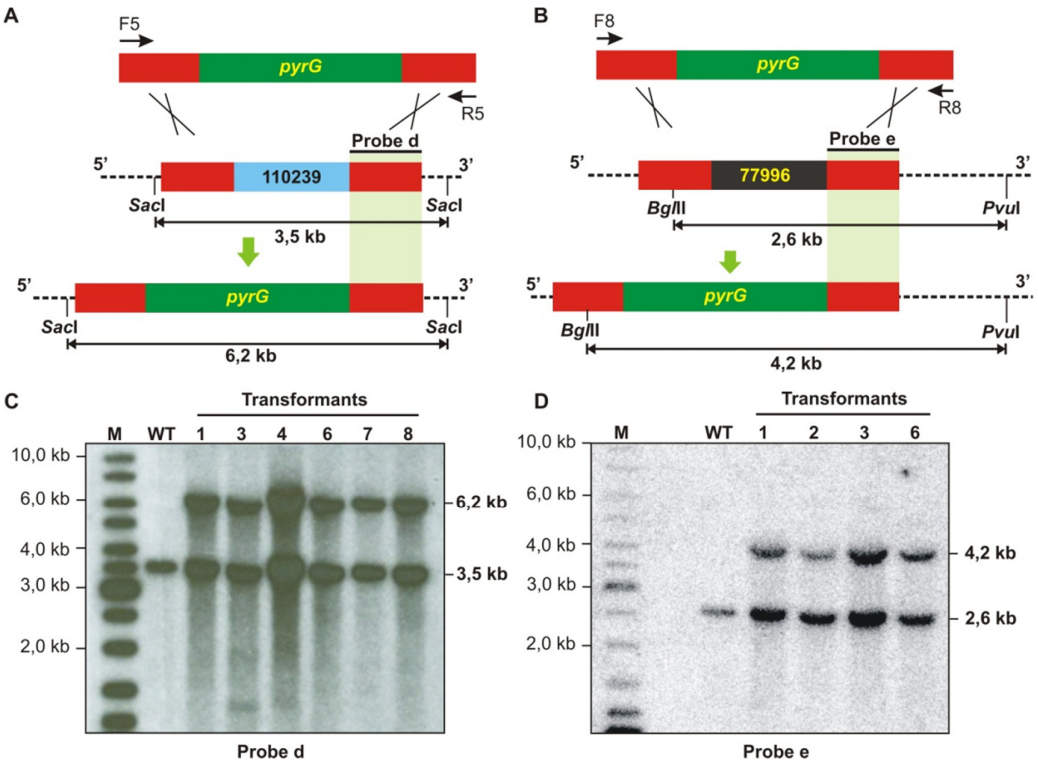

Figure 32. Disruption of the 110239 and 77996 genes. **(A)** Schematic representation of the wild-type 110239 locus (middle) and after homologous recombination with the disruption fragment (below). The color code is the same as **Figure 30**. The position of the probe used (probe *d*) and the expected sizes of the *Sac*I restriction fragments are indicated. Probe *d* corresponds to a 0,8 kb fragment of the 110239 downstream region amplified by the primer pair F6/R5 (**Table 5**). The primers used to amplify the disruption fragment from the knockout vector pMAT763 (F5 and R5) are shown. **(B)** Similar representation of the 77996 locus in the wild-type and disrupted strains. The position of the probe used (probe *e*) and the expected sizes of the *Bgl*II/*Pvu*I restriction fragments are indicated. Probe *e* corresponds to a 1,0 kb fragment of the 77996 downstream region amplified by the primer pair F9-pyrG/R8 (**Table 5**). Primers F8 and R8 were used to amplify the disruption fragment from the knockout vector pMAT770. **(C)** Southern blot analysis of the wild-type strain R7B and six 110239 transformants grown in selective medium for ten vegetative cycles. Genomic DNA (1 µg) was digested with *Sac*I and hybridized with probe *d*, which recognized the wild-type and disrupted alleles but could discriminate between them. All transformants analyzed are heterokaryons, since they generate fragments corresponding to both mutant (6,2 kb) and wild type (3,5 kb) alleles. **(D)** Southern blot analysis of the wild-type strain R7B and four 77996 transformants grown in selective medium for ten vegetative cycles. Genomic DNA (1 µg) was double digested with *Bgl*II and *Pvu*I and hybridized with probe *e*, which recognized the wild-type and disrupted alleles but could discriminate between them. All transformants analyzed are heterokaryons, since they generate fragments corresponding to both mutant (4,2 kb) and wild type (2,6 kb) alleles. The positions and sizes of the GeneRuler DNA ladder mixture (M) (Fermentas) size markers are indicated.

III.6. The RNase III R3B2 participates in the *rdrp*-dependent *dicer*-independent RNA degradation pathway

To investigate the role of the candidate RNases in the non-canonical RNA degradation pathway we first analyzed the accumulation of mRNA of representative loci regulated by this pathway (P1 to P3, see section III-2) in the MU412 mutant

(*r3b2*$^-$) and in the null mutants for gene 136157, MU450 and MU451. All tested mRNAs up-regulated in the *rdrp-1*$^-$ and/or *rdrp-2*$^-$ mutants compared to the wild-type strain and *dicer*$^-$ mutant were also up-regulated in the *r3b2*$^-$ mutant, in samples isolated during both exponential (**Figure 21A**, lane 5) and stationary growth (**Figure 21D**, lane 5). In fact, the increase in mRNA accumulation of the target genes in the *r3b2*$^-$ mutant relative to the wild type strain was roughly two-fold, similarly to the *rdrp-1*$^-$ and *rdrp-2*$^-$ mutants (**Figures 21B** and **21E**), suggesting that the *r3b2* gene encodes an RNase required for the degradation of specific mRNAs by the *rdrp*-dependent, *dicer*-independent non-canonical pathway. In contrast, mRNA accumulation of target genes in the MU450 and MU451 mutants, which are deficient in the putative RNase protein 136157, was similar to the wild type and *dicer*$^-$ mutant (**Figure 33**), indicating that this RNase does not participate in the non-canonical RNA degradation pathway. Lack of homokaryotic null mutants for genes 110239 and 77996 precluded the analysis on their participation in the *rdrp*-dependent, *dicer*-independent pathway.

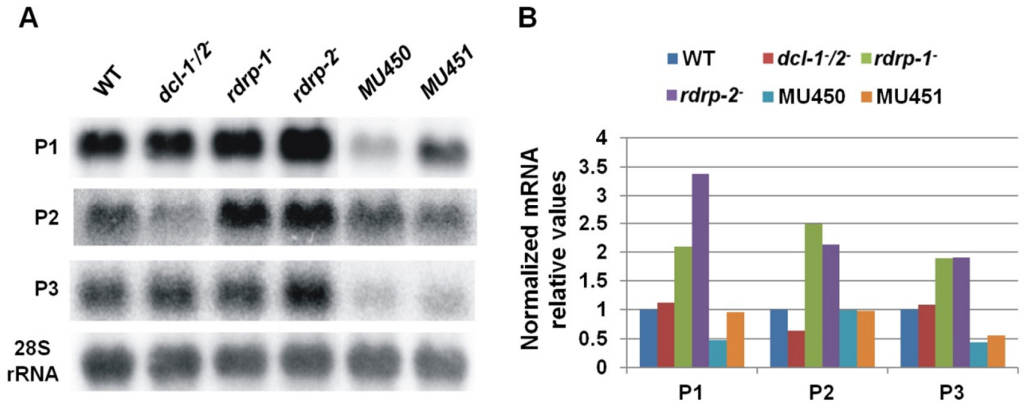

Figure 33. Accumulation of mRNAs in wild type and silencing mutants. **(A)** Accumulation of mRNA from the rdRNA-producing exons (P1 to P3) in mutants affected in the 136157 RNase. Total RNA (50 µg) extracted from the MU450 and MU451 mutants, affected in the 136157 RNase gene, as well as the wild type strain and *dcl*$^-$ and *rdrp*$^-$ mutants grown 24 hours in liquid MMC medium was hybridized with gene specific probes (**Table 6**). The membrane was reprobed with a 28S rRNA probe as loading control. Images are representative of two independent experiments. **(B)** Densitometric analysis of expression data shown in (A). Signal intensities were quantified and normalized to rRNA levels. All data were again normalized with respect to the expression value of the wild type strain (R7B) for each gene.

The presumed role of the RNase III R3B2 in the generation of rdRNAs by the *rdrp*-dependent, *dicer*-independent non-canonical pathway was confirmed by deep sequencing of the sRNA content (18-25 nt) in the *r3b2*$^-$ mutant and its comparison

with the wild type strain. Almost 1560 exonic loci were identified that showed a significant reduction in normalized sRNA reads in the *r3b2*$^{-}$ mutant relative to the wild type (**Supplementary Table S2**). Those loci were selected as those showing at least a fourfold decrease in normalized reads in the *r3b2*$^{-}$ mutant compared to wild type, and a normalized abundance count of more than 50 in the wild type. All but one of the 531 rdRNA loci of the *rdrp*-dependent *dicer*-independent class were found among those significantly down-regulated in the *r3b2*$^{-}$ mutant, as shown in **Table 9** and **Supplementary Table S3**. In fact, the $\log_2$ fold change values in the *r3b2*$^{-}$ mutant relative to the wild type strain was even more significant than that of the *rdrp*$^{-}$ strains for most of the *rdrp*-dependent *dicer*-independent exonic loci, pointing to the relevant role of R3B2 in the biogenesis of these rdRNAs. The lower rdRNA levels in the *r3b2*$^{-}$ mutant can be also seen in genes involved in heme biosynthesis, which show at least a 38-fold reduction in rdRNA accumulation relative to the wild type strain (**Figure 34A**). The presumed up-regulation of those genes in the *r3b2*$^{-}$ mutant should be responsible for the increased resistance to oxidative stress shown by this strain relative to the wild type (**Figure 34B**). In fact, as occurs with the *rdrp-1*$^{-}$ and *rdrp-2*$^{-}$ mutants, *r3b2*$^{-}$ strain shows a higher ability to germinate in the presence of hydrogen peroxide, confirming its involvement in the *rdrp*-dependent *dicer*-independent RNA degradation pathway and suggesting a role for this pathway in the response to specific environmental signals. All together, these results demonstrate the participation of the R3B2 protein in the biogenesis of the *rdrp*-dependent *dicer*-independent rdRNAs, strongly suggesting that it is indeed the RNase involved in the degradation process of specific mRNAs by the non-canonical silencing pathway.

sRNA class		No. of exons	% of down-regulated in *r3b2*⁻	Average log_2 fold change *r3b2*⁻ vs WT[a]
***dicer*-independent (rdRNAs)**	*rdrp-1* and *rdrp-2*-dependent	288	100	**-6,24**
	rdrp-1-dependent	223	100	**-5,70**
	rdrp-2-dependent	20	95 (19 out of 20)	**-3,73**
***dicer*-dependent[b] (ex-siRNAs)**	Class I	9	33,3 (3 out of 9)	-0,07
	Class II	222	66,2 (147 out of 222)	**-2,57**
	Class III	88	97,7 (86 out of 88)	**-6,92**
	Class IV	5	80 (4 out of 5)	**-5,24**

Table 9. Accumulation of different classes of exonic sRNAs in the *r3b2*⁻ mutant. [a]Average value of the log_2 fold change of the different classes of exonic sRNAs in the *r3b2*⁻ *M. circinelloides* mutant compared to wild type. Log_2 fold changes in **Supplementary Tables S3** (*dicer*-independent) and **S4** (*dicer*-dependent) were used to calculate the averages. Numbers in bold indicate a higher than four-fold down-regulation in the *r3b2*⁻ mutant relative to wild type. [b]*dicer*-dependent ex-siRNAs are classified as previously described (Nicolás et al., 2010; Cervantes et al., 2013).

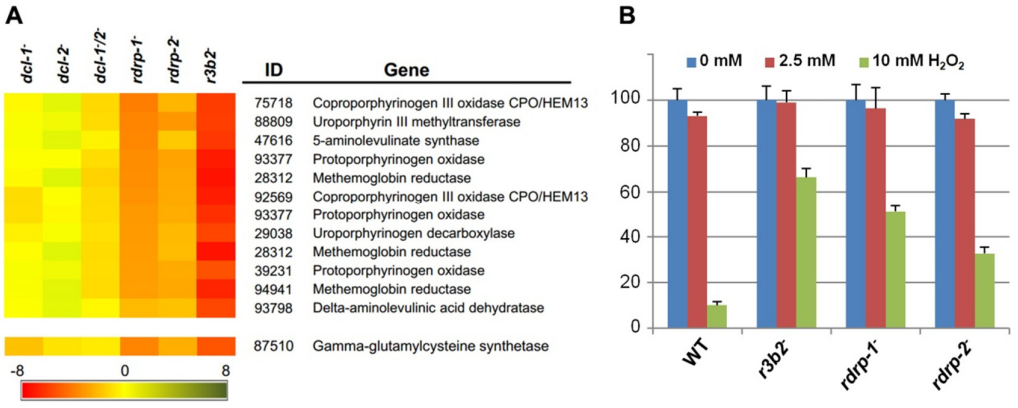

Figure 34. Differential regulation of genes involved in heme B biosynthesis or metabolism and oxidative stress response in the *r3b2*⁻ mutant. **(A)** Accumulation of rdRNAs from genes involved in heme B biosynthesis or metabolism. The heat map shown in **Figure 23** has been extended to include data from the mutant affected in the RNase gene *r3b2*. Each colored cell in the heat map represents the log_2 fold change of rdRNAs in the different mutants relative to wild type strain. Expression levels above 0 represent up-accumulation, whereas those below 0 represent down-accumulation. Data were taken from **Supplementary Tables S1** and **S3**. **(B)** Oxidative stress response in the *r3b2*⁻ mutant. Spores of the wild type strain (R7B) and *r3b2*⁻ and *rdrp*⁻ mutants were inoculated in YNB plates pH 3.2 containing different concentration of hydrogen peroxide (0, 2.5 and 10 mM) and the percentage of germinated spores was calculated. The values are means and standard error of three independent experiments.

III.7. R3B2 also participates in the canonical *dicer*-dependent RNA silencing pathway

As it was stated in the Introduction section, different types of *dicer*-dependent ex-siRNAs were previously identified and classified based on the components of the silencing machinery required for their biogenesis (Nicolás et al., 2010). Most of those classes were also found among the exonic sRNAs significantly down-regulated in the *r3b2*$^-$ mutant (**Table 9** and **Supplementary Table S4**). The majority of ex-siRNAs of the *dicer*-dependent classes II, III and IV showed at least a four-fold reduction in the *r3b2*$^-$ mutant relative to the wild type, whereas only three out of nine loci of class I were significantly reduced in the mutant strain. These results indicate that R3B2, besides its role in the non-canonical pathway, also participates in the production of the majority of canonical *dicer*-dependent ex-siRNAs, although its contribution varies among the different ex-siRNA classes. Particularly interesting is the large decrease in ex-siRNAs of class III in the *r3b2*$^-$ mutant. Class III ex-siRNAs can be produced both by Dcl-1 and Dcl-2, since their reduction is only seen in the double *dcl-1*$^-$*/dcl-2*$^-$ mutant, and its biogenesis requires the participation of both RdRP-1 and RdRP-2 proteins (Nicolás et al., 2010). The structural characteristic of this ex-siRNA class and its lack of binding to Ago-1 indicated that class III ex-siRNAs are not *bona fide* ex-siRNAs and it had been proposed that they could be produced by degradation of specific mRNAs by unknown RNases (Nicolás et al., 2010; Cervantes et al., 2013). The structural and functional similarities between class III of *dicer*-dependent ex-siRNAs and the *rdrp*-dependent *dicer*-independent rdRNAs and the large decrease of both classes in the *r3b2*$^-$ mutant (**Table 9**) might suggest that they can be produced by the same RNase, the R3B2 protein. In fact, comparing the reduction of the class III ex-siRNA levels in the double *dcl-1*$^-$*/dcl-2*$^-$ mutant [average $\log_2$ fold change from wild type -3,21 (Nicolás et al., 2010)] with their reduction in the *r3b2*$^-$ mutant (-6,92; **Table 9**) suggests that R3B2 plays the more prominent role in the production of this class of ex-siRNAs (see Discussion).

To confirm the participation of the *r3b2* gene in the *dicer*-dependent canonical pathway, we analyzed the capacity of the *r3b2*$^-$ mutant to activate the silencing mechanism by exogenous sequences. For that, we transformed the *r3b2*$^-$ mutant and the wild type strain with two different self-replicative silencing vectors containing sequences of the *carB* gene (phytoene dehydrogenase) expressed from the

Plasmid[a]	Strain[b]	Number of transformants[c]			Silencing frequency (%)
		Albino	Bright yellow	Total	
pMAT1279 (s-transgene)	wild-type	90	23	113	79,6
	MU412 (*r3b2*$^-$)	5	103	108	**4,6**
	MU450	17	5	22	77,2
	MU451	65	12	77	84,4
pMAT1253 (hpRNA)	wild-type	130	21	151	86,0
	MU412 (*r3b2*$^-$)	14	206	220	**6,4**
	MU450	50	2	52	96,1
	MU451	51	9	60	85
pMAT771 (hpRNA/*r3b2*^{wt})	wild-type	57	204	261	21,8
	MU412 (*r3b2*$^-$)	44	111	155	28,4
pMAT772 (hpRNA/*r3b2**)	wild-type	76	211	287	26,5
	MU412 (*r3b2*$^-$)	10	215	225	**4,4**
pLEU4 (control)[d]	wild-type	0	312	312	0
	MU412 (*r3b2*$^-$)	0	79	79	0
	MU450	0	17	17	0
	MU451	0	11	11	0

Table 10. Gene silencing by sense and inverted repeat transgenes in candidate RNase mutants. [a]s-transgene, construct expressing the sense transgene; hpRNA, construct expressing hpRNA. [b]Strain MU412 is the null mutant for the *r3b2* gene. Mutants MU450 and MU451 are affected in the candidate RNase 136157. [c]The colors of the *M. circinelloides* transformants were observed after 48 h under illumination with white light. Colonies with patches of albino and wild type (bright yellow) phenotype were considered as albino, since most of the silenced primary transformants showed patches of different phenotypes due to the presence of several nuclei in the *M. circinelloides* protoplasts, but they turned uniformly albino after a cycle of vegetative growth in selective medium. [d]Control plasmid without a silencing construct.

strong promoter of the *gpd1* gene (glycerol-3-phosphate dehydrogenase) as silencing reporter, since *carB* function is required for the production of colored carotenoids. Plasmid pMAT1279 contains a sense *carB* transgene (s- transgene) (Calo et al., 2012), whereas plasmid pMAT1253 expresses a *carB* hairpin RNA (hpRNA) (de Haro et al., 2009). Both plasmids were able to efficiently activate silencing of the endogenous *carB* gene in the wild type strain, giving rise to a high proportion of transformants that remained albino in the light, because of the absence of the *carB*

function (**Table 10**). However, the frequency of albino transformants was severely reduced in the *r3b2*$^{-}$ mutant, in which only a few colonies with albino patches were obtained. These results indicated that *r3b2* is required for efficient transgene-induced silencing regardless the nature of the silencing trigger, since sense and inverted repeat transgenes showed a similar reduction in the efficiency of silencing compared to the wild type strain. As expected, null mutants for the candidate RNase 136157 (MU450 and MU451 strains), which was previously demonstrated does not participate in the non-canonical silencing pathway (**Figure 33**), showed silencing frequencies similar to the wild type strain (**Table 10**), indicating that this putative RNase does not play any role in the canonical silencing pathway either.

III.8. The RNase III-like domain is essential for accurate R3B2 function in RNA silencing

III.8.1. Plasmid construction and site directed mutagenesis

The R3B2 protein (ID 80729) is annotated in the *M. circinelloides* genome (v2.0) as containing an amino-terminal RNase III catalytic domain-like of the SCOP (Structural Classification of Proteins) superfamily SSF 69065, and two C-terminal dsRNA-binding domains (**Figure 35A**). Comparison of the RNase III catalytic domain-like of R3B2 with the Ribonuclease III family signature (Prosite PS00517) identified several substitutions in conserved amino acids (**Figure 35B**). In fact, the invariant glutamic acid in the signature is changed to asparagine in R3B2 and the aspartic acid residue that is essential for catalysis *in vitro* (Sun et al., 2004) is substituted by glutamic acid.

To confirm that the R3B2 function in RNA silencing relies on its RNase III domain-like, we performed directed mutagenesis to change several residues of the domain and analyzed the ability of the mutant allele to complement the lack of R3B2 function in the *r3b2*$^{-}$ null mutant. The R3B2 residues H49, G55 and E56, which correspond to the highly conserved E38, G44 and D45 residues of the *E. coli* RNase III (Sun et al., 2004), were simultaneously changed to alanine (**Figure 35B**).

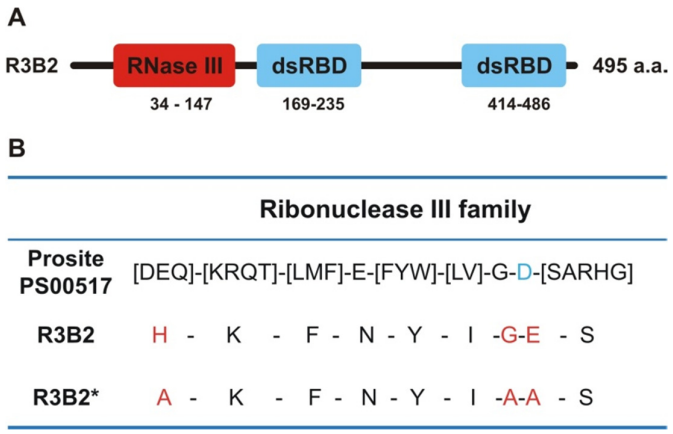

Figure 35. Domain structure and conserved residues of the *M. circinelloides* RNase III R3B2. **(A)** Domain organization of the R3B2 protein. Domains are shown by boxes with the starting and stopping amino acid of each domain indicated. RNase III: RNase III catalytic domain-like; dsRBD: dsRNA binding domain. **(B)** Signature motif of the Ribonuclease III family (Prosite PS00517). The conserved aspartic acid residue that has been demonstrated to be required for catalytic activity *in vitro* (Sun et al., 2004) is shown in blue. The corresponding sequences in the wild type R3B2 and mutant R3B2* proteins are shown below the signature, with the residues that have been changed in the mutant protein marked in red.

The *r3b2* mutant allele (*r3b2**), which contains the missense substitutions H49A, G55A and E56A, was generated by site-directed mutagenesis on genomic DNA by overlap extension using fusion PCR (Aiyar et al., 1996; Ho et al., 1989). Briefly, two overlapping PCR fragments of *r3b2* were amplified in a first round of PCR using the inner primers MutRev and MutFow (**Table 5**), which correspond to the sequences to be mutated, and primers F13 and R11 (**Table 5**) corresponding to upstream and downstream sequences to the sequences to be mutated (outer primers) (**Figure 36**). In a second round of PCR, the mutagenized *r3b2** region was generated with only outer primers and the first-round PCR products as templates. The authenticity of the sequence of the *r3b2** mutant allele was confirmed by sequencing. The 3,44 kb fragment containing the complete coding and regulatory regions of the *r3b2** mutant allele was cloned into the pMAT1253 plasmid, which expresses a *carB* hairpin RNA (hpRNA) under the control of the *gpd1* promoter, giving rise to plasmid pMAT772 (**Figure 36**). As a control, plasmid pMAT771, which contains a wild type *r3b2* allele and the hairpin *carB* transgene, was also constructed (**Figure 36**).

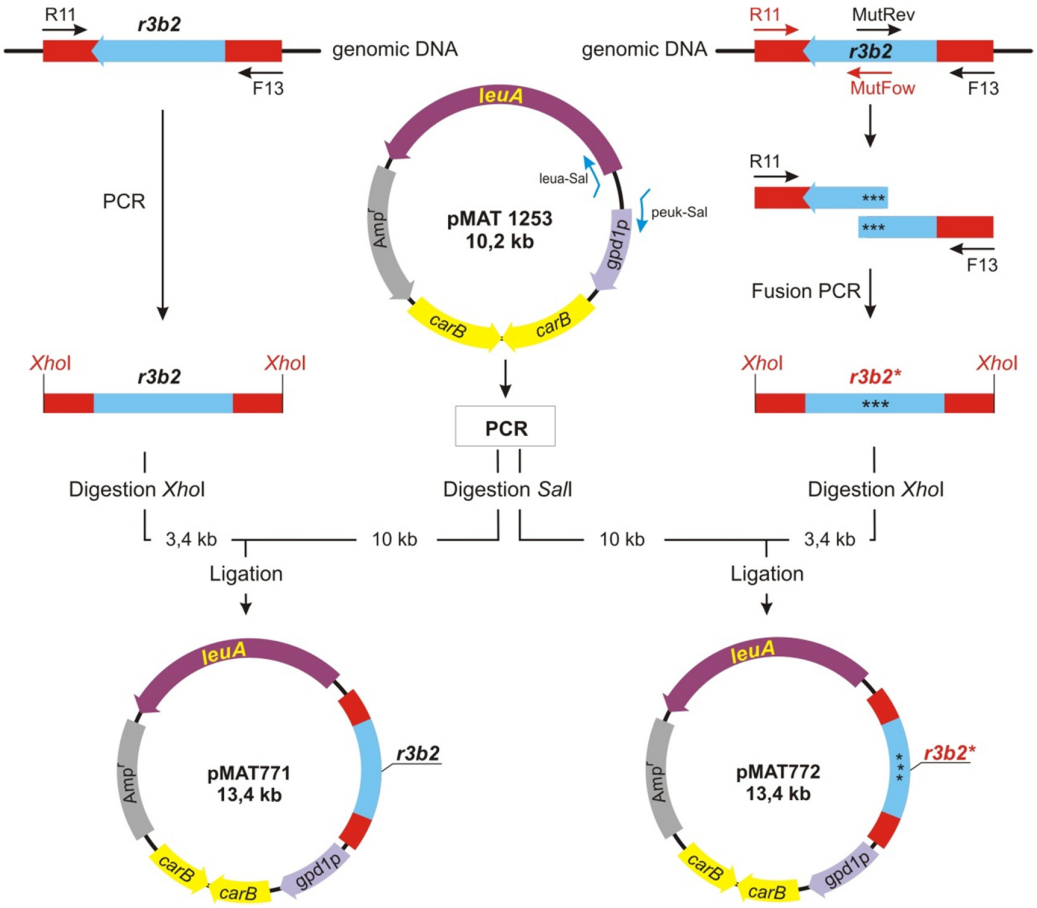

Figure 36. Construction of plasmids used for complementation analysis of the *r3b2*⁻ mutant. Plasmid pMA771 was constructed to complement the *r3b2*⁻ mutant. A 3,44 kb fragment of genomic DNA containing the *r3b2* coding region (light blue) and adjacent sequences (red) was amplified with primers F13 and R11 (**Table 5**), which include *Xho*I restriction sites. The *Xho*I-digested fragment was ligated to a 10 kb *Sal*I-digested fragment that had been amplified from pMAT1253 (de Haro et al., 2009) using primers leuA-Sal and peuk-Sal (**Table 5**). The obtained plasmid, pMAT771, contains the wild type allele of the *r3b2* gene, a silencing-reporter *carB* transgene expressing a hairpin RNA and the *leuA* gene as selectable marker. Plasmid pMAT772 contains the *r3b2** mutant allele, the hairpin RNA-expressing *carB* transgene and the *leuA* marker (purple boxes). The *r3b2** mutant allele, which contains the missense substitutions H49A, G55A and E56A affecting conserved residues of the R3B2 RNase III-like domain, was generated by site-directed mutagenesis using fusion PCR. The 3,44 kb fragment containing the *r3b2** mutant allele was cloned into the 10 kb *Sal*I-digested pMAT1253 fragment to give plasmid pMAT772.

III.8.2. Complementation analysis by self-replicative plasmids

Plasmids pMAT771 and pMAT772 were used to transform the wild type and null *r3b2*⁻ mutant strains and the ability of the transformants to silence the expression of the endogenous *carB* gene was analyzed. Transformation of the *r3b2*⁻ mutant with the control plasmid pMAT771 should simultaneously complement the null *r3b2*⁻ mutation and induce silencing of the *carB* gene. In fact, the silencing frequency in the *r3b2*⁻ mutant when transformed with this complementing plasmid was similar to

the wild type strain (**Table 10, Figure 37**), demonstrating that the *r3b2* wild type allele is perfectly able to complement lack of R3B2 function in the *r3b2*$^{-}$ mutant strain. The reduction observed in the efficiency of pMAT771 to induce silencing relative to other silencing vectors is probably due to the large size of this plasmid. This could result in a low plasmid copy number in the transformants, which has been demonstrated to negatively affect silencing efficiency (Nicolás et al., 2003). A similar silencing frequency was obtained when the silencing vector containing the *r3b2** mutant allele (plasmid pMAT772) was used to induce silencing in the wild type strain. However, this plasmid was barely able to activate silencing in the *r3b2*$^{-}$ mutant, indicating that substitutions of conserved residues in the RNase III domain-like of R3B2 greatly abolish the activity of this protein in the canonical transgene-induced RNA silencing pathway (**Table 10, Figure 37**).

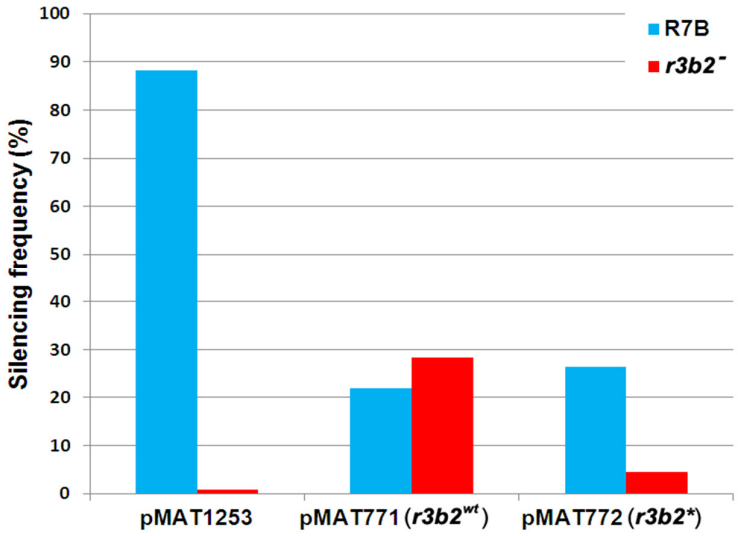

Figure 37. Complementation of the null *r3b2*$^{-}$ mutant with the wild type and mutant *r3b2** alleles. Graph represents the silencing frequencies of *carB* gene in the wild type and *r3b2*$^{-}$ mutant strains transformed with different silencing vectors. The silencing frequency of *r3b2*$^{-}$ mutant is dramatically reduced relative to the wild type strain when silencing is induced by the hpRNA-expressing vector pMAT1253 (Calo et al., 2012). Complementation with the wild type *r3b2* allele restores the R3B2 function in the *r3b2*$^{-}$ mutant, triggering silencing at similar frequencies as the wild type strain. However, the *r3b2** mutant allele was unable to complement the lack of R3B2 function and activate silencing in the *r3b2*$^{-}$ mutant.

III.8.3. Complementation analysis by integration at the *carRP* locus

To confirm the requirement of an intact RNase III-like domain for the R3B2 function in the non-canonical RNA degradation pathway, we constructed stable strains containing the wild type and *r3b2** mutant alleles integrated at the *carRP* locus. Integration at the *carRP* locus can be easily detected due to the color change provoked by the disruption of the *carRP* gene, which encode a bifunctional enzyme with phytoene synthase and lycopene cyclase activities (Velayos et al., 2000b). For the integrative complementation analysis, disruption fragments containing the wild type and mutant *r3b2** alleles flanked by sequences of the *carRP* locus were constructed (plasmids pMAT787 and pMAT788) (**Figure 38**). Plasmid pMAT787 was constructed to integrate the *r3b2* gene into the *carRP* locus. To construct this plasmid, the 3,4 kb *Xho*I fragment isolated from pMAT771 was cloned into pMAT1476 (Rodriguez-Frometa et al., 2013), a plasmid that includes the *M. circinelloides leuA* marker gene flanked by upstream and downstream sequences of the *carRP* gene. The *Xho*I site of pMAT1476 allows cloning of *r3b2* gene just downstream of *leuA* and, thus, keeping *r3b2* within the sequences flanked by the *carRP* upstream and downstream regions. Plasmid pMAT788 was constructed in a similar way, except that the *r3b2* fragment was excised from plasmid pMAT772 and contains point mutations in conserved residues of the R3B2 RNase III-like domain (*r3b2** mutant allele). A 9,8 kb integration fragment was released from plasmids pMAT787 and pMAT788 by *Cfr*9I digestion, amplified with primers carRP-F1 and carRP-R1 (**Table 5**) and introduced into the MU412 (*r3b2*$^-$ *leuA*$^-$) strain by transformation.

Only transformants that remain albino in the light were selected, since integration at the *carRP* locus provokes the disruption of the *carRP* gene and avoids accumulation of colored carotenoids. Those transformants were analyzed by Southern blot hybridization using as a probe a *carRP* fragment that recognized the wild type and disrupted alleles but could discriminate between them (**Figure 39A**).Results indicated that all but one of the five *r3b2*$^-$ transformants harboring the *r3b2** mutant allele were homokaryotic and had correctly integrated the mutant allele at the *carRP* locus (**Figure 39B**). Those strains were named MU458 to MU461. As a control, also three transformants harboring the wild type *r3b2* allele integrated at the *carRP* locus were obtained and were named MU455 to MU457 (**Figure 39B**).

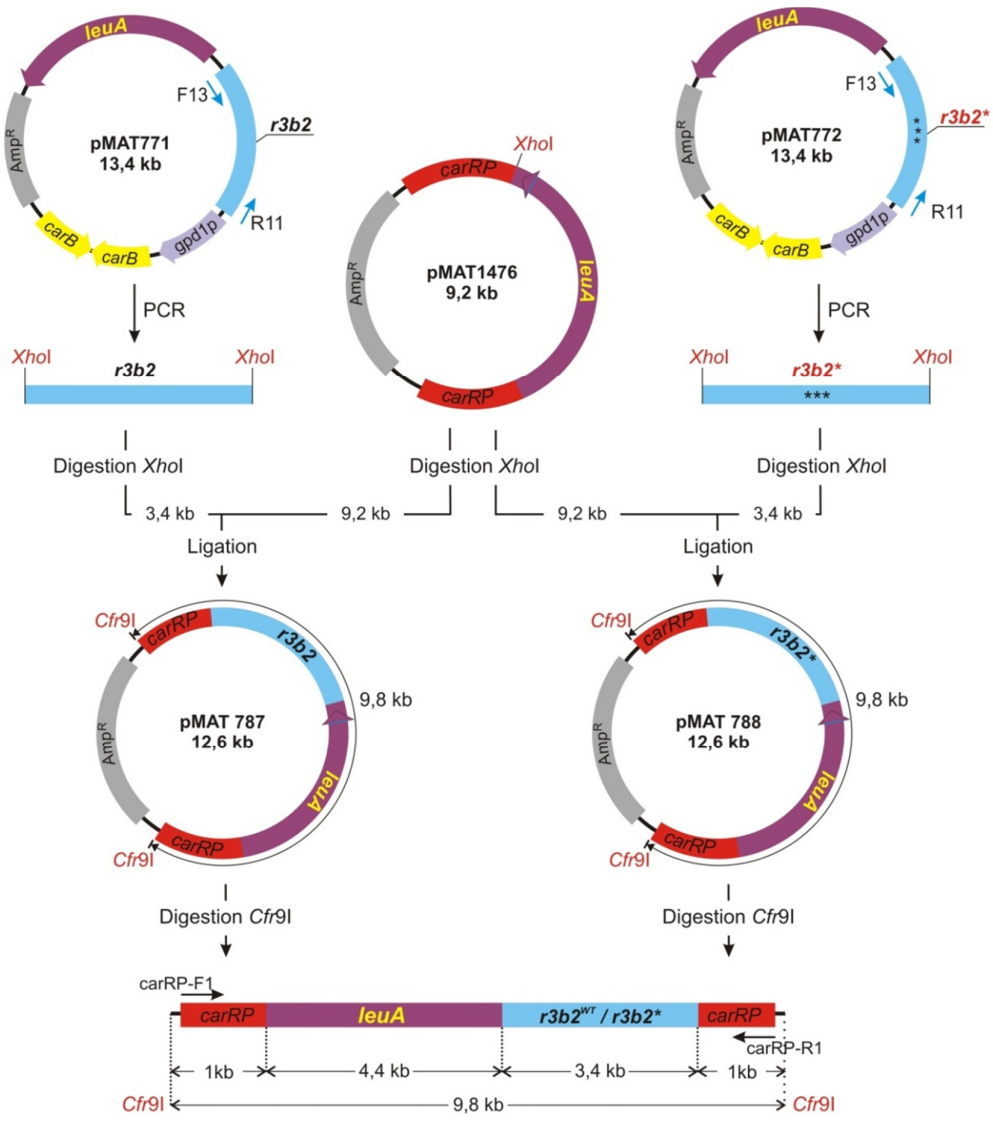

Figure 38. Construction of replacement fragments used for integrative complementation analysis. Plasmid pMAT1476 (Rodriguez-Frometa et al., 2013) contains the *leuA* marker gene (purple boxes) flanked by 1 kb of upstream and downstream sequences of the *carRP* gene (red boxes). The 9,8 kb disruption fragments contain wild type or mutant *r3b2* alleles (light blue boxes) and the *leuA* gene flanked by *carRP* sequences. Positions of restriction sites and primers used for cloning are indicated.

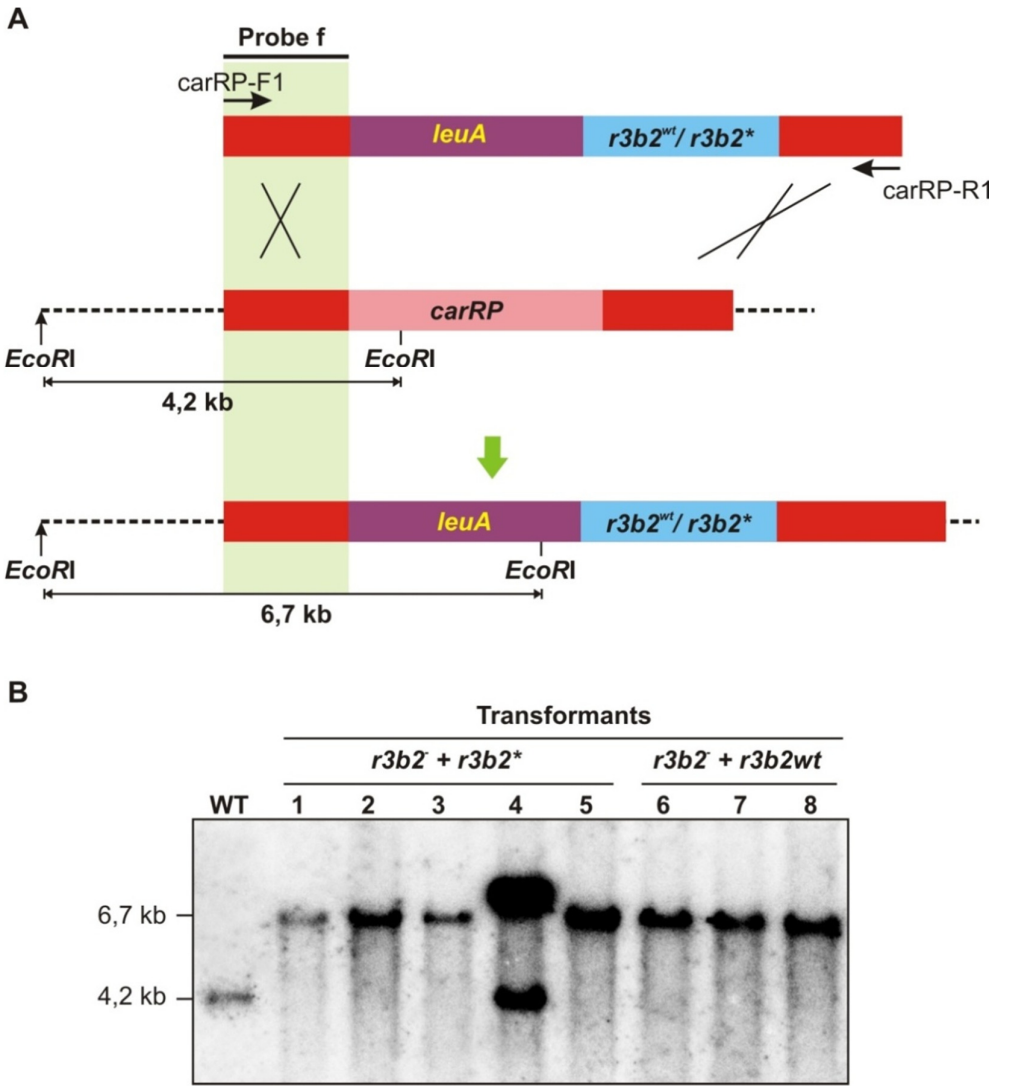

Figure 39. Integration of *r3b2* alleles into the *carRP* locus. **(A)** Schematic representation of the wild-type *carRP* locus (middle) and after homologous recombination with the disruption fragment (below). The disruption fragment contains the wild type or mutant *r3b2* alleles ($r3b2^{wt}$ and *r3b2**, respectively) (light blue boxes) and the *leuA* selectable marker (purple boxes) flanked by upstream and downstream sequences of the *carRP* gene (red boxes). Dashed lines indicate sequences not included in the disruption fragment. The position of the probe used (probe *f*) and the expected sizes of the *Eco*RI restriction fragments are indicated. The primers used to amplify the disruption fragment from the knockout vectors pMAT787 ($r3b2^{wt}$) and pMAT788 (*r3b2**) (carRP-F1 and carRP-R1) are shown (**Table 5**). **(B)** Southern blot analysis of the wild-type strain and transformants of the $r3b2^{-}$ null mutant strain containing the *r3b2** mutant allele (transformants 1-5) or $r3b2^{wt}$ wild type allele (transformants 6-8) integrated into the *carRP* locus. Genomic DNA (1 µg) was digested with *Eco*RI and hybridized with probe *f*, which corresponds to a 1,0 kb fragment that was PCR-amplified with primers carRP-F1 and carRP-R2 (**Table 5**).

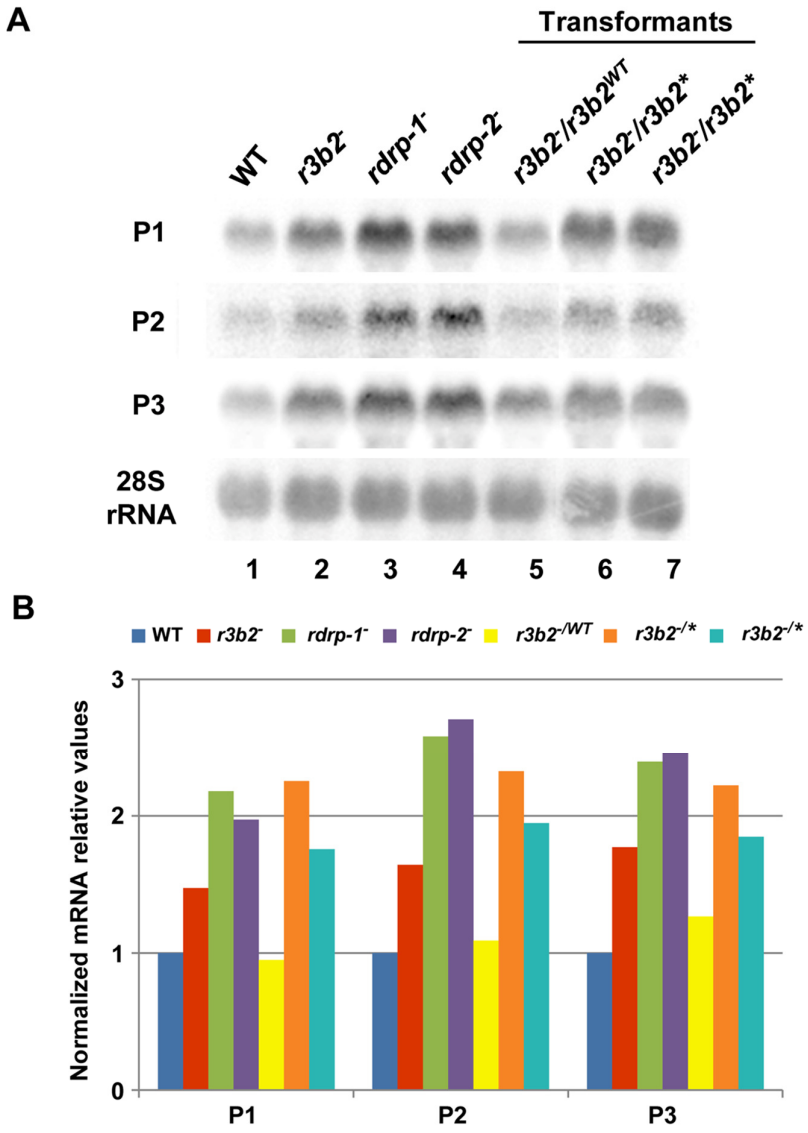

Figure 40. The RNase III domain-like of R3B2 is essential for R3B2 function. **(A)** Accumulation of mRNAs in *r3b2*$^{-}$ transformants harboring *r3b2* wild type or mutant alleles integrated at the *carRP* locus. Northern blots of high molecular weight RNAs corresponding to rdRNA-producing exons (genes P1 to P3) were carried out using total RNA (50 µg) extracted from wild type (R7B), *r3b2*$^{-}$ and *rdrp*$^{-}$ mutant strains (lanes 1-4) and transformants of the *r3b2*$^{-}$ mutants containing the wild type *r3b2* allele (*r3b2*^{WT}, lane 5) or the *r3b2* allele carrying mutations in conserved residues of the RNase III-like domain (*r3b2**, lanes 6 and 7) grown 24 hours in liquid MMC medium. Samples were separated in 1,2% denaturing agarose gel, transferred to membranes and hybridized with gene specific probes (**Table 6**). Genes P1 to P3 correspond to those indicated in **Figure 21**. Wild type and mutant *r3b2*$^{-}$ transformants correspond to transformants 6, 3 and 5 in **Figure 39**, respectively. Membranes were reprobed with a 28S rRNA probe as loading control. Images are representative of two independent experiments. **(B)** Densitometric analysis of expression data shown in (A). Signal intensities were quantified and normalized to rRNA levels. All data were again normalized with respect to the expression value of the wild type strain (R7B) for each gene.

Transformants containing the wild type or mutant *r3b2* alleles integrated at the *carRP* locus were used to analyze mRNA accumulation of genes regulated by the *rdrp*-dependent *dicer*-independent pathway. The three rdRNA-producing exons P1 to P3 were again used to analyze the expression of the corresponding genes by Northern blot hybridization (**Figure 40**). Results indicated that the *r3b2* wild type allele integrated at the *carRP* locus efficiently complements the effect of the *r3b2*$^-$ mutation on mRNA accumulation of target genes, since all tested genes up-regulated in the *r3b2*$^-$, *rdrp-1*$^-$ and *rdrp-2*$^-$ mutants recovered their wild type expression levels in the complemented strain (**Figures 40A** and **40B**, lane 5). However, the *r3b2*$^-$ transformants harboring the *r3b2** mutant allele integrated at the *carRP* locus showed an increased mRNA accumulation of the target genes similar to the recipient strain (**Figures 40A** and **40B**, lanes 6 and 7), demonstrating that the *r3b2** mutant allele was unable to complement the *r3b2*$^-$ mutation. Together, those results indicate that the RNase-like domain of R3B2 is required for the correct function of this protein both in the canonical *dicer*-dependent RNAi pathway and in the *rdrp*-dependent *dicer*-independent RNA degradation pathway.

III.9. An RNase family specific to mucorales

The domain architecture of R3B2 is unusual, since prokaryotic and fungal class 1 RNase IIIs contain only one dsRNA binding domain, besides the RNase III catalytic motif, whereas classes 2 and 3 of eukaryotic RNase III are larger proteins with several structural domains, as occurs in Drosha and Dicer (MacRae and Doudna, 2007). In fact, no proteins with the same domain architecture as R3B2 could be identified in the Conserved Domain Architecture Retrieval Tool (CDART) (Geer et al., 2002). To investigate the presence of proteins similar to R3B2 in the fungal kingdom, the fungal and oomycete genomics resource FungiDB (http://fungidb.org/fungidb/) (Stajich et al., 2012) was used. Sixty four organisms from 14 fungal classes are included in this data base, which allows searching for genes using different criteria. Searching for proteins similar to R3B2 identified nine proteins of this database with an expected value lower than one; all of them belonging to the order mucorales (**Figure 41A**). No other proteins were identified when using less stringent conditions, indicating that, within the fungal kingdom, the

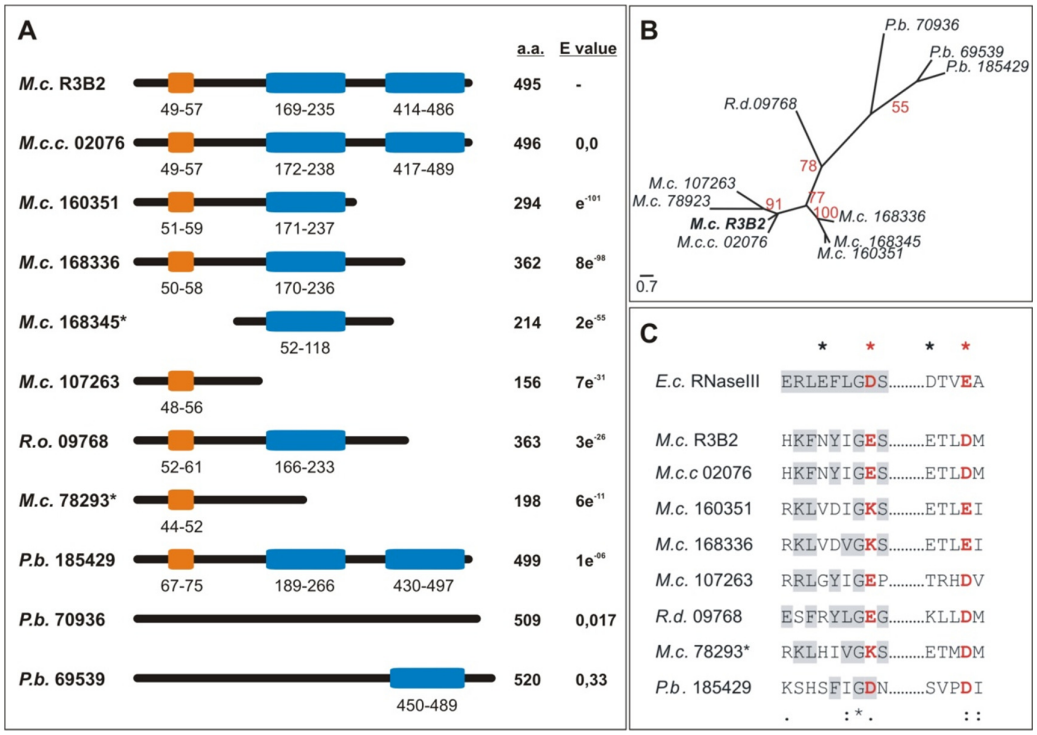

Figure 41. The Murcoralean RNase III family. **(A)** The domain organization of proteins identified in the FungiDB genomics database by their similarity to R3B2 is shown. Orange boxes signal the position of the RNase III family signature, with the starting and stopping amino acid indicated. Blue boxes correspond to dsRNA-binding domains. Total number of amino acid residues and the e- value obtained in the BLAST analysis with R3B2 are also shown. Asterisks indicate manual annotation of the corresponding sequences. **(B)** Phylogenetic relationship of *M. circinelloides* R3B2 protein (M.c. R3B2) and other mucoralean proteins. Phylogenetic tree was constructed using PhyML v3.0 aLRT method (maximum likelihood) (Guindon and Gascuel, 2003) from sequence alignment created using MUSCLE 3.7 with default setting (Edgar, 2004), using the Phylogeny software (http://www.phylogeny.fr) (Dereeper et al., 2008). Branch lengths are proportional to the number of substitutions per site (bars). The numbers at the nodes are bootstrap values (%) for 100 replications. FungiDB accession number of the proteins were: *M. circinelloides* QYA_80729 (*M.c.* R3B2), QYA_160351 (*M.c.* 160351), QYA_168336 (*M.c.* 168336), QYA_168345 (*M.c.* 168345), QYA_107263 (*M.c.* 107263) and QYA_78293 (*M.c.* 78293), *Rhizopus delemar* RO3G_09768 (*R.d.* 09768) and *P. blakesleeanus* PHYBL_185429 (*P.b.* 185429), PHYBL_70936 (*P.b.* 70936) and PHYBL_69539 (*P.b.* 69539). GeneBank accession number of the *M. circinelloides f. circinelloides* protein was HMPREF1544_02076 (*M.c.c.* 02076). **(C)** Amino acid residues of the R3B2 protein family in conserved regions of the RNase III domain. Signature motif in the RNase III domain and the catalytic residues of the *E. coli* RNase III are shown on the top. The strictly conserved acidic residues that coordinate metal binding are marked by asterisks, the red ones being demonstrated to be essential for catalysis in *E. coli* (Sun et al., 2004). *E. coli* sequences correspond to residues 38-46 and 114-118 (SWISS-PROT P0A7Y0). The amino acid residues of the corresponding regions in the R3B2 protein family are shown below. Residues matching the signature motif are highlighted in grey.

R3B2 protein family seems to be specific of the order mucorales. Most of the proteins identified contain RNase III-like and/or dsRNA binding domains, although the majority of them are smaller than R3B2. The phylogenetic relationship among the R3B2 protein family shows several *M. circinelloides* paralogous proteins highly similar to R3B2 (**Figure 41B**). It is not known if those proteins are expressed and if

their structure has been correctly annotated. However, it could be possible that one or several of them might play accessory roles in RNA silencing pathways, since some of them contain similar residues at the catalytic sites of their RNase III-like domains as R3B2 (**Figure 41C**). In fact, most of the proteins of the R3B2 family contain acidic residues at the catalytic positions, although three out of four *M. circinelloides* R3B2 paralogs have a positively charged lysine residue in one of these positions, raising doubts about their functionality. Moreover, none of the R3B2 paralogs have been annotated as containing RNase III domains in the *Mucor* genome, suggesting that their differences with the consensus sequence for this domain are too high to allow their detection as putative RNase IIIs.

We have also investigated the presence of proteins similar to R3B2 among sequences included at the National Center for Biotechnology Information Server (NCBI). No proteins, except those present in the publicly available *M. circinelloides f. circinelloides*1006PhL (ID HMPREF1544_02076) and *Rhizopus delemar* RA 99-880 (ID RO3G_09768) genomes were identified (**Figure 41**). Strikingly, the RNase III-like domain of R3B2 showed a limited similarity (best e-value 0,15) with the RNase III domain of different bacteria of the order *Burkholderiales*, although the domain of these bacterial proteins contains all the conserved residues of the RNase III signature. These data could suggest a horizontal transfer event between *Burkholderia* and an ancestor of the order mucorales and the generation of a fusion protein, with subsequent duplications and diversifications in different mucoralean lineages.

IV. RESULTS. CHAPTER II

The *M. circinelloides* genome sequence is now available. However, like in many other organisms, the relationships between sequence data, gene functions and phenotypes are still the main challenge for scientists. In this study, we developed a large-scale analysis of functional genomics to screen the relationships between genes and phenotypes in *M. circinelloides*. RNAi, a valuable tool for the analysis of gene function by knocking down gene expression, has been used to develop a functional genomics screening method in *M. circinelloides* by constructing genome-wide dsRNA libraries.

M. circinelloides is an emerging opportunistic human pathogen that causes the rare but lethal infection mucormycosis (or zygomycosis) in immunocompromised patients, such as those with diabetes, organ-transplanted, AIDS, hematologic malignancies, or trauma (Marr et al., 2002; Roden et al., 2005; Neblett Fanfair et al., 2012). Little is known about the virulence determinants in *Mucor*. Some pathogenic fungi present dimorphism, a process in which they can grow like hyphae or like yeast, depending on the environmental conditions. This yeast-hyphae transition contributes to fungal virulence. *M. circinelloides* is also a dimorphic fungus that grows as hyphal mycelium in aerobic condition and as yeast in anaerobic/high CO_2 condition. The transition between those two forms in this fungus was demonstrated to be involved in virulence, as the yeast phase is not pathogenic (Lee et al., 2013; Calo et al., 2014). In addition, the size of sporangiospores is also related to virulence in *M. circinelloides,* being pathogenic only the strains producing large multinucleated spores (Li et al., 2011). These results suggested that dimorphism and other phenotypic characteristics could be used as markers for a preliminary evaluation of virulence in this fungus. Thus, we have carried out large screening of phenotype changes using RNAi based libraries in order to identify candidate genes that could be involved in *Mucor* pathogenicity. For this purpose, we focused the screenings on phenotypes affecting dimorphism, growth and morphogenesis. These screenings identified two candidate genes that play important roles in the morphology of *M. circinelloides* and might be good candidates for further analyses of *Mucor* pathogenesis.

IV.1. Construction of genomic libraries

To construct genomic DNA (gDNA) libraries based on RNAi, vector pMAT1812 was used (see section II.9.1, **Figures 18** and **19**). This plasmid harbors two opposite promoters flanking a multi cloning site that allows the expression of dsRNA from the DNA fragment cloned between both promoters. It also contains a *carB* gene fragment that was used as a silencing marker (**Figure 18**). *M. circinelloides* gDNA was digested using different restriction enzyme combinations and then ligated with linear pMAT1812 (**Figure 19**) to generate the library. The ligation mixtures were transformed into *E. coli* DH5α to obtain libraries containing high copy numbers of each plasmid. Two gDNA libraries were isolated from *E. coli* DH5α and transformed into *M. circinelloides* with high efficiencies (**Table 11**). The first gDNA library obtained from ~35000 *E. coli* transformants was transformed into R7B strain producing ~14000 *M. circinelloides* transformants with a *carB* silencing (albino phenotype) frequency of 68,8%. For the second library, ~10000 *E. coli* transformants were obtained and after transformation of R7B, ~2800 *Mucor* transformants were obtained with a *carB* silencing frequency of 72,1% (**Table 11**). The presence of albino colonies indicated that the *carB* fragment present in the silencing vector produces dsRNA that triggers silencing of the endogenous *carB,* a gene required for the production of colored carotenoids (Nicolás et al., 2003). The high albino frequencies obtained demonstrated that the RNAi-based genomic libraries worked properly inside *M. circinelloides* cells.

Libraries	No. of *E. coli* transformants	No. of *M. circinelloides* transformants	Silencing frequencies (%)
1	35000	14000	68,8
2	10000	2800	72,1

Table 11. Transformants of two gDNA libraries. Numbers of *E. coli* and *M. circinelloides* transformants that were obtained after transformation with DNA from amplified RNAi-based libraries are shown. Silencing frequencies represent the percentage of albino colonies among transformants grown from spores obtained from the total number of primary *Mucor* transformants.

However, those silencing frequencies are lower than those obtained when silencing of the *carB* gene was triggered by other dsRNA-expression constructs,

such as pMAT1253 (Calo et al., 2012). This reduction could be the result of silencing with large size plasmids after ligation with digested gDNA. The *carB* fragment is located between the two promoters in pMAT1812. These promoters will generate dsRNA molecules from DNA fragments cloned between them, including the *carB* and fragments derived from cleaved gDNA. Thus, if the total fragment resulting from cloning the gDNA into pMAT1812 is too large, the two inverted promoters might not be able of producing dsRNA from all along the insert. In these cases, only ssRNA will be generated from both ends of the fragment, which triggers silencing less efficiently than dsRNA.

IV.2. Screening for abnormal growth or morphology phenotypes

The complex relationship between morphology and pathogenesis has been investigated in fungi, such as *M. circinelloides* (Li et al., 2011) and *C. albicans* (Kashem et al., 2015). The yeast form of *M. circinelloides* presents a hypovirulent phenotype (Lee et al., 2013; Calo et al., 2014), suggesting that strains with abnormal dimorphism could show altered virulence. Therefore, in order to find candidate genes involved in *Mucor* pathogenesis, we focused the screening on the abnormal growth and morphology of silenced strains. Thus, silenced strains were selected based on their changes in growth rate, sporulation efficiency and colony morphology compared with the control strain, which contains the empty plasmid pMAT1812. Spores collected from *Mucor* transformants were allowed to grow on YNB pH 2,8 medium to screen for rare and relatively stable abnormal growth or morphology phenotypes. Besides spores inoculated in YNB pH 2,8, small pieces of albino transformants were picked and grown on YNB pH 4,5 medium to characterized their morphology alterations at a different pH. After screening of colonies grown on YNB medium, we selected 11 transformants showing abnormal phenotypes (**Figure 42** and **Table 12**). The strain numbers 1 and 3 to 9 were collected from library 1, and strains 2, 10 and 11 from library 2. The phenotypes of these transformants are reversible, as they are easily converted to the wild-type phenotype by growing several vegetative cycles in rich medium. This suggests that the observed phenotypes are due to silencing of the clones genes, since silencing plasmids are gradually lost during growth on non-selective medium.

Strain	Growth rate	Sporulation	Colony characteristics
1	-	-	Very compact colony, growing like yeast
2	-	-	Very compact colony
3	-	-	Compact colony
4	-	-	Quite compact colony
5	-	-	Quite compact colony
6	+	-	Normal
7	-	-	Normal
8	-	-	Quite compact colony
9	+	-	Normal
10	-	-	Compact colony
11	-	-	Compact colony

Table 12. Characteristics of selected transformants. The minus signs show reduction of the corresponding characteristic compared to control strain (R7B strain transformed with empty plasmid pMAT1812). Strains 10 and 11 have similar phenotypes (**Figure 42**).

IV.3. Identification of candidate genes

One of the advantages of *M. circinelloides* as a model organism is the self-replicative nature of its plasmids, which are maintained as episomes and do not integrate into the host genome. Thus, to identify the sequence of the DNA fragments which are responsible for silencing of endogenous genes, size-selected DNA was isolated from the transformants and PCR-amplifications were carried out with two primers, peuka-1 and carbsal-1, flanking the insert fragment (**Table 5**, **Figure 18**) (see section II.9.2). The highest intensity PCR products from each transformant were purified and sequenced (**Figure 43**).

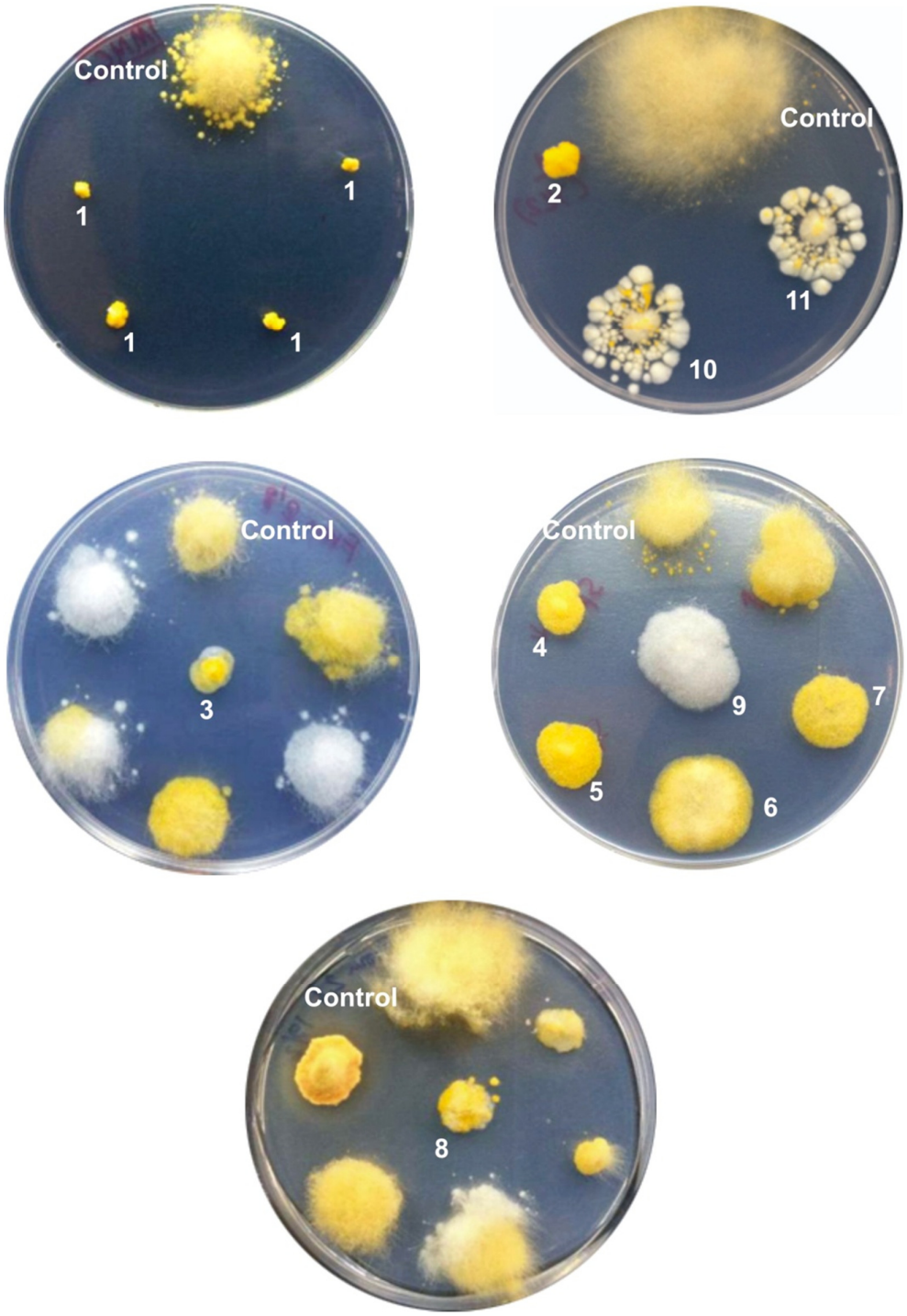

Figure 42. Selected *M. circinelloides* transformants after transformation with gDNA libraries. Control strain is R7B transformed with empty plasmid pMAT1812. The unnumbered colonies correspond to strains which loss their phenotypes after several vegetative cycles in selective medium. YNB pH 3,2 medium was used for growing those strains.

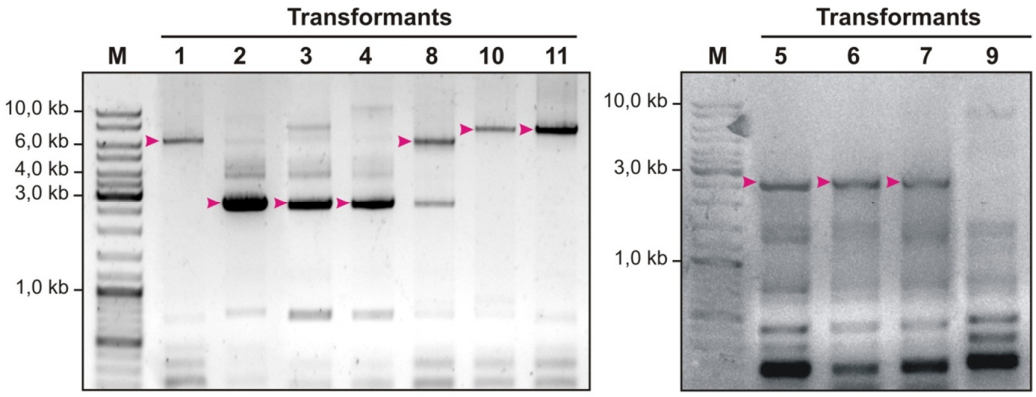

Figure 43. PCR amplification of the insert fragments cloned into pMAT1812. The numbers of transformants correspond to the selected strains (**Figure 42**). Transformants 2 to 7 have PCR products of the same size. Strain 9 did not amplify any specific fragment. The arrow heads indicate the PCR bands which were selected for sequencing. M, GeneRuler DNA ladder mixture (Fermentas).

Strains no. 2 to no. 7 generated a PCR product of the same size. It could be explained if these strains had the same inserted fragment. The variable copy number of transgenes inside the cells could result in different degrees of silencing and therefore diverse phenotypes. Strains no. 10 and no. 11 also generated the same size PCR products, and they also exhibited a similar phenotype. Therefore, it could be the result of silencing with the same plasmid. Several transformants produced a PCR product with a size of around 0,9 kb which was identified as the fragment resulting from an empty plasmid pMAT1812 (data not shown).

Once the sequences of inserted fragments were obtained, it was confirmed that transformants 2 to 7 had the same insert, as did transformants 10 and 11 with a different insert. The sequences were used to identify their locations in the genome using BLAST program in the genome database of *M. circinelloides* v2.0 filtered transcripts. The positions (coordinates) of the inserted fragments are shown in **Figure 44**.

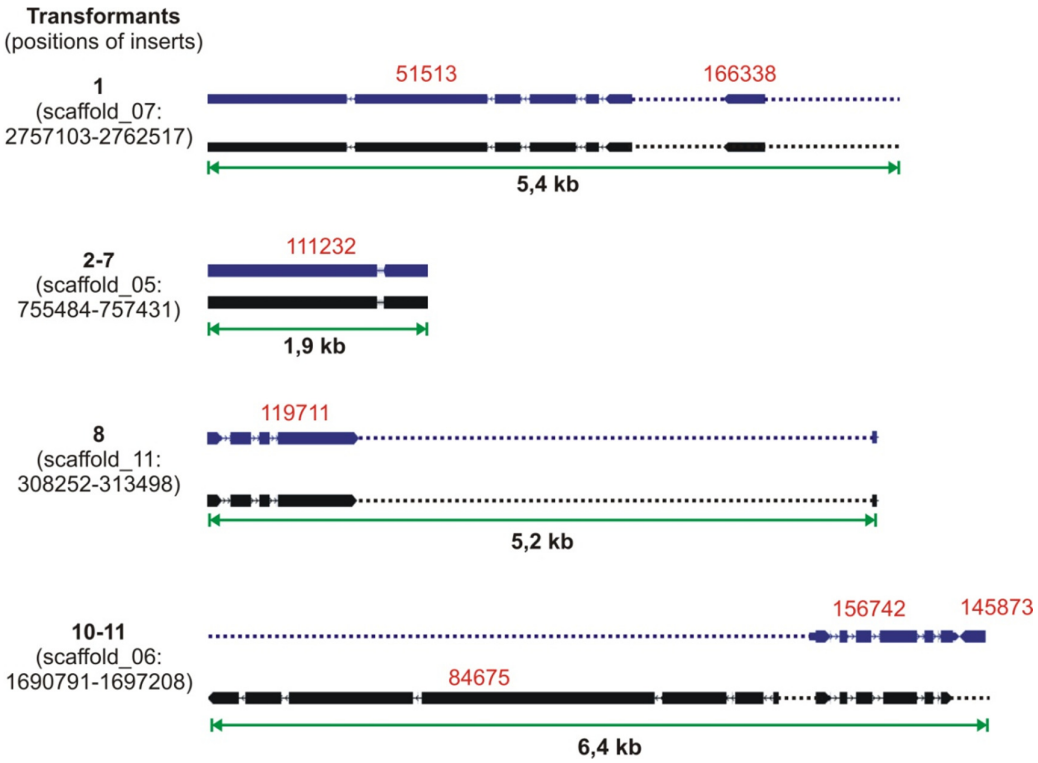

Figure 44. Identification of candidate genes in the *M. circinelloides* genome browser. The positions of each insert fragment corresponding to the selected strains are indicated as scaffold coordinates. The black and blue boxes indicate the genes that are annotated in genome version 1 and 2, respectively. Boxes and solid lines denote exons and introns, respectively. The orientations of boxes indicate the orientations of mRNA transcripts. The dashed lines denote the intergenic regions. The red numbers above each candidate genes denote their IDs. The green arrows with sizes in kb indicate the total length of insert sequences.

The identified candidate gene IDs correspond to their annotation in *Mucor* genome version 2.0, except for gene 84675 which is only annotated in the version 1.0. **Table 13** shows the size and brief functional descriptions of each candidate gene annotated in the JGI server (http://genome.jgi-psf.org/Mucci2/Mucci2.home.html).

IV.4. Silencing candidate genes

Several fragments from the RNAi library plasmids contained more than one gene. To identify the gene whose silencing was responsible for the abnormal phenotypes selected above, we constructed new silencing vectors for each candidate gene. These silencing vectors were used to transform the recipient strain R7B in order to validate the phenotypes obtained with the gDNA library (see **Figure 42**). If a silencing vector

generates a similar phenotype to the previously obtained with the library, it will confirm the role of the candidate gene in the phenotype observed.

Transformants	Candidate gene IDs	Sizes	Descriptions
1	**51513**	5,5 kb	Myosin class V heavy chain
	166338	0,3 kb	No description
2 - 7	**111232**	5,8 kb	Protein kinase of the PI-3 kinase family involved in mitotic growth, DNA repair and meiotic recombination.
8	**119711**	1 kb	Nucleic acid binding protein, RNA recognition motif, RNP-1
10 - 11	**84675 (v1.0)**	4,1 kb	Proton (H^+)-transporting two-sector ATPase complex
	156742	1,1 kb	Intracellular protein transport
	145873	1,9 kb	DNA repair protein RAD51/RHP55

Table 13. Functional description of candidate genes.

IV.4.1. Construction of silencing vectors

In order to construct dsRNA-expressing vectors with the target candidate genes, plasmid pMAT1812 was used as a cloning vector. Insert fragments corresponding to the 5' end of each candidate gene (0,5-2 kb) were amplified with primers containing *Not*I and *Xho*I restriction sites to facilitate cloning into pMAT1812 (**Figure 45**).

Plasmid pMAT828 harbors a 2 kb fragment of the gene 51513 which was PCR-amplified using primer pairs FYL1 and RYL1 (**Table 5**). Plasmid pMAT798 contains a 0,9 kb fragment of gene 166338 that was amplified by PCR reactions using primer pairs FYL1.2 and RYL1.2 (**Table 5**). Those two plasmids were constructed to confirm which gene was involved in the yeast-like phenotype of transformant 1 (**Figure 42**). To confirm the role of the gene 111232 in the phenotype of transformants 2-7 (**Figure 42**), plasmid pMAT831 was constructed by cloning a 1,2 kb fragment of this gene into pMAT1812, using primer pairs FYL2 and RYL2

(**Table 5**). Plasmid pMAT822 contains a 0,9 kb fragment of the gene 119711 that was obtained by PCR amplification with primer pairs F.YL8 and R.YL8 (**Table 5**). It was constructed to confirm the role of this gene in the phenotype observed in transformant 8 (**Figure 42**).

To identify the candidate gene responsible for the phenotype of transformants 10 and 11 (**Figure 42**), three different plasmids were constructed: pMAT823, pMAT824 and pMAT825. These plasmids contain 1,2 kb, 0,9 kb and 0,5 kb fragments corresponding to the genes 84675, 156742 and 145873, which were amplified using primer pairs FYL10.1/RYL10.1, FYL10.2/RYL10.2 and FYL10.3/RYL10.3, respectively (**Table 5**).

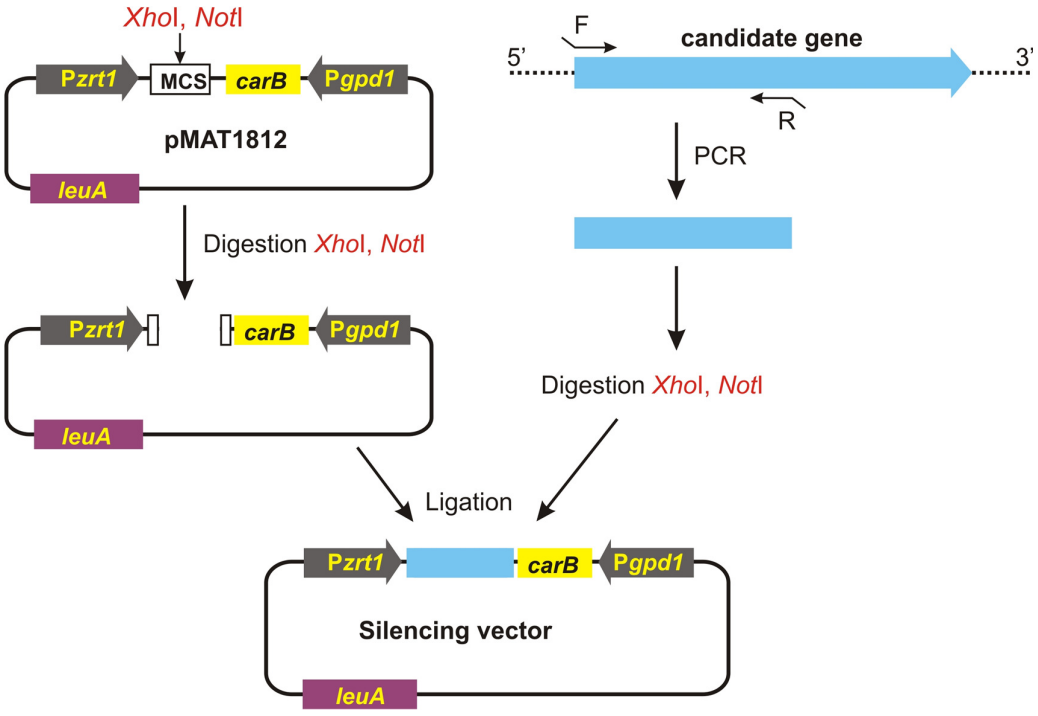

Figure 45. Construction of silencing vectors. Plasmid pMAT1812, containing two opposite promoters (gray boxes) flanking the reporter *carB* gene (yellow box) and a MCS (multi cloning site) region, was double digested with *Xho*I and *Not*I. A 0,5-2 kb fragment from the 5' end of each candidate gene (light blue box) was PCR-amplified using primers (F/R) containing *Xho*I and *Not*I restriction sites. The *Xho*I and *Not*I digested fragments were ligated into linearized pMAT1812 to produce the silencing vectors.

IV.4.2. Phenotypic analysis of silenced strains

Silencing vectors corresponding to each candidate gene were introduced into the recipient strain R7B in order to confirm the phenotypes obtained with the RNAi

libraries and to match single genes to their corresponding phenotypes. The results of these transformations are shown in **Table 14**.

Spores of the new transformants were screened on selective medium YNB pH 2,8 looking for similar phenotypes to those observed in the original transformants. Among the tested plasmids, only pMAT828 and pMAT823 induced the phenotypes previously observed in transformants no. 1 and no. 10-11, respectively (**Figure 46**). It is possible that the low silencing efficiency obtained with plasmids pMAT831 and pMAT822 precluded the observations of the phenotypes due to silencing of the candidate genes. More experiments will be needed to identify the genes responsible for the phenotypes of transformants 2-7 and 8. However, the results obtained confirmed the role of genes 51513 and 84675 in the induction of the phenotypes observed in transformants 1 and 10-11, respectively.

Original transformants	Plasmids	Target genes	No. of transformants	Silencing frequency (%)
1	pMAT828	51513	227	84,6
	pMAT798	166338	198	7,5
2 ~ 7	pMAT831	111232	205	12,6
8	pMAT822	119711	168	25,0
10 ~ 11	pMAT823	84675	183	65,0
	pMAT824	156742	228	47,9
	pMAT825	145873	159	62,3

Table 14. Transformation with different silencing vectors of the wild type R7B strain. Silencing frequency refers to the proportion of albino colonies among transformants.

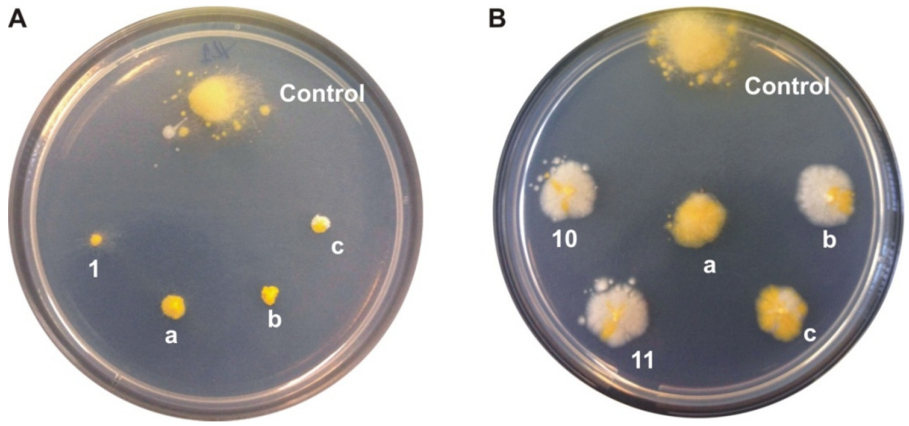

Figure 46. Confirmation of the phenotypes induced by silencing of the genes 51513 and 84675. **(A)** Strain 1 isolated from the original genomic library transformants grows like yeast and generates very compact colonies (**Figure 42**). Strains a, b and c were obtained after introduction of plasmid pMAT828 into R7B strain. **(B)** Similarly, strains 10 and 11 were isolated from the genomic library transformants (**Figure 42**). Strains a, b and c were obtained after transformation with the plasmid pMAT823 of the R7B strain. Control strain is a Leu^+ transformant collected after introduction of the empty plasmid pMAT1812 into R7B strain. Those strains were grown on YNB pH 3,2 plates at 26ºC during 72 hours under continuous light.

IV.4.3. Molecular analysis of silenced strains

In previous sections, the candidate genes were supposedly silenced by transgenes present in the RNAi libraries and later in the silencing vectors. Here, we will validate the silencing of the target genes in these isolated strains, both by testing the mRNAs degradation and the generation of the corresponding small RNA molecules.

IV.4.3.1. mRNA degradation in silenced strains

Northern blot hybridizations were performed using total RNA from the control strain (R7B transformed with pMAT1812) and the silenced strains obtained with both the genomic libraries and the silencing vectors. The membranes were hybridized with probes from loci 51513 (**Figure 47A**) and 84675 (**Figure 47B**). The results shown in **Figure 47** indicate a very low or no mRNA accumulation from the target genes in the silenced strains, both in the genomic libraries transformants (lane 2 in **Figure 47C**; lanes 2 and 3 in **Figure 47D**), and in the strains silenced by pMAT828 (lane 3, 4 and 5 in **Figure 47C**) and pMAT823 (lane 4, 5 and 6 in **Figure 47D**). These results demonstrated the action of a silencing mechanism that resulted in a significant reduction of mRNA accumulation.

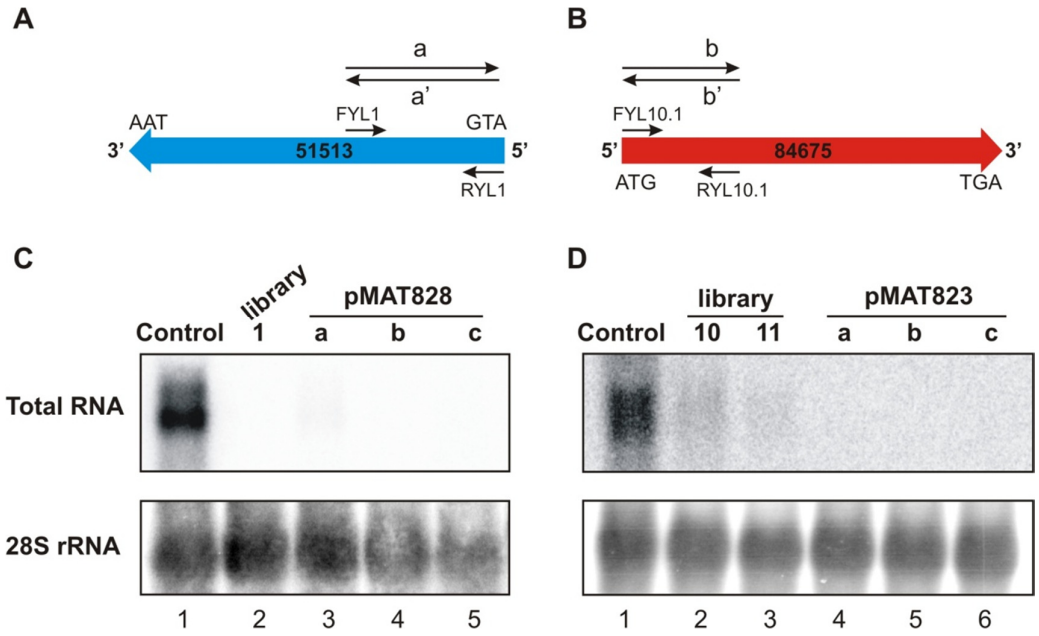

Figure 47. Northern blot analyses of transformants containing silencing constructs for candidate genes. Schematic representation of transcripts of candidate genes 51513 (**A**) and 84675 (**B**). The translation start and termination codons are indicated. The primer pairs FYL1/RYL1 and FYL10.1/RYL10.1 were used for PCR-amplification of probes for genes 51513 and 84675, respectively. Above the scheme, sense and antisense-specific riboprobes (a/a' and b'/b) used to detect small RNAs from genes 51513 and 84675, respectively (see **Figure 48**). **(C)** Accumulation of mRNAs in transformants containing silencing constructs for gene 51513. Total RNA (50 µg) was extracted from control (lane 1), silenced strain no. 1 isolated from genomic library transformants (lane 2) and three silenced strains a, b and c, selected from transformations with pMAT828 (lanes 3-5), grown for 48 hours at 26 ºC in liquid YNB pH 4,5 medium under light conditions. RNA samples were separated in 1,2% denaturing agarose gel, transferred to membranes and hybridized with gene specific probe prepared from PCR-amplification using the primer pair FYL1 and RYL1 (**Table 5**). The membrane was reprobed with a 28S rRNA probe as loading control. Images are representative of three independent experiments. **(D)** Accumulation of mRNAs in transformants containing silencing constructs for gene 84675. The experimental conditions were similar as those described in C. Northern blots were carried out using total RNA extracted from control (lane 1), silenced strains no. 10 and 11 isolated from genomic library transformants (lanes 2-3) and three silenced strains a, b and c, selected from transformations with pMAT823 (lanes 4-6). The corresponding probe was PCR-amplified with primers FYL10.1 and RYL10.1 (**Table 5**).

IV.4.3.2. Small interfering RNAs in silenced strains

To validate the presence of siRNAs in the silenced strains, we performed Northern blot analyses of small RNAs derived from 51513 and 84675 genes (**Figure 48**). Low molecular weight RNAs were isolated from control and silenced strains and analyzed as described in sections II.8.2, II.8.4 and II.8.5. The expected short antisense RNAs from silenced strains were detected at both 51513 and 84675 loci (**Figure 48**). These small antisense RNAs were detected as discrete bands of 20-25nt. However, small sense RNAs were not detected, probably because of the low

production and stability of this class of siRNAs, as it has been previously described (Nicolás et al., 2003) (**Figure 48**). The presence of small antisense RNAs in all the strains harboring silencing constructs and their absence in the wild type strain confirms that those constructs are triggering silencing of the target genes in the recipient strains and validates RNA silencing as the mechanism responsible for the lack of function of the target genes that causes the observed phenotypes in the transformant strains.

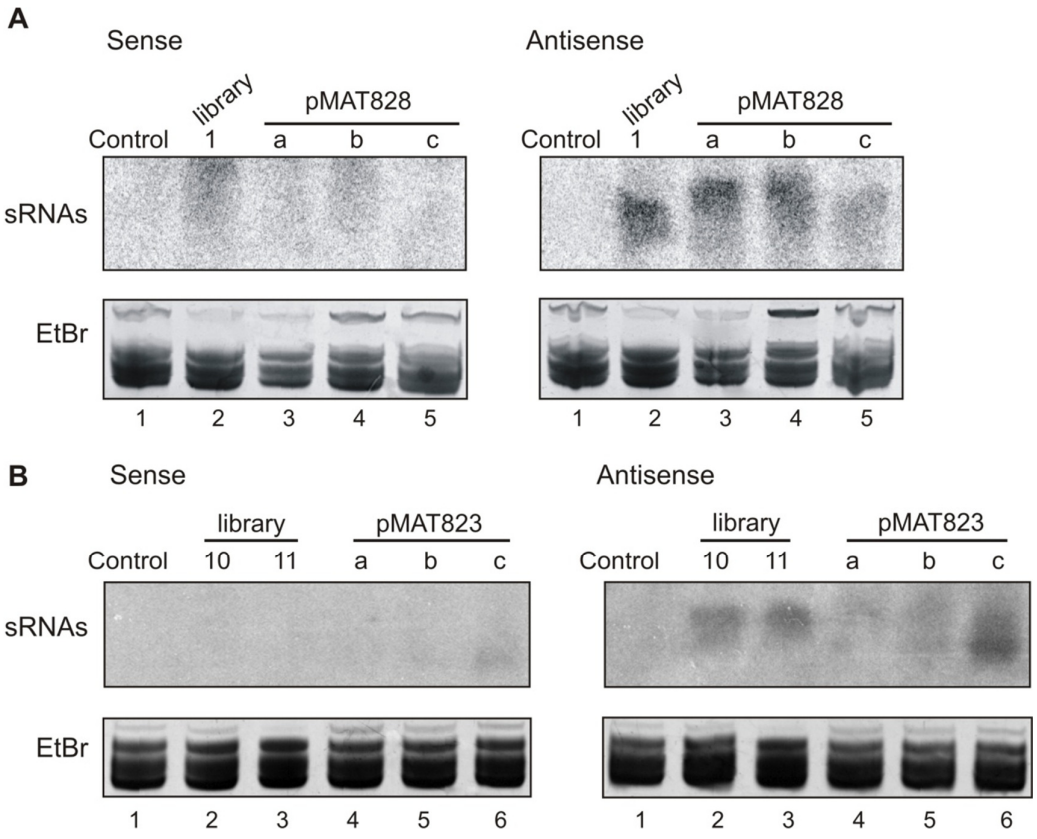

Figure 48. siRNAs associated with silencing of genes 51513 and 84675. **(A)** Accumulation of siRNAs in transformants containing silencing constructs for gene 51513. Northern blots of sRNAs corresponding to gene 51513 were carried out using low molecular weight RNAs (20 µg) isolated from total RNA. Lane 1: control sample (R7B transformed with pMAT1812); lane 2: silenced strain no. 1 selected from transformants obtained from genomic libraries; lanes 3-5: silenced strains a, b and c, obtained with pMAT828. Samples were grown 72 hours in liquid YNB medium pH 4,5 at 26ºC. Membranes were hybridized with sense and antisense-specific riboprobes (probes a and a' in **Figure 47A**, respectively). The predominant RNA species in the sRNA samples were stained with EtBr as a loading control. **(B)** Accumulation of siRNAs in transformants containing silencing constructs for gene 84675. Lane 1: control strain; lane 2 and 3: silenced strains no. 10 and 11 selected from transformants obtained from genomic libraries; lanes 4-6: silenced strains a, b and c, transformed with pMAT823. Samples were hybridized with sense and antisense-specific riboprobes (probes b' and b in **Figure 47B**, respectively).

IV.5. Two new candidate genes for *Mucor* pathogenesis

The silenced strains of each gene exhibited a significant reduction in growth rate and sporulation relative to the wild type. The defects on normal growth and sporulation (gene 84675) and yeast-like phenotype (gene 51513) could be related to pathogenesis in *Mucor*, since the rapid invasive hyphal growth that is required for virulence could be affected in these strains. Therefore, we decided to disrupt and analyze more deeply these two candidate genes. *In silico* analysis of the 51513 and 84675 genes using BLASTp application, NCBI and FungiDB identified those genes as homologs of *myo5* gene (coding Myosin class V) and *clasp* gene (coding Cytoplasm linker-associated protein), respectively.

IV.5.1. Nucleotide and amino acid sequences

The nucleotide and amino acid sequences of genes 84675 and 51513 were obtained from the *M. circinelloides* genome sequences (JGI). The size of 84675 gene (scaffold_8:261584-265746, *M. circinelloides* genome v1.0) is 4,1 kb, containing 7 exons and 6 introns (**Figures 49A** and **50**). The length of 51513 gene (scaffold_07:2754918-2760433) is 5,5 kb, containing 9 exons and 8 introns (**Figures 49B** and **53**).

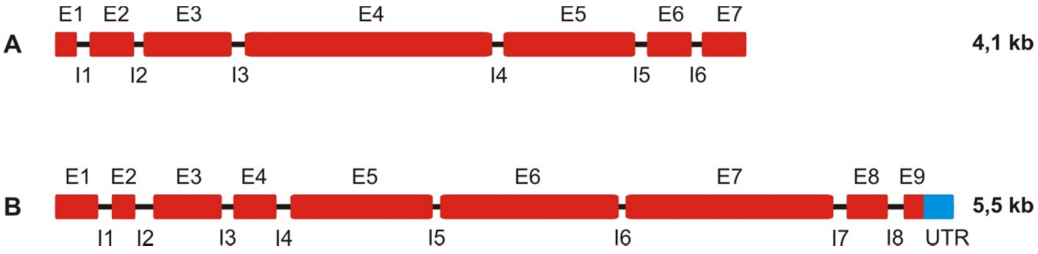

Figure 49. Schematic representation of genes 84675 and 51513. **(A)** Gene 84675 contains 7 exons (E1-E7, red boxes) and 6 introns (I1-I6, black bars). The lengths of red boxes and black bars indicate the relative lengths of exons and introns, respectively. **(B)** Gene 51513 contains 9 exons (E1-E9, red boxes) and 8 introns (I1-I8, black bars) and an untranslated 3´ region (UTR, blue box).

IV.5.1.1. Gene 84675

The phenotype observed after silencing of gene 84675 shows reduced growth rate and sporulation, suggesting that this gene could be involved in morphogenesis of *M. circinelloides*. This gene is unique in *Mucor* genome, since no homologous loci have been detected using BLAST program. By analyzing the entire sequence of this

gene, a region of 66 bp pyrimidine-rich sequence was observed upstream of the putative start codon, suggesting a promoter region (**Figure 50**). The gene 84675 contains a core promoter CAAT box-like sequence (CAAC) at 192 nt upstream of the ATG codon. This putative CAAT box-like has been also found in the *pyrG* gene of the fungus *Blakeslea trispora* (Quiles-Rosillo et al., 2003). The presence of CT-rich region suggested that 84675 could be a highly expressed gene in *M. circinelloides* (Gurr et al., 1987). This gene does not contain the canonical motif TATAAA at its promoter region. Instead, we found a TATAAT sequence (-167) located in the upstream region of gene 84675 that could be a putative TATA box (**Figure 50**). This putative TATA box sequence has been also found in the *pcbC* gene of *Penicillium chrysogenum* (Gurr et al., 1987). The complete coding sequence of gene 84675 contains 4163 nt and it is shown in **Figure 50**.

GAGCTCTGAACCGCCAGCAGAAGATGCCATGTTGTGTTGAGTAGGTACTGATAACAGGAAAAAAGTGT
AGAAAGGAAGAAAGACCTTGGCATTGCTGTATGCTGCAACAGCTGTTTCCATTGTGTGTGCTATAATC
TCCGTCTCATCACGTGCAGAGCAAAAAAGACATACATATGTGTGTGTTTCTCCTTCTCTCTCTCTCTC
TCTTTCTCTATTCCTCCTCTCTTCTTTTTATTTCCTTCTTTCTCGCTATATTGCTGTTTCATTGTATT
GGTACTTGACAATCAATCGGCAGCATGACTATACACAAAGATGAATCCACAGACGTAGATCCTGTACA
GGTAAAGCCCAACATCAAAGAAGAAGAGAAAAAAAAAAGGCACCCTTCAGGTACCAACACACACTTCT
AGATATGGAGTGCCAAAGACTTGGAGGCAGAATTCAACAAAATGCTGAAAGCATACCACGACAAGGAA
ACAGAGTTTAATTGGGAGGCAAGAGATCAAGCCATAACACGTTTGAGAGGTATTCTTCGAGGAAACGC
AACAGAATCACCGTACCTTGAAGTATTGATGCCATGTATGAAGCAGATGGTGGATGGCATTGTCAAAG
CCGTAAGTGCATGCGCTGTGCTCTGTGGGCCTGGAAACACACGCTAACAAACACACACACACAGGTCG
AGAGTCTTCGTACCCAACTGGCAGTCAAGGCCCTACTGCTGGTGACAGACATTGGTATCTACATTGGC
AGACATTTGGACAACTACACTACAGATCAGATCCTGCTGTGTATGATGCGGTGCTCTAGCTTGACCAA
AAAGATGGTCGCCAGCGCCTCGCTAGAGACCACCAAATCCTTTCTCAAGCACACCCAGTTCTACCCCA
AGATCACGAACATGCTCCACTTGTCCATGAACGAGAAGAACAGCCAGGTGAGACTGTATGCCATGGTG
TACACAAAGACACTGCTGCAGACACATGCGCATCATGACCGCACTCGACAAACCATGGATCGCAGCCA
CAGCACAGAGCAGTGCGAGACGATTCTGGTCAAGGGGCTAAATGATCCAATCCCGGCTGTGAAGGAAG
TGTGCAGAGAGGCATTTTGGATATTCTGGGAGCATTGGAGAGACAGAGGCGAGGGGTAACTATGATGA
CAGTCATGCTCGAGTAGGCTGCAAAACTAACACCGTGTACAGCATCCTGAGACAGCTGCCTCCAGCCG
CACAGAAGCAGCTGGAAAAGTCGAAAACCACCGCTCCCAAAGCCAACACGACCAGATCCATGCATAGT
CCCACGATATCGCCTCGCGCATCCAGTTCCTTGGGCAGACATCGCCACCACGACCTGTCGCCCTCCAC
CTCCAGCGCCTCAAACGGATCCCTCAAGCGATCCATGTCGCCCGCCAACAACCGAGCCGTGTCGCCAC
CGCATCTACGATCGCCCCCACCGCCGTCGTCAATCTCGTCTCAGATGCAGCAGGAACACCATCCACCT
CCTGCCCACAAAACGCGCGTACCCACATTGAACCGAAAAAAGTCAGCTGTCAGTTTAATCAAGCGAAA
GCCTACCAGCAATTTCATGAATCTGATCACAAGCGATGATGTGTTTCAGCGAGGTGAGGGCATTGTAC
TACTTGCAAAGAAACTGGCCCCTTTCCCTCCCTCATTTGATACCAACAACAACAACAACAATGAAATC
CAGCTGGATGTCCCCAACAGCCCGCCCGTCAGTGGCGACCAACTGCGTACGCTTGTCGTCAAGCTGTG
GGACGATCACTATCCAGAGCCCCTGTTTAGCTGGGATGCCGTCACTTGCATCATGTTTCGACTGCTGA
CGTTTGAAGAGTACATTCCCAAGTTGATACTGGAGGCCAATGCCGACGGCAAATCCGAGCATGATCTA
GTGAAACAGCAGCTGGCCCAAATGGGTCTCGTGAGAGCAAAGCTGTTTCTGCAATCCCAGCATCCTGC
GCTGGTGGACACCTTGTTCAACAGTCTGATCCAGTACGGCAACTTTGCTTCCACGACACACACCTCCT
CGTCGTTTGATAGAGTGGCGATTGGCAGCAAAAAAGACATGACCCGGTTGCCAGCCAACAGACGAAAA
CTCACTAGACAGTTTTTGGAATGGATGGACGAGCTTGTGACACCATTGATCGGGTTGAGCGAGGATGT
CGATGTTACAGCCAGAGCCTTTGAAGGCGTGCCTGCAGAGTATGTGGATCTCGTCAGCAACAGGGATA
GCCATGCAGCAGCAGCCTCCGCCACCTCAGAGTGGTTTGAATCCGATGACAACATACGACAATGCTTG
GCCATCCTGCTGCCTCTGATTACCACGTCAACTTCAGGCACCATGTGGCACGCTCCACTCGTCACCTT
TATCAAACACATCCGACTGCTCAACCAACGGCTGTTTGAGATGGTCACCACCACCTACGACGACTACT
CGGTCAACAAGATTTGCAGAGTGCTAGGCATCCACATCAGAATAGAGCCGCCTCTGTCAATCGTGCCA
CAGCAGCAACTCCTCGCCGAGGAACCCATGATGGCAGCGGCGGAGGATGATGAGCCTCTGTTTGAAGC

AGAGACACTGCCGCCCGCTCCCTTGATGGAATCCAGCGAGCCACCTGTCGCTGTGGACGAAGTGCTGT
TTGATGATCCTCCGCTCCATGCATCCAGCTCAGACTCGACATCGCAGCCCCTCATTGACGCCCCTTTA
GTAGACAGACTCACTATACAGGAGAACAACGACATTTTGGATCACGACGCTGATTTGATGCCCTCCTC
CACCGTCGCCGCCGCCGCCGCTACTGCCACACATTTCGATCATAGAAAGGAACAAGATGAAATTCCTA
TCCCTGACTACTTTAGCCCCAAGCAGAATGTAGTCGATGTTATGGTATGACAAGCATACACATCCGAT
TCGTATTATCAACTAAAAAGAAAAAAATCTTGATAGTATACTCACGACACTGATGGCTCTCCTACTGC
ATCCATATTAGACGGTCGCACGGTCTCTGGTACATCTACGTCAACAAAAACAACAAAGCAGGTTGTAT
CATCGTCTCCTCTTTTACCCCCTATTGATGCACCTCAACCAGTGACAAGCCAATCTGAGAAATCCTCG
TCAGAGCCACCACCACCATCCACAGTGACACCATTACCACAATCAGGATCAGAGTATGTGGCACCATC
TCCACCAGCGCCCACAGCAGCAGCGCCCACATCAGCAGCAGCAACACCGCCTCATGTCCCTGCACCCA
CAACACAGCTGCTGCCCTCTGAACCTAATTTAGAGACATATCCTCTACCCACTCACGTTCCATTCTTT
GCCCCTGAAAAAGTCAATTTCCCAAATCCCGTATTCAGATCCAATGTGCGAGCCAACATTGTCGCCGC
TTCTCAATCCACGACGACGACTTCCACGACGACCAATGGTACTTCCAACGCAAGACATCTCAAGGACA
AGACGACGCTGCTGTATACGTTGATAGATAAATTAAATTCTGCGACATTAGTGCCACCCGCAACAACA
ACAGCCCATGCCGATACATTTCGCAAATTGACCCGCTTGTTCAAGGAAGTGCCTATCCGAAGACGCTG
GGATCAAGGAGGCATTGAAGAAACCGGGAGCGAGACATGGGCTGGTGCGCTGGGTGATGCCGGCAACT
TTGTAGAAACGGTGCAAGCGATTCTGCCTCATCTGGACAACAACATTGTGGCATTGGAGTGCATCCGT
CAATTAGCAGTAACTCAAACGGGCCTGTTTCGTTACTATGAGCGAAAACTAGATGATCAAGGCAAGAG
CTTGGAATCGCAGCTCATGGAAAAACTATTGGACATTCGATGCAACGACAATCCTACGGTGAGTACGG
TCCTTTTGTTTATCGTACGCAATGCTGACGGTTTTCGGGTTTAGATTTGCGTTGCTGCAGAAGATGCA
TTAGATGCAGTTTTGGGTACATTGAACCCTCCCACGGCTTTCGAGATGCTAATGGCATTTGTTATTTA
TCGACTCTTAATATTGCCATGTAGCGAGGAATTGACCGACGTCAGATATCATCCTGTAGGCTCGGCAT
TTACGTATCTCGGTAAATGGGTCAAGGAGATGAACGAGACATTCTACATTGATGAATGGCTATCCAAG
CGTGGTGGCGTGAATGCCATTTTCAAGGCAAGTGTAACCATAGCAACGGACTGACCTATGATCTCATC
TTTCAGACATGATAGGCCATCAATCACCCTCTGATCAACATACGAAAGTCGTGCGTGGATGCCTTGGT
CGCCTTTCACGAAGTTCTTGGAGACGACATGTACCAATTTTTGGCAGATTTCAGGGAAGATCAACTCA
ATCTCCTCAAGTACTATGTTGCGAAATCACAAAAGAAGAAGATCAGTCTTCGGAGAGACAACAACATC
AATAACAACAACAACAACATGAGCAACGGTCAATTTTGATTTCAAAATATTTACAAACAAATCATTTG
TCCTTTTTGGACATTGCTGATTGATTTCGAGCTGCTTTTGCGATATACCCACCTTTTATTTCTCCCTC
TCTCTCTATATATCTCACTCTAACCTATATAAATAGTATCGTAATATATCACATTTTGGGGGAA
GCGTCAAAGAGTGAGAAACAGACATTGGATAAATATTTGGATTTATGCATCTTGGCCATGGTGAAATG
TGTAGCACATACACACGCACACGCATCATTTTACCCGCCACTTTCTATAATTTTCTTCTTGTTTCTCC
TTGATCGTCTCTGCGGGTGTGTGGGATGAATGGAATAATGCGAATGAAATAGATCCTGATTTACCCCT
GGATGTGTAATACTAGTGTATATCATTTGGCTGGTTAATTAAAAAAAAAAATAGAAAAAGGCTCTTTA
TATAAAAAAGGGTTTAATAACGCTTGATTTAGAAAAAGGGTTTGATTTTCTGCTCGTTCGGGT

Figure 50. Nucleotide sequence of gene 84675 (v1.0). The complete coding sequence and 296 and 500 nt of upstream and downstream regions, respectively, are shown. A putative CAAT box (-192) and a TATA box (-167) are indicated as blue and yellow boxes, respectively. The pyrimidine-rich sequence is underlined. The start and stop codons are highlighted as green boxes. Red and black letters denote exon and intron sequences, respectively. A putative polyadenylation sequence is indicated as a pink box. The upstream and downstream regions are indicated in gray letters.

Amino acid sequence

Protein 84675 contains 1271 amino acid residues (**Figure 51**). Using BLASTp application of NCBI server, we identified CLIP-associated proteins (CLASPs) as the more similar proteins to 84675, with a best E-value of 4e-39 for protein STU1 (XP_009266029.1), which is a member of the CLASP family in the fungus *Wallemia ichthyophaga* (excluding hypothetical proteins). The amino acid sequence of protein 84675 contains a cytoplasmic linker-associated protein domain (CLASP_N, Pfam12348, E = 1,46e-57) (**Figure 52A)** that is located between positions 22 and 253 of the amino acid sequence (**Figure 52B**). CLASP proteins are

widely conserved microtubule plus-end-tracking proteins that regulate the stability of dynamic microtubules, playing essential roles in cell division, motility and morphogenesis. In yeast, *Drosophila* and *Xenopus*, a single CLASP orthologous is present. In mammals, there is a second paralogue (CLASP2) which has some functional overlap with CLASP1 (Grallert et al., 2006; Pereira et al., 2006).

MTIHKDESTDVDPVQIWSAKDLEAEFNKMLKAYHDKETEFNWEARDQAITRLRGILRGNATESPYLEVLM
PCMKQMVDGIVKAVESLRTQLAVKALLLVTDIGIYIGRHLDNYTTDQILLCMMRCSSLTKKMVASASLET
TKSFLKHTQFYPKITNMLHLSMNEKNSQVRLYAMVYTKTLLQTHAHHDRTRQTMDRSHSTEQCETILVKG
LNDPIPAVKEVCREAFWIFWEHWRDRGEGILRQLPPAAQKQLEKSKTTAPKANTTRSMHSPTISPRASSS
LGRHRHHDLSPSTSSASNGSLKRSMSPANNRAVSPPHLRSPPPPSSISSQMQQEHHPPPAHKTRVPTLNR
KKSAVSLIKRKPTSNFMNLITSDDVFQRGEGIVLLAKKLAPFPPSFDTNNNNNNEIQLDVPNSPPVSGDQ
LRTLVVKLWDDHYPEPLFSWDAVTCIMFRLLTFEEYIPKLILEANADGKSEHDLVKQQLAQMGLVRAKLF
LQSQHPALVDTLFNSLIQYGNFASTTHTSSSFDRVAIGSKKDMTRLPANRRKLTRQFLEWMDELVTPLIG
LSEDVDVTARAFEGVPAEYVDLVSNRDSHAAAASATSEWFESDDNIRQCLAILLPLITTSTSGTMWHAPL
VTFIKHIRLLNQRLFEMVTTTYDDYSVNKICRVLGIHIRIEPPLSIVPQQQLLAEEPMMAAAEDDEPLFE
AETLPPAPLMESSEPPVAVDEVLFDDPPLHASSSDSTSQPLIDAPLVDRLTIQENNDILDHDADLMPSST
VAAAAATATHFDHRKEQDEIPIPDYFSPKQNVVDVMYTHDTDGSPTASILDGRTVSGTSTSTKTTKQVVS
SSPLLPPIDAPQPVTSQSEKSSSEPPPPSTVTPLPQSGSEYVAPSPPAPTAAAPTSAAATPPHVPAPTTQ
LLPSEPNLETYPLPTHVPFFAPEKVNFPNPVFRSNVRANIVAASQSTTTTSTTTNGTSNARHLKDKTTLL
YTLIDKLNSATLVPPATTTAHADTFRKLTRLFKEVPIRRRWDQGGIEETGSETWAGALGDAGNFVETVQA
ILPHLDNNIVALECIRQLAVTQTGLFRYYERKLDDQGKSLESQLMEKLLDIRCNDNPTICVAAEDALDAV
LGTLNPPTAFEMLMAFVIYRLLILPCSEELTDVRYHPVGSAFTYLGKWVKEMNETFYIDEWLSKRGGVNA
IFKASAINHPLINIRKSCVDALVAFHEVLGDDMYQFLADFREDQLNLLKYYVAKSQKKKISLRRDNNINN
NNNNMSNGQF

Figure 51. Amino acid sequence of protein 84675. The sequence and location of the amino-terminal CLASP domain (positions 23-253) is indicated in red color.

Based on the conserved domain CLASP_N identified in protein 84675 and comparing with other protein sequences in CLASP family (**Figure 52**), we propose *mcclasp* as the new name for gene 84675 of *M. circinelloides*. Using the alignment program ClustalW2 (http://www.ebi.ac.uk), we analyzed the genetic relationship of Mcclasp with other CLASP proteins (**Figure 52C**). These analyses showed that the Clasp protein of *M. circinelloides* seems to be early diverged during evolution, as expected from the evolutionary distance between *Mucor* and other model organisms (**Figure 52C**). Given the phenotypes shown by transformants in which the *mcclasp* gene has been silenced, it is tempting to speculate that this gene could be involved in

the cell division process by regulating spindle microtubule dynamics, as it has been demonstrated in other organisms (Maiato et al., 2003).

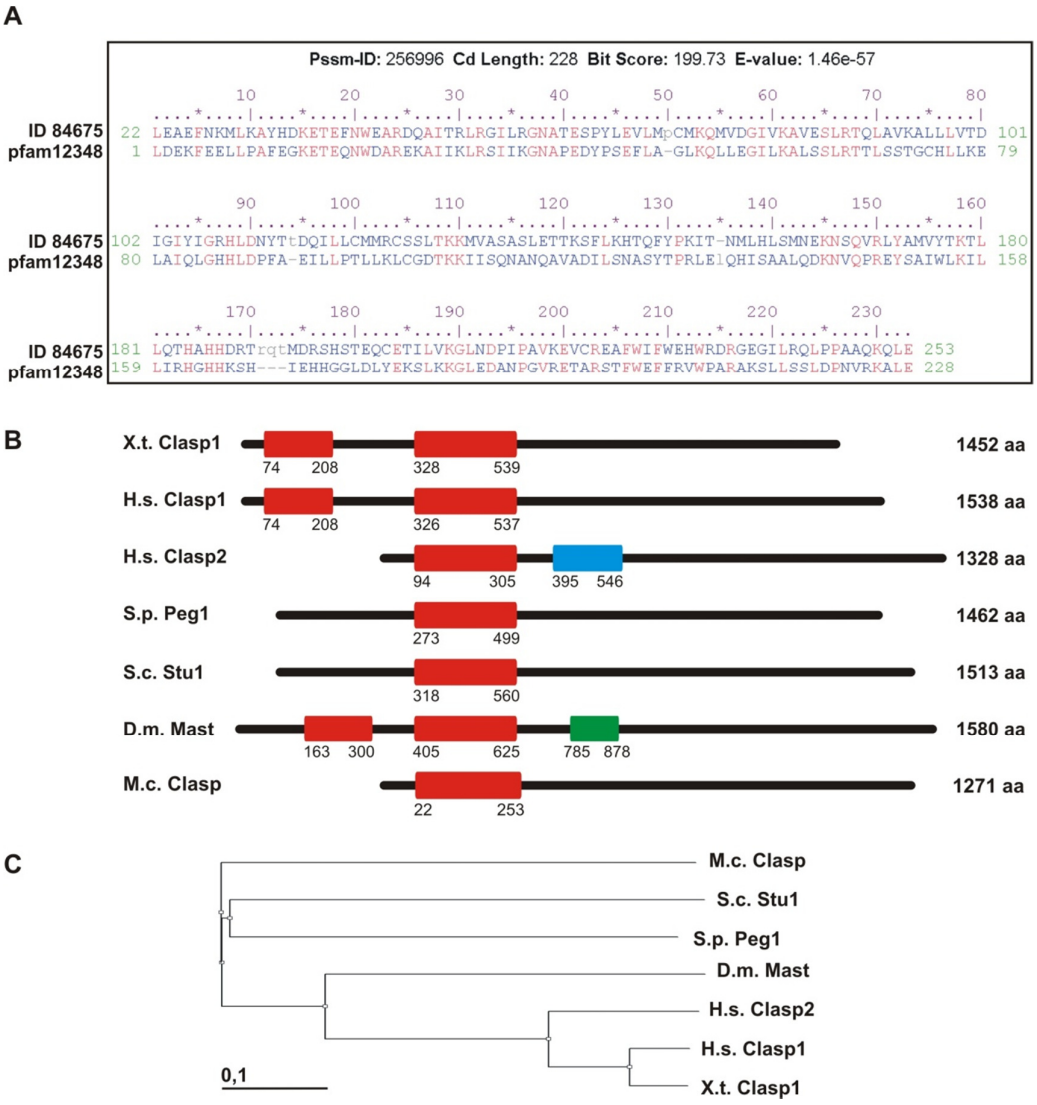

Figure 52. Domain structure of *M. circinelloides* Clasp and its genetic relationship with other Clasp proteins. **(A)** Alignment of amino acid sequence of protein 84675 with CLASP_N domain (Pfam12348). E-value is indicated. **(B)** The domain structure of the *M. circinelloides* Clasp predicted protein is compared to CLASP proteins from different species. The name and length of each protein and the positions of their domains are indicated. The red, blue and green boxes indicate CLASP_N domains, DUF2967 domain (cl12728), and senescence regulator domain (cl04561), respectively. X.t., *Xenopus tropicalis*; H.s., *Homo sapiens*; S.p., *Schizosaccharomyces pombe*; S.c., *Saccharomyces cerevisiae*; D.m., *Drosophila melanogaster*; M.c., *M. circinelloides.* These domains were identified using the Conserved Domain Database (CDD) search of NCBI (http://www.ncbi.nlm.nih.gov/cdd). **(C)** Phylogenetic tree showing the relationship and genetic distances among CLASP proteins from different species. The abbreviated names are the same as in part B. The tree was built using ClustalW2 program (http://www.ebi.ac.uk).

IV.5.1.2. Gene 51513

The coding sequence of gene 51513 is 5516 nt long (**Figure 53**). Results from previous sections suggested that gene 51513 also plays a significant role in *M. circinelloides* morphogenesis, since the 51513-silenced strains grow like yeast under normal growth conditions (aerobic, 26°C). There are several proteins in the *Mucor* genome that have high similarity to protein 51513 (**Table 15**).

Analyses of the nucleotide sequence of gene 51513 showed that it contains 9 exons and 8 introns. A region of 29 bp pyrimidine-rich sequence located upstream of the putative start codon could correspond to a possible promoter region. We also found a TATA box-like sequence (TATATC) at position 195 nt upstream from the ATG codon (**Figure 53**). This putative TATA box has the same sequence as the TATA box-like that is located at position -264 of the promoter of *EfPKS1* gene of the citrus pathogenic fungus *Elsinoë fawcettii* (Liao and Chung, 2008) and *ymL33* gene of *S. cerevisiae* (Kang et al., 1991). Gene 51513 seems to lack the conserved canonical CAAT box. It contains the sequences CAAT and CAAG at positions -409 and -244, respectively, although they may be too far to have a positive function. The presence of CT-rich region suggests that gene 51513 could be highly expressed in this fungus (Gurr et al., 1987).

CATATCAATCAAGGTCAAATCAAGCGAAAAAAAAATCAAGTTGTAGTACAAAATCAAAGCCATCAAGA
TGAAGCCAAATAGCCTATTCAAATCTTGCAAAATCAAAAGCTGCCTAATATTTCACTGAATAAAGTTA
TATATATATCTCAAAAAGCCCATTGCTTATGCCATTAACGAGAATGCTTATATACCAATCTCTTGAGG
CTTTCAAGAGCCTTCTCTGTTGAGATGTGCTGGGGGGGAGGCAGCTGGCAACTTTTCAGATCATTTCA
TGGCTTCACTTTCTGCCACATTGCATCTGGTTTAGTTGGCGCAAGCTTTCTCAGCAGATCAACTACTA
CTACCACTGCTACTAGCAAGTGTCATCCTGTATTGGATTCAGATTAAAACTCACTAAATTGTGGC**TAT**
ATCCCCCTCCCCCCCTTTATTTGAAGTTGCCTAATCCGTCTCTCTCTGGTACTCGTTACACACAAAGG
TTTTTTGTATTTATTTGTGTGTGCGAGAGAGCTCATATTATTCGGCTTTCTTTCTTCTTTCCATCTTT
TATTTTATATCTATCCGTACATCGACTCACACAGATCCAAGCTATAGATATAAAATATGGACAGTCTA
TCTTCAGGAGTAGCACAAGCTGTTCAAGTATACACAAAAGGTACCAAAGCCTGGTTTGAAGACGAAGA
CGAGGCTTGGGTGTCAGCCTCCGTACTTTCAAAAGAAGAATCAGGCACAGGTGTCAAGATTATATTTC
AAGACGATAAAGACGAAGGAAGGGTAAGCATCAAGATGGTGTGGGATTGCAGCATGTCAACTCATGTT
GTCTGTTCTAGGAACATGTCTTTGAGTGCACCTATGCTTTGCTCGAGAAGCAAAAAGGTGCCAATTTA
CCGCCACTTCGTAACCCACCGAGACTAGAGAATACAGAGGATCTAACCAACCTGAGTTACTTGAACGA
ACCCTCAGGTAAGTGAAAGAGTGCTTCCCCCACCCTTTATTCAAATAACAAGAGAGCACTACTGAAAC
GCTGTACCTTTTTTTTTTCTAGTTTTAAATACAATTCGAACACGTTACTTTCAACGTAATATTTACAC
CTACTCTGGCATCGTTTTGATTGCAGCGAATCCATTTGCCAGTGTACCATTGTATGAGCCTGATATCA
TTCAGCAGTATTCGGGCAGAAGACGTGGAGAGCTGGAGCCTCACTTGTTTGCCATTGCCGAAGATGCG
TATCGCTGCATGGTCAGAGAAAAGTCAAATCAAACAGTGGTTGTGTCTGGTGAAAGTGGTGCAGGTAA
AACTGTATCTGCCACGCACATTATGCGTTATTTCGCTACGGCTGATGATCAAGAATCTGGAAAAATCA
AGGATGTTGCGCAAGGCATGACAGAAGTGGAAGAACAAATCATGGGTAAACAGTGCACGCTCTCGCCT
TGGAAATCGACTAAGCCCTCGTCTAATCACCAAGCTTTTTTTTTTCTTAGCCACAAATCCTATTATGG
AGGCATTTGGTAATGCTAAAACAACGAGAAACAACAACAGTTCGAGATTTGGTAAATACATTGAAATC
CAGTTTGATAATCGATGCAACATTGTGGGCGCCAAAATCAGAACCTACCTTTTGGAGAGATCAAGATT

GATTTTCCAGCCCGAGTCCGAGAGAAATTATCACATCTTCTATCAGGTACGTTTTATAATAGACTATA
CAGCCCATCTGTTGATATCATTCTCACATGGGGGGATTAGCTCTGTACAGGTGCGCCCATCAACGAAC
GCAAAAATTTGGAATTGGGCGATTGGAACAAATTTCACTATCTCAACCAAAGTGGCGTTGGATCCATT
CCTGGTGTAGACGATGCTGCCGAATTCGAGTTGACTCAAAAGTCCCTGTCGTTGGTCGGTATCTCTGT
CGAAGCGCAATGGCACATTTTCAAGCTCTTGGCTGCCTTGCTTCACATTGGTAACATTGAAATCGGCG
GACGACAAGACGCCACCTTGACAGAAGATCAGCCTGCCTTGATCACTGCTACCAAACTACTGGGCATC
AAGACGTCCGAATTCAAAAAGTGGTTGGTCAAGAAGCAAATCATCACTCGCAACGAAAAGATTGTCAA
GAACCTAAACCCCACACAGGCCACTGTGGTCAGAGATTCCGTGGCCAAATACATTTATGCAAGCTTGT
TTGACTGGCTGGTCAAGGTGGTCAATGACAGTCTATCGTGTCAAGAAGAAGGACTGGTGCGCACCTTC
ATTGGTGTGTTGGATATCTACGGTTTCGAGCATTTCAAAAAGAACTCGTTTGAGCAGTTTTGTATCAA
TTACGCCAACGAAAAGTTACAGCAGCAGTTCAATCAACACGTCTTCAAGCTGGAGCAAGAGGAATACG
TCAAGGAAAAGATTGACTGGAAGTTTATTGATTTCAGCGACAATCAAAAGTGTATCGAGGTCATTGAG
TCCAAGCTGGGTATCTTGTCCCTGCTGGATGAGGAATCCAGAATGCCCTCAGGCACGGATCAAGGCTT
CATCAACAAGCTGTATTCCAGTTTTGCGGATCCCAAATACAAGGATTACTTCAAGAAGCCTCGTTTCT
CCAACAGCGCTTTCACCGTGGTGCATTATGCGCACGAAGTCGAATACGATGCCGAGGGCTTTATCGAT
AAGAACAAGGATACTGTGCCTGATGAACTGTTGACCTTGCTGCAAAATGCGGAATCAACCTTTTTAGT
GGACATGCTTCAAACAGCCACTGCTGCTGCTTCTGCTGCCAGCCAAGAAGCCAAGGTAATGTAGCTAA
TGATTGCCCCCCCCCCTCGCCCCGCCTTATCCACCAACACCTTATTTCTTTATAGCCTACGCCTGTCA
AAAAGGTGGGTATGGCCATTGCCAAAAAGCCCACACTGGGTTCCATCTTCAAGCTCTCACTGATCAGT
CTAATGGACACCATCAGCAAAACCAACGTGCACTATATTCGCTGTATCAAGCCAAACGAAGCCAAGGT
AGCTTGGGGATTTGAGCCCAACATGGTCCTGTCGCAACTGCGTGCATGTGGTGTGCTCGAGACGATTC
GCATCAGTTGTGCTGGCTACCCCTCGCGATGGACATTTGAAGATTTCGCAGAGAGATTCTACGCGCTT
GTCAACTCACAATACTGGGACCCCAACTTATCGCCCGACATCAACAAGCTGTGTCATGTCATTTTGGA
CAAGTACATCAAGGACGCTGACAAGTACCAGATTGGTTTGACCAAGATCTTCTTCCGTGCGGGTCAAC
TTGCCTACCTGGAAAAGTGCAGACGCGAGCGTTGGGACGAATGCACCATTTTGCTGCAAAAGAACATG
CGTCGCTTCATTGTGCGTATTGGCTACCTTCGTAAACTGGACCTGATTTCGCGCCTGCAACGTGTGGC
TCGACAAAAGATGGGCGTCCGAAAGCTGGAACTGGCGCGTCAAGAGATTGCTGCCATCAAGATACAAA
CCGAATGGCGTCGCTACATTCAACGCAAGCGCTACTTGAAGCAACGTGCCTTTGTCATTCATTTGCAA
GCCGCCTGTCGATCGCATCTCACGCGCAAGACGTTTGCTCACATCCGAGAGCATTTCGCTGCCATCAA
GATTCAAAGCATGGTGCGTGGATGGCGTGTGCGCAAGGAGTTTTTGGCCAAACGTCAAGTGGCTATCC
AGATCCAAACCTGTATTCGTCGTCGCTTGGCTCGCAAGGCGCTATTGGCTCTCAAGCAGGATGCTCGT
TCTGCCAACCATTTCAAGGAAGTCTCCTACAAGCTGGAAAGCAAGGTAGTCGAGCTCACTCAGAGCGT
CACTCAGTACAAGGATGAAAAGGATCAATTGCGTCTCAAGGCAAACGCGCTGGAAATGCAGGTCAAGG
ATTGGAGCGAAAAGTACGAGAAACTGGGCGAAAAGGCACGCTCCCTGGAGCAGTCTGCCGATACCTCT
GAACTGGAGCGTCAACTAGAGAGCTTGCAAGTGGAGCGCAATGGCATCCAAAACGATTATCGAAACTC
GTTGGAGCGCATCAAGAAACAAGACATGGAGATTGCTCGCTTGAATGAAGAGCTGCAGCGTCACAAGG
ATGAAATCACCAAGCTCAAGCAAGCCCACAACCAACAGCAACTGCGATCGCCCGTCAGTCCCAGTAGT
GCGTCTCCCTTTTCTGCTTCTGCGGGTGGTGGCGATGAAGAAGTGGCTGAACTCAAGAGTCAGATTGT
CGCCTTAAAGGCACAACTCTCTCAATCGCTCAAGAACCATCCCAAGCGTCAAGCCTCCATCAATGCGT
ACCGCACCTTGTCTCCTCAACGTAGTGGTGATCGTCGTGGCATGTCACCTGATTACAACCGTGGACGC
TCTCCCAGTGCCGATCCTCGTAACCGATCTCCCAGTTCATTGGCTGTGCGTCGTAGCAGCATAGGTGA
TAGAAGAACCGAGCCCAATGGCAACAACAACCACTATGCCAACACGGGCGGTGCTAATGGTGGTGCTA
ATGCCGCCAAGATGATTTATGCTGAGCCCGAGCAAATGATACCCAAGCAAATCGGCCAACGTGGTAGT
CTGGACGCGGACAAGATTGGCAACCCAGAAGACGCCATCAACGCGCTTTTGCAAGACAGCGAACTGTT
GGAAGAAGAGATCATTGAGGGCCTGATTCAAACACTCAAGATTGTGCCTCCCGAGCTGCAAAAACTGC
CTGCACGCGAAGAAGTTGTGTTCCCAGTGCACATTATTGGCAAAGTCGTGACACAAATGTGGCGTTTG
GGCTACTTGGTGGAATCCGAGCGATTGCTGTTTAGAGCCATGGATACCATTCAAAAGGACTGTCTGTC
CTTTACAGGCGAAGACACCATTGTACCTTGCTCCTACTGGCTGTCCAACACACACGAGCTGTTGTCGT
TGGTGTATTCTGTGGAGCAAGAGCTGGAGAGAGAAATGCACTACAACTCGATCCACGGACGCCGCGCT
GTCGGATGGCACGATTTTGAAAAGCTGGTGTCCACCATGAAGTTTGAGCTGCAGTGCCTGGAAGACAA
CATTTACCACCACTGGCTGTCTGAGCTCAAGAAGAAGCTCAACAAGATGGCGATCCCTGCCGTCATTG
AGAACCAGTCGTTGCCCGGCTTCATTGCCAGTGATTCCAACCGATTCTTTGGCAAGATCCTGTCCAGC
AACAACCAGCCTGCCTTCTCCATGGACGATCTGCTCAACTACCTGAACCGTATCTACCGTACCATGAA
GTCCTACTATGTGGAGCCCTATGTCATTGAGCAAGTCTTGACAGAACTGCTCAAGCTGATTGGTATCA
CCACGTTCAATGATTTGGTCATGAGACGCAACTTCAATTCATGGAAGCGTGCCATGCAAATTCAGTAC
AACATTACGCGTTTGGAGGAATGGTGCAAAGCGCATGACGTGTCAGAAGCCACGAATCAACTGGAGCA
TTTGATGCAAGCGACCAAGTTGTTGCAGCTCAAGAAGGCTACATTGGAGGATATCAAGATTATCTATG
ATGTGTGTTGGTTCCTGGCTCCTACTCAGGTCCAAAAGTTGATTCAAAACTACTGTGTGGCTGATTAT
GAGGTAAGAAGGGGTTACTAAAAACGAAAATTTAGAGCTATACACTTACATTACATTCTACTTGTAGG
ATCCCATCAGCAATGAAATTCTGAGAGCTGTTGCTTCTCGTGTCAGTAGCAGCGATACAGGCGATATC
TTATTGCTGGATAACGTGTCGATTGAAGACAGTGATTATGATCAACCCGAGCCACACAATGTGGTAGC

CAGCTCTTATATCCCCAGTTATGTAAGTGTGTCGTATGTGTTTCTTGAATCCATCCAACTAAGTGCCT
TTTTTTTTCTCTCCAGTTGAACTTGCAACATGTCCAAAAGTTGATTGCCTTGGTCACCTTGAATGAAA
AACATAGACCTCAACGCATGGATTCCATGTAGTTTTTATGAGCCGTATGTAATTTTATTGCTATTATG
AGCCAAATTTTTCCCTCCCCAAAAAACTCCCTTTATTTAACACCTCTCTATATATATAACTGACATAT
GTTTCTATCTTGATATTTTAATTCAATACATTTATACTTCAATAAACTCTACCATTCGCTATGTAAAT
GCCGACCATCTTACACATCCAAGTGCCTGAAACCTTGACATGTCTGATTTGAATGACTGTAATTAGCT
ACTGTGTATAATGTCCCGCTTGTGAACGCCAATACAGTAAAAGACAAAAACGCAAAATGTAATAGTAA
TACAACTTGGAAAGAAGATACAAATGATTACTTTATTAAAATCAGCACACTCGTAAAAAAAAAAAAAA
AAAAAAAAAAAACTACAACCTGCGTTCAATTTTTGGTGAGCTTCTAGCGCTACTTTTTGGAGATAATG
GTGAATTGGAGCCATCTATATCATTATGACAAGTAGCAGCAAAGTTGTGCCATTGAGACAGCGAGGGA
GAGGGAGTAGGAGGAGGAACCACCGTGGTGTGGTCAGATGGAGGTGTAGGTGTTGTGGATGGTTGTTG
CTGTTGTGGTTGTGCTTTGCCAATGGTATCTTTTGATTCTGTTTCATCATCATCATCGTTATTATCTT
GTCTAAGAATCTCGTGCTCATCATCTGAAAGATCTGCATCAGCAAATCGATCCTCTTCGTTATCTTCT
TCCTCTTCCTCCTGTGGTTGTGGCTCGTTGTTTTCTAAAGGCTCTGTATTGA

Figure 53. Nucleotide sequence of gene 51513. The complete coding sequence and 600 nt of upstream and downstream regions are shown. A putative TATA box (-195) is indicated as yellow box. The pyrimidine-rich sequence is underlined. The start and stop codons are highlighted as green boxes. Red and black letters denote exon and intron sequences, respectively. The putative polyadenylation sequence is marked as a pink box. Blue letters indicates the 3' untranslated region. The upstream and downstream regions are indicated in gray letters.

Amino acid sequence

Protein 51513 contains 1615 amino acids (**Figure 54**). This protein contains several conserved domains that were detected using BLASTp program of NCBI and Pfam servers (**Figure 55**). The first domain is a MYSc_Type_V domain (cl00286, E = 0e+00), a motor domain located from amino acid 90 to 773. Two IQ domains (Calmodulin-binding motif) were found between residues 835-856 and 887-904 (smart00015, E = 2,90e-03; pfam00612, E = 5,26e-03, respectively). And a fMyo2p_CBD domain (Cargo binding domain of fungal myosin 2) was detected at the C-terminal end of the protein using BLASTp of NCBI (cd15480, E = 1,67e-159). A DIL domain of unknown function was also detected using PFAM (PF01843, E = 2,8e-31) (**Figures 54** and **55**). Besides those domains, a coiled-coil region formed by two partially overlapping domains, SPEC (Spectrin repeats, cl02488, E = 5,38e-04) and LRS4 (Monopolin complex subunit, pfam10422, E = 6,88e-05), were found between residues 947-1088 and 1028-1157, respectively (**Figure 55**).

MDSLSSGVAQAVQVYTKGTKAWFEDEDEAWVSASVLSKEESGTGVKIIFQDDKDEGRVSIKMVWDCSMST
HKQKGANLPPLRNPPRLENTEDLTNLSYLNEPSVLNTIRTRYFQRNIYTYSGIVLIAANPFASVPLYEPD
IIQQYSGRRRGELEPHLFAIAEDAYRCMVREKSNQTVVVSGESGAGKTVSATHIMRYFATADDQESGKIK
DVAQGMTEVEEQIMATNPIMEAFGNAKTTRNNNSSRFGKYIEIQFDNRCNIVGAKIRTYLLERSRLIFQP
ESERNYHIFYQLCTGAPINERKNLELGDWNKFHYLNQSGVGSIPGVDDAAEFELTQKSLSLVGISVEAQW
HIFKLLAALLHIGNIEIGGRQDATLTEDQPALITATKLLGIKTSEFKKWLVKKQIITRNEKIVKNLNPTQ
ATVVRDSVAKYIYASLFDWLVKVVNDSLSCQEEGLVRTFIGVLDIYGFEHFKKNSFEQFCINYANEKLQQ
QFNQHVFKLEQEEYVKEKIDWKFIDFSDNQKCIEVIESKLGILSLLDEESRMPSGTDQGFINKLYSSFAD
PKYKDYFKKPRFSNSAFTVVHYAHEVEYDAEGFIDKNKDTVPDELLTLLQNAESTFLVDMLQTATAAASA
ASQEAKPTPVKKVGMAIAKKPTLGSIFKLSLISLMDTISKTNVHYIRCIKPNEAKVAWGFEPNMVLSQLR
ACGVLETIRISCAGYPSRWTFEDFAERFYALVNSQYWDPNLSPDINKLCHVILDKYIKDADKYQIGLTKI
FFRAGQLAYLEKCRRERWDECTILLQKNMRRFIVRIGYLRKLDLISRLQRVARQKMGVRKLELARQEIAA
IKIQTEWRRYIQRKRYLKQRAFVIHLQAACRSHLTRKTFAHIREHFAAIKIQSMVRGWRVRKEFLAKRQV
AIQIQTCIRRRLARKALLALKQDARSANHFKEVSYKLESKVVELTQSVTQYKDEKDQLRLKANALEMQVK
DWSEKYEKLGEKARSLEQSADTSELERQLESLQVERNGIQNDYRNSLERIKKQDMEIARLNEELQRHKDE
ITKLKQAHNQQQLRSPVSPSKVAELKSQIVALKAQLSQSLKNHPKRQASINAYRTLSPQRSGDRRGMSPD
YNRGRSPSADPRNRSPSSLAVRRSSIGDRRTEPNGNNNHYANTGGANGGANAAKMIYAEPEQMIPKQIGQ
RGSLDADKIGNPEDAINALLQDSELLEEEIIEGLIQTLKIVPPELQKLPAREEVVFPVHIIGKVVTQMWR
LGYLVESERLLFRAMDTIQKDCLSFTGEDTIVPCSYWLSNTHELLSLVYSVEQELEREMHYNSIHGRRAV
GWHDFEKLVSTMKFELQCLEDNIYHHWLSELKKKLNKMAIPAVIENQSLPGFIASDSNRFFGKILSSNNQ
PAFSMDDLLNYLNRIYRTMKSYYVEPYVIEQVLTELLKLIGITTFNDLVMRRNFNSWKRAMQIQYNITRL
EEWCKAHDVSEATNQLEHLMQATKLLQLKKATLEDIKIIYDVCWFLAPTQVQKLIQNYCVADYEDPISNE
ILRAVASRVSSSDTGDILLLDNVSIEDSDYDQPEPHNVVASSYIPSYLNLQHVQKLIALVTLNEKHRPQR
MDSM

Figure 54. Amino acid sequence of protein 51513. The dark blue box indicates the motor domain (MYSc_Type_V). Two IQ domains are indicated as blue boxes. The fMyo2p_CBD domain is denoted as a yellow box.

Protein 51513 contains the regular domains found in class V Myosin, one of the molecular motors in cells. Myosin class V is a widely conserved protein family that belongs to the myosin superfamily. This superfamily consists in at least 35 different classes of myosins (Odronitz and Kollmar, 2007). Myosin superfamily contains actin-based motor proteins that play diverse functions in cells, including cytokinesis, cell adhesion, endocytosis, exocytosis, movement of mRNA, movement of pigment granules and cell motility (Hammer and Sellers, 2012). Class V myosin is specifically identified through the presence of a head of motor domain, a neck including up to 6 IQ motifs and a tail with diverse domains containing a coiled-coil region and a globular tail domain (GTD), which might contain AF6/cno/DIL domains (Weber et al., 2003; Wei et al., 2013) (**Figure 55A**). The SPEC and LRS4 domains identified in the *Mucor* protein (**Figure 55B**) have been also found in

myosins class V of other organisms, such as myosin-Va (*Saimiri boliviensis*, XP_003941669.1), myosin-Va isoform X1 (*Balaenoptera acutorostrata*, XP_007194954.1), myosin-Vc (*Sorex araneus*, XP_004602030.1) and myosin-Va isoform X1 (*Acromyrmex echinatior*, XP_011065929.1). Taken together, these results suggest that protein 51513 should be classified as a member of Myosin class V protein in *Mucor*. Therefore we named the candidate gene 51513 in *M. circinelloides* as *mcmyo5*. The structure of this protein, its domain architecture and the genetic relationship with homologous proteins from other fungi are shown in **Figure 55**. The putative Myosin V proteins found in *M. circinelloides* and *M. ambiguous* could be orthologs, since the genetic distance between them is very low (**Figure 55C**). As occurs in most systems, *M. circinelloides* seems to have several myosin genes, since several proteins highly similar to 51513 have been identified in the *Mucor* genome (**Table 15**).

Protein ID	E-value	Protein ID	E-value
179665	0e+00	**140500**	1,05e-108
154518	0e+00	**116620**	2,99e-108
138262	0e+00	**153118**	2,92e-55
149958	3,3e-160	**104542**	1,95e-52
136314	1,25e-120		

Table 15. Similar proteins to Myo5 (51513) found in the *M. circinelloides* genome (v2.0)

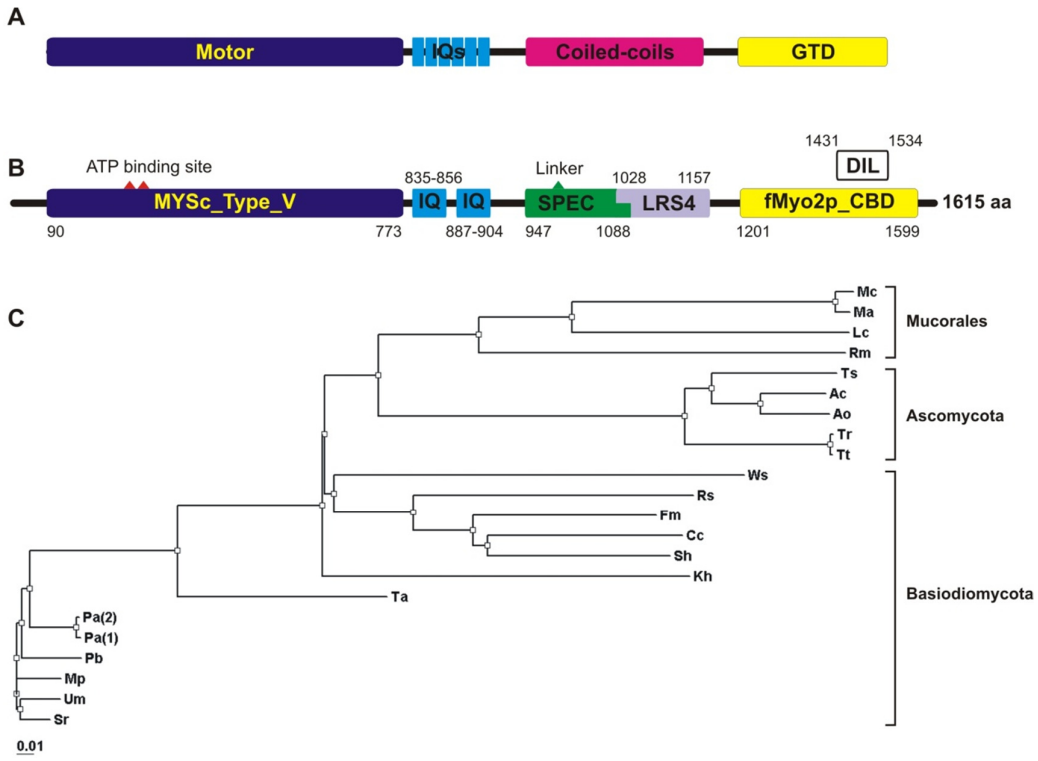

Figure 55. Domain architecture of *M. circinelloides* Myo5 and its genetic relationship with other fungal Myosin class V. **(A)** General domain architecture of Myosin class V, which contains a motor domain (dark blue box), several Calmodulin-binding motifs (IQs, blue boxes) and a coiled coil (pink box) and a globular tail (GTD, yellow box) domains (Wei et al., 2013). **(B)** Domain structure of protein ID 51513, which includes MYSc_type_V (motor domain), two IQ motifs, two overlapping SPEC (Spectrin repeats) and LRS4 (Monopolin complex subunit) domains and a fMyo2p_CBD domain (Cargo binding domain of fungal myosin 2). The color code is the same as part (A). An ATP binding site (orange band) is located within MYSc_type_V domain and a linker region (green triangle) is located in the SPEC domain. An unknown function DIL domain was detected by PFAM search (http://pfam.xfam.org/). The starting and stopping amino acid of each domain is indicated. **(C)** A phylogenetic tree of fungal myosin class V proteins from different species of Mucorales (Mc, *M. circinelloides*; Ma, *Mucor ambiguous*; Lc, *Lichtheimia corymbifera* and Rm, *Rhizopus microspores*), Ascomycota (Ts, *Talaromyces stipitatus*; Ac, *Aspergillus clavatus*; Ao, *Aspergillus oryzae*; Tr, *Trichophyton rubrum* and Tt, *Trichophyton tonsurans*), and Basidiomycota (Ws, *Wallemia sebi*; Rs, *Rhizoctonia solani*; Fm, *Fomitiporia mediterranea*; Cc, *Coprinopsis cinerea* okayama; Sh, *Stereum hirsutum*; Kh, *Kwoniella heveanensis*; Ta, *Tilletiaria anomala*; Pa(1), *Pseudozyma antarctica*; Pa(2), *Pseudozyma aphidis*; Pb, *Pseudozyma brasiliensis*; Mp, *Melanopsichium pennsylvanicum*; Um, *Ustilago maydis* and Sr, *Sporisorium reilianum*) fungi. The phylogenetic tree was built using ClustalW2 program (http://www.ebi.ac.uk).

IV.5.2. Disruption of candidate genes

The silenced strains showing altered morphogenesis have unstable phenotypes, since they partially revert to the wild type phenotype after a long-time incubation. For further analyses of the function of the candidate genes and their roles in *M. circinelloides* pathogenesis, null mutant strains are required.

To disrupt the candidate genes, a *pyrG* selective marker was fused with adjacent sequences of the candidate coding regions using fusion PCRs, generating a gene replacement fragment (see section II.7.5). This fragment was cloned into the pGEMT-easy vector and used to disrupt the candidate genes via homologous recombination (see section II.5). The recipient strain was the leucine and uracil auxotroph MU402. The transformants were grown on selective medium MMC pH 3,2, which contains leucine but not uracil, for several vegetative cycles. The putative disruptants were easily detected after screening their phenotypes on a selective medium. Homokaryotic strains were selected by phenotype, PCR screenings and Southern blot analyses.

IV.5.2.1. Disruption of *mcclasp* gene

Plasmid pMAT833 was constructed to disrupt the *mcclasp* gene. It contains a 4,2 kb fragment that includes the *pyrG* gene flanked by upstream and downstream sequences of the target locus. It was constructed by PCR-amplification using primer pairs FYL10U/RYL10-pyrG and FYL10-pyrG/RYL10D (**Table 5**), which amplified 1,3 kb of upstream and downstream sequences of *mcclasp* gene, respectively. Those fragments were used in a fusion PCR together with a 2 kb *pyrG* fragment amplified from plasmid pATA5 using primers F-pyrG and R-pyrG (**Table 5, Figure 17**). The 4,2 kb fusion fragment was amplified with internal primers FYL10 and RYL10 (**Table 5, Figure 56**) and cloned into pGEM-T easy to produce plasmid pMAT833. The 4,2 kb replacement fragment was released from plasmid pMAT833 by *Not*I digestion, amplified with primers FYL10 and RYL10 (**Figure 56**) and introduced into the strain MU402 (Leu^-, Ura^-) by electroporation. The selectable marker *pyrG* gene of *M. circinelloides* supplements the uracil auxotrophy of the recipient strain.

Thirty two $pyrG^+$ transformants were obtained on minimal medium MMC. Transformants were subjected to successive cycles of vegetative growth in selective medium in order to increase the proportion of $pyrG^+$ nuclei. After 5 vegetative cycles, one transformant was selected for subsequent analyses based on its stability and similar phenotype to the silenced strains obtained previously with plasmid pMAT823 (**Figures 46B** and **58**).

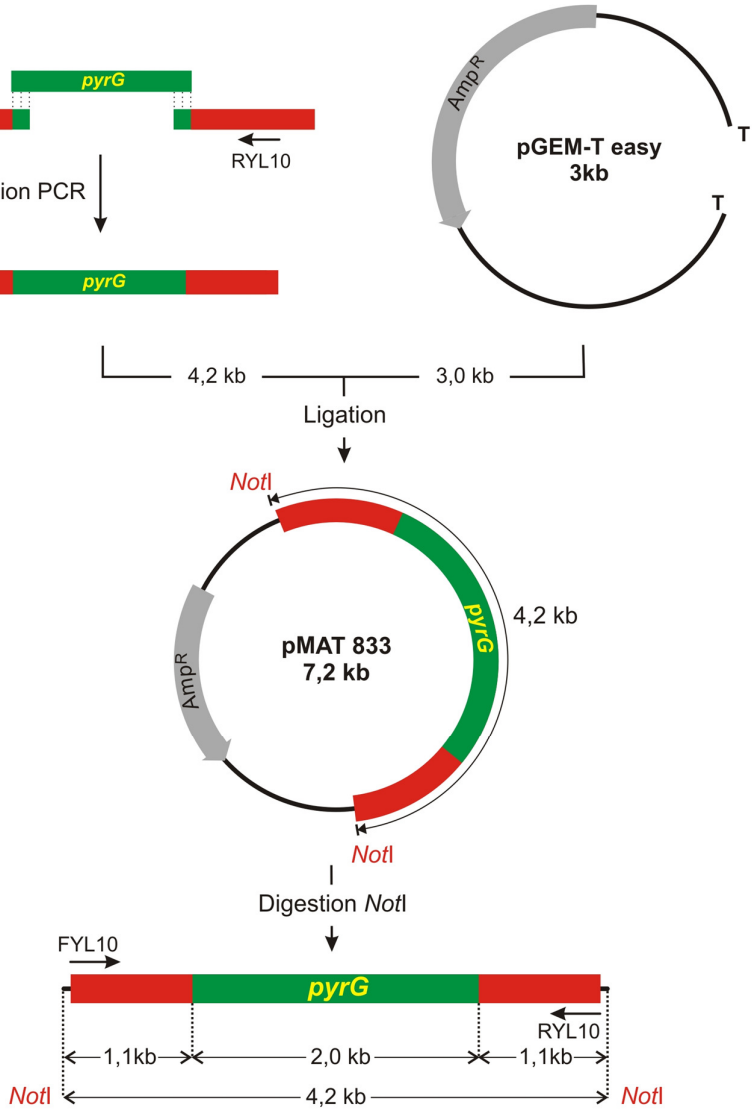

Figure 56. Construction of the replacement fragment used to disrupt the *mcclasp* gene. Overlapping PCR was used to fuse three fragments and generate a replacement fragment that includes upstream and downstream regions (red boxes) of the target gene and the selective marker *pyrG* (dark green box). This fragment was cloned into pGEMT-easy to give plasmid pMAT833. A 4,2 kb replacement fragment released from plasmid pMAT833 by *Not*I digestion was used as template for PCR-amplification with primer pair FYL10/RYL10 (**Table 5**). The positions of restriction sites and primers used for cloning are indicated.

In order to check the correct homologous recombination that removes *mcclasp* gene and the possible existence of additional ectopic integrations, a Southern blot analysis was carried out. Genomic DNA isolated from the wild-type strain R7B and the transformant showing the expected phenotype was digested with the restriction enzyme *Sal*I and was hybridized with two different probes that differentiate the wild type *mcclasp* and mutant alleles (**Figure 57A**, probes i and j).

The results revealed that the selected strain showed the expected fragments for homologous integration, indicating that the *mcclasp* gene was replaced successfully (**Figure 57B**). The transformant was named MU464 and, as indicated previously, it showed the same growth and sporulation defects as the silenced strain (**Figure 58**), allowing its use to characterize *mcclasp* gene function.

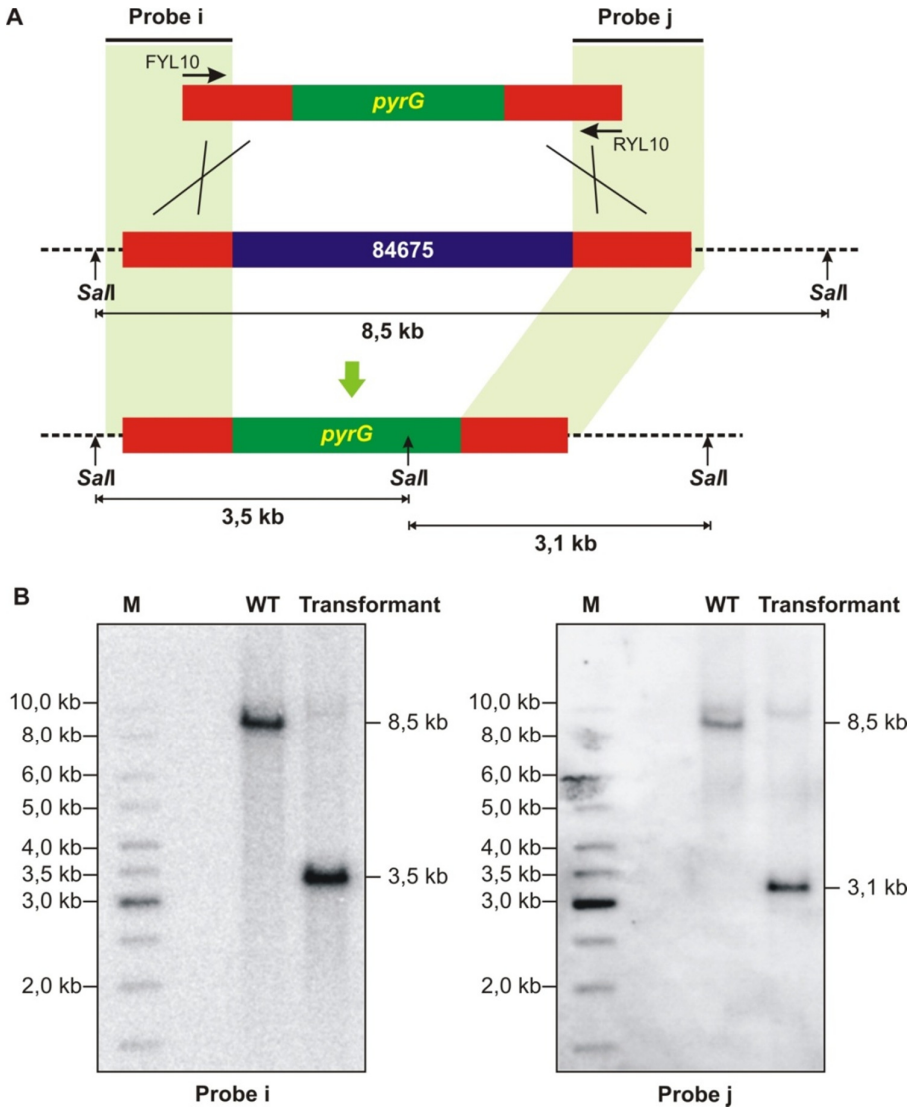

Figure 57. Disruption of *mcclasp* gene. **(A)** Schematic representation of the wild-type *mcclasp* locus (middle) and after homologous recombination with the disruption fragment (below). Dark blue and red boxes represent *mcclasp* gene and adjacent sequences, respectively; dark green boxes, *pyrG* selectable marker; dashed lines, sequences not included in the disruption fragment. The probes *i* (1,2 kb) and *j* (1,4 kb) were generated by PCR-amplification with primer pairs FYL10U/RYL10-pyrG and FYL10-pyrG/RYL10D, respectively (**Table 5**). The positions of the probes and the expected sizes of the *Sal*I restriction fragments are indicated. The primers used to amplify the disruption fragment from the knockout vector pMAT833 (FYL10 and RYL10) are shown (**Table 5**). **(B)** Southern blot analysis of the wild-type strain R7B and *mcclasp* transformant. Genomic DNA (1 µg) was digested with *Sal*I and hybridized with probe i (left) and with probe j (right). M, GeneRuler DNA ladder mixture (Fermentas).

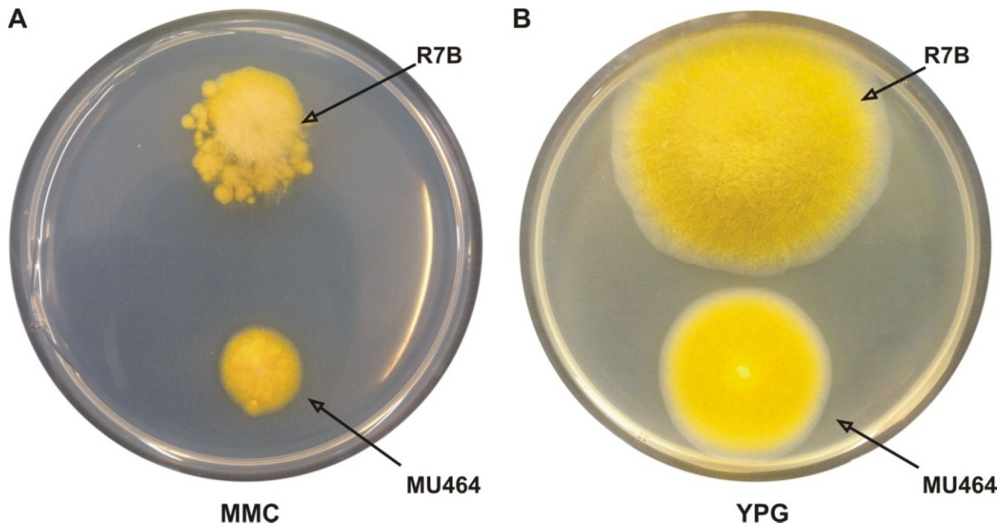

Figure 58. Morphologic phenotype of the *mcclasp*⁻ mutant. The wild-type R7B strain and the *mcclasp*⁻ null mutant strain (MU464) were grown at 26°C under continuous light on minimal medium MMC pH 3,2 for 72 hours **(A)** and on rich medium YPG pH 4,5 for 48 hours **(B).**

IV.5.2.2. Disruption of *mcmyo5* gene

Plasmid pMAT832 was constructed to disrupt *mcmyo5* gene. This plasmid contains *pyrG* gene flanked by upstream and downstream sequences of the target gene. It was constructed by PCR-amplification using primer pairs FYL1U/RYL1-pyrG and FYL1-pyrG/RYL1D (**Table 5**) to amplify 1,3 kb of upstream and downstream sequences of the *mcmyo5* gene, respectively. Those fragments were fused together with a 2 kb *pyrG* gene amplified from plasmid pATA5 using primers F-pyrG and R-pyrG (**Table 5, Figure 17**) by overlapping PCR. The 4,1 kb fusion fragment was amplified with internal primers FYL1N and RYL1N (**Table 5, Figure 59**) and cloned into pGEM-T easy to produce plasmid pMAT832. The 4,1 kb replacement fragment was released from plasmid pMAT832 by *Eco*RI digestion, amplified with primers FYL1N and RYL1N (**Figure 59**) and introduced into MU402 by electroporation.

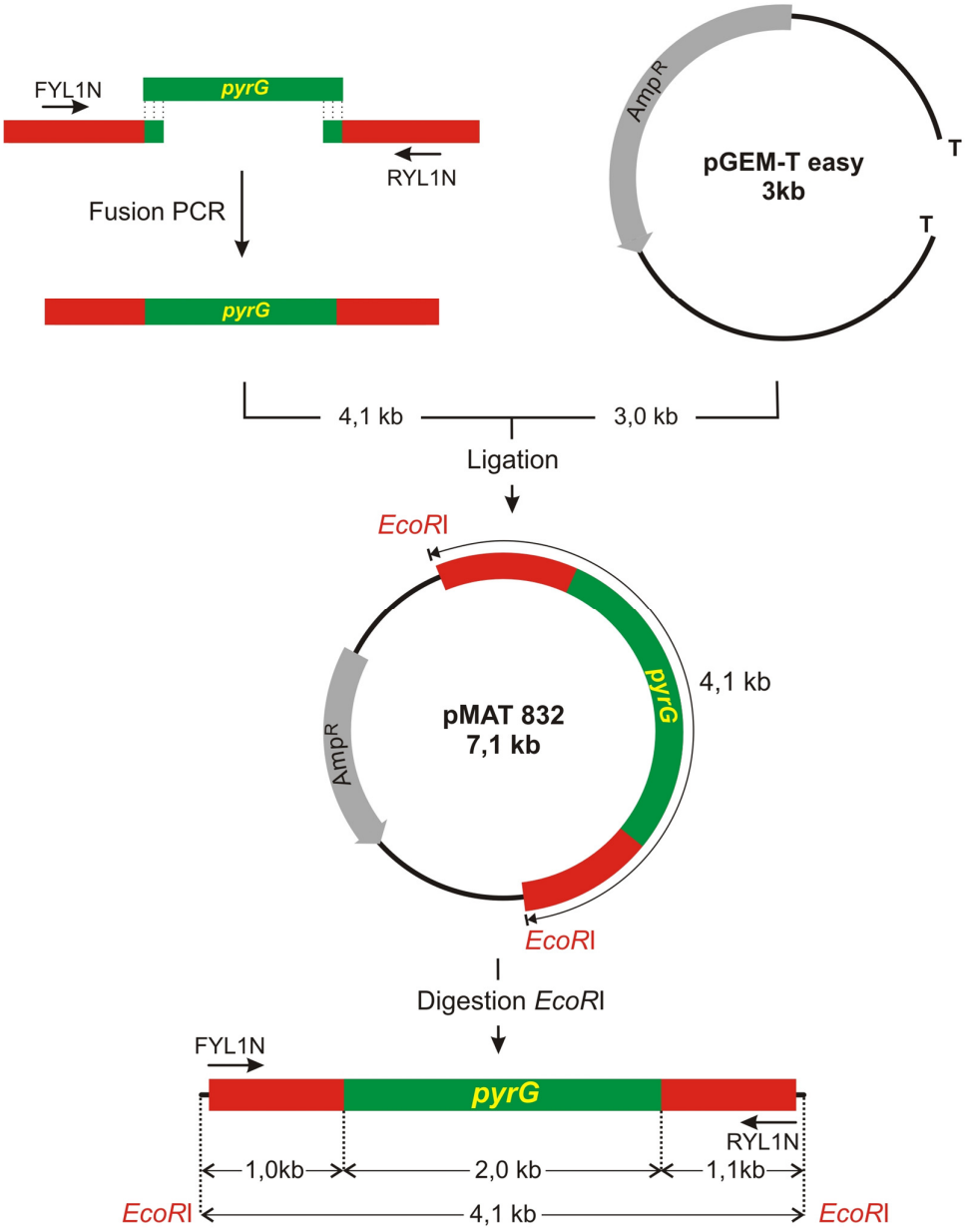

Figure 59. Construction of the replacement fragment to disrupt the *mcmyo5* locus. Overlaping PCR reaction was used to fuse three fragments and generate a replacement fragment that includes flanking regions (red boxes) of target gene and the selective marker *pyrG* (green box). This fragment was cloned into pGEMT-easy to generate plasmid pMAT832. A 4,1 kb replacement fragment released from plasmid pMAT832 by *Eco*RI digestion was PCR-amplified with primer pair FYL1N/RYL1N (**Table 5**). The positions of restriction sites and primers used for cloning are indicated.

To disrupt *mcmyo5* gene, a similar strategy used for disruption of *mcclasp* gene was applied. Thirteen *pyrG*$^{+}$ transformants were obtained after transformation of MU402 with the disruption fragment. Those transformants were subjected to successive cycles of vegetative growth in selective medium to increase the

proportion of *pyrG*$^{+}$ nuclei. The screening for transformants with a similar phenotype to the silenced strains (R7B strain transformed with pMAT828, **Figure 46A**) yielded two transformants with stable phenotype after 7 vegetative cycles. These two transformants were selected for subsequent analyses.

To check the correct homologous recombination at the *mcmyo5* locus and the homokaryosis of the two selected strains, Southern blot hybridization was performed. Genomic DNA isolated from the wild-type strain R7B and the two transformants showing the expected phenotypes was digested with the restriction enzyme *Bgl*II and hybridized with a probe that can discriminate between the wild type and mutant alleles (**Figure 60A**).

The results of Southern blot experiments revealed that one of the selected strains exhibited the expected fragment for homologous integration at the *mcmyo5* locus, although it also revealed a low proportion of wild-type nuclei, since a 3,5 kb fragment corresponding to the wild-type allele was detected (**Figure 60B**). The other transformant had an ectopic integration, as it did not show the expected 4,1 kb fragment. Usually, the homokaryotic state is reached after 2 or 3 vegetative cycles in selective medium. The transformant with the correct integration was grown through 7 vegetative cycles although it remained as a heterokaryon strain. These results suggest that *mcmyo5* gene could play an essential role in the viability of *M. circinelloides*, being impossible to reach a 100% of mutant nuclei. Nevertheless, the heterokaryotic transformant (number 2, **Figure 60B**) with high proportion of mutant nuclei showed a very stable yeast-like phenotype, even after growing in non-selective rich medium YPG for a long-time incubation (**Figure 61**). Thus, we decided to continue analyzing the function of *mcmyo5* gene in *M. circinelloides*. The heterokaryotic transformant was named MU465.

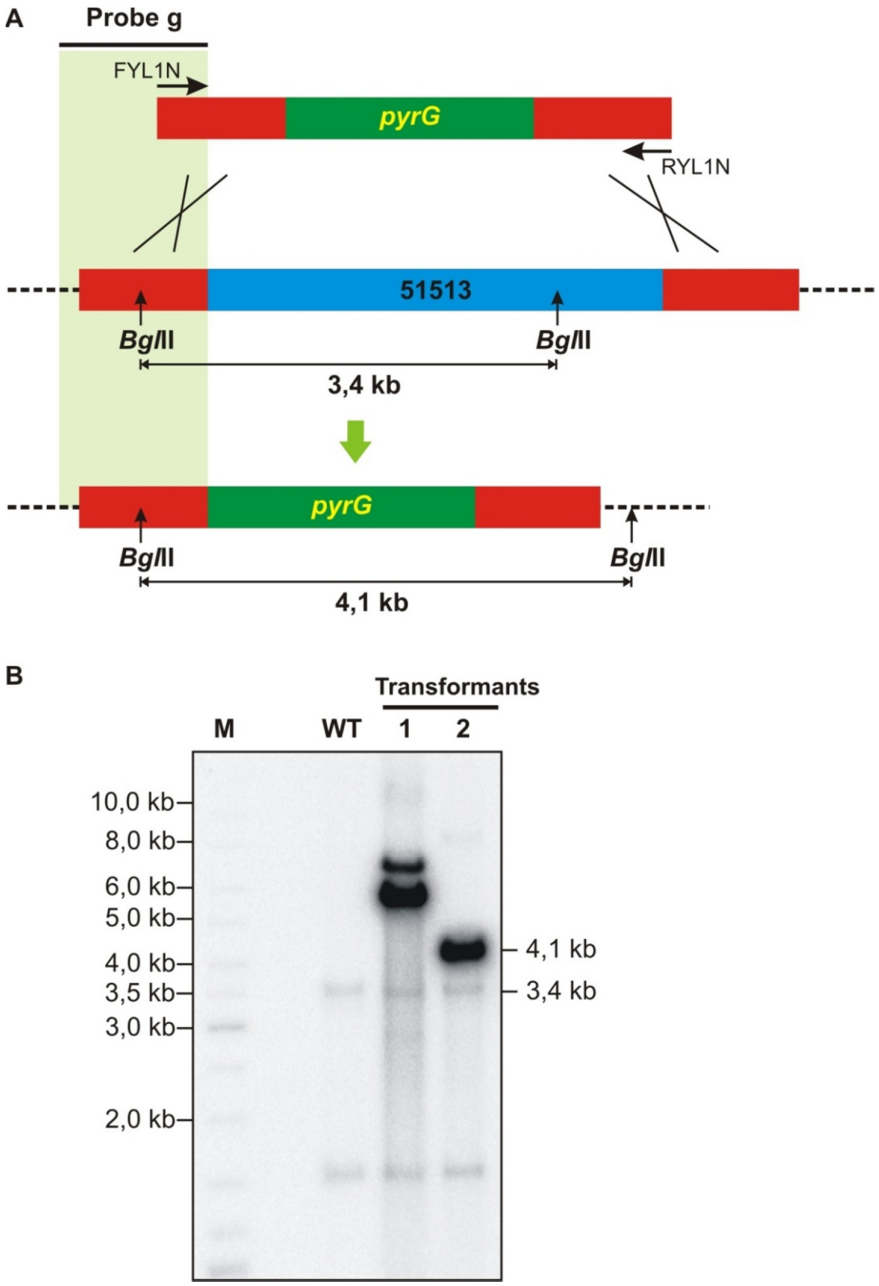

Figure 60. Disruption of the *mcmyo5* gene. **(A)** Schematic representation of the wild-type *mcmyo5* locus (middle) and after homologous recombination with the disruption fragment (below). Light blue and red boxes represent *mcmyo5* gene and adjacent sequences, respectively; dark green boxes, *pyrG* selectable marker; dashed lines, sequences not included in the disruption fragment. The probes *g* (1,3 kb) was generated by PCR-amplification with primer pair FYL1U/RYL1-pyrG (**Table 5**). The position of the probe and the expected sizes of the *Bgl*II restriction fragments are indicated. The primers used to amplify the disruption fragment from the knockout vector pMAT832 (FYL1N and RYL1N) are shown (**Table 5**). **(B)** Southern blot analysis of the wild-type strain R7B and two *mcmyo5* transformants. Genomic DNA (1 µg) was digested with *Bgl*II and hybridized with probe g. M, GeneRuler DNA ladder mixture (Fermentas).

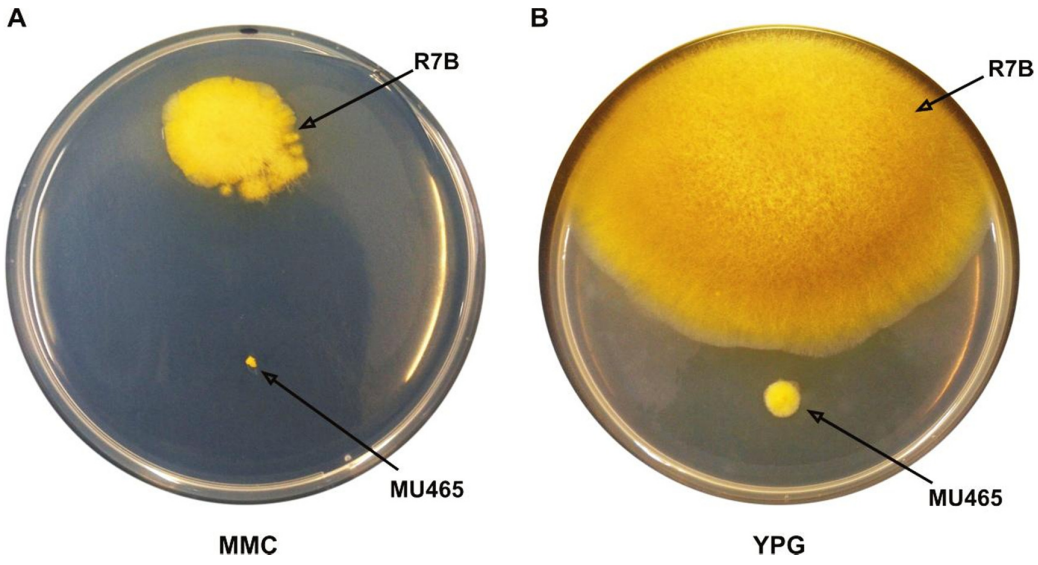

Figure 61. Morphologic phenotype of the *mcmyo5*⁻ mutant. The wild-type R7B strain and the *mcmyo5*⁻ heterokaryotic transformant strain (MU465) were grown at 26°C during 72 hours under continuous light on minimal medium MMC pH 3,2 **(A)** and rich medium YPG pH 4,5 **(B)**.

IV.5.3. Phenotypic analyses

The results shown in the previous sections showed the drastic changes in the phenotypes of the mutants obtained in the two selected genes from the screening of the genomic libraries. Interestingly, mutant strain MU465 showed a yeast-like growing phenotype that could be directly related to pathogenesis. In this section, several phenotypic aspects, such as growth rate, sporulation, morphology and virulence were analyzed in both mutant strains.

IV.5.3.1. Growth rate

To measure the growth rate of the wild-type and mutant strains, small pieces (~1 mm in diameter) of mycelium of each strain (n = 15) were plated on solid medium MMC pH 3,2 and incubated under continuous light at 26°C. The diameters of the colonies were measured after 24, 48 and 72 hours and the average values and standard errors were calculated (**Figure 62**).

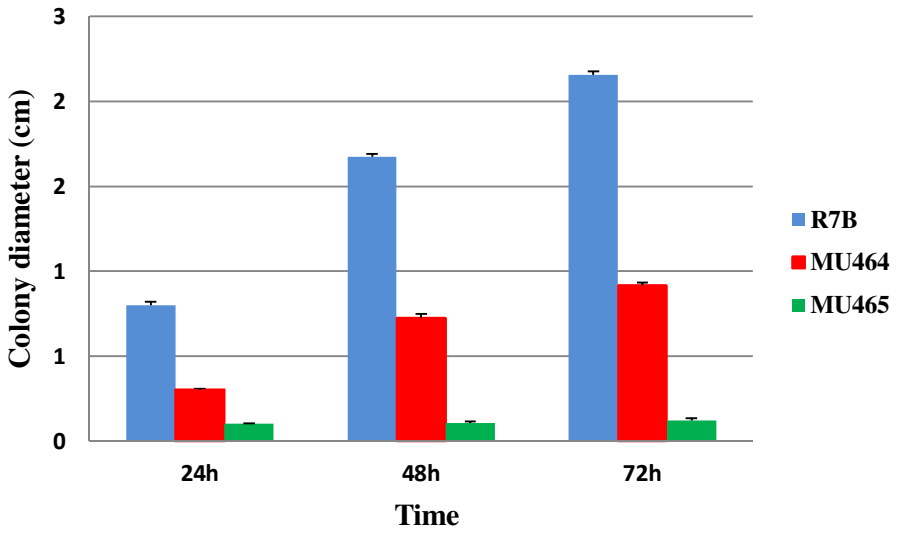

Figure 62. Growth analysis of mutants MU464 and MU465. Growth of the wild type strain R7B and MU464 (*mcclasp*$^-$) and MU465 (heterokaryotic *mcmyo5*$^-$) mutants on MMC medium was monitored periodically by measuring colony diameter. Average and standard errors from 15 independent colonies of each strain are shown.

The above results indicated that although *mcmyo5* gene was not completely eliminated from the heterokaryotic strain MU465, its growth rate was much lower than MU464 and wild-type strain R7B (**Figure 62**). In fact, the MU465 strain seems not to grow during the incubation time. Also the growing rate of the MU464 strain was lower than the wild-type strain R7B, showing a reduction of about 2,5 fold (**Figure 62**). These results indicated that lack of function of these genes (*mcmyo5* and *mcclasp*) strongly reduces the growth rate of *M. circinelloides*, suggesting that these genes might play an important role for the expanding of hyphal mycelium during the growing processes.

IV.5.3.2. Sporulation efficiency

In order to quantify the participation of these two proteins, Clasp and Myo5, in the process of vegetative sporulation, we compared the total vegetative spore production of wild-type and the two mutant strains. All strains were plated on solid medium MMC pH 3,2 and incubated for 72 hours at 26^o C under continuous light or dark conditions (n=10). Asexual spores were collected and counted and the area of the mycelium was measured to represent the production of spores per cm^2 (see section II.10.1) (**Figure 63**).

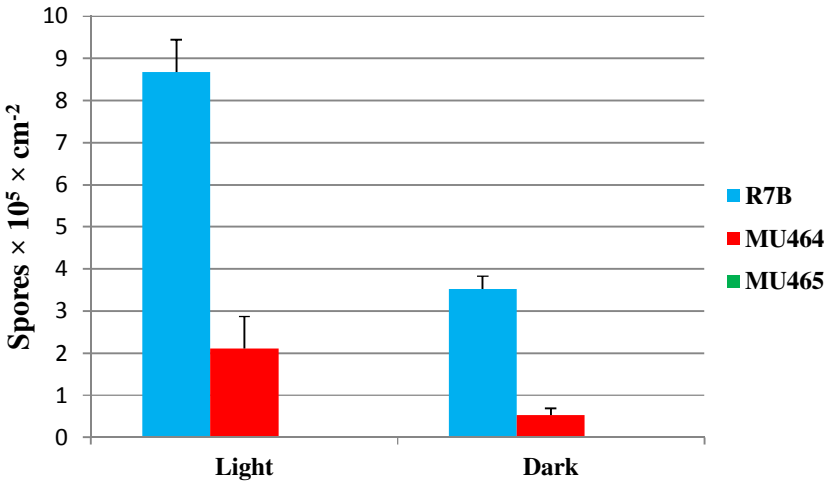

Figure 63. Asexual sporulation in mutants MU464 and MU465. Production of asexual spores in mycelia of the wild-type strain R7B and MU464 (*mcclasp*$^{-}$) and MU465 (heterokaryotic *mcmyo5*$^{-}$) mutants grown under white light and dark conditions for 3 days is shown. The values are means and standard errors of 10 independent measurements.

These results showed that the heterokaryotic strain MU465 did not produce any asexual spore during 72 hours of growth in both light and dark conditions, suggesting that the incomplete production of Myo5 protein completely blocks the process of vegetative sporulation in *M. circinelloides*. Similarly, a significant reduction of sporulation was also observed in the *mcclasp* null mutant, since MU464 strain produced 4,1 fold (light) and 6,6 fold (dark) less spores than the wild-type strain (**Figure 63**). These results suggested that the Clasp protein also plays a relevant role in the asexual sporulation process of *M. circinelloides*.

IV.5.3.3. Polarity index

The polarity index is the quotient of the cell length divided by the cell width (Schuster et al., 2012). This index measures the polarized growth of filamentous fungi. As indicated before, *M. circinelloides* is a dimorphic fungus that grows in a mycelial morphology in aerobic condition and as yeast in anaerobic condition. To calculate the polarity indexes of the wild type and mutant strains, the three strains were grown in anaerobic conditions to generate yeast-like cells. About 10^7 spores of the strains R7B and *mcclasp*$^{-}$ and cells collected by vigorous vortexing of the heterokaryotic *mcmyo5*$^{-}$ mutant were inoculated in 2 ml eppendorf tubes filled up

with liquid MMC pH 4,5, paraffin covered, and incubated overnight under dark conditions, at 26°C without shaking. Once cells of the three strains were growing as yeast-like cells, they were transferred to aerobic liquid MMC medium to allow the transition to mycelial growth. This process was monitored under the light microscope. Photographs were taken and used to measure polarity indexes of the three strains using ImageJ application (**Figure 64**). Briefly, straight lines corresponding to the length and width of cells were drawn (n = 10), and the "Measure" tool in "Analyze" menu was used to get the data in pixels. The polarity index of a cell was obtained by dividing its length by its width (Schuster et al., 2012).

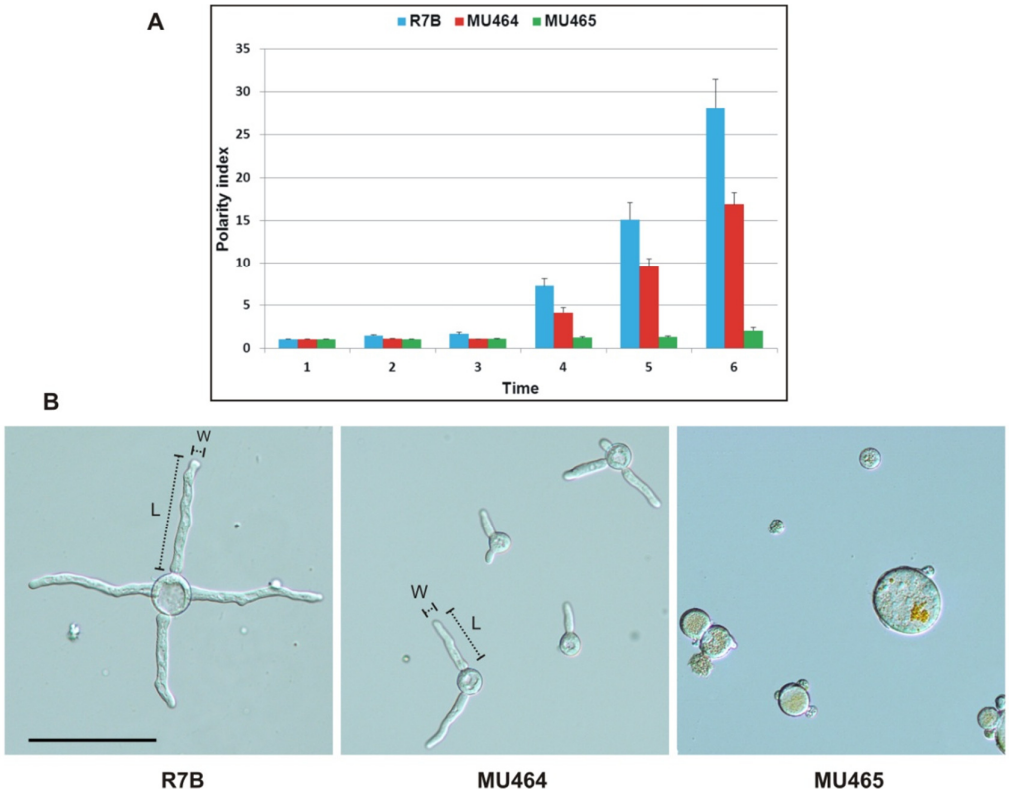

Figure 64. Polarity indexes of wild-type and mutant strains. **(A)** The polarity indexes of the strains R7B, MU464 (*mcclasp*$^{-}$) and MU465 (heterokaryotic *mcmyo5*$^{-}$) at different growing times are shown. These strains were grown on liquid medium MMC pH 4,5 at 26°C under dark condition with shaking (200 rpm). The values are means and standard errors of 10 independent measurements. **(B)** Figures showing the morphology of R7B, MU464 and MU465 strains after 3 hours growing in the conditions described in (A). The bars L and W denote the length and width of hyphae, respectively. Scale bar = 100 µm.

The results showed a strong reduction of polarity indexes of both mutant strains (*mcclasp*$^{-}$ and *mcmyo5*$^{-}$) compared to the wild type strain (**Figure 64A**). During the first two hours of growth, there were no significant differences in the polarity index between wild type and mutant strains, probably because this is an incubation time required for activation of hyphal growth. However, after 3-hours, cells started to produce hyphae, showing significant differences in the polarity indexes of the three strains. The MU465 strain exhibited the lowest polarity index compared with the two other strains. In fact, MU465 seems to lack the ability for hyphal growth and keep isotropic growth during the complete incubation time (**Figure 64A**). Oppositely, the wild-type strain showed the highest polarity index, going from 1,04 to 28,13 after 5 hours of incubation. The *mcclasp* null mutant, MU464, also exhibited a reduction of the polarity index compared with wild-type strain, being about 1,7 fold lower than the wild type (**Figure 64A**). The differences in the polarity indexes of these strains could explain the differences in the growth rates previously observed. These results also suggested that the loss of Myo5 protein does not allow regular mycelial growth. Therefore, Myosin-V plays an essential role in polarized hyphal growth in *M. circinelloides*, as was previously described in *U. maydis* (Weber et al., 2003; Schuchardt et al., 2005).

Although the polarization of *mcclasp*$^{-}$ strain is not as affected as in the Myo5 lacking strain, lack of *M. circinelloides* Clasp protein also generates an abnormal phenotype. After 5 hour of growth, this mutant produced structures like “pseudo-septa” inside mycelia and generates more secondary branches than the wild-type strain (**Figure 65**). As a consequence, its hyphae become thicker than the wild-type strain. These results suggest that Clasp is also involved in polarized hyphal growth in *M. circinelloides*, although cells lacking Clasp protein do not completely abolish polarization.

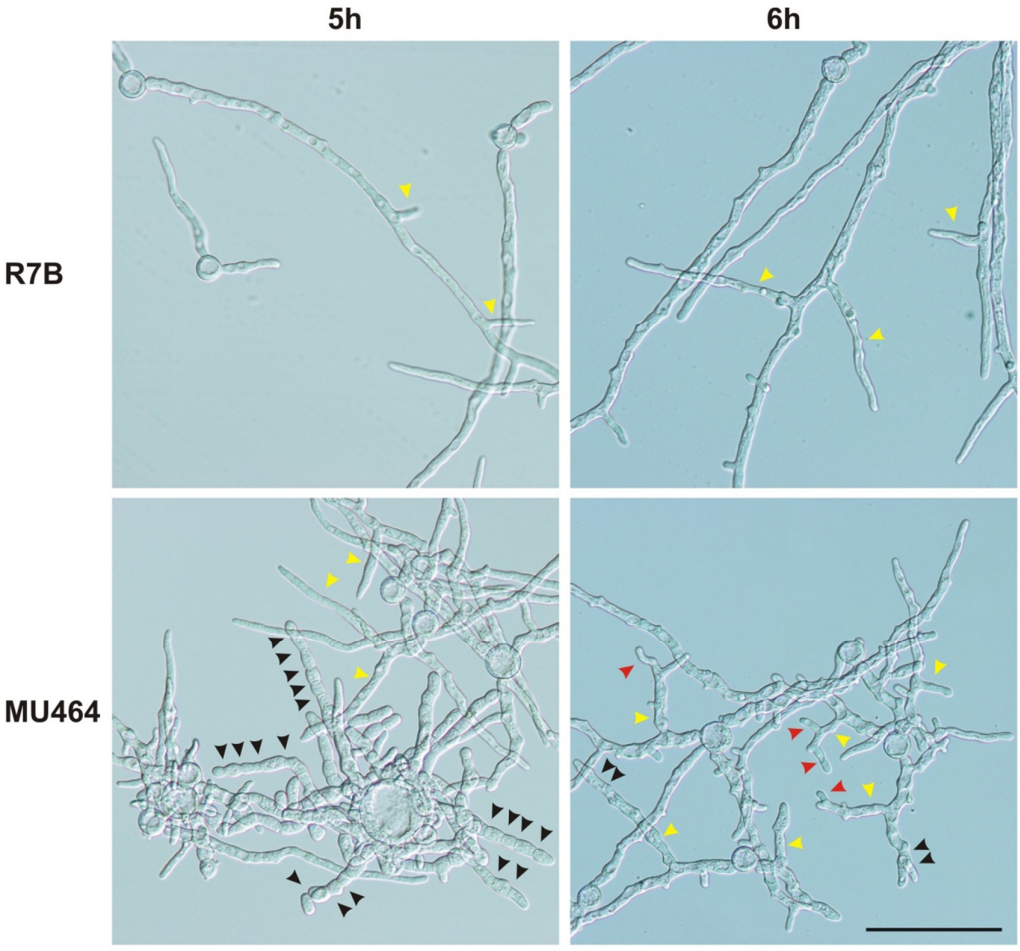

Figure 65. Hyphal morphology of wild-type and *mcclasp* mutant strains. Strains R7B (upper) and MU464 (lower) were grown on liquid medium MMC pH 4,5 under dark condition with shaking (200 rpm) at 26°C. Photographs were taken after 5 hours (left) and 6 hours (right) of growth. The black, yellow and red arrow heads indicate "pseudo-septa", secondary and third branches, respectively. Scale bar = 100 µm.

IV.5.3.4. Virulence analysis

Virulence assays were developed using the study model *Galleria mellonella*. The larva state of this insect is a reproducible and inexpensive model than has been used previously as a host model for *Mucor circinelloides* (Bastidas et al., 2012). It is a versatile model that allows infection with both spores and yeast cells, which helped us to overcome the complete lack of sporulation in MU465 (Bastidas et al., 2012). Infections were carried out injecting *G. mellonella* larvae (n=10) with 5000 spores in the case of MU464 and 20000 yeast cells in the case of MU465. The virulence of these two mutant strains was compared with a negative control (PBS), a non-virulent strain (NRRL3236) and a virulent strain (R7B) during 8 days post-injection (**Figure**

66). The results of these assays showed that strain MU464 presented almost the same virulence than the control R7B. MU464 reached 90% of mortality, a 10% lower than R7B, which is not a significant reduction of mortality (**Figure 66A**). However, strain MU465 showed a strong reduction of mortality, as it killed only 40% of the hosts, whereas R7B killed 100% of them when it was injected as yeast cells (**Figure 66B**). These results showed that MU465 presents a seriously reduced virulence and corroborate that the ability for hyphal growth is a virulence factor for *M. circinelloides*.

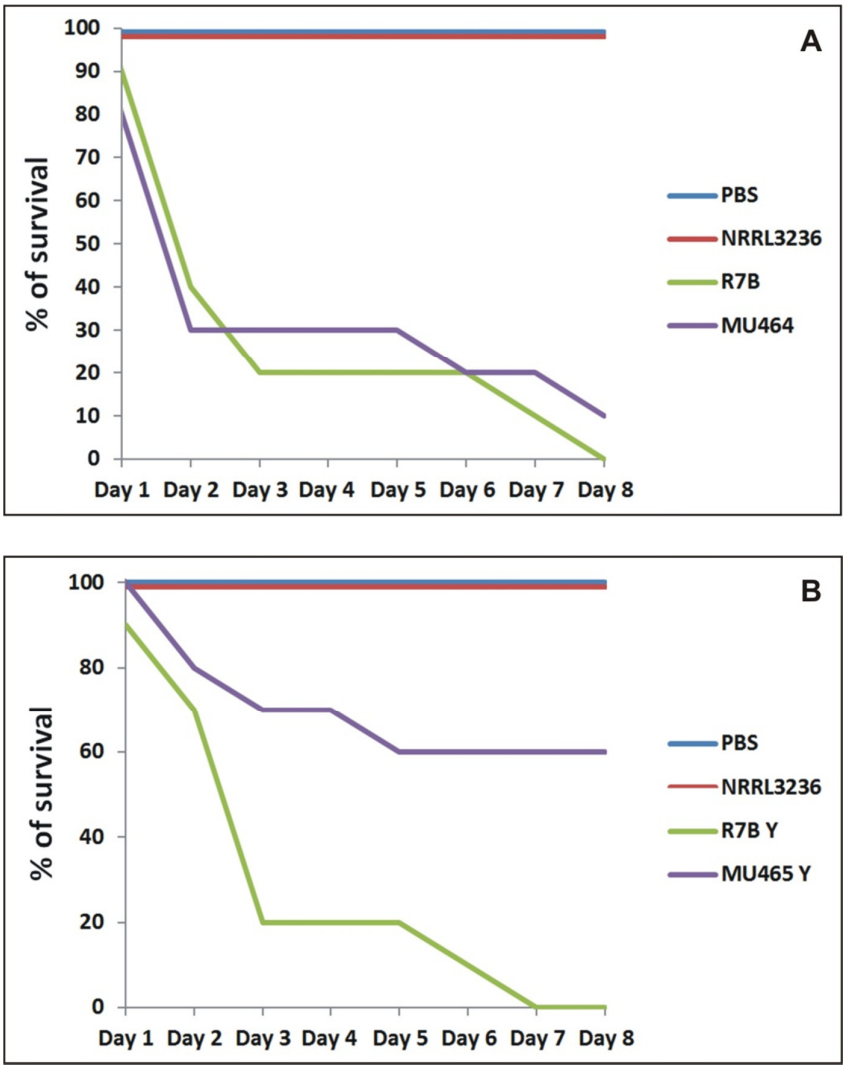

Figure 66. Virulence assays of mutants MU464 and MU465 in *G. mellonella*. (**A**) Survival percentages using spores of the strain MU464 (*mcclasp*$^{-}$, violet) compared with a negative control (PBS, blue), a non-virulent strain (NRRL3236, red) and a virulent strain (R7B, green). (**B**) Survival percentage using yeast cells of the strain MU465 (heterokaryotic *mcmyo5*$^{-}$, violet) compared with a negative control (PBS, blue), a non-virulent strain (NRRL3236, red) and a virulent strain (R7B, green).

V. DISCUSSION

V.1. A novel mRNA degradation mechanism in *M. circinelloides*

V.1.1. A novel pathway to regulate mRNA accumulation

Several RdRP proteins have been involved in the production of endogenous siRNAs in plants and nematodes (Fischer, 2010; Bologna and Voinnet, 2014). In those organisms, RdRPs show functional diversification in distinct endogenous silencing pathways as they are linked to the action of specific Dicer enzymes and/or Argonaute proteins. Also in *M. circinelloides* the two RdRP proteins described are functionally different. The RdRP-1 protein is involved in activation of silencing by sense transgenes and produces antisense RNAs corresponding to transgene transcripts (Calo et al., 2012). It is also required for the production of the largest class of *dicer*-dependent ex-siRNAs (Nicolás et al., 2010). RdRP-2 is involved in the amplification process that produces secondary siRNAs (Calo et al., 2012) and it has a role in the production of several classes of *dicer*-dependent ex-siRNAs (Nicolás et al., 2010). We have shown here that, besides playing an essential role in this endogenous silencing pathway, the RdRP enzymes are also involved in a novel mechanism that control degradation of specific mRNAs. By deep sequencing, more than 500 loci corresponding to exons were observed to produce short RNAs in an *rdrp*-dependent but *dicer*-independent manner. However, no discrete RNA species could be detected by northern blot, suggesting that they may be degradation products of mRNAs. Sequence analysis of these short RNA molecules and their flanking genomic regions indicated that this degradation was not random and suggested the existence of a *M. circinelloides* RNase that preferentially cleaves mRNAs two nucleotides downstream of any uracil. Besides the preference for uracil in the penultimate position, sequence logos also showed a biased purine/pyrimidine distribution, the rdRNAs being biased towards an A/G rich population. This bias is not specific to *Mucor* rdRNAs, since it is has been also found in canonical ex-siRNAs (Nicolás et al., 2010) and the small RNA datasets of seven different plant species (Aryal et al., 2012). It has been suggested that the distorted purine pyrimidine ratio in cellular sRNA populations implies that cells selectively accumulates purine rich strands and eliminates the pyrimidine rich strands, although the molecular mechanism for this active strand selection is not known (Aryal et al., 2012).

Different RNase-based mechanisms have been involved in the control of mRNA stability but an RdRP enzyme was not demonstrated to participate in any of those mechanisms (Akimitsu, 2008). Our results indicate that RdRP-1 and/or RdRP-2 proteins have a functional role in the degradation of specific mRNAs, since the levels of these mRNAs were significantly increased in *rdrp*$^-$ mutants. Thus, reduction of the mRNA degradation rate in the *rdrp*$^-$ mutants would be associated with a low accumulation of degradation products (rdRNAs), leading to the identification of the corresponding loci as *rdrp*-dependent. Confirming the non-canonical nature of this *rdrp*-dependent *dicer*-independent rdRNAs, only a minority of them were found associated with Ago-1, the *M. circinelloides* Argonaute protein involved in exogenous and endogenous RNAi canonical pathways (Cervantes et al., 2013). Although two other *ago* genes have been identified in *Mucor*, their genomic sequences and expression patterns do not suggest a role for their protein products in the degradation pathway described in this study (Cervantes et al., 2013).

We have analyzed the biological functions of genes regulated by this novel degradation pathway (**Table S1**). Although the large number of affected genes makes it difficult to precisely understand the processes regulated by this degradation pathway, it can be emphasized that many of those genes code for metabolic enzymes or proteins involved in regular cellular functions, such as mRNA processing, translation or signaling. Particularly interesting is the regulation of genes involved in heme biosynthesis or metabolism (**Figure 23**). Heme B, the most abundant heme, is synthetized by eight enzymatic steps, some of which occur in the cytoplasm and some in the mitochondrion (Franken et al., 2011) (**Figure 67A**). Five out of eight proteins involved in heme biosynthesis are regulated by the *rdrp*-dependent *dicer*-independent degradation pathway (**Figure 67B**), suggesting a role for this pathway in the regulation of heme-containing protein(s). Curiously, a *M. circinelloides* protein (ID 95051) highly similar to the ferrochetalase enzyme, which is required to bind iron to protoporphyrin IX, is regulated by *dicer*-dependent ex-siRNAs of class III (**Table S4**), which share some characteristics with the *rdrp*-dependent *dicer*-independent rdRNAs (see below). In addition to that, the uroporphyrinogen III methyltransferase, which controls the first of the three steps leading to the formation of siroheme from uroporphyrinogen III, is also regulated by this pathway (**Figure 67**). Siroheme is a heme-like prosthetic group for sulfite and nitrite reductases that is

required for methionine and cysteine synthesis (Franken et al., 2011). Finally, two proteins highly similar to methemoglobin reductases, which are involved in heme metabolism by reducing the iron in the heme group from the ferric state (methemoglobin) to the ferrous state of the normal hemoglobin, are also regulated by the *rdrp*-dependent *dicer*-independent degradation pathway (**Figure 67**).

A

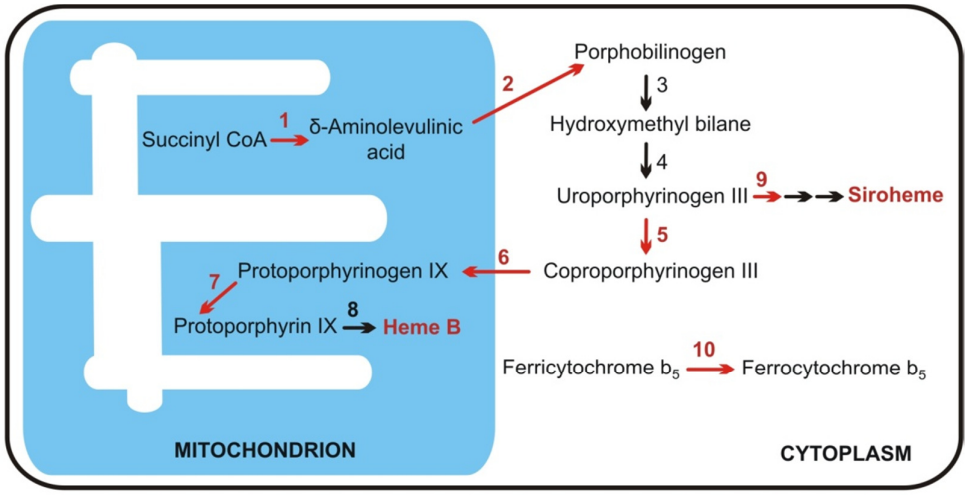

B

No.	Enzyme	*Mucor* protein
1	ALA synthase	ID 47616
2	ALA dehydratase	ID 93798
3	PGB deaminase	
4	Uroporphyrinogen III synthase	
5	Uroporphyrinogen III decarboxylase	ID 29038
6	Coproporphyrinogen III oxidase	ID 75718, ID 92569
7	Protoporphyrinogen oxidase	ID 93377, ID 39231
8	Ferrochelatase	
9	Uroporphyrinogen III methyltransferase	ID 88809
10	Methemoglobin reductase	ID 28312, ID 94941

Figure 67. Regulation of the heme group biosynthesis pathway by the non-canonical RNA degradation pathway. **(A)** Heme B biosynthesis pathway. Some reactions occur in the cytoplasm and some in the mitochondrion (blue). Substrates and products of each enzymatic step are indicated. The numbers correspond to the enzymatic activities shown in (B). The side branch leading to siroheme synthesis is schematically shown. Steps indicated in red are controlled by enzymes regulated by the *rdrp*-dependent *dicer*-independent degradation pathway. **(B)** *M. circinelloides* proteins corresponding to the enzymatic activities involved in heme biosynthesis pathway shown in (A).

Impairment of the degradation pathway in the *rdrp*$^-$ mutants would result in an increased accumulation of the mRNAs corresponding to the mentioned genes and

thus, an up-regulation of heme biosynthesis and, consequently, an increase of intracellular heme levels. In fungi, hemes are found in a number of biological relevant proteins, i.e. peroxidases, cytochrome, flavohemoglobins and others (Franken et al., 2011). Many of these proteins are involved in the response to different environmental stresses, such as low oxygen conditions (Hillmann et al., 2014). Interestingly, one of the most relevant fungal hemoproteins is catalase, which is essential for protecting the cell from oxidative damage (Hansberg et al., 2012).

The *M. circinelloides* glutamate cysteine ligase-like protein 87510 is also regulated by the *rdrp*-dependent *dicer*-independent degradation pathway (**Figure 23**). This enzyme, also named gamma-glutamylcysteine synthetase, catalyzes the first and rate-limiting step in the production of cellular antioxidant glutathione, which plays key roles in the response to several stress situations in fungi, including oxidative stress (Pocsi et al., 2004). Several other genes regulated by the *rdrp*-dependent *dicer*-independent pathway also encode antioxidant proteins, such as thioredoxin (ID 87683), glutaredoxin (ID 37397) and peroxiredoxin (ID 25842 and ID 51186). Up-regulation of these genes in the *rdrp*$^-$and *r3b2*$^-$mutants, together with the increase in heme biosynthesis, could explain the better response to oxidative stress shown by these strains relative to the wild type, manifested by their increased ability to germinate in presence of hydrogen peroxide (**Figure 34**). Detailed analysis of each of the above genes would be required to assess their specific roles in the responses of *M. circinelloides* to oxidative stress and other environmental signals. Besides their better response to oxidative stress, the *rdrp*$^-$ and *r3b2*$^-$ mutants showed defects in sexual interaction and production of zygospores, although these developmental processes were not affected in the *dcl*$^-$ and *ago-1*$^-$mutants (Nicolás et al., 2015; Trieu et al., 2015). The high number of genes regulated by the *rdrp*-dependent *dicer*-independent pathway containing domains involved in transcriptional regulation or signal transduction, makes difficult to ascertain the gene(s) responsible(s) for the sexual behavior of the *rdrp-1*$^-$, *rdrp-2*$^-$ and *r3b2*$^-$ mutants. However, it is worth noting that one of the genes regulated by this pathway codes for a protein (ID 43858) highly similar to the mating factor M secretion protein Mam1 of *Schizosaccharomyces pombe* ($1{,}3e^{-125}$), which is responsible for the secretion of the mating pheromone (Christensen et al., 1997). It is tempting to speculate that modulation of *M. circinelloides* protein expression in mutants affected in the *rdrp*-

dependent *dicer*-independent pathway could be responsible, at least in part, of the defects shown by those mutants in their sexual behavior.

V.1.2. The role of R3B2 in canonical and non-canonical RNA silencing pathways

We have identified the RNase III-like protein R3B2 as the RNase involved in the *rdrp*-dependent *dicer*-independent RNA degradation pathway. More than 1500 exonic loci were identified that produced sRNAs in a R3B2-dependent manner (**Table S2**). These loci included all but one *rdrp*-dependent *dicer*-independent loci, revealing the participation of this RNase in the degradation pathway (**Table S3**). Surprisingly, also a significant number of *dicer*-dependent ex-siRNA loci, mainly those belonging to the class III ex-siRNAs, were found to be dependent on R3B2 for their biogenesis (**Table S4**). Class III ex-siRNAs share several structural and functional features with the *rdrp*-dependent *dicer*-independent rdRNAs (Nicolás et al., 2010; Cervantes et al., 2013). They have the same polarity as mRNA and a random spread of size distribution, as well as a very strong preference for uracil in the penultimate position, and they do not specifically bind to Ago-1, as occurs with the *rdrp*-dependent *dicer*-independent rdRNAs. This allowed us to propose that class III ex-siRNAs are not produced by a canonical RNAi pathway (Nicolás et al., 2010). The difference with the *rdrp*-dependent *dicer*-independent rdRNAs relies in the participation of Dcl-1 or Dcl-2 in the biogenesis of class III ex-siRNAs. Thus, it can be suggested that the activity of RdRP-1 and/or RdRP-2 on target transcripts, presumably aberrant transcripts lacking normal processing signals such as a 5′ cap or a polyA tail, generates discrete dsRNA stretches that could be directly recognized by the RNase III-like R3B2, targeting those transcripts for degradation (*rdrp*-dependent, *dicer*-independent rdRNAs) or could be firstly processed by either Dcl-1 or Dcl-2 and after the initial cleavage the single stranded portions of mRNAs would be degraded by R3B2 (class III ex-siRNAs) (**Figure 68**).

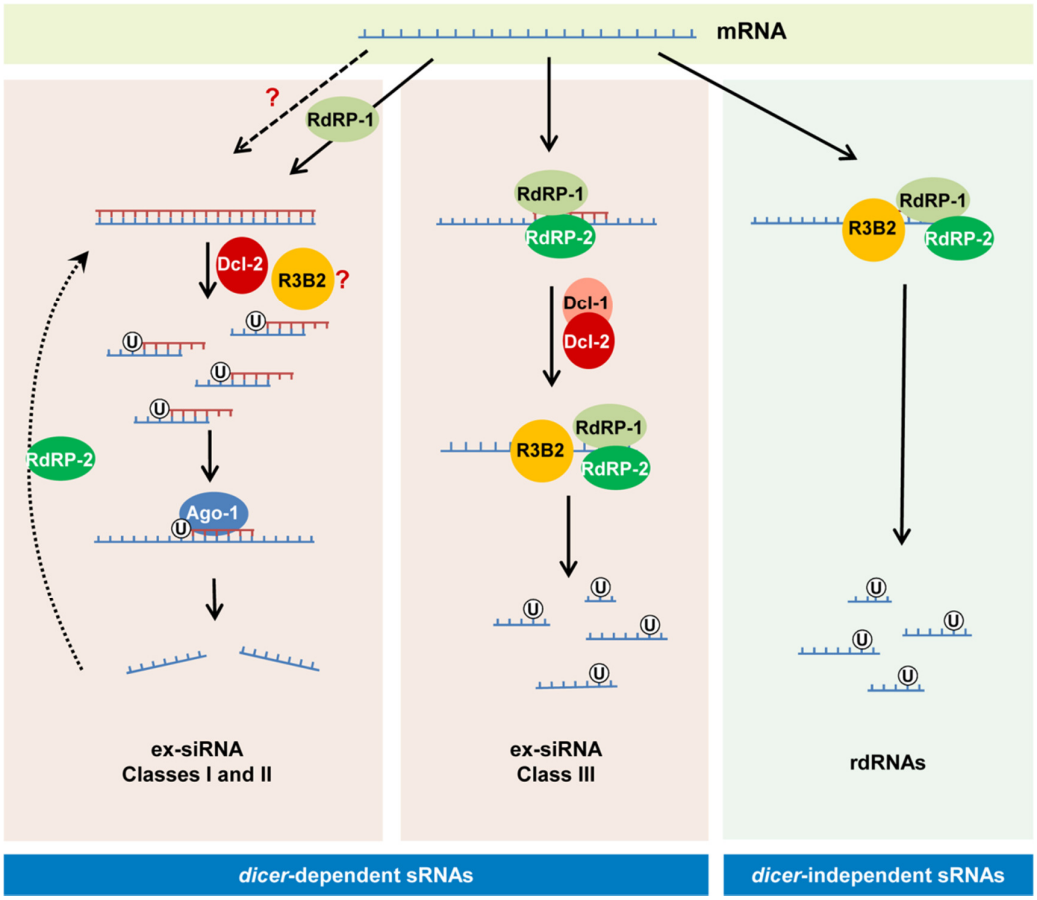

Figure 68. Models for production of the different classes of sRNAs in *M. circinelloides*. The *dicer*-independent sRNAs studied in this work (right) derive from specific transcripts that are targeted for degradation by RdRP-1 and/or RdRP-2 binding. The RdRP proteins bound to these transcripts may be able to make a short complementary strand that signals the RNase III-like protein R3B2 for degradation. This protein preferentially cleaves mRNAs two nucleotides downstream of any uracil, giving rise to different size fragments with a uracil in the penultimate position (rdRNAs). The *dicer*-dependent ex-siRNAs (left) can be classified into four classes depending on the component of the silencing machinery required for their biogenesis. Classes I and II correspond to Ago-1-bound ex-siRNAs that are processed by Dcl-2 from dsRNAs derived from cellular transcripts by the action of RdRP-1 (class II, solid arrows) or RdRP-2 (Class I, broken arrows). R3B2 plays a role in the production of some of these ex-siRNAs, although its specific role is not yet known. Classes I and II are canonical ex-siRNAs with a defined size of 23-24 nt and a preference for uracil at the 5' position. The structural characteristics of class III ex-siRNAs are similar to those of rdRNAs, suggesting that these ex-siRNAs are also degradation products generated by R3B2. The involvement of Dcl-1 or Dcl-2 in the biogenesis of class III ex-siRNAs suggests that the discrete dsRNA stretches produced by RdRP proteins must be processed by either Dcl-1 or Dcl-2 and after the initial cleavage the single stranded portions of mRNAs would be degraded by R3B2. Class IV ex-siRNAs, which require Dcl-1 and both RdRP-1 and RdRP-2 proteins for their biogenesis, are not indicated since they represent a small number of ex-siRNAs derived from only five exons.

R3B2contains a catalytic RNase III domain and two dsRBDs, which differ from typical class 1 RNase IIIs in terms of the number of dsRBDs. Only a single protein from *Arabidopsis thaliana*, the RNase III-like protein 2 (AtRTL2, At3g20420) display this unusual domain organization, although its catalytic domain

contains a canonical RNase III signature motif (Comella et al., 2008). Class 1 RNase IIIs are normally involved in the processing of ribosomal RNA precursors and some mRNAs. However, AtRTL2 has no effect on rRNA maturation *in vivo*, which suggests that it may function differently to RNase IIIs of class 1 (Kiyota et al., 2011). In fact, this protein cleaves dsRNAs *in vitro* giving rise to cleavage products of longer size than other class 1 RNases, and it is involved in the production of small RNAs derived from transgenes *in vivo*. This raised the possibility that AtRTL2 may interact with other *A. thaliana* Dicer enzymes to positively affect the Dicer activity in siRNA generation (Kiyota et al., 2011). Although the sequence similarity between AtRTL2 and *M. circinelloides* R3B2 is low, their similar and unique domain organization supports that R3B2 also has functions distinct from those of other class 1 RNase IIIs *in vivo*. Results shown here indicate that the RNase III domain-like of R3B2 is required for efficient R3B2 function in RNA silencing, although it lacks a canonical RNase III signature motif. The biochemical requirements for RNA cleavage by R3B2 are unknown, but the presence of two dsRBD, which might be utilized for protein–protein interactions (Fierro-Monti and Mathews, 2000), suggests that it may interact with other members of the RNAi machinery (e.g. RdRP or Dicer proteins) to degrade target transcripts or positively affect siRNA production.

Due to the participation of R3B2 in both, the canonical and non-canonical RNA pathways, the null *r3b2*$^-$ mutant presented phenotypes associated to alterations in cellular processes controlled by those pathways (Trieu et al., 2015). The *dcl-2*$^-$, *ago-1*$^-$ and *rdrp-2*$^-$ mutants, which participate in the canonical *dicer*-dependent ex-siRNA pathway, are affected in cellular processes connected with nutrient sensing of the cells, such as production of vegetative spores and autolysis induced by nutrient starvation (de Haro et al., 2009; Cervantes et al., 2013; Nicolás et al., 2015). Those processes are also affected in the *r3b2*$^-$ mutant, which initiates autolysis of aged mycelia induced by nutritional stress at earlier state than the wild type strain (Trieu et al., 2015) and presents a reduction in the production of vegetative spores relative to the wild-type (Trieu et al., 2015). Similarly, and besides their better response to oxidative stress demonstrated in this work (**Figure 34**), the *rdrp*$^-$ and *r3b2*$^-$ mutants showed defects in sexual interaction and production of zygospores (Nicolás et al., 2015; Trieu et al., 2015). These phenotypes have not been observed in *dcl*$^-$ or *ago-1*$^-$ mutants, suggesting that those processes are specifically regulated by the non-

canonical *rdrp*-dependent *dicer*-independent RNA degradation pathway and indicating that different silencing pathways regulate the response to specific environmental signals.

V.1.3. A genetic link between mRNA degradation and post-transcriptional RNA silencing

Most genes regulated by the *rdrp*-dependent *dicer*-independent pathway seem to be highly expressed, as denoted by the high number of sequences derived from those genes that are included in the EST repertoire sequenced from *M. circinelloides* (http://genome.jgi-psf.org/Mucci2/Mucci2.home.html). For instance, all but one of genes involved in heme biosynthesis and metabolism shown in **Figure 23** are present in the *Mucor* EST collection, whereas the global percentage of genes with ESTs in the *Mucor* genome is only 33%. It is tempting to speculate that this RdRP-dependent degradation process is a control mechanism for genes with high levels of expression, since elevated transcription increases the production of aberrant RNAs (Gazzani et al., 2004; Luo and Chen, 2007). All eukaryotic cells, including fungi, contain general and specialized mRNA decay pathways that target aberrant transcripts for degradation. Besides these quality control systems, the correct RNA turnover of mRNAs, carried out by defined degradation mechanisms, can play an important role in setting the basal level of mRNA expression and how that level is modulated by environmental stimuli (Parker, 2012). Although numerous components of the RNA degradation mechanisms have already been identified, no RdRP enzyme has been demonstrated to be involved in any of those mechanisms. However, several evidences suggest that proteins involved in proper mRNA turnover or RNA quality-control systems compete with the RNAi machinery for aberrant transcripts (Voinnet, 2008; Thran et al., 2012; Lange et al., 2014). In all the reported cases, the efficiency of transgene-induced gene silencing increased in mutants affected in the mRNA degradation pathways, suggesting that degradation of aberrant transcripts limits their entry into the RNAi pathway and providing insights into the interplay between mRNA degradation and post-transcriptional gene silencing. Here, we have shown a genetic link, the *rdrp* genes, between these two processes. The RdRP proteins bound to aberrant transcripts may be able to either make a short complementary strand that signals the RNase R3B2 for preferential degradation or synthesize long dsRNA

molecules that trigger the RNAi mechanism. How the RdRP enzymes discriminate what RNAs are directed to the canonical silencing pathway or to the degradation pathway is not known yet. However, it is worth noting that the results obtained in this work agree with the enhanced activation of the RNAi-induced epimutation pathway observed in the *rdrp-1*$^{-}$ mutants (Calo et al., 2014). It has been shown that spontaneous resistance to an antifungal drug via an epigenetic RNAi-mediated pathway that silences the drug target gene is highly increased in the *rdrp-1*$^{-}$ mutants, suggesting that in these mutants the RNA degradation pathway has been abolished and mRNAs are primarily directed to the canonical RNAi silencing pathway. The involvement of RdRPs in RNA degradation could represent the first step in the evolution of the RNAi mechanism. RNAi is a complex process and it is unlikely that the entire process developed at once. The RdRP could be the first player that somehow marked mRNAs for degradation. Later on, Dicer may have appeared and cleaved the RdRP products. Finally, Argonaute proteins evolved to acquire the siRNAs produced by Dicer and use them for further RNA degradation. It is tempting to speculate that in *M. circinelloides*, and probably other members of the mucoralean basal lineage of the fungal kingdom, all of these mechanisms are still simultaneously operating.

V.2. Functional analysis of *M. circinelloides* genome

The rapid development of sequencing techniques has allowed many genomic DNA sequences becoming available. However, a principal challenge is how to establish the connections between the DNA sequences and their functions in an organism. Large-scale analyses of gene functions have been performed in bacteria, yeast, animals and plants.

In animals, Fraser *et al* (2000) and Kamath *et al* (2003) performed systematic analyses of gene functions using RNAi. RNAi libraries were generated by cloning PCR fragments from total protein-coding genes into dsRNA-producing constructs to inhibit ~86% of the 19427 genes of *C. elegans.* As a result, 1722 genes were identified that control different phenotypes in this organism (Kamath et al., 2003). Also in plants, several genome-wide RNAi analyses have been performed, some of them using procedures for RNAi inactivation of several genes simultaneously. In an

Arabidopsis thaliana study, family-specific artificial microRNAs (amiRNAs) were designed using computational tools and utilized to identify several morphological phenotypes. Novel morphological and abscisic acid-insensitive germination mutants were identified for amiRNAs targeting zinc finger homeodomain transcription factors and MAPKKK, respectively (Hauser et al., 2013).

In fungi, several genome-wide analyses based on RNAi have been also performed. A functional genomic analysis using antisense RNA was carried out in the human pathogenic fungus *Candida albicans* (De Backer et al., 2001). Antisense RNAs were generated from antisense cDNA cloned into a vector with a GAL1 promoter. Those antisense RNAs could block translation by complementary binding with homologous sense RNAs transcribed from endogenous genes, resulting in the inhibition of the corresponding loci. After transformation and analyses of transformants, 86 genes critical for growth were identified, including 45 with unknown function (De Backer et al., 2001). Within filamentous fungi, the first silencing vector containing two opposite promoters was developed for the ascomycete *M. oryzae* and was used to identify genes involved in calcium-signalling by knocking down gene expression using dsRNA (Nguyen et al., 2008). After that, few attempts have been carried out in other fungi, probably because silencing is relatively inefficient compared to that with the hairpin system, perhaps due to the low efficiency of formation of dsRNA (Dang et al., 2011).

The molecular knowledge of the RNAi mechanism in *M. circinelloides* and the relevance of this organism as an emerging opportunistic pathogen make *Mucor* a suitable subject for RNAi-based functional analysis. In recent years, the number of cases of mucormycosis is becoming a public health issue due to an increasing population of patients suffering a compromised immunity (Kontoyiannis and Lewis, 2006). Besides that, an increasing number of cases of mucormycosis in immunocompetent, otherwise healthy individuals, has been reported in the last years (Bharathi and Arya, 2012; Pahwa et al., 2013; Verma et al., 2014; Matsudate et al., 2015). This makes an ongoing need to identify new targets and develop new therapeutic interventions for mucormycosis. Particularly, more than 200 people got digestive illness after ingestion of commercial yogurt which was contaminated with this fungus (Lee et al., 2014). The *M. circinelloides* f. *circinelloides* subspecies, the most virulent *Mucor* subspecies that is commonly associated with human infections,

was isolated from the contaminated yogurt (Lee et al., 2014). Very few virulence determinants have been identified in *Mucor*. As indicated before, a relationship between virulence and the size of the sporangiospores was demonstrated a few years ago (Li et al., 2011). Besides that, the calcineurin pathway seems to play an important role in the dimorphic transition and its relationship with virulence (Lee et al., 2013; Calo et al., 2014).

RNAi mechanisms in *M. circinelloides* are well known. Those include the canonical *dicer*-dependent RNA silencing and the non-canonical *dicer*-independent RNA degradation pathways (Nicolás et al., 2003; Trieu et al., 2015). Therefore, RNAi can be used as a tool for knockdown a gene in a genome-wide screening. We have carried out this study to specifically identify candidate genes to be involved in pathogenesis, among the 11719 genes annotated in the *Mucor* genome. Our goals included the construction of effective RNAi-based gDNA libraries for *M. circinelloides* and their use to identify candidate genes that participate in *Mucor* morphogenesis.

V.2.1. RNAi-based functional analysis of the *M. circinelloides* genome

RNAi pathways require the presence of triggered dsRNA molecules that are generated from aberrant transcripts or dsRNA-expressing constructs. To increase silencing efficiency, we have constructed genomic libraries using a dsRNA-expressing vector. This vector, pMAT1812 (**Figure 18**), can generate dsRNA molecules from inserts cloned between two opposite promoters. In order to increase representation, the gDNA isolated from the wild-type strain was digested with 7 different combinations of three restriction enzymes that produce compatible sticky ends to generate two genomic libraries (**Table 11**). Although using genomic DNA for cloning could produce plasmids containing only intergenic regions, the high gene density of the *Mucor* genome and the DNA size selected for cloning suggested that this situation should affect a low number of the recombinant plasmids. In theory, the dsRNAs generated from those dsRNA-expressing constructs, after transforming into *M. circinelloides* cells, can inhibit the expressions of the corresponding target genes through RNAi pathway activation. Screening and analyses of abnormal growth or morphogenesis phenotypes would allow identification of the candidate genes that are

responsible for these phenotypic changes. However, this method for knocking down gene expression is only effective if the corresponding endogenous genes are highly expressed, particularly during vegetative growth, since a threshold of gene expression is required for the target genes to be silenced (Nicolás et al., 2009). Therefore, genes with low-expression or those whose expression are only activated by specific signals, as may happen for some genes involved in pathogenesis, could not be detected by this strategy.

To validate the efficiency of the RNAi-based genomic libraries, a fragment of the carotenogenic gene *carB* was used as a silencing marker (**Figure 18**). Silencing of *carB* provokes the albino phenotype in *M. circinelloides* due to a significant reduction of β-carotene accumulation (Nicolás et al., 2003; Nicolás-Molina et al., 2008). The albino frequencies obtained after transformation with the two genomic libraries (68,8 and 72,1%; **Table 11**), indicated that those libraries efficiently activated the RNAi mechanism. As indicated before, the slight reduction of the silencing efficiency relative to that of hairpin RNA-producing constructs (Calo et al., 2012) could be due to the excessive size of the DNA fragment cloned between the opposite promoters, which would produce incomplete dsRNA molecules. In summary, RNAi-based genomic libraries could be used as an effective large-scale method for functional analyses in *M. circinelloides*. Further improvements could be performed to eliminate some of the potential problems of the libraries used, such as construction of an RNAi-based cDNA library. However, this library would only contain genes that are transcribed in a specific culture condition, which limits its use for analyzing phenotypes expressed under different conditions.

Analysis of the transformants obtained with the silencing libraries identified two genes, 51513 and 84675, whose silencing was responsible for the growth and morphogenesis phenotypes of strains 1 and 10-11, respectively (**Figure 46**). Those silenced strains showed reduced growth rate and asexual sporulation. The silenced strain 1 grew like yeast; it generated very compact colonies and was unable to produce vegetative spores. The strains 10 and 11 were also affected in their growth ability and sporulation (**Figure 46**). The involvement of RNAi in the abnormal phenotypes shown by those strains was demonstrated by Northern blot analyses, which showed a significant reduction of mRNA accumulations of the target genes and the presence of antisense siRNAs in the silenced strains relative to the wild type

(**Figures 47** and **48**). The sense siRNAs were non-detectable, a situation described previously in *M. circinelloides* (Nicolás et al., 2003) and *C. elegans* (Tijsterman et al., 2002) silencing. These results implied that a canonical RNAi mechanism was triggered in those silenced strains. The analyses of domain architectures of the proteins corresponding to genes 51513 and 84675 demonstrated that they encode Myosin class V and CLASP proteins, respectively.

V.2.2. Identification of two new candidate genes for *Mucor* pathogenesis

As mentioned above, two candidate genes, 51513 and 84675, were identified in the RNAi-based screening for phenotypes with a possible role in *Mucor* pathogenesis. Those genes encoded Myosin class V and CLASP proteins, respectively. Here, we discuss the putative structures and functions of these proteins in *M. circinelloides.*

V.2.2.1. Myo5 protein as a cargo transporter

Motor proteins are required for all cells to move, localize and segregate their organelles. Motor proteins include actin-based myosins, and microtubule-dependent kinesins and dyneins. Myosins play important roles in morphogenesis of filamentous fungi, since they are involved in the establishment and/or maintenance of polarity (reviewed by Harris, 2006). Myosin superfamily includes more than 35 classes (Odronitz and Kollmar, 2007) and plays important roles in many cellular processes, such as cytokinesis, cell adhesion, endocytosis, exocytosis, cell motility, mRNA and pigment transportation (reviewed by Hammer and Sellers, 2012). As indicated before, myosin proteins generally contain three regions, including head, neck and tail (Widenius, 2008; **Figure 55A**). The head region contains the motor domain and binds ATP and actin. The neck region is a connection between head and tail regions. And the tail region includes dimerization and cargo binding domains. The tail structure is the most important factor for classifying of distinct myosin classes (Hammer and Sellers, 2012).

Class V myosin, one of the most extensively studied myosins, has a wide-range distribution, being present in most of the higher eukaryotic cells (Provance and Mercer, 1999). This class of myosin differs from others by an extended neck and tail domains that allow dimerization. Myosin-V members have been found in a wide

range of species, such as animals, yeasts and plants (Provance and Mercer, 1999). In humans, three genes encoding class V myosins have been identified among the 38 myosin family genes. In *S. cerevisiae*, five myosin genes were identified, including two class V myosin genes (*myo2* and *myo4*) (Berg et al., 2001). In the dimorphic pathogenic fungus *U. maydis*, a single Myosin class V protein encoded by *myo5* is involved in mating, hyphal growth and pathogenicity (Weber et al., 2003).

In this study, we found that gene 51513 encodes a myosin class V protein in *M. circinelloides*. The 51513 protein has all the conserved domains found in Myosin class V family, including a motor domain (MYSc_type_V), two IQ motifs and a fMyo2p_CBD domain (**Figure 55B**). This finding strongly suggested that protein 51513 is a member of Myosin class V family in *M. circinelloides* and the corresponding gene and protein were named *mcmyo5* and Myo5, respectively. The absence of Myo5 protein inhibits hyphae formation and results in yeast-like growth, even though the analyzed strain was not homokaryotic. This suggested that *Mucor* cells require an adequate accumulation of myosin class V for normal hyphal growth. Unlike members of Myosin class V family in other organisms, *mcmyo5* gene could not be completely deleted from *Mucor* genome, suggesting that this member of Myosin-V plays other roles along with a cargo transporter that are essentials for *M. circinelloides* viability. Besides that, preliminary experiments on *Mucor* virulence using an insect host system have showed a significant reduction of virulence in *mcmyo5*$^{-}$ (MU465) mutant strain. This result suggested that Myo5 plays an important role in *M. circinelloides* pathogenesis, probably through its requirement for hyphal growth, and confirmed the relationship between yeast-like growth and hipovirulence (Lee et al., 2013; Calo et al., 2014). As indicated in **Table 15**, several proteins highly similar to Myo5 have been identified in the *Mucor* genome, suggesting that *Mucor* might contain more than one myosin class V protein. However, their putative functions are not redundant with Myo5, since the phenotypes observed correspond to the lack of function of the single *mcmyo5* gene. Further functional analyses would be required to decipher the role of the other myosins.

Filamentous fungi are defined by their ability to generate highly polarized hyphal growth (Harris, 2006). Unlike *U. maydis*, where the loss of Myo5 did not affect the tip growth of hyphae and sporidia (Weber et al., 2003), the loss of Myo5 in *Mucor* resulted in loss of cell polarity, since it generated the yeast-like morphology

under normal growth conditions. *M. circinelloides mcmyo5*$^{-}$ mutant cells only increase diameter, resulting in isotropic growth. Loss of polarized growth could be explained by the absence of transporters that deliver the secretory vesicles to the growth regions (Steinberg, 2011). It is possible that some of the vesicles that are specific cargo of Myo5 in *Mucor* constitute the Spitzenkörper (apical body), a structure found in fungal hyphae that acts as the organizing center for hyphal growth and morphogenesis. It consists of many small vesicles and is present in growing hyphal tips, during spore germination and where branch formation occurs (Bartnicki-Garcia, 2002). Its position in the hyphal tip correlates with the direction of hyphal growth, thus, lack of the appropriate vesicle concentration at specific points during germination of *mcmyo5*$^{-}$ mutant should avoid its polarized hyphal growth.

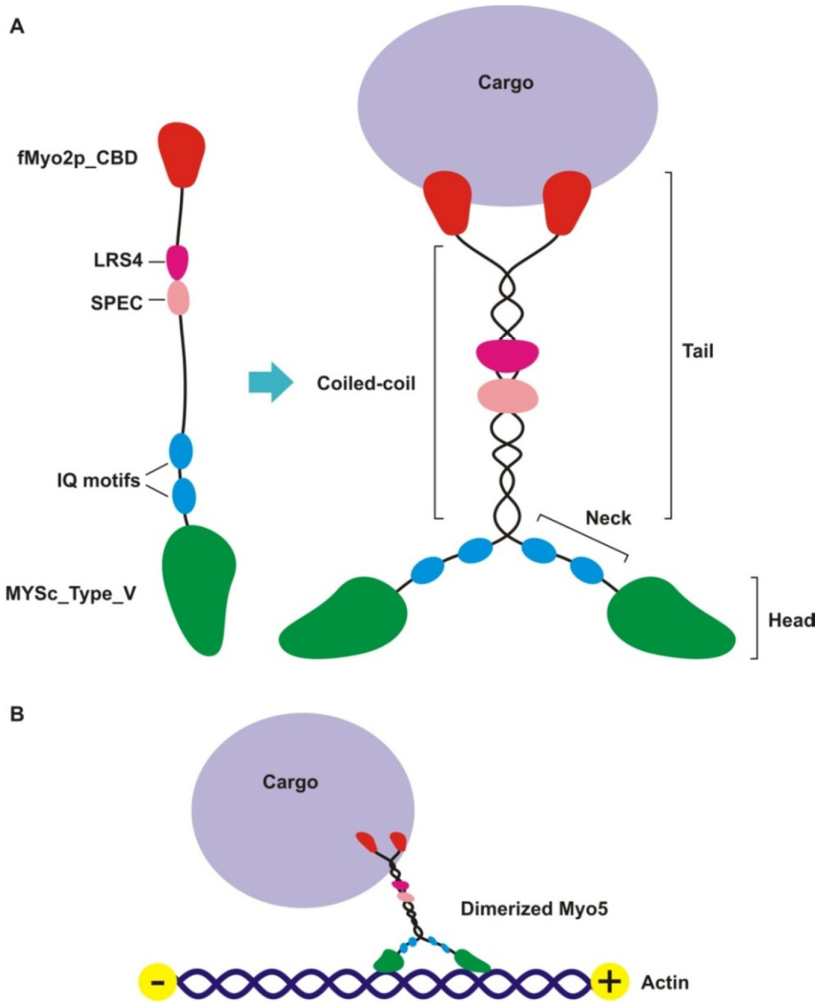

Figure 69. Putative structure and function of class V Myosin protein (51513) in *M. circinelloides*. **(A)** Domain architecture of Myo5 as monomer (inactive state) is shown on the left. The dimer structure of Myo5 in an active cargo-transporting state is indicated on the right. **(B)** The active dimer of Myo5 protein delivers a cargo by "walking" on actin filaments.

Mucor Myo5 protein might also be involved in pigment transportation, since colonies with albino phenotype were observed when the heterokaryotic strain MU465 was grown in MMC medium (data not shown). On the other hand, it was easy to observe the accumulation of large vesicles containing yellow pigments, probably carotenoids, in the cytoplasm of *mcmyo5*$^{-}$ cells (**Figure 64B**). Based on the characteristics of myosin class V, a model for Myo5 functions as a cargo transporter in *M. circinelloides* can be proposed. In this model, the active protein would consist in a homodimer, as proposed for this class of myosins (Hammer and Sellers, 2012) (**Figure 69A**), which would move on actin filaments as a cargo transporter (**Figure 69B**).

V.2.2.2. CLASP promotes microtubule assembly

Microtubules (MTs), a component of eukaryotic cytoskeleton, are dynamic protein polymers that are used to transport and organize cellular components for processes such as cell division, membrane trafficking and cell morphogenesis (Al-Bassam and Chang, 2011). In cells, MTs can grow and shrink at their ends by two inverse processes, called “rescue” and “catastrophe”, respectively. The MT dynamic depends on the balance of these two processes. The regulation of MT dynamics contributes to cell polarity and cell division (Al-Bassam et al., 2010).

CLASP (Cytoplasmic Linker ASsociated Protein) and XMAP215/Dis1 are two conserved families belonging to MAPs (Microtubule-associated proteins). XMAP215 proteins function as microtubule polymerases at MT (+) ends to promote MT assembly, while CLASPs accelerate MT recue and inhibit MT catastrophe processes. These two families are conserved from yeast to humans and regulate MT dynamics in the mitotic spindle and interphase (Bratman and Chang, 2008; reviewed by Al-Bassam and Chang, 2011).Those two MAP protein families have similar structures, XMAP215 containing two TOG domains (tumor overexpressed gene) and CLASP containing one or more TOG-like domains (TOGL). The TOG domains interact with soluble tubulin heterodimers, the building block of MTs (Slep, 2009).

Analysis of the crystal structure of the TOG3 domain in Zyg-9, a member of XMAP215/Dis1 family in *C. elegans*, revealed a conserved structure throughout all members of this family (Al-Bassam et al., 2007). This domain consists of six

conserved HEAT (Huntingtin, Elongation factor 3, the PR65/A subunit of protein phosphatase 2A and the lipid kinase Tor) repeat elements that are stacked side by side. Each HEAT domain includes two α-helices that are connected by a single loop. The loops between HEAT repeats and between individual α helices run along the narrow face of the domain, and this face is necessary for binding to αβ-tubulin heterodimers (Al-Bassam et al., 2007).

In *M. circinelloides*, gene 84675 encodes a protein of the CLASP family. This protein contains the conserved domain found in the CLASP family, CLASP_N (**Figure 52**), and the corresponding gene and protein were named *mcclasp* and Clasp, respectively. Searching the *Mucor* genome for proteins similar to Clasp did not give any results, suggesting that only one CLASP protein is found in *M. circinelloides*. A single CLASP orthologue has been also identified in several organisms, such as yeasts, *Drosophila*, and *Xenopus*, although two homologs, Clasp1 and Clasp2, are present in mammals, including humans (Lemos et al., 2000; Akhmanova et al., 2001; Mimori-Kiyosue et al., 2005; Grallert et al., 2006; Hannak and Heald, 2006; Ortiz et al., 2009), and three have been found in *C. elegans* (Espiritu et al., 2012). In mammals, Clasp1 protein plays an important role in the cell division process, since it regulates the spindle microtubule dynamics and is required for normal chromosome alignment and segregation (Maiato et al., 2003). Similarly, Clasp2 localizes at kinetochores, centrosomes, and spindle throughout mitosis. It has been suggested that the partial redundancy of CLASP functions during mitosis could be a possible mechanism to prevent aneuploidy in mammals (Pereira et al., 2006). The single *mcclasp* gene found in *Mucor* could be also involved in the mitotic process, since the mutant *mcclasp*$^{-}$ strain exhibits several growth defects.

Lack of Clasp protein also results in the abnormal hyphal morphology of *M. circinelloides* mycelia (**Figure 65**). We have identified the TOG-like domain within the Clasp protein of *M. circinelloides* by searching its full-length amino acid sequence for the canonical sequence of the HEAT domain of the XMAP215 family. Four putative HEAT units were identified (**Figure 70**), two of them located in the CLASP_N domain (**Figure 52**). Those results suggested that *M. circinelloides* Clasp could contain one or more TOGL domains that may play a role in binding tubulin heterodimers. This binding probably helps Clasp protein to accelerate rescue and reduce catastrophe of MTs, resulting in the stability of MTs in *M. circinelloides* wild

type. However, like other CLASP members (Al-Bassam and Chang, 2011), TOGL domains of *M. circinelloides* Clasp also share weak sequence homology with TOG domains of XMAP215/Dis1 family. Therefore, further functional analysis of these putative TOGL domains are required to understand how *Mucor* Clasp protein works.

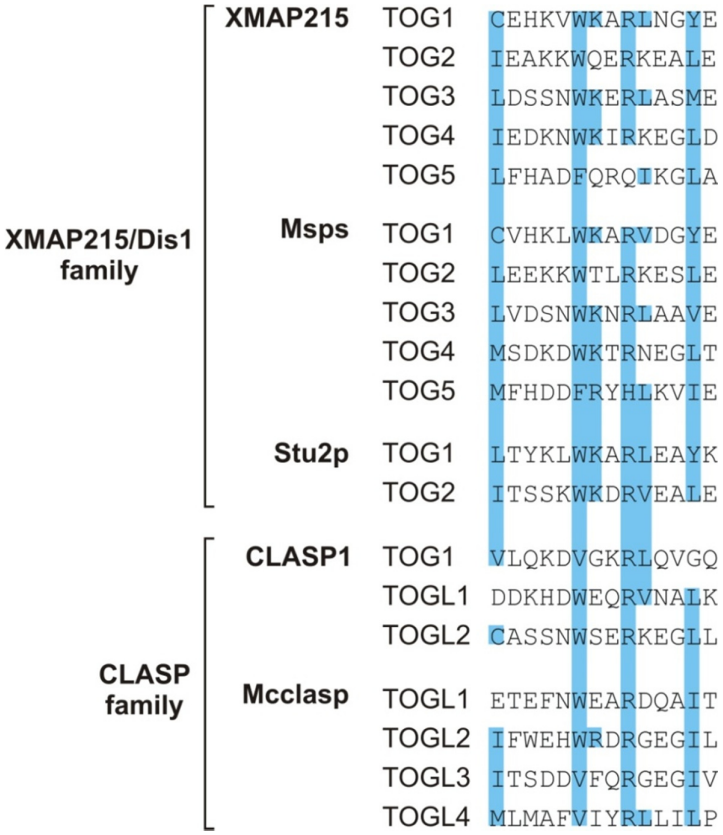

Figure 70. Sequence alignment of the conserved intra-HEAT loop region of XMAP215 and CLASP families. This region is necessary for binding of those proteins to αβ-tubulin heterodimers. XMAP215 family includes XMAP215 (*Xenopus laevis*, GenBank: CAB61894.1), Msps (*D. melanogaster,* GenBank: CAB55772.1) and Stu2p (*S. cerevisiae,* GenBank: AJV86374.1). CLASP family includes CLASP1 (*H. sapiens,* UniProtKB/Swiss-Prot: Q7Z460.1) and Mcclasp (*M. circinelloides*, ID 84675). The alignments of Msps, Stu2 and CLASP1 proteins were collected from Slep (2009).

As indicated before, Clasp proteins are involved in the stability of MTs, which are essential for the motility of motor proteins, such as kinesins and dyneins. Kinesins participate in the maintenance of the polarity of filamentous fungi (reviewed by Harris, 2006), which could explain the reduction of polarity indexes of *mcclasp*$^{-}$ null mutant relative to the wild-type strain (**Figure 64**). On the other hand, unlike Myo5, kinesins are not involved in polarity establishment. Therefore, the *Mucor* strain without Clasp protein is still able to generate hyphal growth, but its expanding rate is lower than the wild-type strain (**Figure 62**). The *mcclasp*$^{-}$ null

mutant strain (MU464) also exhibits a strong reduction of growth rate and sporulation (**Figures 62** and **63**) relative to the wild-type strain. Additionally, this mutant generates more secondary branches and "pseudo-septa" than the wild-type strain (**Figure 65**). The increase of secondary branches could be a result of changes in vesicle distributions, since lack of Clasp protein in the mutant strain could produce shorter and/or unstable MTs, which are the roads for the vesicle transporters, such as kinesins. It is tempting to speculate that the abnormal distribution of vesicles containing growth factors in smaller areas along hyphae can produce more branches than the wild type strain. Finally, and contrary to the *mcmyo5*$^-$ mutant strain, the *mcclasp*$^-$ mutant did not show a significant reduction of virulence relative to the wild type in an insect host system (**Figure 66**). This preliminary result suggested that Clasp protein, although essential for MTs stability, does not play an important role in *M. circinelloides* pathogenesis. However, further analysis would be required to investigate if the strong reduction of growth rate and vegetative sporulation in the *mcclasp* mutant could have any role in *Mucor* virulence.

VI. CONCLUSIONS

The results obtained of this study lead to the following conclusions:

1. A novel non-canonical RNA silencing mechanism promoting mRNA degradation in *M. circinelloides* has been identified and characterized. This pathway requires the presence of RdRP-1 and RdRP-2, but neither DCL-1 nor DCL-2 proteins. The degradation mechanism produces small RNA fragments that have been named as *rdrp*-dependent degraded RNA (rdRNA).

2. The rdRNA class includes molecules that correspond almost exclusively to exonic regions of protein-coding loci. They are exclusively sense to the mRNAs and show a random spread of size distribution with a strong preference for uracil at the penultimate position. Most of these rdRNA molecules are not specifically bound to Ago-1 protein.

3. The *rdrp*-dependent *dicer*-independent non-canonical pathway regulates the expression of more than 500 loci by degrading their mRNA transcripts. The regulated genes are involved in metabolism, information storage and processing, and cellular processes and signaling. The RNA degradation pathway also participates in the response to specific environmental signals.

4. Four candidate genes were identified as putative RNases to be involved in the non-canonical RNA degradation pathway. Functional analysis of the corresponding disruption mutants indicated that one of those candidates, named as *r3b2*, participates not only in the non-canonical *rdrp*-dependent degradation pathway but also in the canonical *dicer*-dependent RNAi pathway. The R3B2 protein plays a crucial role in both rdRNA and class III ex-siRNA biogenesis.

5. R3B2 protein has unique domain architecture, with an RNase III-like domain and two dsRBD domains. R3B2 belongs to a protein family that seems to be specific of the order mucorales.

6. The catalytic RNase III-like domain of R3B2 is required for accurate functions of this protein in both, the canonical *dicer*-dependent RNA silencing and the non-canonical *rdrp*-dependent RNA degradation

mechanisms. Mutations in the conserved acidic residues of this domain cause defective protein which loses its catalytic functions.

7. A new approach for large-scale functional genomics using RNAi has been successfully developed in *M. circinelloides*. RNAi-based genomic libraries were constructed to suppress expression of endogenous genes through the canonical silencing mechanism.

8. Gene silencing resulting in abnormal growth and morphogenesis was selected as an indication of a possible role of the silenced genes in *Mucor* pathogenesis. Silencing assays and molecular analyses identified two out of seven candidate genes whose silencing provokes a significant reduction in growth rate and vegetative sporulation.

9. The *mcmyo5* gene encodes a member of Myosin class V family in *M. circinelloides*. The Mcmyo5 protein contains the canonical domains found in this family and probably functions as a cargo transporter. The absence of gene *mcmyo5* results in a yeast-like morphology of *M. circinelloides*, due to a significant reduction of growth rate and a complete loss of polarized growth, as well as a reduction in the production of vegetative spores. This Myosin class V protein also plays an important role in the virulence of *M. circinelloides* in an insect host model.

10. The *mcclasp* gene encodes a protein of the CLASP family. The Mcclasp protein contains a CLASP_N domain and it is probably involved in the dynamics of microtubules. Only one member of the CLASP family is present in *M. circinelloides*. The null *mcclasp*$^-$ mutant shows a strong decrease in growth rate, vegetative sporulation and cell polarity index relative to wild-type strain, although it is able to perform polarized growth. However, Clasp protein does not play any significant role in *Mucor* pathogenesis.

VII. REFERENCES

Aiyar, A., Xiang, Y., and Leis, J. (1996). Site-directed mutagenesis using overlap extension PCR. *Methods in Molecular Biology* 57, 177-191.

Akhmanova, A., Hoogenraad, C.C., Drabek, K., Stepanova, T., Dortland, B., Verkerk, T., Vermeulen, W., Burgering, B.M., De Zeeuw, C.I., Grosveld, F., et al. (2001). Clasps are CLIP-115 and -170 associating proteins involved in the regional regulation of microtubule dynamics in motile fibroblasts. *Cell* 104, 923-935.

Akimitsu, N. (2008). Messenger RNA surveillance systems monitoring proper translation termination. *Journal of Biochemistry* 143, 1-8.

Al-Bassam, J., and Chang, F. (2011). Regulation of microtubule dynamics by TOG-domain proteins XMAP215/Dis1 and CLASP. *Trends in Cell Biology* 21, 604-614.

Al-Bassam, J., Larsen, N.A., Hyman, A.A., and Harrison, S.C. (2007). Crystal structure of a TOG domain: conserved features of XMAP215/Dis1-family TOG domains and implications for tubulin binding. *Structure* 15, 355-362.

Al-Bassam, J., Kim, H., Brouhard, G., van Oijen, A., Harrison, S.C., and Chang, F. (2010). CLASP promotes microtubule rescue by recruiting tubulin dimers to the microtubule. *Developmental Cell* 19, 245-258.

Alexander, W.G., Raju, N.B., Xiao, H., Hammond, T.M., Perdue, T.D., Metzenberg, R.L., Pukkila, P.J., and Shiu, P.K. (2008). DCL-1 colocalizes with other components of the MSUD machinery and is required for silencing. *Fungal Genetics and Biology* 45, 719-727.

Altschul, S.F., Madden, T.L., Schaffer, A.A., Zhang, J., Zhang, Z., Miller, W., and Lipman, D.J. (1997). Gapped BLAST and PSI-BLAST: a new generation of protein database search programs. *Nucleic Acids Research* 25, 3389-3402.

Aryal, R., Yang, X., Yu, Q., Sunkar, R., Li, L., and Ming, R. (2012). Asymmetric purine-pyrimidine distribution in cellular small RNA population of papaya. *BMC Genomics* 13, 682.

Bartel, D.P. (2004). MicroRNAs: genomics, biogenesis, mechanism, and function. *Cell* 116, 281-297.

Bartnicki-García, S. (2002). Hyphal tip growth: Outstanding questions. In "Molecular Biology of Fungal Development" (H. D. Osiewacz, Ed.). *Marcel Dekker, New York.* pp. 29-58.

Bartnicki-García, S., and Nickerson, W.J. (1962). Induction of yeast-like development in *Mucor* by carbon dioxide. *Journal of Bacteriology* 84, 829-840.

Bastidas, R.J., Shertz, C.A., Lee, S.C., Heitman, J., and Cardenas, M.E. (2012). Rapamycin exerts antifungal activity in vitro and in vivo against *Mucor circinelloides* via FKBP12-dependent inhibition of Tor. *Eukaryotic Cell* 11, 270-281.

Benito, E.P., Diaz-Minguez, J.M., Iturriaga, E.A., Campuzano, V., and Eslava, A.P. (1992). Cloning and sequence analysis of the *Mucor circinelloides pyrG* gene encoding orotidine-5'-monophosphate decarboxylase: use of *pyrG* for homologous transformation. *Gene* 116, 59-67.

Berg, J.S., Powell, B.C., and Cheney, R.E. (2001). A millennial myosin census. *Molecular Biology of the Cell* 12, 780-794.

Bharathi, R., and Arya, A.N. (2012). Mucormycosis in an immunocompetent patient. *Journal of Oral and Maxillofacial Pathology* 16, 308-309.

Bi, E., Chiavetta, J.B., Chen, H., Chen, G.C., Chan, C.S., and Pringle, J.R. (2000). Identification of novel, evolutionarily conserved Cdc42p-interacting proteins and of redundant pathways linking Cdc24p and Cdc42p to actin polarization in yeast. *Molecular Biology of the Cell* 11, 773-793.

Bologna, N.G., and Voinnet, O. (2014). The diversity, biogenesis, and activities of endogenous silencing small RNAs in *Arabidopsis. Annual Review of Plant Biology* 65, 473-503.

Bratman, S.V., and Chang, F. (2008). Mechanisms for maintaining microtubule bundles. *Trends in Cell Biology* 18, 580-586.

Brown, J. (2005). Zygomycosis: an emerging fungal infection. *American Journal of Health-system Pharmacy* 62, 2593-2596.

Calo, S. (2010). Polimerasas de RNA y su papel en el silenciamiento génico mediado por RNA en *Mucor circinelloides*. *Tesis Doctoral. Universidad de Murcia.*

Calo, S., Nicolás, F.E., Vila, A., Torres-Martínez, S., and Ruiz-Vázquez, R.M. (2012). Two distinct RNA-dependent RNA polymerases are required for initiation and amplification of RNA silencing in the basal fungus *Mucor circinelloides*. *Molecular Microbiology* 83, 379-394.

Calo, S., Shertz-Wall, C., Lee, S.C., Bastidas, R.J., Nicolás, F.E., Granek, J.A., Mieczkowski, P., Torres-Martínez, S., Ruiz-Vázquez, R.M., Cardenas, M.E., et al. (2014). Antifungal drug resistance evoked via RNAi-dependent epimutations. *Nature* 513, 555-558.

Carreras-Villasenor, N., Esquivel-Naranjo, E.U., Villalobos-Escobedo, J.M., Abreu-Goodger, C., and Herrera-Estrella, A. (2013). The RNAi machinery regulates growth and development in the filamentous fungus *Trichoderma atroviride*. *Molecular Microbiology* 89, 96-112.

Catalanotto, C., Azzalin, G., Macino, G., and Cogoni, C. (2002). Involvement of small RNAs and role of the *qde* genes in the gene silencing pathway in *Neurospora. Genes and Development* 16, 790-795.

Catalanotto, C., Pallotta, M., ReFalo, P., Sachs, M.S., Vayssie, L., Macino, G., and Cogoni, C. (2004). Redundancy of the two *dicer* genes in transgene-induced posttranscriptional gene silencing in *Neurospora crassa. Molecular and Cellular Biology* 24, 2536-2545.

Cervantes, M., Vila, A., Nicolás, F.E., Moxon, S., de Haro, J.P., Dalmay, T., Torres-Martínez, S., and Ruiz-Vázquez, R.M. (2013). A single *argonaute* gene participates in exogenous and endogenous RNAi and controls cellular functions in the basal fungus *Mucor circinelloides. PloS One* 8, e69283.

Chang, S.S., Zhang, Z., and Liu, Y. (2012). RNA interference pathways in fungi: mechanisms and functions. *Annual Review of Microbiology* 66, 305-323.

Chayakulkeeree, M., Ghannoum, M.A., and Perfect, J.R. (2006). Zygomycosis: the re-emerging fungal infection. *European Journal of Clinical Microbiology and Infectious Diseases* 25, 215-229.

Chesneau, L., Dupre, S., Burdina, A., Roger, J., Le Panse, S., Jacquet, M., and Cuif, M.H. (2004). Gyp5p and Gyl1p are involved in the control of polarized exocytosis in budding yeast. *Journal of Cell Science* 117, 4757-4767.

Christensen, P.U., Davey, J., and Nielsen, O. (1997). The *Schizosaccharomyces pombe* mam1 gene encodes an ABC transporter mediating secretion of M-factor. *Molecular and General Genetics* 255, 226-236.

Cogoni, C., and Macino, G. (1997). Isolation of quelling-defective (*qde*) mutants impaired in posttranscriptional transgene-induced gene silencing in *Neurospora crassa. Proceedings of the National Academy of Sciences of the United States of America* 94, 10233-10238.

Cogoni, C., and Macino, G. (1999a). Gene silencing in *Neurospora crassa* requires a protein homologous to RNA-dependent RNA polymerase. *Nature* 399, 166-169.

Cogoni, C., and Macino, G. (1999b). Posttranscriptional gene silencing in *Neurospora* by a RecQ DNA helicase. *Science* 286, 2342-2344.

Comella, P., Pontvianne, F., Lahmy, S., Vignols, F., Barbezier, N., Debures, A., Jobet, E., Brugidou, E., Echeverria, M., and Saez-Vasquez, J. (2008). Characterization of a ribonuclease III-like protein required for cleavage of the pre-rRNA in the 3'ETS in *Arabidopsis. Nucleic Acids Research* 36, 1163-1175.

Dang, Y., Yang, Q., Xue, Z., and Liu, Y. (2011). RNA interference in fungi: pathways, functions, and applications. *Eukaryotic Cell* 10, 1148-1155.

De Backer, M.D., Nelissen, B., Logghe, M., Viaene, J., Loonen, I., Vandoninck, S., de Hoogt, R., Dewaele, S., Simons, F.A., Verhasselt, P., et al. (2001). An antisense-based functional genomics approach for identification of genes critical for growth of *Candida albicans. Nature Biotechnology* 19, 235-241.

de Haro, J.P. (2010). Silenciamiento génico en *Mucor circinelloides*: análisis estructural y funcional del gen *dicer-2*. *Tesis Doctoral. Universidad de Murcia*.

de Haro, J.P., Calo, S., Cervantes, M., Nicolás, F.E., Torres-Martínez, S., and Ruiz-Vázquez, R.M. (2009). A single *dicer* gene is required for efficient gene silencing associated with two classes of small antisense RNAs in *Mucor circinelloides. Eukaryotic Cell* 8, 1486-1497.

Dereeper, A., Guignon, V., Blanc, G., Audic, S., Buffet, S., Chevenet, F., Dufayard, J.F., Guindon, S., Lefort, V., Lescot, M., et al. (2008). Phylogeny.fr: robust phylogenetic analysis for the non-specialist. *Nucleic Acids Research* 36, W465-469.

Dlakic, M. (2006). DUF283 domain of Dicer proteins has a double-stranded RNA-binding fold. *Bioinformatics* 22, 2711-2714.

Drinnenberg, I.A., Fink, G.R., and Bartel, D.P. (2011). Compatibility with killer explains the rise of RNAi-deficient fungi. *Science* 333, 1592.

Edgar, R.C. (2004). MUSCLE: multiple sequence alignment with high accuracy and high throughput. *Nucleic Acids Research* 32, 1792-1797.

Emri, T., Molnar, Z., Szilagyi, M., and Pocsi, I. (2008). Regulation of autolysis in *Aspergillus nidulans*. *Applied Biochemistry and Biotechnology* 151, 211-220.

Espiritu, E.B., Krueger, L.E., Ye, A., and Rose, L.S. (2012). CLASPs function redundantly to regulate astral microtubules in the *C. elegans* embryo. *Developmental Biology* 368, 242-254.

Feinberg, A.P., and Vogelstein, B. (1983). A technique for radiolabeling DNA restriction endonuclease fragments to high specific activity. *Analytical Biochemistry* 132, 6-13.

Feinberg, A.P., and Vogelstein, B. (1984). "A technique for radiolabeling DNA restriction endonuclease fragments to high specific activity". Addendum. *Analytical Biochemistry* 137, 266-267.

Fierro-Monti, I., and Mathews, M.B. (2000). Proteins binding to duplexed RNA: one motif, multiple functions. *Trends in Biochemical Sciences* 25, 241-246.

Fire, A., Xu, S., Montgomery, M.K., Kostas, S.A., Driver, S.E., and Mello, C.C. (1998). Potent and specific genetic interference by double-stranded RNA in *Caenorhabditis elegans*. *Nature* 391, 806-811.

Fischer, S.E. (2010). Small RNA-mediated gene silencing pathways in *C. elegans*. *The International Journal of Biochemistry and Cell Biology* 42, 1306-1315.

Franken, A.C., Lokman, B.C., Ram, A.F., Punt, P.J., van den Hondel, C.A., and de Weert, S. (2011). Heme biosynthesis and its regulation: towards understanding and improvement of heme biosynthesis in filamentous fungi. *Applied Microbiology and Biotechnology* 91, 447-460.

Fraser, A.G., Kamath, R.S., Zipperlen, P., Martinez-Campos, M., Sohrmann, M. and Ahringer, J. (2000). Functional genomic analysis of *C. elegans* chromosome I by systematic RNA interference. *Nature* 408:325–330.

Galagan, J.E., Calvo, S.E., Borkovich, K.A., Selker, E.U., Read, N.D., Jaffe, D., FitzHugh, W., Ma, L.J., Smirnov, S., Purcell, S., et al. (2003). The genome sequence of the filamentous fungus *Neurospora crassa. Nature* 422, 859-868.

Gazzani, S., Lawrenson, T., Woodward, C., Headon, D., and Sablowski, R. (2004). A link between mRNA turnover and RNA interference in *Arabidopsis. Science* 306, 1046-1048.

Geer, L.Y., Domrachev, M., Lipman, D.J., and Bryant, S.H. (2002). CDART: protein homology by domain architecture. *Genome Research* 12, 1619-1623.

Ghildiyal, M., and Zamore, P.D. (2009). Small silencing RNAs: an expanding universe. *Nature Reviews Genetics* 10, 94-108.

Gooday, G.W., Fawcett, P., Green, D. and Shaw, G. (1973). The formation of fungal sporopollenin in the zygospore wall of *Mucor mucedo*: a role for the sexual carotenogenesis in the Mucorales. *Journal of General Microbiology* 74, 233-239.

Grallert, A., Beuter, C., Craven, R.A., Bagley, S., Wilks, D., Fleig, U., and Hagan, I.M. (2006). *S. pombe* CLASP needs dynein, not EB1 or CLIP170, to induce microtubule instability and slows polymerization rates at cell tips in a dynein-dependent manner. *Genes and Development* 20, 2421-2436.

Green M.R. and Sambrook, J. (2012). Molecular cloning: a laboratory manual. *New York: Cold Spring Harbor Laboratory Press.*

Gurr S.J., Unkles S.E. and Kinghorn J.R. (1987). The structure and organization of nuclear genes of filamentous fungi. In “Gene structure in eukaryotic microbes”. *IRL Press.* pp 93-140.

Gutierrez, A., Lopez-Garcia, S., and Garre, V. (2011). High reliability transformation of the basal fungus *Mucor circinelloides* by electroporation. *Journal of Microbiological Methods* 84, 442-446.

Hammer, J.A. 3rd, and Sellers, J.R. (2012). Walking to work: roles for class V myosins as cargo transporters. *Nature Reviews. Molecular Cell Biology* 13, 13-26.

Hammond, T.M., Andrewski, M.D., Roossinck, M.J., and Keller, N.P. (2008). *Aspergillus* mycoviruses are targets and suppressors of RNA silencing. *Eukaryotic Cell* 7, 350-357.

Hammond, T.M., Xiao, H., Boone, E.C., Perdue, T.D., Pukkila, P.J., and Shiu, P.K. (2011). SAD-3, a putative helicase required for meiotic silencing by unpaired DNA, interacts with other components of the silencing machinery. *G3* 1, 369-376.

Hammond, T.M., Xiao, H., Boone, E.C., Decker, L.M., Lee, S.A., Perdue, T.D., Pukkila, P.J., and Shiu, P.K. (2013). Novel proteins required for meiotic silencing by unpaired DNA and siRNA generation in *Neurospora crassa*. *Genetics* 194, 91-100.

Hanahan, D. (1983). Studies on transformation of *Escherichia coli* with plasmids. *Journal of Molecular Biology* 166, 557-580.

Hannak, E., and Heald, R. (2006). Xorbit/CLASP links dynamic microtubules to chromosomes in the *Xenopus* meiotic spindle. *The Journal of Cell Biology* 172, 19-25.

Hansberg, W., Salas-Lizana, R., and Dominguez, L. (2012). Fungal catalases: function, phylogenetic origin and structure. *Archives of Biochemistry and Biophysics* 525, 170-180.

Harris, S.D. (2006). Cell polarity in filamentous fungi: shaping the mold. *International Review of Cytology* 251, 41-77.

Hauser, F., Chen, W., Deinlein, U., Chang, K., Ossowski, S., Fitz, J., Hannon, G.J., and Schroeder, J.I. (2013). A genomic-scale artificial microRNA library as a tool to investigate the functionally redundant gene space in *Arabidopsis. The Plant Cell* 25, 2848-2863.

Hillmann, F., Linde, J., Beckmann, N., Cyrulies, M., Strassburger, M., Heinekamp, T., Haas, H., Guthke, R., Kniemeyer, O., and Brakhage, A.A. (2014). The novel globin protein fungoglobin is involved in low oxygen adaptation of *Aspergillus fumigatus. Molecular Microbiology* 93, 539-553.

Ho, S.N., Hunt, H.D., Horton, R.M., Pullen, J.K., and Pease, L.R. (1989). Site-directed mutagenesis by overlap extension using the polymerase chain reaction. *Gene* 77, 51-59.

Holmes, D.S., and Quigley, M. (1981). A rapid boiling method for the preparation of bacterial plasmids. *Analytical Biochemistry* 114, 193-197.

Jaskiewicz, L., and Filipowicz, W. (2008). Role of Dicer in posttranscriptional RNA silencing. *Current Topics in Microbiology and Immunology* 320, 77-97.

Jinek, M., and Doudna, J.A. (2009). A three-dimensional view of the molecular machinery of RNA interference. *Nature* 457, 405-412.

Kamath, R.S., Fraser, A.G., Dong, Y., Poulin, G., Durbin, R., Gotta, M., Kanapin, A., Le Bot, N., Moreno, S., Sohrmann, M., et al. (2003). Systematic functional analysis of the *Caenorhabditis elegans* genome using RNAi. *Nature* 421, 231-237.

Kang, W., Matsushita, Y., Grohmann, L., Graack, H.R., Kitakawa, M., and Isono, K. (1991). Cloning and analysis of the nuclear gene for YmL33, a protein of the large subunit of the mitochondrial ribosome in *Saccharomyces cerevisiae. Journal of Bacteriology* 173, 4013-4020.

Kashem, S.W., Igyarto, B.Z., Gerami-Nejad, M., Kumamoto, Y., Mohammed, J., Jarrett, E., Drummond, R.A., Zurawski, S.M., Zurawski, G., Berman, J., et al. (2015). *Candida albicans* morphology and dendritic cell subsets determine T helper cell differentiation. *Immunity* 42, 356-366.

Kiyota, E., Okada, R., Kondo, N., Hiraguri, A., Moriyama, H., and Fukuhara, T. (2011). An *Arabidopsis* RNase III-like protein, AtRTL2, cleaves double-stranded RNA in vitro. *Journal of Plant Research* 124, 405-414.

Kontoyiannis, D.P., and Lewis, R.E. (2006). Invasive zygomycosis: update on pathogenesis, clinical manifestations, and management. *Infectious Disease Clinics of North America* 20, 581-607.

Lakatos, L., Csorba, T., Pantaleo, V., Chapman, E.J., Carrington, J.C., Liu, Y.P., Dolja, V.V., Calvino, L.F., Lopez-Moya, J.J., and Burgyan, J. (2006). Small RNA binding is a common strategy to suppress RNA silencing by several viral suppressors. *The EMBO Journal* 25, 2768-2780.

Lange, H., Zuber, H., Sement, F.M., Chicher, J., Kuhn, L., Hammann, P., Brunaud, V., Berard, C., Bouteiller, N., Balzergue, S., et al. (2014). The RNA helicases AtMTR4 and HEN2 target specific subsets of nuclear transcripts for degradation by the nuclear exosome in *Arabidopsis thaliana. PLoS Genetics* 10, e1004564.

Larkin, M.A., Blackshields, G., Brown, N.P., Chenna, R., McGettigan, P.A., McWilliam, H., Valentin, F., Wallace, I.M., Wilm, A., Lopez, R., et al. (2007). Clustal W and Clustal X version 2.0. *Bioinformatics* 23, 2947-2948.

Lasker, B.A., and Borgia, P.T. (1980). High-frequency heterokaryon formation by *Mucor racemosus. Journal of Bacteriology* 141, 565-569.

Lee, D.W., Pratt, R.J., McLaughlin, M., and Aramayo, R. (2003). An argonaute-like protein is required for meiotic silencing. *Genetics* 164, 821-828.

Lee, H.C., Chang, S.S., Choudhary, S., Aalto, A.P., Maiti, M., Bamford, D.H., and Liu, Y. (2009). qiRNA is a new type of small interfering RNA induced by DNA damage. *Nature* 459, 274-277.

Lee, H.C., Aalto, A.P., Yang, Q., Chang, S.S., Huang, G., Fisher, D., Cha, J., Poranen, M.M., Bamford, D.H., and Liu, Y. (2010a). The DNA/RNA-dependent RNA polymerase QDE-1 generates aberrant RNA and dsRNA for RNAi in a process requiring replication protein A and a DNA helicase. *PLoS Biology* 8.

Lee, H.C., Li, L., Gu, W., Xue, Z., Crosthwaite, S.K., Pertsemlidis, A., Lewis, Z.A., Freitag, M., Selker, E.U., Mello, C.C., et al. (2010b). Diverse pathways generate microRNA-like RNAs and Dicer-independent small interfering RNAs in fungi. *Molecular Cell* 38, 803-814.

Lee, S.C., Li, A., Calo, S., and Heitman, J. (2013). Calcineurin plays key roles in the dimorphic transition and virulence of the human pathogenic zygomycete *Mucor circinelloides. PLoS Pathogens* 9, e1003625.

Lee, S.C., Billmyre, R.B., Li, A., Carson, S., Sykes, S.M., Huh, E.Y., Mieczkowski, P., Ko, D.C., Cuomo, C.A., and Heitman, J. (2014). Analysis of a food-borne fungal pathogen outbreak: virulence and genome of a *Mucor circinelloides* isolate from yogurt. *mBio* 5, e01390-01314.

Lemos, C.L., Sampaio, P., Maiato, H., Costa, M., Omel'yanchuk, L.V., Liberal, V., and Sunkel, C.E. (2000). Mast, a conserved microtubule-associated protein required for bipolar mitotic spindle organization. *The EMBO Journal* 19, 3668-3682.

Li, L., Chang, S.S., and Liu, Y. (2010). RNA interference pathways in filamentous fungi. *Cellular and Molecular Life Sciences* 67, 3849-3863.

Li, C.H., Cervantes, M., Springer, D.J., Boekhout, T., Ruiz-Vázquez, R.M., Torres-Martínez, S.R., Heitman, J., and Lee, S.C. (2011). Sporangiospore size

dimorphism is linked to virulence of *Mucor circinelloides*. *PLoS Pathogens* 7, e1002086.

Liao, H.L., and Chung, K.R. (2008). Genetic dissection defines the roles of elsinochrome Phytotoxin for fungal pathogenesis and conidiation of the citrus pathogen *Elsinoë fawcettii*. *Molecular Plant-microbe Interactions* 21, 469-479.

Lubbehusen, T.L., Nielsen, J., and McIntyre, M. (2003). Morphology and physiology of the dimorphic fungus *Mucor circinelloides* (syn. *M. racemosus*) during anaerobic growth. *Mycological Research* 107, 223-230.

Luo, Z., and Chen, Z. (2007). Improperly terminated, unpolyadenylated mRNA of sense transgenes is targeted by RDR6-mediated RNA silencing in *Arabidopsis*. *The Plant Cell* 19, 943-958.

MacRae, I.J., and Doudna, J.A. (2007). Ribonuclease revisited: structural insights into ribonuclease III family enzymes. *Current Opinion in Structural Biology* 17, 138-145.

MacRae, I.J., Zhou, K., Li, F., Repic, A., Brooks, A.N., Cande, W.Z., Adams, P.D., and Doudna, J.A. (2006). Structural basis for double-stranded RNA processing by Dicer. *Science* 311, 195-198.

Maiato, H., Fairley, E.A., Rieder, C.L., Swedlow, J.R., Sunkel, C.E., and Earnshaw, W.C. (2003). Human CLASP1 is an outer kinetochore component that regulates spindle microtubule dynamics. *Cell* 113, 891-904.

Maiti, M., Lee, H.C., and Liu, Y. (2007). QIP, a putative exonuclease, interacts with the *Neurospora* Argonaute protein and facilitates conversion of duplex siRNA into single strands. *Genes and Development* 21, 590-600.

Marr, K.A., Carter, R.A., Crippa, F., Wald, A., and Corey, L. (2002). Epidemiology and outcome of mould infections in hematopoietic stem cell transplant recipients. *Clinical Infectious Diseases* 34, 909-917.

Matsudate, Y., Murao, K., Urano, Y., Yarita, K., Kamei, K., Takeichi, H., and Kubo, Y. (2015). Primary cutaneous mucormycosis caused by *Mucor irregularis* in an immunocompetent patient. *The Journal of Dermatology* 42, 267-268.

Miller, J.H. (1972). Experiments in molecular genetics. *New York: Cold Spring Harbor Laboratory Press.* pp. 325-355.

Mimori-Kiyosue, Y., Grigoriev, I., Lansbergen, G., Sasaki, H., Matsui, C., Severin, F., Galjart, N., Grosveld, F., Vorobjev, I., Tsukita, S., et al. (2005). CLASP1 and CLASP2 bind to EB1 and regulate microtubule plus-end dynamics at the cell cortex. *The Journal of Cell Biology* 168, 141-153.

Motamedi, M.R., Verdel, A., Colmenares, S.U., Gerber, S.A., Gygi, S.P., and Moazed, D. (2004). Two RNAi complexes, RITS and RDRC, physically interact and localize to noncoding centromeric RNAs. *Cell* 119, 789-802.

Nakayashiki, H., Kadotani, N., and Mayama, S. (2006). Evolution and diversification of RNA silencing proteins in fungi. *Journal of Molecular Evolution* 63, 127-135.

Napoli, C., Lemieux, C., and Jorgensen, R. (1990). Introduction of a Chimeric Chalcone Synthase Gene into Petunia Results in Reversible Co-Suppression of Homologous Genes in trans. *The Plant Cell* 2, 279-289.

Navarro, E., Lorca-Pascual, J.M., Quiles-Rosillo, M.D., Nicolás, F.E., Garre, V., Torres-Martínez, S., and Ruiz-Vázquez, R.M. (2001). A negative regulator of light-inducible carotenogenesis in *Mucor circinelloides. Molecular Genetics and Genomics* 266, 463-470.

Neblett Fanfair, R., Benedict, K., Bos, J., Bennett, S.D., Lo, Y.C., Adebanjo, T., Etienne, K., Deak, E., Derado, G., Shieh, W.J., et al. (2012). Necrotizing cutaneous mucormycosis after a tornado in Joplin, Missouri, in 2011. *The New England Journal of Medicine* 367, 2214-2225.

Ng, K.K., Arnold, J.J., and Cameron, C.E. (2008). Structure-function relationships among RNA-dependent RNA polymerases. *Current Topics in Microbiology and Immunology* 320, 137-156.

Nguyen QB, Kadotani N, Kasahara S, Tosa Y, Mayama S, Nakayashiki H. (2008). Systematic functional analysis of calcium-signalling proteins in the genome of the rice-blast fungus, *Magnaporthe oryzae*, using a high-throughput RNA-silencing system. *Molecular Microbiology* 68:1348-1365.

Nicolás, F.E., Torres-Martínez, S., and Ruiz-Vázquez, R.M. (2003). Two classes of small antisense RNAs in fungal RNA silencing triggered by non-integrative transgenes. *The EMBO Journal* 22, 3983-3991.

Nicolás, F.E., de Haro, J.P., Torres-Martínez, S., and Ruiz-Vázquez, R.M. (2007). Mutants defective in a *Mucor circinelloides dicer*-like gene are not compromised in siRNA silencing but display developmental defects. *Fungal Genetics and Biology* 44, 504-516.

Nicolás, F.E., Calo, S., Murcia-Flores, L., Garre, V., Ruiz-Vázquez, R.M., and Torres-Martínez, S. (2008). A RING-finger photocarotenogenic repressor involved in asexual sporulation in *Mucor circinelloides. FEMS Microbiology Letters* 280, 81-88.

Nicolás, F.E., Torres-Martínez, S., and Ruiz-Vázquez, R.M. (2009). Transcriptional activation increases RNA silencing efficiency and stability in the fungus *Mucor circinelloides. Journal of Biotechnology* 142, 123-126.

Nicolás, F.E., Moxon, S., de Haro, J.P., Calo, S., Grigoriev, I.V., Torres-Martínez, S., Moulton, V., Ruiz-Vázquez, R.M., and Dalmay, T. (2010). Endogenous short RNAs generated by Dicer 2 and RNA-dependent RNA polymerase 1 regulate mRNAs in the basal fungus *Mucor circinelloides. Nucleic Acids Research* 38, 5535-5541.

Nicolás, F.E., Torres-Martínez, S., and Ruiz-Vázquez, R.M. (2013). Loss and retention of RNA interference in fungi and parasites. *PLoS Pathogens* 9, e1003089.

Nicolás, F.E., Vila, A., Moxon, S., Cascales, M.D., Torres-Martínez, S., Ruiz-Vázquez, R.M., and Garre, V. (2015). The RNAi machinery controls distinct responses to environmental signals in the basal fungus *Mucor circinelloides. BMC Genomics* 16, 237.

Nicolás-Molina, F.E., Navarro, E., and Ruiz-Vázquez, R.M. (2008). Lycopene over-accumulation by disruption of the negative regulator gene *crgA* in *Mucor circinelloides. Applied Microbiology and Biotechnology* 78, 131-137.

Nolan, T., Braccini, L., Azzalin, G., De Toni, A., Macino, G., and Cogoni, C. (2005). The post-transcriptional gene silencing machinery functions independently of DNA methylation to repress a LINE1-like retrotransposon in *Neurospora crassa. Nucleic Acids Research* 33, 1564-1573.

Nunes, C.C., Gowda, M., Sailsbery, J., Xue, M., Chen, F., Brown, D.E., Oh, Y., Mitchell, T.K., and Dean, R.A. (2011). Diverse and tissue-enriched small RNAs in the plant pathogenic fungus, *Magnaporthe oryzae. BMC Genomics* 12, 288.

Odronitz, F., and Kollmar, M. (2007). Drawing the tree of eukaryotic life based on the analysis of 2,269 manually annotated myosins from 328 species. *Genome Biology* 8: R196.

Orlowski, M. (1991). Mucor dimorphism. *Microbiological Reviews* 55, 234-258.

Ortiz, J., Funk, C., Schafer, A., and Lechner, J. (2009). Stu1 inversely regulates kinetochore capture and spindle stability. *Genes and Development* 23, 2778-2791.

Pahwa, M., Pahwa, A.R., Girotra, M., and Chawla, A. (2013). Isolated renal mucormycosis in a healthy immunocompetent patient: atypical presentation and course. *Korean Journal of Urology* 54, 641-643.

Pall, G.S., Codony-Servat, C., Byrne, J., Ritchie, L., and Hamilton, A. (2007). Carbodiimide-mediated cross-linking of RNA to nylon membranes improves the detection of siRNA, miRNA and piRNA by northern blot. *Nucleic Acids Research* 35, e60.

Parker, R. (2012). RNA degradation in *Saccharomyces cerevisae*. *Genetics* 191, 671-702.

Pocsi, I., Prade, R.A., and Penninckx, M.J. (2004). Glutathione, altruistic metabolite in fungi. *Advances in Microbial Physiology* 49, 1-76.

Pereira, A.L., Pereira, A.J., Maia, A.R., Drabek, K., Sayas, C.L., Hergert, P.J., Lince-Faria, M., Matos, I., Duque, C., Stepanova, T., et al. (2006). Mammalian CLASP1 and CLASP2 cooperate to ensure mitotic fidelity by regulating spindle and kinetochore function. *Molecular Biology of the Cell* 17, 4526-4542.

Pickford, A., Braccini, L., Macino, G., and Cogoni, C. (2003). The QDE-3 homologue RecQ-2 co-operates with QDE-3 in DNA repair in *Neurospora crassa*. *Current Genetics* 42, 220-227.

Prigent, M., Boy-Marcotte, E., Chesneau, L., Gibson, K., Dupre-Crochet, S., Tisserand, H., Verbavatz, J.M., and Cuif, M.H. (2011). The RabGAP proteins Gyp5p and Gyl1p recruit the BAR domain protein Rvs167p for polarized exocytosis. *Traffic* 12, 1084-1097.

Provance, D.W., and Mercer, J.A. (1999). Myosin-V: head to tail. *Cellular and Molecular Life Sciences* 56, 233-242.

Prufer, K., Stenzel, U., Dannemann, M., Green, R.E., Lachmann, M., and Kelso, J. (2008). PatMaN: rapid alignment of short sequences to large databases. *Bioinformatics* 24, 1530-1531.

Qi, Y., and Hannon, G.J. (2005). Uncovering RNAi mechanisms in plants: biochemistry enters the foray. *FEBS Letters* 579, 5899-5903.

Quiles-Rosillo, M.D., Ruiz-Vázquez, R.M., Torres-Martínez, S., and Garre, V. (2003). Cloning, characterization and heterologous expression of the *Blakeslea trispora* gene encoding orotidine-5'-monophosphate decarboxylase. *FEMS Microbiology Letters* 222, 229-236.

Ribes, J.A., Vanover-Sams, C.L., and Baker, D.J. (2000). Zygomycetes in human disease. *Clinical Microbiology Reviews* 13, 236-301.

Roden, M.M., Zaoutis, T.E., Buchanan, W.L., Knudsen, T.A., Sarkisova, T.A., Schaufele, R.L., Sein, M., Sein, T., Chiou, C.C., Chu, J.H., et al. (2005). Epidemiology and outcome of zygomycosis: a review of 929 reported cases. *Clinical Infectious Diseases* 41, 634-653.

Rodriguez-Frometa, R.A., Gutierrez, A., Torres-Martínez, S., and Garre, V. (2013). Malic enzyme activity is not the only bottleneck for lipid accumulation in the oleaginous fungus *Mucor circinelloides. Applied Microbiology and Biotechnology* 97, 3063-3072.

Rogers, T.R. (2008). Treatment of zygomycosis: current and new options. *The Journal of Antimicrobial Chemotherapy* 61 Suppl 1, i35-40.

Romano, N., and Macino, G. (1992). Quelling: transient inactivation of gene expression in *Neurospora crassa* by transformation with homologous sequences. *Molecular Microbiology* 6, 3343-3353.

Roncero, M.I., Jepsen, L.P., Stroman, P., and van Heeswijck, R. (1989). Characterization of a *leuA* gene and an ARS element from *Mucor circinelloides. Gene* 84, 335-343.

Ruiz-Vázquez, R.M. and Torres-Martínez, S. (2003). Production of carotenes in Mucorales: structural and regulatory genes. In: Barredo JL (ed) Useful organism

for health care, foods and enzyme production. *Research Signpost, Kerala, India,* pp 69–84.

Schipper, M.A.A. (1976). On *Mucor circinelloides*, *Mucor racemosus* and related species. *Studies of Mycology* 12, 1-40.

Schuchardt, I., Assmann, D., Thines, E., Schuberth, C., and Steinberg, G. (2005). Myosin-V, Kinesin-1, and Kinesin-3 cooperate in hyphal growth of the fungus *Ustilago maydis. Molecular Biology of the Cell* 16, 5191-5201.

Schuster, M., Treitschke, S., Kilaru, S., Molloy, J., Harmer, N.J., and Steinberg, G. (2012). Myosin-5, kinesin-1 and myosin-17 cooperate in secretion of fungal chitin synthase. *The EMBO Journal* 31, 214-227.

Segers, G.C., van Wezel, R., Zhang, X., Hong, Y., and Nuss, D.L. (2006). Hypovirus papain-like protease p29 suppresses RNA silencing in the natural fungal host and in a heterologous plant system. *Eukaryotic Cell* 5, 896-904.

Seto, A.G., Kingston, R.E., and Lau, N.C. (2007). The coming of age for Piwi proteins. *Molecular Cell* 26, 603-609.

Shiu, P.K., and Metzenberg, R.L. (2002). Meiotic silencing by unpaired DNA: properties, regulation and suppression. *Genetics* 161, 1483-1495.

Shiu, P.K., Raju, N.B., Zickler, D., and Metzenberg, R.L. (2001). Meiotic silencing by unpaired DNA. *Cell* 107, 905-916.

Shiu, P.K., Zickler, D., Raju, N.B., Ruprich-Robert, G., and Metzenberg, R.L. (2006). SAD-2 is required for meiotic silencing by unpaired DNA and perinuclear localization of SAD-1 RNA-directed RNA polymerase. *Proceedings of the National Academy of Sciences of the United States of America* 103, 2243-2248.

Sijen, T., Fleenor, J., Simmer, F., Thijssen, K.L., Parrish, S., Timmons, L., Plasterk, R.H., and Fire, A. (2001). On the role of RNA amplification in dsRNA-triggered gene silencing. *Cell* 107, 465-476.

Silva, F., Torres-Martínez, S., and Garre, V. (2006). Distinct white collar-1 genes control specific light responses in *Mucor circinelloides. Molecular Microbiology* 61, 1023-1037.

Silva, F., Navarro, E., Penaranda, A., Murcia-Flores, L., Torres-Martínez, S., and Garre, V. (2008). A RING-finger protein regulates carotenogenesis via proteolysis-independent ubiquitylation of a white collar-1-like activator. *Molecular Microbiology* 70, 1026-1036.

Slep, K.C. (2009). The role of TOG domains in microtubule plus end dynamics. *Biochemical Society Transactions* 37, 1002-1006.

Son, H., Min, K., Lee, J., Raju, N.B., and Lee, Y.W. (2011). Meiotic silencing in the homothallic fungus *Gibberella zeae. Fungal Biology* 115, 1290-1302.

Sorefan, K., Pais, H., Hall, A.E., Kozomara, A., Griffiths-Jones, S., Moulton, V., and Dalmay, T. (2012). Reducing ligation bias of small RNAs in libraries for next generation sequencing. *Silence* 3, 4.

Stajich, J.E., Harris, T., Brunk, B.P., Brestelli, J., Fischer, S., Harb, O.S., Kissinger, J.C., Li, W., Nayak, V., Pinney, D.F., et al. (2012). FungiDB: an integrated functional genomics database for fungi. *Nucleic Acids Research* 40, D675-681.

Steinberg, G. (2011). Motors in fungal morphogenesis: cooperation versus competition. *Current Opinion in Microbiology* 14, 660-667.

Sun, W., Li, G., and Nicholson, A.W. (2004). Mutational analysis of the nuclease domain of *Escherichia coli* ribonuclease III. Identification of conserved acidic

residues that are important for catalytic function in vitro. *Biochemistry* 43, 13054-13062.

Sun, Q., Choi, G.H., and Nuss, D.L. (2009). A single Argonaute gene is required for induction of RNA silencing antiviral defense and promotes viral RNA recombination. *Proceedings of the National Academy of Sciences of the United States of America* 106, 17927-17932.

Suzuki, N., Maruyama, K., Moriyama, M., and Nuss, D.L. (2003). Hypovirus papain-like protease p29 functions in trans to enhance viral double-stranded RNA accumulation and vertical transmission. *Journal of Virology* 77, 11697-11707.

Thran, M., Link, K., and Sonnewald, U. (2012). The *Arabidopsis* DCP2 gene is required for proper mRNA turnover and prevents transgene silencing in *Arabidopsis*. *The Plant Journal* 72, 368-377.

Tijsterman, M., Ketting, R.F., Okihara, K.L., Sijen, T., and Plasterk, R.H. (2002). RNA helicase MUT-14-dependent gene silencing triggered in *C. elegans* by short antisense RNAs. *Science* 295, 694-697.

Trieu, T.A., Calo, S., Nicolás, F.E., Vila, A., Moxon, S., Dalmay, T., Torres-Martínez, S., Garre, V., and Ruiz-Vázquez, R.M. (2015). A Non-canonical RNA Silencing Pathway Promotes mRNA Degradation in Basal Fungi. *PLoS Genetics* 11, e1005168.

van Heeswijck, R. and Roncero, M.I. (1984). High frequency transformation of *Mucor* with recombinant plasmid DNA. *Carlsberg Research Communications* 49, 597-609.

Velayos, A., Blasco, J.L., Alvarez, M.I., Iturriaga, E.A., and Eslava, A.P. (2000a). Blue-light regulation of phytoene dehydrogenase (*carB*) gene expression in *Mucor circinelloides*. *Planta* 210, 938-946.

Velayos, A., Eslava, A.P., and Iturriaga, E.A. (2000b). A bifunctional enzyme with lycopene cyclase and phytoene synthase activities is encoded by the *carRP* gene of *Mucor circinelloides. European Journal of Biochemistry* 267, 5509-5519.

Verma, R., Nair, V., Vasudevan, B., Vijendran, P., Behera, V., and Neema, S. (2014). Rare case of primary cutaneous mucormycosis of the hand caused by *Rhizopus microsporus* in an immunocompetent patient. *International Journal of Dermatology* 53, 66-69.

Vicente G, Bautista LF, Rodríguez R, Gutiérrez FJ, Sádaba I, Ruiz-Vázquez RM, Torres-Martínez S, Garre V. (2009). Biodiesel production from biomass of an oleaginous fungus. *Biochemical Engineering Journal* 48, 22-27.

Vicente G, Bautista LF, Gutiérrez FJ, Rodríguez R, Martínez V, Rodríguez-Frómeta RA, Ruiz-Vázquez RM, Torres-Martínez S, Garre V. (2010). Direct transformation of fungal biomass from submerged cultures into biodiesel. *Energy Fuels* 24, 3173-3178.

Voinnet, O. (2008). Use, tolerance and avoidance of amplified RNA silencing by plants. *Trends in Plant Science* 13, 317-328.

Wang, X., Hsueh, Y.P., Li, W., Floyd, A., Skalsky, R., and Heitman, J. (2010). Sex-induced silencing defends the genome of *Cryptococcus neoformans* via RNAi. *Genes & Development* 24, 2566-2582.

Watson, J. D., Baker, T. A. Bell, S., Gann, A., Levine, M. W., and Losick, R. (2008). Molecular biology of the gene. *Pearson/Benjamin Cummings*.

Weber, I., Gruber, C., and Steinberg, G. (2003). A class-V myosin required for mating, hyphal growth, and pathogenicity in the dimorphic plant pathogen *Ustilago maydis. The Plant Cell* 15, 2826-2842.

Wei, K.F., Wu, L.J., Chen, J., Chen, Y.F., and Xie, D.X. (2012). Structural evolution and functional diversification analyses of argonaute protein. *Journal of Cellular Biochemistry* 113, 2576-2585.

Wei, Z., Liu, X., Yu, C., and Zhang, M. (2013). Structural basis of cargo recognitions for class V myosins. *Proceedings of the National Academy of Sciences of the United States of America* 110, 11314-11319.

Widenius, M. (2008). Myosins - A Superfamily of Molecular Motors. *Springer.*

Wilkins, M.R., Gasteiger, E., Bairoch, A., Sanchez, J.C., Williams, K.L., Appel, R.D., and Hochstrasser, D.F. (1999). Protein identification and analysis tools in the ExPASy server. *Methods in Molecular Biology* 112, 531-552.

Xue, Z., Yuan, H., Guo, J., and Liu, Y. (2012). Reconstitution of an Argonaute-dependent small RNA biogenesis pathway reveals a handover mechanism involving the RNA exosome and the exonuclease QIP. *Molecular Cell* 46, 299-310.

Zhang, X., and Nuss, D.L. (2008). A host dicer is required for defective viral RNA production and recombinant virus vector RNA instability for a positive sense RNA virus. *Proceedings of the National Academy of Sciences of the United States of America* 105, 16749-16754.

Zhang, X., Segers, G.C., Sun, Q., Deng, F., and Nuss, D.L. (2008). Characterization of hypovirus-derived small RNAs generated in the chestnut blight fungus by an inducible DCL-2-dependent pathway. *Journal of Virology* 82, 2613-2619.

RESUMEN EN CASTELLANO

RESUMEN

Identificación de componentes del mecanismo no canónico de silenciamiento mediado por RNA en *Mucor circinelloides*

Introducción: Desde el descubrimiento del mecanismo de RNA de interferencia (RNAi) en *Caenorhabditis elegans*, nuestro conocimiento sobre el papel crucial de los pequeños RNAs endógenos (esRNAs) como riboreguladores ha aumentado drásticamente. Se han identificado múltiples clases de esRNAs, incluyendo microRNAs (miRNAs) y pequeños RNAs de interferencia (siRNAs), tanto en metazoos como en eucariotas inferiores. La biogénesis de la mayoría de estos esRNAs requiere una maquinaria común que incluye una RNasa III denominada Dicer, que procesa precursores de RNA de doble cadena (dsRNA) en moléculas de pequeños RNAs (sRNA), y una endonucleasa denominada Argonauta, que se une a los sRNAs y los utiliza como una guía para identificar y cortar los RNAm diana con secuencias complementarias. Además, algunos organismos, incluyendo plantas, nematodos y hongos, requieren la participación de RNA polimerasas dependientes de RNA para generar las moléculas de dsRNA inductoras del silenciamiento a partir de cadenas sencillas de RNA, o para amplificar las señales de silenciamiento. Además de esta ruta canónica, se han descrito diferentes rutas alternativas no canónicas, en las que no participan las proteínas Dicer, como responsables de la biogénesis de esRNAs específicos, no sólo los conocidos como RNAs que interaccionan con Piwi (piRNAs), sino también ciertos miRNAs y moléculas similares a los miRNAs (milRNAs). En estos casos, la actividad catalítica de proteínas de la familia Argonauta y la actividad degradativa de exonucleasas específicas son las que participan en la producción de los esRNAs maduros. Sin embargo, la mayoría de las moléculas de miRNAs que se generan por rutas no canónicas están mal conservadas y su abundancia es limitada, lo que arroja dudas sobre su funcionalidad.

El hongo basal *Mucor circinelloides*, un patógeno humano oportunista emergente del orden Mucorales, es un gran modelo para investigar el papel funcional de los esRNAs. En este hongo se han descrito esRNAs derivados de exones, denominados ex-siRNAs, que regulan la expresión de muchos genes que codifican proteínas. Las distintas clases de ex-siRNAs identificadas son dependientes de Dicer,

ya que requieren una de las proteínas Dicer (Dcl) de *M. circinelloides* para su biogénesis. El papel de los ex-siRNAs dependientes de Dicer en la regulación de genes endógenos se ha confirmado experimentalmente, ya que la reducción de ex-siRNAs específicos en mutantes afectados en la maquinaria de RNAi está asociada con un aumento en la acumulación de los mRNAs diana correspondientes. De hecho, el análisis transcriptómico a escala genómica de mutantes de silenciamiento en *M. circinelloides* ha permitido identificar cientos de genes que muestran expresión diferencial en comparación con la estirpe silvestre. El análisis detallado de los genes expresados diferencialmente ha permitido la identificación de candidatos que pueden ser responsables de los fenotipos que presentan los mutantes afectados en la maquinaria de RNAi, tales como defectos en el crecimiento vegetativo, la morfología de las hifas, la producción de esporas vegetativas o la respuesta diferencial al estrés nutricional. La mayoría de estos fenotipos están relacionados con respuestas a señales de desarrollo endógenas y ambientales, lo que sugiere que la maquinaria de RNAi modula la expresión de genes implicados en estas respuestas. Esto viene apoyado por la capacidad de *M. circinelloides* para adaptarse al medio ambiente mediante un nuevo mecanismo epigenético basado en el silenciamiento génico mediado por RNA, lo que señala la importancia del mecanismo de RNAi en el control de la plasticidad fenotípica.

Los análisis previos de los esRNAs en *M. circinelloides* se centraron exclusivamente en los producidos a través de rutas dependientes de Dicer, ya que sólo se consideraron los esRNAs que mostraron una reducción significativa en cualquiera de los mutantes *dcl*$^-$ en relación con la estirpe silvestre. Por otra parte, el estudio de los fenotipos mostrados por los diferentes mutantes en la maquinaria de RNAi reveló que varios fenotipos eran compartidos por los mutantes *rdrp-1*$^-$ y *rdrp-2*$^-$ pero no por los *dcl*$^-$, sugiriendo la existencia de una nueva clase de esRNAs dependientes de *rdrp* pero independientes de *dicer*. En efecto, el análisis del contenido completo de esRNAs en la estirpe silvestre y los mutantes de silenciamiento permitió identificar esta nueva clase de esRNAs, que deriva casi exclusivamente de exones de genes que codifican proteínas. Estos esRNAs muestran unas características estructurales atípicas. Así, presentan un sesgo muy fuerte en la polaridad de las cadenas, todas ellas con la misma orientación que el mensajero correspondiente, y una distribución aleatoria de tamaños, lo que sugiere que son

productos de degradación de RNAm endógenos. Sin embargo, no es una degradación inespecífica, ya que requiere la presencia de las proteínas RdRP-1 y/o RdRP-2 que señalan, de alguna forma, los mensajeros que deben ser degradados por una nucleasa desconocida. El objetivo global de esta tesis es caracterizar esta posible ruta de degradación de RNAm, identificar la RNasa implicada y utilizar los mecanismos de silenciamiento de *Mucor* para realizar un análisis funcional a escala genómica. Estos objetivos globales se concretan en los siguientes:

Objetivos: i) Análisis de la función de la ruta independiente de Dicer y dependiente de RdRp en la regulación de la expresión génica. ii) Identificación *in silico* de RNasas de *M. circinelloides* candidatas a participar en la ruta de degradación independiente de Dicer. iii) Análisis del papel de los genes candidatos en la producción de esRNAs independientes de Dicer y dependientes de RdRP. iv) Construcción de genotecas genómicas para el análisis funcional de genes mediante RNA de interferencia (RNAi), utilizando vectores de silenciamiento para identificar secuencias de *M. circinelloides* con un posible papel en patogénesis. v) Generación de mutantes nulos de los genes candidatos para confirmar el fenotipo e investigar su papel en la patogénesis de *Mucor*.

Métodos: El análisis de la función génica se llevó a cabo mediante manipulaciones genéticas *in vitro* e *in vivo*. Estas incluyen métodos para aislar, amplificar y analizar la expresión de genes específicos y para la transformación genética de células vivas. Se construyeron genotecas de DNA genómico en vectores de silenciamiento con promotores duales para el análisis funcional del genoma y la identificación de genes candidatos con un posible papel en la patogénesis de *Mucor*. Se utilizaron análisis fenotípicos para evaluar las funciones de los genes candidatos en el crecimiento, la morfogénesis y la virulencia de este hongo.

Resultados y Discusión: La secuenciación de las genotecas de sRNAs comprendidos entre 18-25nt permitió identificar 531 nuevos loci que producían esRNAs derivados de exones mediante un mecanismo independiente de Dicer, pero dependiente de RdRP-1 y/o RdRP-2. Las características estructurales de estos esRNAs sugerían que eran productos de degradación de mRNAs específicos, por lo que se denominaron rdRNAs (*r*drp-dependent *d*egraded RNA). Los análisis de expresión de varios *loci* productores de rdRNAs demostraron que la nueva ruta independiente de Dicer y dependiente de RdRP regula la expresión génica mediante

la degradación específica de los RNAm por una RNasa previamente desconocida. Es decir, los RNAm de los genes regulados por esta ruta de degradación mostraron una mayor acumulación en los mutantes *rdrp*$^-$, en los que la ruta no está operativa, en relación con la estirpe silvestre y los mutantes *dcl*$^-$. Esta ruta regula principalmente genes conservados implicados en metabolismo y procesos de señalización celular, tales como los requeridos para la biosíntesis del grupo hemo, y controla las respuestas a señales ambientales específicas.

La búsqueda en el genoma de *Mucor* identificó cuatro genes candidatos (80729, 136157, 110239 y 77996) para la posible RNasa implicada en la ruta de degradación. Se obtuvieron mutantes nulos por disrupción génica para cada uno de los genes candidatos, aunque para dos de ellos (110239 y 77996) no se pudieron obtener estirpes homocarióticas, sugiriendo que estos genes podrían cumplir funciones esenciales para la viabilidad celular. El análisis funcional de los mutantes nulos para los otros dos genes permitió demostrar que la proteína RNasa III 80729 (denominada ahora R3B2) está implicada en la ruta no canónica de silenciamiento en *M. circinelloides*. Todos los genes cuya expresión aumentaba en los mutantes *rdrp*$^-$ respecto a la estirpe silvestre mostraron también una mayor acumulación de RNAm en el mutante *r3b2*$^-$, indicando que esta proteína participa en la ruta de degradación dependiente de *rdrp* e independiente de *dicer*. La secuenciación de los sRNAs (18-25 nt) acumulados en el mutante *r3b2*$^-$ confirmó que R3B2 es esencial para la producción de los rdRNA, sugiriendo que esta proteína es la RNasa implicada en la ruta de degradación. Se identificaron casi 1.560 *loci* exónicos que mostraron una reducción significativa en la producción de sRNA en el mutante *r3b2*$^-$ en relación con la estirpe silvestre. Todos menos uno de los 531 loci productores de rdRNA mediante la ruta independiente de Dicer y dependiente de RdRP se encontraron entre aquellos significativamente reducidos en el mutante *r3b2*$^-$. Los niveles reducidos de rdRNAs en el mutante *r3b2*$^-$ también se observaron en los genes implicados en la biosíntesis del grupo hemo, que muestran al menos una reducción de 38 veces en los niveles de rdRNAs en relación con la estirpe silvestre. La presumible sobre-expresión de los genes correspondientes en el mutante *r3b2*$^-$ podría ser la responsable de la mayor resistencia al estrés oxidativo que muestra este mutante en relación con la estirpe silvestre. Esto sugiere un papel para esta ruta de degradación en la respuesta a señales ambientales específicas.

El análisis detallado de los 1.560 *loci* productores de sRNA que requieren R3B2 para su producción demostró que esta proteína no sólo está implicada en la ruta no canónica de degradación, sino que también participa en la producción de ex-siRNAs por la ruta canónica de RNAi. En concreto, los ex-siRNAs de la clase III, que muestran unas características estructurales parecidas a las de los rdRNAs, requieren la presencia de R3B2 para su producción. La confirmación de este resultado se obtuvo al estudiar el papel de *r3b2* en el silenciamiento inducido por transgenes, que opera mediante la ruta canónica de silenciamiento. El mutante *r3b2*$^-$ es prácticamente incapaz de silenciar genes endógenos mediante la introducción de transgenes, lo que confirma el papel de R3B2 en la ruta de RNAi.

La combinación única de dominios que presenta la proteína R3B2 y el hecho de que el dominio RNasa III no presentase todos los residuos conservados característicos de este tipo de dominios, podría sugerir que la función de R3B2 en las distintas rutas en las que participa no estuviese determinada por su actividad RNasa III. Para descartar este extremo, se realizaron experimentos de mutagénesis dirigida, alterando residuos conservados del dominio RNasa III, y se analizó la capacidad de esta versión mutante de la proteína para complementar la falta de función en el mutante nulo *r3b2*$^-$. Los resultados obtenidos indican que el dominio RNasa III es necesario para la correcta función de R3B2, tanto en la ruta no canónica de degradación como en la ruta canónica de silenciamiento. Existen varias proteínas similares a R3B2 en el genoma de *Mucor*, aunque no deben tener funciones solapantes. Curiosamente, esta familia de proteínas parece ser exclusiva de Mucorales, ya que no se han identificado proteínas similares fuera de este orden.

Experimentos similares llevados a cabo con mutantes afectados en la presunta RNasa 136157 demostraron que esta proteína no está implicada en la ruta no canónica de degradación, ya que la expresión de los genes regulados por esta ruta no mostró ninguna diferencia en estos mutantes respecto a los valores obtenidos en la estirpes silvestre y mutantes *dcl*$^-$. Así mismo, los mutantes nulos para 136157 son capaces de activar el silenciamiento por transgenes a niveles similares a los de la estirpe silvestre, indicando que este gen tampoco está implicado en la ruta canónica de silenciamiento mediado por RNA. La falta de mutantes nulos homocarióticos para los genes 110239 y 77996 impidió el análisis de su participación en la ruta independiente de Dicer y dependiente de RdRP. En conjunto, estos resultados

demuestran la participación de la proteína R3B2 en la biogénesis de los rdRNAs independientes de Dicer y dependientes de RdRP, lo que señala de forma contundente a R3B2 como la RNasa involucrada en el proceso de degradación de los RNAm específicos por la ruta no canónica de silenciamiento.

En la segunda parte de esta tesis se ha utilizado el mecanismo canónico de silenciamiento para llevar a cabo análisis funcional a escala genómica en *Mucor*. Para ello, se han construido dos genotecas genómicas en un vector de clonación portador de dos promotores de *Mucor* en orientaciones opuestas. La clonación de fragmentos de DNA genómico entre los dos promotores generará, tras la introducción de los plásmidos recombinantes en *Mucor*, moléculas de dsRNA que activaran el silenciamiento de los genes con secuencias homólogas. Para la construcción de las genotecas, el DNA genómico aislado de la estirpe silvestre se digirió con tres enzimas de restricción en siete combinaciones diferentes y se clonó en este vector. La introducción de estas genotecas en *M. circinelloides* dio lugar a frecuencias de silenciamiento del gen chivato *carB* de 68,8% y 72,1%. Un fragmento de DNA de este gen chivato estaba incorporado en el vector de clonación, entre los dos promotores, para poder estimar la eficacia del silenciamiento, ya que la falta de función de *carB* da lugar a un fenotipo albino fácilmente identificable. Las frecuencias de silenciamiento obtenidas indican que el sistema funciona correctamente en *Mucor* y que esta estrategia es adecuada para analizar la función génica mediante la supresión de la expresión por silenciamiento mediado por RNA

La introducción de estas genotecas en *M. circinelloides* permitió identificar varios transformantes con fenotipos anormales, relacionados con defectos en la tasa de crecimiento, morfología de las colonias o producción de esporas vegetativas. Se seleccionaron estos fenotipos por su posible papel en la patogénesis de *Mucor*, ya que el mayor interés en este primer escrutinio de la genoteca de RNAi fue identificar genes candidatos con posibles efectos sobre patogénesis. Se utilizó un método basado en la amplificación por PCR para identificar los fragmentos clonados en los transformantes con fenotipos anormales, lo que dio como resultado la detección de siete genes candidatos. Los análisis moleculares y de silenciamiento demostraron que dos de estos genes, 51513 y 84675, eran los responsables de las alteraciones fenotípicas estudiadas en dos grupos de transformantes con fenotipos diferentes. Uno de estos genes, 51513, codifica una miosina de clase V y se denominó *mcmyo5*. El

fenotipo debido al silenciamiento de este gen es muy acusado, ya que produce colonias con una velocidad de crecimiento reducida, nula producción de esporas e incapacidad para el crecimiento polarizado, dando lugar a colonias en forma de levaduras en vez de mostrar crecimiento micelial normal. Este mismo fenotipo se obtiene al provocar la disrupción del gen, demostrando el papel esencial de *mcmyo5* en la morfogénesis de *Mucor*. El mutante *mcmyo5*$^-$ muestra también una virulencia reducida en un sistema modelo que utiliza la larva de la polilla, *Galleria mellonella*, como hospedador de *Mucor*, lo que corrobora que la capacidad de crecimiento filamentoso es un factor de virulencia para *M. circinelloides*. Dado que la miosina de clase V funciona como un transportador de vesículas y otros componentes celulares a lo largo de los filamentos de actina, se podría sugerir que la falta de Mcmyo5 podría resultar en la imposibilidad de formación del Spitzenkörper (cuerpo apical), una estructura formada por vesículas que se forma en el extremo apical de la hifa y que es responsable del crecimiento polarizado. En el modelo propuesto, la proteína Mcmyo5 activa consistiría en un homodímero, que se movería a lo largo de los filamentos de actina como un transportador de carga para entregar vesículas en posiciones concretas de las células.

El otro gen identificado, 84675, cifra una proteína de la familia CLASP, que regula la dinámica de los microtúbulos, y se denominó *mcclasp*. El silenciamiento de este gen provoca una reducción significativa en la velocidad de crecimiento, una reducción en la producción de esporas y una disminución en el índice de polaridad, lo que provoca que las hifas sean más gruesas y ramificadas que las de la estirpe silvestre y se generen colonias más compactas. De nuevo, esos mismos fenotipos se apreciaron en el mutante nulo correspondiente, que al contario que *mcmyo5*$^-$, no presentó diferencias significativas en virulencia respecto a la estirpe silvestre. El papel esencial de las proteínas CLASP en la dinámica de los microtúbulos durante los procesos de mitosis podría explicar los defectos de crecimiento que presenta el mutante *mcclasp*$^-$. Por otro lado, los microtúbulos constituyen el citoesqueleto celular por el que se desplazan las proteínas motoras, como kinesinas y dineínas, que están implicadas en el mantenimiento de la polaridad en hongos filamentosos, lo que podría explicar el menor índice de polaridad que muestra el mutante *mcclasp*$^-$. En conjunto, los genes identificados en este estudio parecen jugar papeles esenciales en

procesos de morfogénesis, que podrían, en algún caso, afectar la virulencia de los mutantes correspondientes.

Conclusiones: Se ha identificado y caracterizado una nueva ruta no canónica de silenciamiento, independiente de Dicer y dependiente de RdRP, que regula la expresión génica mediante la degradación de RNAm específicos. La RNasa implicada en esta ruta, denominada R3B2, presenta una arquitectura de dominios única, es específica de hongos basales y también está implicada en el mecanismo canónico de RNAi. Estos resultados asignan un nuevo papel para las proteínas RdRP en un proceso de degradación de RNA que podría representar el primer paso en la evolución del RNAi. Se ha desarrollado con éxito un procedimiento para realizar análisis funcional a gran escala utilizando RNAi, lo que ha permitido identificar dos genes que participan en la morfogénesis de *Mucor*. El gen *mcmyo5* codifica una miosina de clase V que juega un papel esencial en la morfogénesis y la patogénesis de *Mucor*. El gen *mcclasp* codifica una proteína CLASP, que también participa en la morfogénesis, pero no juega ningún papel importante en la patogénesis de *Mucor*.

SUPPLEMENTARY INFORMATION

Table S1. Log_2 fold change and strand bias of *rdrp*-dependent *dicer*-independent sRNAs in different mutants compared to wild type. Normalized reads were used to calculate the fold change of sRNAs in each mutant compared to wild type strain. The sRNA-producing loci are separated into *rdrp-1* and *rdrp-2* dependent (yellow background), only *rdrp-1* dependent (white background) and only *rdrp-2* dependent (blue background). Among each class, data were sorted for the fold change in *rdrp-1*$^-$ and/or *rdrp-2*$^-$ strains. Values that represent a fourfold or larger change are in bold. Decrease in expression is shown in red and increase in expression is shown in green. The coordinates correspond to the exonic loci where small RNAs map (http://genome.jgi-psf.org/Mucci1/Mucci1.home.html [v1]). Strand bias indicates orientation to mRNAs, where 1 corresponds to all sRNAs in the same orientation as the mRNA, 0 to equal mixture of sRNAs on both strands and -1 to all sRNAs antisense to mRNAs. The fold change of Ago-1 bound sRNAs in the WT compared with the *ago-1*$^-$ mutant is shown for the exonic *rdrp*-dependent *dicer*-independent sRNAs identified among those bound to Ago-1. n.d.: sRNAs not detected among those specifically bound to Ago-1. Only loci with a normalized abundance count higher than 50 in the wild type strain and a log_2 fold change ≤ -2 (fourfold or larger change) were considered.

ID	WT strand bias	dcl1$^-$ log_2 fold change vs WT	dcl2$^-$ log_2 fold change vs WT	dcl1$^-$/2$^-$ log_2 fold change vs WT	rdrp1$^-$ log_2 fold change vs WT	rdrp2$^-$ log_2 fold change vs WT	Ago-1 bound WT log_2 fold change vs ago-1$^-$
90984	1	-0.17	1.46	-1.37	**-4.93**	**-2.91**	n.d.
95912	0.99	0.01	1.50	-1.99	**-4.87**	**-3.11**	n.d.
90984	1	0.88	**2.11**	-1.18	**-4.77**	**-2.38**	n.d.
33232	1	-0.79	0.86	-1.69	**-4.71**	**-3.29**	n.d.
94432	1	-1.20	-0.17	-1.48	**-4.68**	**-2.85**	n.d.
26072	1	0.28	0.96	-0.52	**-4.62**	**-2.27**	**6.44**
33232	1	-0.75	0.17	-1.56	**-4.59**	**-3.46**	n.d.
80802	0.98	0.25	-0.43	-1.85	**-4.54**	**-3.86**	n.d.
91526	0.99	-0.76	0.26	-1.30	**-4.40**	**-2.04**	n.d.
92910	1	-0.68	0.15	-1.44	**-4.40**	**-2.61**	n.d.
95769	1	-1.62	-1.47	-1.91	**-4.32**	**-3.67**	n.d.
90984	0.99	0.15	1.63	-0.71	**-4.30**	**-2.40**	n.d.
85485	0.99	-0.51	0.28	-1.96	**-4.26**	**-2.92**	n.d.
93701	1	-0.35	0.73	-1.41	**-4.18**	**-2.93**	n.d.
32935	1	0.33	1.17	-1.43	**-4.18**	**-2.77**	n.d.
86723	1	0.25	0.70	-1.59	**-4.16**	**-2.80**	n.d.
78876	1	-0.88	0.19	-1.84	**-4.14**	**-3.15**	n.d.
49491	1	-0.37	0.14	-1.52	**-4.13**	**-2.88**	n.d.
31063	1	-0.69	0.65	-1.91	**-4.09**	**-2.93**	n.d.
82069	1	-0.15	0.69	-0.40	**-4.06**	**-2.39**	n.d.
94060	1	-0.22	1.32	-1.43	**-4.06**	**-2.09**	n.d.
75718	1	-0.24	0.88	-1.48	**-4.00**	**-2.26**	n.d.
49570	1	-0.61	0.22	-1.53	**-3.96**	**-2.01**	n.d.
95442	1	-1.06	0.13	-1.03	**-3.96**	**-2.77**	n.d.
9772	1	-0.35	0.45	-1.86	**-3.94**	**-3.06**	n.d.
31113	1	-0.90	-1.31	-1.62	**-3.91**	**-3.15**	n.d.
46819	1	0.45	**2.63**	-1.75	**-3.89**	**-2.12**	n.d.
83076	0.99	-0.13	0.04	-1.13	**-3.88**	**-2.29**	n.d.
45935	1	-0.59	0.99	-1.56	**-3.85**	**-2.12**	n.d.
88809	1	0.18	0.43	-1.93	**-3.84**	**-3.21**	n.d.
30744	1	0.34	1.15	-1.91	**-3.82**	**-2.68**	n.d.
49230	1	-0.80	-0.32	-1.85	**-3.81**	**-2.80**	n.d.
30003	0.95	0.58	1.21	-0.78	**-3.74**	**-2.74**	n.d.
90984	1	0.61	**2.05**	-0.52	**-3.73**	**-2.37**	n.d.
39013	1	-0.12	1.21	-0.83	**-3.73**	**-2.32**	n.d.
91672	1	0.23	1.23	-1.58	**-3.72**	**-2.73**	n.d.
94795	1	-0.11	0.69	-0.82	**-3.68**	**-2.11**	**3.37**
90840	1	-0.03	0.90	-1.50	**-3.68**	**-3.18**	n.d.
88521	1	-0.77	0.39	-1.73	**-3.67**	**-3.39**	n.d.
95916	1	-0.12	0.69	-1.18	**-3.67**	**-2.65**	n.d.
76286	1	0.28	0.98	-1.59	**-3.66**	**-3.09**	n.d.
32205	1	-0.43	-0.09	-1.93	**-3.61**	**-3.32**	n.d.
48786	1	-0.16	0.71	-1.80	**-3.60**	**-3.85**	n.d.
89824	0.89	-0.43	0.36	-1.94	**-3.57**	**-3.62**	n.d.
30895	1	-0.48	-0.59	-1.65	**-3.57**	**-3.42**	n.d.
82643	1	1.27	1.46	-0.97	**-3.56**	**-2.58**	n.d.
30682	1	0.53	0.94	-1.16	**-3.56**	**-2.29**	n.d.
90216	1	-1.60	-0.07	-1.89	**-3.55**	**-2.89**	n.d.
93377	1	0.08	0.07	-1.69	**-3.55**	**-2.85**	n.d.
28312	1	-0.19	1.08	-1.79	**-3.52**	**-2.68**	n.d.
49864	1	-0.40	0.73	-1.17	**-3.52**	**-2.22**	n.d.
93704	1	-1.35	-0.65	-1.75	**-3.50**	**-2.78**	n.d.
86459	1	0.02	0.71	-1.48	**-3.50**	**-2.45**	n.d.
69078	1	-0.85	0.22	-1.58	**-3.48**	**-2.88**	n.d.
89415	1	-0.04	0.31	-1.95	**-3.48**	**-2.97**	n.d.
90050	1	-0.27	0.19	-1.28	**-3.47**	**-3.01**	n.d.
87875	1	-0.29	-0.05	-1.23	**-3.47**	**-2.09**	n.d.
93667	1	-0.01	0.54	-1.61	**-3.47**	**-2.64**	n.d.
72589	1	-0.28	1.12	-1.04	**-3.46**	**-2.85**	n.d.
48894	1	0.21	0.88	-1.07	**-3.44**	**-2.94**	n.d.
89958	1	-1.31	0.10	-1.72	**-3.43**	**-3.23**	n.d.
50847	1	-0.22	0.74	-1.51	**-3.43**	**-2.68**	n.d.
87389	1	0.06	1.06	-1.39	**-3.40**	**-2.43**	n.d.
31161	1	0.13	0.20	-1.64	**-3.40**	**-2.71**	n.d.
79772	1	-0.93	0.14	-1.39	**-3.39**	**-2.77**	n.d.
92569	1	-1.08	0.12	-1.48	**-3.38**	**-2.64**	n.d.
46783	1	-0.34	0.19	-1.59	**-3.38**	**-3.26**	n.d.
80695	1	-0.73	-0.20	-1.87	**-3.36**	**-2.52**	n.d.
88703	1	-1.55	-0.96	-1.71	**-3.35**	**-2.87**	n.d.
46104	1	-0.95	-0.18	-1.18	**-3.34**	**-2.63**	n.d.

ID	WT strand bias	dcl1⁻ log_2 fold change vs WT	dcl2⁻ log_2 fold change vs WT	dcl1⁻/2⁻ log_2 fold change vs WT	rdrp1⁻ log_2 fold change vs WT	rdrp2⁻ log_2 fold change vs WT	Ago-1 bound WT log_2 fold change vs ago-1⁻
83434	1	-0.17	0.43	-1.60	**-3.33**	**-3.23**	n.d.
73842	1	-0.94	-0.23	-1.77	**-3.32**	**-2.78**	n.d.
51719	1	-0.68	0.04	-1.41	**-3.31**	**-2.54**	n.d.
43928	0.99	-0.42	0.36	-1.63	**-3.31**	**-2.96**	n.d.
44126	1	-0.48	0.34	-0.88	**-3.30**	**-2.77**	n.d.
33806	1	-0.20	1.16	-1.80	**-3.29**	**-2.11**	n.d.
90407	1	-1.96	-1.21	-1.18	**-3.28**	**-2.57**	n.d.
36942	1	-0.52	0.88	-1.39	**-3.28**	**-2.65**	n.d.
93671	1	0.38	1.09	-0.95	**-3.27**	**-2.10**	n.d.
50312	-0.83	-0.99	0.46	-1.39	**-3.27**	**-2.81**	n.d.
51948	1	0.12	1.45	-1.33	**-3.26**	**-2.35**	n.d.
48566	1	0.21	0.93	-0.58	**-3.26**	**-2.06**	n.d.
85633	1	0.47	1.45	-1.04	**-3.26**	**-2.21**	n.d.
79712	1	-0.75	-0.03	-1.21	**-3.26**	**-2.82**	n.d.
27316	1	-0.90	0.41	-1.39	**-3.26**	**-2.52**	n.d.
48456	1	-0.34	0.28	-1.29	**-3.25**	**-2.63**	n.d.
75510	1	-0.56	-0.07	-1.08	**-3.23**	**-2.66**	n.d.
77712	1	-0.48	0.91	-1.34	**-3.23**	**-2.68**	n.d.
84716	1	0.02	-0.10	-1.55	**-3.22**	**-2.87**	n.d.
85759	0.99	0.51	0.62	-1.35	**-3.21**	**-2.59**	n.d.
40368	1	-0.49	-0.01	-1.58	**-3.21**	**-2.26**	n.d.
94671	1	-0.97	-0.05	-1.62	**-3.21**	**-2.81**	n.d.
90427	1	-0.33	0.16	-1.20	**-3.21**	**-3.09**	n.d.
92297	1	-0.83	0.31	-1.33	**-3.21**	**-2.41**	n.d.
23700	1	-0.97	-0.33	-1.42	**-3.21**	**-2.34**	n.d.
41731	1	-0.01	0.63	-1.46	**-3.20**	**-2.87**	n.d.
88521	1	-0.23	0.17	-1.46	**-3.20**	**-2.77**	n.d.
93377	1	-1.04	-0.25	-1.43	**-3.18**	**-2.50**	n.d.
92837	1	-1.53	-0.56	-1.60	**-3.14**	**-2.99**	n.d.
81329	0.99	-0.85	-0.32	-1.77	**-3.14**	**-3.12**	n.d.
87875	1	-0.64	0.08	-1.04	**-3.13**	**-2.63**	n.d.
76389	1	-0.60	0.09	-1.82	**-3.13**	**-2.39**	n.d.
27189	1	-1.41	-1.01	-1.59	**-3.12**	**-2.69**	n.d.
93112	1	-0.31	0.51	-1.01	**-3.12**	**-2.08**	n.d.
29038	1	-0.46	0.21	-0.92	**-3.12**	**-2.11**	n.d.
92909	0.99	-0.28	0.88	-1.10	**-3.11**	**-2.50**	n.d.
28312	1	-0.03	0.94	-1.09	**-3.10**	**-2.06**	n.d.
68839	1	-0.68	0.16	-1.26	**-3.10**	**-2.32**	n.d.
81601	1	-0.07	1.00	-1.47	**-3.10**	**-2.94**	n.d.
80729	1	0.25	0.44	-0.94	**-3.09**	**-2.14**	n.d.
72128	1	-0.51	-0.02	-1.34	**-3.09**	**-2.41**	n.d.
76861	1	-0.39	-0.05	-1.25	**-3.08**	**-2.71**	n.d.
78974	1	-0.93	-0.25	-1.85	**-3.07**	**-3.49**	n.d.
26855	1	-0.91	0.13	-1.16	**-3.07**	**-2.68**	n.d.
85759	1	-1.02	-0.44	-1.58	**-3.07**	**-2.62**	n.d.
90989	1	-0.42	0.08	-1.39	**-3.07**	**-3.35**	n.d.
22420	1	-0.38	0.37	-0.97	**-3.07**	**-2.31**	n.d.
95180	1	-0.60	0.01	-1.92	**-3.07**	**-3.32**	n.d.
84236	1	-0.79	0.34	-1.27	**-3.05**	**-2.31**	n.d.
83427	1	0.07	1.16	-0.96	**-3.05**	**-2.16**	n.d.
90661	1	1.00	0.66	-0.57	**-3.03**	**-2.34**	n.d.
39231	0.98	0.22	0.44	-1.56	**-3.03**	**-2.61**	n.d.
80392	1	-0.16	0.19	-1.56	**-3.03**	**-3.20**	n.d.
84935	0.99	-0.71	0.41	-1.60	**-3.02**	**-2.71**	n.d.
37397	1	-0.32	0.46	-1.66	**-3.01**	**-2.73**	n.d.
36402	1	-0.55	0.67	-1.29	**-3.01**	**-2.35**	n.d.
71319	1	-0.27	0.65	-1.62	**-3.01**	**-2.82**	n.d.
78510	1	0.56	1.04	-1.26	**-3.01**	**-2.28**	n.d.
88759	1	-1.04	0.41	-1.22	**-3.00**	**-2.32**	n.d.
35570	1	0.18	0.78	-1.35	**-3.00**	**-2.83**	n.d.
86091	1	-0.23	-0.04	-0.78	**-3.00**	**-2.27**	n.d.
84211	1	-0.25	0.72	-0.90	**-3.00**	**-2.21**	n.d.
26919	1	-0.99	-0.41	-1.53	**-3.00**	**-2.38**	**4.89**
33319	1	-0.69	0.14	-1.87	**-2.99**	**-3.06**	n.d.
78974	1	-0.67	0.11	-1.74	**-2.99**	**-3.26**	n.d.
84311	1	-1.14	0.39	-0.80	**-2.99**	**-2.15**	n.d.
93567	1	-0.84	0.64	-1.60	**-2.98**	**-2.18**	n.d.
89243	1	0.02	0.88	-0.46	**-2.98**	**-2.27**	n.d.
94941	1	0.16	0.93	-1.23	**-2.98**	**-2.69**	n.d.
12399	1	-1.49	-0.08	-1.45	**-2.98**	**-2.83**	n.d.
76134	1	-0.23	-0.32	-1.09	**-2.97**	**-2.65**	n.d.
75313	1	-0.45	0.33	-1.61	**-2.96**	**-2.19**	n.d.
33458	1	-1.05	-0.50	-0.58	**-2.96**	**-2.56**	n.d.
84114	1	-0.06	0.66	-1.24	**-2.95**	**-2.63**	n.d.
90057	1	-0.74	-0.30	-1.65	**-2.95**	**-2.81**	n.d.
89950	1	-0.19	0.47	-1.50	**-2.95**	**-2.84**	n.d.
34025	1	0.52	1.15	-0.67	**-2.95**	**-2.04**	n.d.
29487	1	-0.22	0.51	-1.54	**-2.94**	**-2.86**	n.d.
70091	0.98	-0.88	-0.52	-1.44	**-2.93**	**-2.89**	n.d.
91230	1	-1.43	-0.36	-1.69	**-2.93**	**-2.64**	n.d.
50500	1	-0.45	-0.60	-1.63	**-2.92**	**-2.52**	n.d.
45044	1	0.80	0.86	-0.90	**-2.92**	**-2.59**	n.d.
93787	1	-0.31	0.94	-1.42	**-2.92**	**-2.28**	n.d.
48059	1	-0.45	0.30	-1.92	**-2.91**	**-2.60**	n.d.
95140	1	0.09	0.64	-1.00	**-2.91**	**-2.45**	n.d.
82159	1	-0.59	0.93	-1.15	**-2.90**	**-2.35**	n.d.
90918	1	-0.23	0.23	-1.33	**-2.89**	**-2.38**	n.d.
82482	1	-1.18	-0.11	-1.64	**-2.88**	**-3.08**	n.d.
48786	1	-0.16	0.54	-1.19	**-2.88**	**-2.24**	n.d.
93782	1	-0.40	-0.45	-1.86	**-2.88**	**-3.04**	n.d.
80802	1	0.09	0.12	-0.76	**-2.86**	**-2.04**	n.d.
20075	1	-1.67	-0.58	-1.51	**-2.86**	**-2.67**	n.d.
92734	1	-0.35	0.98	-1.20	**-2.85**	**-2.56**	n.d.
51408	1	-1.24	-0.66	-1.20	**-2.84**	**-3.00**	n.d.
50238	1	-0.83	0.13	-0.75	**-2.84**	**-2.59**	n.d.
91591	1	-0.38	0.17	-1.40	**-2.84**	**-3.14**	n.d.

ID	WT strand bias	dcl1⁻ log_2 fold change vs WT	dcl2⁻ log_2 fold change vs WT	dcl1⁻/2⁻ log_2 fold change vs WT	rdrp1⁻ log_2 fold change vs WT	rdrp2⁻ log_2 fold change vs WT	Ago-1 bound WT log_2 fold change vs ago-1⁻
41987	1	-0.75	0.65	-0.45	**-2.83**	**-2.06**	n.d.
94401	1	-0.73	-0.74	-0.38	**-2.83**	**-2.81**	n.d.
93173	0.99	-0.60	0.40	-0.97	**-2.83**	**-2.37**	n.d.
89017	1	-0.79	0.29	-0.64	**-2.82**	**-2.34**	n.d.
95599	1	-0.27	0.40	-1.28	**-2.82**	**-2.82**	n.d.
29691	1	-0.30	-0.09	-0.47	**-2.81**	**-2.15**	n.d.
82047	1	0.09	0.41	-1.15	**-2.81**	**-2.52**	n.d.
86333	1	-0.24	1.11	-1.30	**-2.81**	**-2.40**	n.d.
13626	1	1.30	1.41	-0.56	**-2.80**	**-2.14**	n.d.
92089	1	0.08	0.48	-1.40	**-2.80**	**-2.21**	n.d.
44205	1	-1.63	0.42	-1.33	**-2.79**	**-2.22**	n.d.
44640	1	-1.19	-0.95	-0.95	**-2.78**	**-2.17**	n.d.
88605	1	-0.10	0.52	-1.10	**-2.77**	**-2.59**	n.d.
46623	1	-0.93	0.36	-0.68	**-2.76**	**-2.29**	n.d.
94991	1	0.26	1.02	-1.04	**-2.76**	**-2.45**	n.d.
44594	1	0.77	0.61	-1.15	**-2.75**	**-2.45**	n.d.
43913	1	-0.78	0.81	-1.42	**-2.75**	**-2.93**	n.d.
93857	1	-0.07	0.76	-0.89	**-2.75**	**-2.23**	n.d.
94013	0.92	-0.56	0.11	-1.38	**-2.75**	**-2.16**	n.d.
50834	1	-0.06	-0.19	-1.08	**-2.75**	**-2.16**	n.d.
87231	1	0.93	1.86	-0.61	**-2.73**	**-2.17**	n.d.
37057	1	0.66	1.09	-0.68	**-2.73**	**-2.08**	n.d.
93155	1	0.33	0.51	-0.82	**-2.71**	**-2.50**	n.d.
91714	1	0.19	-0.01	-0.97	**-2.71**	**-2.49**	n.d.
92731	1	-0.20	0.20	-0.90	**-2.71**	**-2.42**	n.d.
48484	1	0.56	0.59	-1.16	**-2.70**	**-2.79**	n.d.
94942	1	-0.33	0.38	-1.21	**-2.70**	**-2.20**	n.d.
91077	1	-0.07	0.44	-1.24	**-2.70**	**-2.48**	n.d.
93008	0.99	-0.66	-0.32	-0.96	**-2.69**	**-2.16**	n.d.
30046	1	-0.37	-0.08	-1.02	**-2.69**	**-2.27**	n.d.
45044	1	0.27	0.79	-1.21	**-2.68**	**-2.47**	n.d.
79972	1	-0.22	0.47	-1.80	**-2.68**	**-2.79**	n.d.
38120	1	-0.76	0.14	-1.31	**-2.67**	**-2.30**	n.d.
31124	1	-0.60	-0.22	0.31	**-2.67**	**-2.43**	n.d.
30744	1	-1.05	0.11	-0.88	**-2.66**	**-2.36**	n.d.
92017	1	0.33	0.53	-0.83	**-2.66**	**-2.20**	n.d.
77001	1	0.01	0.31	-0.83	**-2.66**	**-2.45**	n.d.
90832	1	0.60	0.56	-0.24	**-2.65**	**-2.03**	n.d.
42284	1	-0.31	0.92	-1.38	**-2.65**	**-3.29**	n.d.
95682	1	-0.30	0.39	-1.11	**-2.65**	**-2.77**	0.98
48444	1	-0.31	1.17	-1.54	**-2.65**	**-2.25**	n.d.
93193	1	-0.60	0.00	-0.80	**-2.65**	**-2.35**	n.d.
81743	1	-1.20	-0.92	-1.02	**-2.64**	**-2.63**	n.d.
77450	0.74	-0.41	0.45	-0.78	**-2.64**	**-2.27**	n.d.
87683	1	-0.56	-0.16	-1.32	**-2.62**	**-2.25**	n.d.
39200	1	0.21	0.67	-0.55	**-2.62**	**-2.23**	n.d.
84536	1	0.34	0.91	-1.31	**-2.62**	**-2.56**	n.d.
93264	0.92	-0.81	0.70	-0.89	**-2.62**	**-2.11**	n.d.
31320	1	-0.85	-0.00	-0.68	**-2.60**	**-2.00**	n.d.
89322	1	-0.49	0.54	-0.95	**-2.58**	**-2.11**	n.d.
90112	1	-0.64	-0.02	-1.16	**-2.58**	**-2.43**	n.d.
93252	1	0.24	0.90	-0.55	**-2.57**	**-2.35**	n.d.
50168	1	-0.20	0.82	-1.18	**-2.57**	**-2.77**	**3.65**
18759	1	-0.18	-0.04	-1.46	**-2.56**	**-2.48**	n.d.
92731	1	-0.32	0.73	-0.53	**-2.56**	**-2.17**	n.d.
81408	1	-0.94	-0.55	-1.16	**-2.56**	**-2.34**	n.d.
94112	1	0.41	1.08	-1.62	**-2.55**	**-2.24**	**5.51**
90782	1	-0.45	0.36	-0.61	**-2.55**	**-2.01**	n.d.
32834	1	0.03	0.07	-0.59	**-2.55**	**-2.05**	n.d.
48455	1	-0.58	0.47	-1.38	**-2.54**	**-2.64**	n.d.
91279	1	-1.00	-0.01	-0.77	**-2.54**	**-2.42**	n.d.
44822	1	-0.39	0.16	-1.23	**-2.54**	**-2.12**	n.d.
80586	1	-0.29	0.72	-1.00	**-2.53**	**-2.49**	n.d.
91915	1	-1.10	0.24	-0.92	**-2.53**	**-2.08**	n.d.
76793	1	0.15	1.10	-1.10	**-2.53**	**-2.14**	n.d.
77377	1	-0.57	0.74	-0.41	**-2.52**	**-2.09**	n.d.
76244	1	-0.56	-0.07	-1.04	**-2.52**	**-2.08**	n.d.
79571	1	-0.38	0.78	-1.09	**-2.50**	**-2.52**	n.d.
46783	1	-0.39	0.23	-1.11	**-2.50**	**-2.24**	n.d.
87333	1	0.32	0.86	-1.26	**-2.49**	**-2.26**	n.d.
94072	1	0.02	0.07	-1.06	**-2.49**	**-2.53**	n.d.
89721	1	-1.38	0.02	-0.69	**-2.49**	**-2.35**	n.d.
78799	1	-0.43	0.20	-0.45	**-2.48**	**-2.11**	n.d.
91374	1	-0.32	0.26	-0.59	**-2.47**	**-2.13**	n.d.
47690	1	-0.86	-0.10	-0.59	**-2.46**	**-2.21**	n.d.
86793	1	-0.25	0.56	-0.90	**-2.46**	**-2.37**	n.d.
25723	1	0.66	1.67	-0.76	**-2.46**	**-2.12**	n.d.
50382	1	-0.65	0.20	-0.89	**-2.44**	**-2.28**	n.d.
79616	1	-0.88	0.38	-1.01	**-2.42**	**-2.15**	n.d.
47807	1	-0.46	0.43	-0.73	**-2.40**	**-2.43**	n.d.
31788	1	0.31	1.38	-1.08	**-2.38**	**-2.04**	n.d.
95473	1	-1.68	0.02	-0.98	**-2.38**	**-2.28**	n.d.
47676	1	-0.39	0.39	-0.59	**-2.38**	**-2.29**	n.d.
94003	1	-0.61	0.01	-1.41	**-2.38**	**-2.61**	n.d.
79227	1	-0.05	0.52	-0.84	**-2.36**	**-2.25**	n.d.
74888	1	-0.02	0.84	-0.93	**-2.35**	**-2.26**	n.d.
91660	0.99	-0.39	0.38	-0.63	**-2.35**	**-2.24**	n.d.
95461	0.95	-0.90	0.00	-0.95	**-2.35**	**-2.26**	n.d.
88998	1	-0.49	0.99	-0.42	**-2.34**	**-2.02**	n.d.
90918	1	-1.00	-0.55	-1.49	**-2.33**	**-2.01**	n.d.
43050	1	0.47	0.58	-0.98	**-2.30**	**-2.31**	n.d.
86763	1	-0.26	0.13	-0.75	**-2.30**	**-2.28**	n.d.
89561	1	-0.13	0.85	-0.57	**-2.29**	**-2.23**	n.d.
95242	1	-0.81	0.69	-0.26	**-2.29**	**-2.13**	n.d.
29487	1	-0.20	0.48	-1.70	**-2.28**	**-2.31**	n.d.
44317	1	-0.43	0.58	-0.76	**-2.27**	**-2.01**	n.d.

ID	WT strand bias	dcl1⁻ log_2 fold change vs WT	dcl2⁻ log_2 fold change vs WT	dcl1⁻/2⁻ log_2 fold change vs WT	rdrp1⁻ log_2 fold change vs WT	rdrp2⁻ log_2 fold change vs WT	Ago-1 bound WT log_2 fold change vs ago-1⁻
81551	1	0.00	0.24	-1.19	**-2.26**	**-2.15**	n.d.
89517	1	-0.98	-0.35	-0.27	**-2.26**	**-2.12**	n.d.
32912	1	-0.49	0.80	-0.38	**-2.26**	**-2.60**	n.d.
78620	1	-0.66	0.70	-0.81	**-2.25**	**-2.16**	n.d.
43858	1	-0.75	-0.63	-1.22	**-2.23**	**-2.75**	n.d.
9964	1	-1.08	0.31	-0.84	**-2.22**	**-2.60**	n.d.
81477	1	-0.67	-0.02	-1.00	**-2.21**	**-2.22**	n.d.
87856	1	-1.20	-0.01	-0.13	**-2.20**	**-2.21**	n.d.
50622	1	-0.09	0.50	-0.95	**-2.19**	**-2.18**	n.d.
93011	1	-0.79	0.03	-0.83	**-2.19**	**-2.15**	n.d.
25842	1	-0.44	0.45	-0.97	**-2.18**	**-2.40**	n.d.
43628	0.99	-0.20	1.07	-1.00	**-2.18**	**-2.08**	n.d.
93656	0.87	-1.54	0.36	-0.67	**-2.17**	**-2.98**	n.d.
90750	1	0.14	0.59	-0.51	**-2.16**	**-2.48**	n.d.
38927	1	-1.09	0.48	-0.54	**-2.14**	**-2.04**	n.d.
46895	1	-0.21	0.74	-0.79	**-2.13**	**-2.05**	n.d.
20135	1	-0.14	1.22	-0.53	**-2.13**	**-2.13**	n.d.
79055	1	0.02	1.10	-0.61	**-2.11**	**-2.15**	n.d.
46410	1	-0.64	0.07	-0.69	**-2.09**	**-2.06**	n.d.
68633	1	0.02	0.42	-0.62	**-2.08**	**-2.00**	n.d.
92598	1	1.30	0.61	-0.32	**-2.05**	**-2.18**	n.d.
48729	1	0.29	1.05	-0.96	**-2.03**	**-2.23**	n.d.
94535	1	0.02	1.17	0.67	**-2.02**	**-2.26**	n.d.
91622	1	0.33	1.18	-0.32	**-2.02**	**-2.12**	n.d.
51186	1	-0.47	-0.29	-0.99	**-2.01**	**-2.19**	n.d.
9831	1	-0.07	0.18	-0.87	**-2.00**	**-2.54**	n.d.
95318	1	-0.33	0.56	-1.58	**-5.25**	-1.97	**3.43**
88145	0.99	-0.26	0.81	-0.82	**-4.85**	-1.65	n.d.
91412	1	0.37	1.85	-0.69	**-4.20**	-1.01	n.d.
94060	1	-0.24	0.87	-0.81	**-3.89**	-1.74	n.d.
95037	1	0.38	1.21	-0.89	**-3.85**	-1.49	n.d.
45935	1	0.33	1.78	-1.38	**-3.84**	-1.98	n.d.
80539	1	0.46	**2.05**	-0.23	**-3.72**	-1.31	n.d.
47616	1	0.25	0.92	-0.35	**-3.71**	-1.63	n.d.
30682	0.97	-0.38	0.48	-0.71	**-3.67**	-1.65	n.d.
80406	1	-0.33	1.10	-0.91	**-3.64**	-1.98	n.d.
87857	1	-0.88	0.67	-0.05	**-3.60**	-1.49	n.d.
93776	1	0.62	1.65	-0.01	**-3.41**	-1.31	n.d.
92625	0.97	0.30	0.67	-1.21	**-3.39**	-1.92	n.d.
49344	0.98	-0.11	1.01	0.02	**-3.38**	-0.56	**3.88**
89960	1	-0.05	0.77	-1.05	**-3.35**	-1.68	n.d.
46568	1	0.62	1.08	-0.03	**-3.30**	-0.81	n.d.
89569	1	-0.20	1.11	-0.07	**-3.27**	-0.61	n.d.
73863	1	0.47	1.09	-1.28	**-3.26**	-1.80	n.d.
91193	0.99	0.23	1.52	-0.68	**-3.24**	-1.41	n.d.
88136	1	0.72	1.60	-0.74	**-3.18**	-1.94	n.d.
48022	1	0.22	1.14	-1.30	**-3.17**	-1.94	n.d.
90890	1	-1.74	-0.83	-0.75	**-3.15**	-1.82	n.d.
85063	1	-0.19	1.19	-0.57	**-3.08**	-1.13	n.d.
47076	0.98	0.80	1.67	0.65	**-3.07**	-0.32	n.d.
49444	1	-0.15	1.19	-1.09	**-3.07**	-1.99	n.d.
91403	1	0.02	0.99	-0.10	**-2.99**	-1.39	n.d.
92884	1	0.04	1.02	-0.57	**-2.98**	-1.83	n.d.
51816	1	-0.88	0.65	-1.26	**-2.97**	-1.74	n.d.
96091	0.98	-0.93	0.26	-0.75	**-2.95**	-1.74	n.d.
86952	0.99	-0.68	1.09	0.59	**-2.95**	0.05	n.d.
49344	0.98	0.61	1.52	0.46	**-2.95**	0.11	**4.27**
77956	1	0.95	1.15	-0.68	**-2.94**	-1.74	n.d.
95369	1	0.55	0.57	-0.49	**-2.94**	-1.39	n.d.
71281	1	0.07	0.70	-0.21	**-2.94**	-1.89	n.d.
94536	1	0.54	0.64	-0.73	**-2.93**	-1.93	n.d.
30682	1	0.02	0.78	-0.53	**-2.91**	-1.61	n.d.
93564	1	0.39	1.41	-0.14	**-2.91**	-1.56	n.d.
47565	1	0.59	1.60	-0.32	**-2.87**	-1.54	n.d.
91173	1	-0.65	0.54	-1.01	**-2.86**	-1.83	n.d.
11610	0.99	0.16	1.34	0.43	**-2.85**	0.03	n.d.
48950	1	-0.03	0.02	-0.47	**-2.85**	-1.80	n.d.
51849	1	0.39	0.79	-0.93	**-2.84**	-1.85	n.d.
78965	1	1.14	1.62	-0.19	**-2.83**	-1.33	n.d.
85005	0.94	-0.80	1.01	-0.59	**-2.82**	-1.73	n.d.
93002	1	0.00	1.21	0.77	**-2.82**	0.13	n.d.
30700	1	-0.72	0.16	-1.22	**-2.81**	-1.83	n.d.
92607	1	-0.09	0.71	-0.85	**-2.80**	-1.71	n.d.
91590	1	-1.33	0.13	-1.26	**-2.78**	-1.82	n.d.
94997	1	-0.02	0.55	0.04	**-2.78**	-0.98	n.d.
76277	1	0.19	0.98	-0.64	**-2.77**	-1.00	n.d.
93592	1	-0.03	0.84	-0.32	**-2.77**	-1.24	n.d.
25571	1	0.19	0.52	-0.72	**-2.76**	-1.96	n.d.
86055	1	-0.26	0.80	-0.09	**-2.75**	-1.65	n.d.
73872	0.98	0.81	1.52	-0.87	**-2.75**	-1.93	n.d.
76823	1	-0.42	1.02	-0.69	**-2.75**	-1.76	n.d.
77714	1	0.54	1.38	-0.29	**-2.74**	-1.84	n.d.
77774	1	-0.05	0.78	-0.87	**-2.73**	-1.90	n.d.
49974	1	-0.69	-0.05	-0.64	**-2.72**	-1.89	n.d.
87147	1	1.10	1.69	-0.76	**-2.71**	-0.89	n.d.
90691	1	-0.25	0.90	-0.64	**-2.70**	-1.83	n.d.
91672	1	0.15	0.89	-0.49	**-2.70**	-1.75	n.d.
92655	1	0.01	1.45	0.03	**-2.69**	-1.68	n.d.
87586	1	-0.07	0.09	-0.99	**-2.68**	-1.62	n.d.
37988	0.65	-0.74	0.22	-0.70	**-2.67**	-1.53	n.d.
26602	1	-0.40	0.18	-0.67	**-2.67**	-1.69	n.d.
75629	1	0.91	1.21	-0.42	**-2.66**	-1.53	n.d.
82167	1	-0.05	0.66	-0.52	**-2.66**	-1.75	n.d.
90890	1	0.33	0.55	0.05	**-2.65**	-1.36	n.d.
28089	1	-0.65	0.10	-0.21	**-2.65**	-1.47	n.d.
89684	1	0.13	0.94	-1.11	**-2.65**	-1.67	n.d.

ID	WT strand bias	dcl1⁻ log_2 fold change vs WT	dcl2⁻ log_2 fold change vs WT	dcl1⁻/2⁻ log_2 fold change vs WT	rdrp1⁻ log_2 fold change vs WT	rdrp2⁻ log_2 fold change vs WT	Ago-1 bound WT log_2 fold change vs ago-1⁻
82741	1	0.62	0.78	0.05	**-2.64**	-1.65	n.d.
69078	1	-0.44	0.97	-0.73	**-2.63**	-1.72	n.d.
87636	1	0.06	1.24	-0.61	**-2.63**	-1.81	n.d.
49981	1	-0.02	0.57	-0.40	**-2.62**	-1.99	n.d.
84769	1	0.11	1.60	-0.33	**-2.62**	-1.58	n.d.
48719	1	0.41	1.12	-0.26	**-2.62**	-1.11	n.d.
89569	1	-0.36	1.05	0.66	**-2.61**	0.27	n.d.
89707	0.89	-0.91	0.55	0.17	**-2.61**	-1.69	n.d.
90924	1	0.01	1.09	0.09	**-2.61**	-1.94	n.d.
85096	1	-0.01	0.37	-0.55	**-2.61**	-1.84	n.d.
49864	0.94	-0.34	0.68	-0.66	**-2.60**	-1.54	n.d.
93760	0.98	-1.21	0.62	0.04	**-2.59**	-0.89	n.d.
17522	1	-0.30	0.67	-0.74	**-2.58**	-1.84	n.d.
94383	1	-0.08	0.99	-0.55	**-2.58**	-1.61	n.d.
46576	1	0.75	1.40	-0.31	**-2.54**	-1.28	n.d.
10358	1	0.34	0.59	-0.45	**-2.54**	-1.66	n.d.
83198	1	-0.01	0.81	-0.30	**-2.54**	-1.59	n.d.
90548	1	0.15	0.87	-0.74	**-2.54**	-1.69	n.d.
82855	1	-0.39	-0.14	-0.69	**-2.53**	-1.71	n.d.
34433	1	-0.60	0.32	-0.74	**-2.53**	-1.82	n.d.
95947	1	-0.07	0.77	0.03	**-2.53**	-0.87	n.d.
81707	0.38	-1.02	0.12	-0.82	**-2.51**	-1.88	n.d.
91279	1	0.19	0.73	-0.33	**-2.51**	-1.70	n.d.
92704	0.96	0.08	0.14	-0.92	**-2.51**	-1.83	n.d.
84389	1	-0.46	0.67	0.02	**-2.51**	-1.38	n.d.
81173	1	-0.57	0.25	-0.12	**-2.50**	-1.76	n.d.
80609	1	-0.12	1.63	-0.64	**-2.50**	-1.39	n.d.
45528	1	-0.24	1.10	-0.18	**-2.49**	-1.59	n.d.
74535	0.98	0.15	0.94	0.09	**-2.47**	-0.81	n.d.
94446	1	0.24	1.37	-0.51	**-2.45**	-1.35	n.d.
25669	1	0.38	1.06	-0.18	**-2.44**	-1.36	n.d.
82711	1	-0.42	0.68	-0.73	**-2.44**	-1.77	n.d.
79080	1	0.04	0.23	-0.99	**-2.43**	-1.90	n.d.
95521	0.98	0.84	0.86	-0.21	**-2.42**	-1.82	n.d.
28514	1	-0.28	0.47	-0.51	**-2.42**	-1.74	n.d.
19077	1	-0.81	-0.33	-0.62	**-2.41**	-1.55	**3.38**
88300	1	0.91	1.65	-0.53	**-2.41**	-1.89	n.d.
94101	0.99	-0.85	0.06	-0.22	**-2.40**	-1.34	n.d.
44832	1	-0.25	0.34	-0.60	**-2.40**	-1.79	n.d.
87442	1	-0.66	-0.20	-0.64	**-2.40**	-1.69	n.d.
32471	1	0.22	0.94	-0.59	**-2.40**	-1.27	n.d.
92041	0.98	-0.11	1.07	-0.35	**-2.39**	-1.45	n.d.
33534	0.88	0.78	1.94	0.11	**-2.39**	-1.32	n.d.
92436	1	0.24	0.54	-0.45	**-2.39**	-1.88	n.d.
91641	1	-0.58	0.28	-0.50	**-2.38**	-1.80	n.d.
77082	1	0.32	1.10	0.17	**-2.38**	-0.75	n.d.
50181	1	0.35	1.23	-0.30	**-2.37**	-1.24	n.d.
91611	1	-0.14	0.59	-0.26	**-2.37**	-1.61	n.d.
91330	1	-0.47	0.26	-0.71	**-2.37**	-1.91	n.d.
89689	1	-0.68	0.86	-0.39	**-2.36**	-1.40	n.d.
87510	0.99	-1.18	-0.53	-0.36	**-2.36**	-1.53	n.d.
88612	1	-0.19	0.66	-0.79	**-2.35**	-1.91	n.d.
46819	1	0.54	1.98	-0.15	**-2.35**	-0.54	n.d.
29806	1	-0.87	0.63	-0.24	**-2.34**	-1.77	n.d.
93704	1	0.21	0.84	-0.38	**-2.34**	-1.78	n.d.
48438	1	-0.67	-0.02	-0.16	**-2.34**	-1.68	n.d.
92587	1	-0.16	0.85	-0.22	**-2.34**	-1.72	n.d.
77340	1	0.57	1.37	-0.77	**-2.33**	-1.89	n.d.
25669	1	0.71	0.90	-0.21	**-2.33**	-0.84	n.d.
49444	1	-0.14	1.11	-0.16	**-2.33**	-1.50	n.d.
26661	1	-0.40	0.15	-0.52	**-2.32**	-1.75	n.d.
93550	1	-0.64	0.45	-0.65	**-2.32**	-1.78	n.d.
89689	1	-0.34	0.64	-0.24	**-2.31**	-1.51	n.d.
84249	0.98	0.26	0.77	-0.27	**-2.31**	-1.69	n.d.
48886	0.99	-0.15	0.85	-0.65	**-2.31**	-1.65	n.d.
77585	1	-0.07	0.65	0.16	**-2.30**	-1.33	n.d.
83388	1	-0.45	0.44	-0.48	**-2.30**	-1.93	n.d.
34228	1	-1.10	-0.18	1.11	**-2.30**	0.64	n.d.
84572	0.97	-0.47	-0.10	-0.94	**-2.30**	-1.96	n.d.
90661	1	1.06	0.13	-0.15	**-2.29**	-1.78	n.d.
78707	1	-0.95	0.54	-0.61	**-2.29**	-1.75	n.d.
91410	1	0.68	1.88	-0.13	**-2.28**	-0.92	n.d.
35064	1	-0.46	0.11	-0.38	**-2.28**	-1.63	n.d.
77450	1	-0.57	0.45	-0.76	**-2.28**	-1.77	n.d.
81582	1	-0.52	0.64	-0.90	**-2.27**	-1.71	n.d.
9840	1	0.60	**2.08**	0.22	**-2.26**	-1.08	n.d.
46467	1	0.26	1.32	0.21	**-2.25**	-1.04	n.d.
90244	1	-0.55	0.05	-0.57	**-2.24**	-1.81	n.d.
89561	1	0.69	1.28	-0.46	**-2.24**	-1.64	n.d.
30173	1	0.54	1.30	-0.47	**-2.24**	-1.48	n.d.
82657	1	-0.99	0.10	-0.47	**-2.24**	-1.80	n.d.
92814	1	-0.24	0.66	-1.12	**-2.23**	-1.78	n.d.
78510	0.98	-0.19	0.85	-0.73	**-2.22**	-1.91	n.d.
51704	1	-0.29	-0.03	-0.54	**-2.22**	-1.77	n.d.
88216	1	0.14	0.63	-0.51	**-2.22**	-1.80	n.d.
80723	1	-0.73	0.27	-0.67	**-2.22**	-1.94	n.d.
49230	1	0.49	1.12	0.01	**-2.20**	-1.46	n.d.
94430	1	-0.61	-0.11	0.01	**-2.20**	-1.91	n.d.
93342	1	-0.20	0.62	0.02	**-2.20**	-1.94	n.d.
90052	1	-0.03	0.41	-0.31	**-2.20**	-1.97	n.d.
94169	1	0.54	1.62	-0.37	**-2.19**	-1.86	n.d.
84708	1	0.16	-0.26	-0.52	**-2.19**	-1.85	n.d.
88585	1	-0.15	0.52	-0.30	**-2.19**	-1.21	n.d.
80329	1	-0.48	0.06	0.07	**-2.19**	-1.38	n.d.
77832	1	-0.18	0.56	-0.47	**-2.18**	-1.93	n.d.
36097	1	-0.24	1.18	-0.84	**-2.18**	-1.26	n.d.

ID	WT strand bias	dcl1⁻ log_2 fold change vs WT	dcl2⁻ log_2 fold change vs WT	dcl1⁻/2⁻ log_2 fold change vs WT	rdrp1⁻ log_2 fold change vs WT	rdrp2⁻ log_2 fold change vs WT	Ago-1 bound WT log_2 fold change vs ago-1⁻
47757	1	-0.48	0.12	-0.94	**-2.17**	-1.98	n.d.
48221	0.99	-0.86	0.05	-0.63	**-2.17**	-1.84	n.d.
92625	1	-0.08	0.90	0.22	**-2.16**	-0.68	n.d.
86682	0.99	-0.00	1.50	-0.18	**-2.16**	-1.14	n.d.
73640	1	-0.01	0.56	-0.36	**-2.16**	-1.53	n.d.
90418	1	-0.19	1.08	0.10	**-2.16**	-1.17	n.d.
93252	1	-0.42	0.72	-0.51	**-2.16**	-1.91	n.d.
47858	1	0.42	0.28	-0.67	**-2.15**	-1.99	n.d.
90087	1	0.32	1.08	-0.11	**-2.15**	-1.59	n.d.
79230	1	0.46	0.75	0.05	**-2.15**	-1.78	n.d.
92548	0.99	-0.33	0.37	-0.21	**-2.13**	-1.53	n.d.
74934	1	-0.71	0.21	-0.42	**-2.13**	-1.59	n.d.
93865	0.97	-0.60	-0.02	-0.82	**-2.13**	-1.90	n.d.
74489	1	-0.25	0.47	-0.57	**-2.13**	-1.93	n.d.
90593	1	0.40	1.31	0.03	**-2.13**	-1.36	n.d.
30389	1	-0.66	0.27	-0.58	**-2.12**	-1.94	n.d.
25671	1	-0.48	-0.14	-0.80	**-2.11**	-1.75	n.d.
87442	0.99	-0.20	0.71	-0.54	**-2.11**	-1.85	n.d.
92956	1	0.24	1.03	-0.02	**-2.11**	-1.54	n.d.
82256	1	0.46	0.95	-0.44	**-2.11**	-1.64	n.d.
90517	1	0.06	0.87	-0.27	**-2.11**	-1.55	n.d.
73075	1	-0.11	0.63	0.20	**-2.10**	-1.08	n.d.
51832	1	-0.28	0.59	-0.05	**-2.10**	-1.79	n.d.
90350	1	0.59	0.66	-0.00	**-2.10**	-1.49	n.d.
93247	1	-0.58	0.51	-0.71	**-2.10**	-1.91	n.d.
72331	1	-0.31	0.54	-0.14	**-2.09**	-1.81	n.d.
30862	1	-0.45	0.37	0.02	**-2.09**	-1.19	n.d.
37276	1	-1.43	-1.05	-0.92	**-2.08**	-1.76	n.d.
85247	1	-0.35	1.22	0.16	**-2.08**	-0.96	n.d.
94219	1	-0.66	0.50	-0.24	**-2.08**	-1.25	n.d.
89581	0.99	-0.35	0.52	-0.58	**-2.08**	-1.95	n.d.
93112	1	0.24	1.31	0.09	**-2.08**	-1.65	n.d.
89911	1	-0.05	0.88	-0.78	**-2.08**	-1.99	n.d.
19729	1	-0.03	0.49	0.38	**-2.08**	-1.65	n.d.
93798	1	0.07	0.87	-0.28	**-2.08**	-1.91	n.d.
87336	0.98	0.02	0.50	0.41	**-2.07**	-0.77	n.d.
92251	1	1.08	1.70	-0.05	**-2.07**	-1.54	n.d.
84389	1	-0.32	0.84	0.03	**-2.07**	-1.44	n.d.
89441	0.92	-0.89	0.23	-0.37	**-2.06**	-1.35	n.d.
93904	1	-1.21	-0.54	-1.01	**-2.05**	-1.92	n.d.
84219	1	-0.22	0.71	-0.23	**-2.05**	-1.84	n.d.
95393	1	-0.44	0.49	-0.12	**-2.05**	-1.81	n.d.
46668	1	-0.20	0.65	-0.56	**-2.05**	-1.39	n.d.
33583	1	0.36	1.22	-0.35	**-2.04**	-1.29	n.d.
49010	0.99	-0.64	0.34	-0.54	**-2.04**	-1.60	n.d.
83708	0.99	0.70	1.41	0.10	**-2.04**	-1.07	n.d.
50610	1	-0.07	1.04	-0.13	**-2.03**	-1.33	n.d.
72170	1	-0.32	0.31	-0.93	**-2.03**	-1.91	n.d.
92495	1	-0.95	0.16	-0.28	**-2.03**	-1.99	n.d.
93496	1	-0.59	0.68	0.08	**-2.03**	-1.20	n.d.
47337	1	-0.77	-0.00	-0.30	**-2.03**	-1.35	n.d.
90047	0.99	-0.61	0.55	-1.06	**-2.03**	-1.94	n.d.
95147	1	-0.26	0.49	-0.45	**-2.03**	-1.91	n.d.
93861	1	0.22	0.94	-0.64	**-2.02**	-1.97	**2.39**
83547	1	-0.42	0.01	-0.55	**-2.02**	-1.64	n.d.
75695	1	-0.70	0.53	-0.75	**-2.01**	-1.94	n.d.
95936	1	0.10	0.98	-0.29	**-2.01**	-1.48	n.d.
92273	1	-0.60	-0.40	-1.87	-1.98	**-2.63**	n.d.
43525	0.99	-0.58	0.67	-0.94	-1.98	**-2.14**	n.d.
84270	0.99	-0.15	0.60	-0.59	-1.96	**-2.13**	n.d.
91591	1	0.95	1.74	-0.63	-1.94	**-2.03**	n.d.
84706	1	-0.21	0.06	-1.21	-1.90	**-2.59**	n.d.
93812	1	-0.56	-1.09	-1.36	-1.85	**-2.14**	n.d.
94340	1	-0.67	-0.02	-1.15	-1.84	**-2.36**	n.d.
27020	1	-0.12	0.85	-0.61	-1.81	**-2.08**	n.d.
81551	1	-0.16	-0.01	-0.63	-1.75	**-2.10**	n.d.
33097	1	-0.36	0.66	-0.57	-1.67	**-2.02**	n.d.
92352	0.99	0.10	1.45	0.23	-1.65	**-2.14**	n.d.
94066	0.9	-1.46	-0.35	0.11	-1.64	**-2.28**	n.d.
11398	1	-0.18	0.71	-0.38	-1.63	**-2.01**	n.d.
94691	1	-1.16	-0.50	-0.81	-1.63	**-2.10**	n.d.
76715	1	-0.44	0.42	-0.91	-1.62	**-2.19**	n.d.
48630	1	-0.47	-0.54	-0.38	-1.59	**-2.17**	n.d.
90057	0.95	-0.16	0.46	-0.74	-1.45	**-2.12**	n.d.
81169	1	-0.52	0.33	-0.42	-1.35	**-2.09**	n.d.
93824	0.95	-1.16	0.29	-0.26	-1.27	**-2.21**	n.d.
76247	0.96	-1.06	0.56	-0.56	-1.25	**-2.05**	n.d.

Table S2. Normalized reads and log_2 fold change of exonic sRNAs in the *r3b2*$^-$ mutant compared to the wild type. Normalized reads in the wild type strain R7B and the *r3b2*$^-$ mutant (WT and *r3b2*$^-$ abundance) of exonic sRNAs corresponding to each locus are shown. The coordinates correspond to the exonic loci where small RNAs maps (http://genome.jgi-psf.org/Mucci1/Mucci1.home.html [v1]). Strand bias indicates orientation to mRNAs, where 1 corresponds to all sRNAs in the same orientation as the mRNA, 0 to equal mixture of sRNAs on both strands and -1 to all sRNAs antisense to mRNAs. Normalized reads were used to calculate the fold change of sRNAs in the *r3b2*$^-$ mutant compared to wild type strain. The data are sorted for the fold change in *r3b2*$^-$ strain. N/A, not applicable. Only loci with a normalized abundance count higher than 50 in the wild type strain and a log_2 fold change ≤ -2 (fourfold or larger change) were considered.

Locus	WT abundance	WT strand bias	*r3b2*$^-$ abundance	*r3b2*$^-$ strand bias	*r3b2*$^-$ log_2 fold change vs WT
scaffold_8:1863231-1863332(+)	4068.33	-1	0.91	-1	**-12.13**
scaffold_5:1078207-1078423(+)	441.7	-0.98	0.23	1	**-10.91**
scaffold_10:633425-634769(-)	748.84	1	0.46	1	**-10.67**
scaffold_10:410047-410184(+)	632.99	1	0.46	1	**-10.43**
scaffold_3:4069661-4070267(-)	1122.46	1	0.91	1	**-10.27**
scaffold_3:668768-668985(+)	545.7	1	0.46	1	**-10.21**
scaffold_2:3893535-3893918(-)	847.98	1	0.91	1	**-9.86**
scaffold_11:77422-77501(+)	200.02	1	0.23	1	**-9.76**
scaffold_4:315603-316078(+)	157.87	1	0.23	1	**-9.42**
scaffold_9:1437628-1437756(-)	155.63	1	0.23	1	**-9.40**
scaffold_1:775153-775844(-)	148.9	1	0.23	1	**-9.34**
scaffold_6:1078899-1078972(-)	296.3	1	0.46	1	**-9.33**
scaffold_1:2712159-2712637(-)	145.28	1	0.23	1	**-9.30**
scaffold_2:833114-833305(+)	140.04	1	0.23	1	**-9.25**
scaffold_1:1335578-1335866(+)	139.67	1	0.23	1	**-9.25**
scaffold_9:1373764-1373990(+)	1099.64	1	1.82	1	**-9.24**
scaffold_3:2508867-2509003(+)	808.33	1	1.37	1	**-9.20**
scaffold_3:2304379-2304432(+)	267.99	1	0.46	1	**-9.19**
scaffold_3:4675739-4675889(-)	392.82	1	0.68	1	**-9.17**
scaffold_2:422848-422919(-)	261.13	1	0.46	1	**-9.15**
scaffold_11:414035-414150(+)	257.89	1	0.46	1	**-9.13**
scaffold_3:1647145-1647199(-)	256.64	1	0.46	1	**-9.12**
scaffold_4:476836-477179(+)	127.7	1	0.23	1	**-9.12**
scaffold_2:4478570-4478892(-)	497.82	1	0.91	1	**-9.10**
scaffold_2:1146109-1146159(-)	123.96	1	0.23	1	**-9.07**
scaffold_5:1190770-1191306(-)	118.22	1	0.23	1	**-9.01**
scaffold_2:4037702-4037778(-)	232.2	1	0.46	1	**-8.98**
scaffold_1:1875448-1875577(-)	1191.29	1	2.39	1	**-8.96**
scaffold_6:2787043-2787225(-)	113.73	1	0.23	1	**-8.95**
scaffold_4:1419174-1419440(-)	1049.5	1	2.28	1	**-8.85**
scaffold_8:817746-818335(-)	114	0.91	0.26	0.5	**-8.78**
scaffold_8:1564394-1564475(-)	96.02	1	0.23	1	**-8.71**
scaffold_8:861011-861516(+)	95.47	1	0.23	1	**-8.70**
scaffold_1:5804803-5804882(-)	94.28	1	0.23	1	**-8.68**
scaffold_3:835093-835143(-)	181.57	1	0.46	1	**-8.62**
scaffold_2:1270527-1271503(+)	90.66	1	0.23	1	**-8.62**
scaffold_2:2414115-2414511(-)	176.33	1	0.46	1	**-8.58**
scaffold_1:3091914-3092147(+)	170.2	1	0.46	1	**-8.53**
scaffold_1:3239157-3239235(+)	84.3	1	0.23	1	**-8.52**
scaffold_4:4157923-4158807(+)	81.61	0.95	0.23	1	**-8.47**
scaffold_6:53513-55201(-)	80.93	0.99	0.23	1	**-8.46**
scaffold_10:834943-835057(-)	236.54	1	0.68	1	**-8.44**
scaffold_4:2316298-2316544(-)	78.31	1	0.23	1	**-8.41**
scaffold_2:976328-976736(+)	3780.01	1	11.39	0.96	**-8.37**
scaffold_3:1288206-1288596(-)	76.07	1	0.23		**-8.37**
scaffold_2:833364-833655(+)	298.42	1	0.91	1	**-8.36**
scaffold_4:2558370-2558802(-)	220.73	1	0.68	1	**-8.34**
scaffold_5:2072131-2072243(+)	148.65	1	0.46	1	**-8.34**
scaffold_1:454420-455337(-)	403.67	1	1.25	1	**-8.34**
scaffold_3:2410408-2410896(-)	145.9	1	0.46	1	**-8.31**
scaffold_6:2835546-2835829(-)	71.83	1	0.23	1	**-8.29**
scaffold_12:720801-721017(-)	71.08	1	0.23	1	**-8.27**
scaffold_1:1594965-1595321(-)	207.38	1	0.68	1	**-8.25**
scaffold_8:1738325-1738747(+)	69.46	1	0.23	1	**-8.24**
scaffold_7:1043176-1043994(+)	69.09	1	0.23	1	**-8.23**
scaffold_2:172737-173161(+)	262.87	1	0.91	1	**-8.17**
scaffold_6:1451186-1451514(-)	66.09	1	0.23	1	**-8.17**
scaffold_1:3325236-3325340(-)	191.05	1	0.68	1	**-8.13**
scaffold_3:803104-803421(-)	190.3	1	0.68	1	**-8.13**
scaffold_9:77586-77676(-)	64.35	1	0.23		**-8.13**
scaffold_3:2976627-2977100(-)	125.08	1	0.46	1	**-8.09**
scaffold_1:4225295-4225441(+)	124.95	1	0.46	1	**-8.09**
scaffold_10:195731-195897(-)	1329.26	1	4.9	1	**-8.08**
scaffold_2:33473-33936(-)	124.68	1	0.46	1	**-8.08**
scaffold_2:3603228-3603475(+)	184.25	1	0.68	1	**-8.08**
scaffold_9:1271467-1271957(+)	61.98	1	0.23	1	**-8.07**
scaffold_5:1769333-1769745(-)	182.82	1	0.68	1	**-8.07**
scaffold_2:832649-832977(+)	61.6	1	0.23	1	**-8.07**
scaffold_1:2880374-2881207(-)	61.1	1	0.23	1	**-8.05**
scaffold_13:300833-301379(-)	149.09	1	0.57	0.33	**-8.03**
scaffold_2:4062599-4062727(+)	60.11	1	0.23	1	**-8.03**
scaffold_4:665357-665660(-)	176.51	1	0.68	0.33	**-8.02**
scaffold_5:1007347-1007690(+)	59.61	1	0.23	1	**-8.02**
scaffold_6:2729235-2729275(+)	118.72	-0.97	0.46	-1	**-8.01**
scaffold_6:1280513-1281396(+)	174.09	1	0.68	1	**-8.00**
scaffold_1:3552377-3552608(-)	399.92	1	1.59	1	**-7.97**
scaffold_11:120581-120657(-)	57.61	0.98	0.23	1	**-7.97**
scaffold_9:1019049-1019816(+)	114.35	1	0.46	1	**-7.96**
scaffold_3:1419586-1420132(-)	904.85	1	3.64	1	**-7.96**
scaffold_3:4296474-4296740(+)	139.04	1	0.57	1	**-7.93**

Locus	WT abundance	WT strand bias	*r3b2*⁻ abundance	*r3b2*⁻ strand bias	*r3b2*⁻ $\log_2$ fold change vs WT
scaffold_6:605338-605904(-)	381.84	1	1.59	1	**-7.91**
scaffold_9:858122-858554(-)	270.86	1	1.14	1	**-7.89**
scaffold_7:1517969-1518442(-)	107.62	1	0.46	1	**-7.87**
scaffold_3:1286663-1288146(-)	107.37	1	0.46	1	**-7.87**
scaffold_8:1879318-1879423(+)	158.71	1	0.68	1	**-7.87**
scaffold_9:1059042-1059197(-)	106.75	1	0.46	1	**-7.86**
scaffold_2:3225639-3225829(+)	53.37	1	0.23	1	**-7.86**
scaffold_2:2556060-2556412(-)	52.87	1	0.23	1	**-7.84**
scaffold_6:893699-893858(+)	207.88	1	0.91	1	**-7.84**
scaffold_2:530534-530679(+)	206.76	1	0.91	1	**-7.83**
scaffold_12:735964-736830(-)	51.88	1	0.23	1	**-7.82**
scaffold_4:2067164-2067348(+)	356.09	1	1.59	1	**-7.81**
scaffold_1:543290-543626(-)	102.38	1	0.46	1	**-7.80**
scaffold_6:1155137-1155291(+)	150.89	1	0.68	1	**-7.79**
scaffold_5:2811886-2812243(+)	200.44	1	0.91	1	**-7.78**
scaffold_5:1585063-1585722(+)	50.63	0.99	0.23	1	**-7.78**
scaffold_1:2827842-2828320(-)	300.54	1	1.37	1	**-7.78**
scaffold_5:1928037-1928308(+)	100.51	1	0.46	1	**-7.77**
scaffold_2:4852907-4853231(-)	56.62	1	0.26	1	**-7.77**
scaffold_2:2694937-2695622(+)	146.28	0.99	0.68	1	**-7.75**
scaffold_11:224101-224417(+)	98.27	1	0.46	1	**-7.74**
scaffold_1:2485876-2487330(+)	104.49	0.99	0.49	1	**-7.74**
scaffold_9:157603-158443(-)	96.77	0.98	0.46	1	**-7.72**
scaffold_5:663800-664020(-)	141.41	1	0.68	1	**-7.70**
scaffold_3:56812-57319(-)	137.67	1	0.68	1	**-7.66**
scaffold_6:2564408-2564641(+)	115.1	1	0.57	1	**-7.66**
scaffold_2:376825-376954(-)	92.22	0.99	0.46	1	**-7.65**
scaffold_3:2508688-2508810(+)	272.6	1	1.37	1	**-7.64**
scaffold_7:596560-59811(-)	94.96	0.99	0.48	0.80	**-7.63**
scaffold_4:1047397-1047798(+)	179.07	1	0.91	1	**-7.62**
scaffold_5:490450-492055(-)	1556.17	1	7.97	1	**-7.61**
scaffold_3:4165338-4165634(+)	679.39	1	3.48	1	**-7.61**
scaffold_11:120728-120823(-)	325.97	1	1.67	1	**-7.61**
scaffold_4:3288040-3288674(-)	110.09	0.99	0.57	1	**-7.59**
scaffold_1:4474181-4474426(+)	130.44	1	0.68	1	**-7.58**
scaffold_2:4469030-4469137(+)	87.29	1	0.46	1	**-7.57**
scaffold_2:3482771-3482859(-)	472.63	1	2.51	1	**-7.56**
scaffold_10:493309-494103(-)	85.86	1	0.46	1	**-7.54**
scaffold_8:530143-530668(-)	85.3	1	0.46	1	**-7.53**
scaffold_2:2853958-2854357(+)	123.96	1	0.68	1	**-7.51**
scaffold_11:32504-32680(-)	496.82	1	2.73	1	**-7.51**
scaffold_8:1931424-1931510(+)	163.49	1	0.91	1	**-7.49**
scaffold_2:832264-832379(+)	82.55	1	0.46	1	**-7.49**
scaffold_1:503811-504313(+)	121.31	0.83	0.68	1	**-7.48**
scaffold_7:69860-70900(+)	1946.37	1	10.93	1	**-7.48**
scaffold_3:1403587-1403798(-)	202.93	1	1.14	1	**-7.48**
scaffold_4:3918917-3919131(-)	405.41	1	2.28	1	**-7.47**
scaffold_4:263791-264100(+)	73.52	1	0.42	1	**-7.45**
scaffold_3:178948-179643(+)	153.86	1	0.88	1	**-7.45**
scaffold_1:3992924-3992966(-)	117.97	1	0.68	1	**-7.44**
scaffold_4:1747335-1747879(-)	157.68	1	0.91	1	**-7.44**
scaffold_6:2713097-2713201(-)	79.56	1	0.46	1	**-7.43**
scaffold_2:4009876-4011005(-)	117.22	1	0.68	1	**-7.43**
scaffold_3:3944931-3946069(-)	196.28	1	1.14	0.60	**-7.43**
scaffold_8:961050-961533(-)	79.06	1	0.46	1	**-7.43**
scaffold_5:386365-387234(-)	1485.22	1	8.88	0.93	**-7.39**
scaffold_2:3605996-3606844(+)	75.82	1	0.46	1	**-7.36**
scaffold_3:2643999-2644281(-)	75.07	1	0.46	1	**-7.35**
scaffold_1:3433294-3433702(-)	110.86	-1	0.68	-1	**-7.35**
scaffold_3:1284618-1285148(+)	497.95	1	3.07	0.73	**-7.34**
scaffold_6:2760005-2760624(-)	109.74	1	0.68	1	**-7.33**
scaffold_7:1155302-1155862(-)	74.17	0.93	0.46	1	**-7.33**
scaffold_5:3036564-3036673(+)	74.07	1	0.46	1	**-7.33**
scaffold_5:815750-816240(-)	128.61	1	0.8	1	**-7.33**
scaffold_9:34064-34309(-)	437.71	1	2.73	1	**-7.32**
scaffold_3:4457807-4458517(-)	78.56	1	0.49	1	**-7.32**
scaffold_10:71641-72390(+)	252.9	1	1.59	1	**-7.31**
scaffold_1:1778876-1779190(+)	180.82	1	1.14	1	**-7.31**
scaffold_1:1123427-1125025(-)	72.58	1	0.46	1	**-7.30**
scaffold_4:3749994-3750330(-)	392.07	1	2.51	1	**-7.29**
scaffold_4:1741060-1741738(-)	71.58	1	0.46	1	**-7.28**
scaffold_12:639143-639242(+)	124.31	1	0.8	1	**-7.28**
scaffold_7:1395096-1395487(-)	70.65	1	0.46	1	**-7.26**
scaffold_2:4058791-4058913(+)	103.75	1	0.68	1	**-7.25**
scaffold_4:261021-263098(+)	69.81	0.95	0.46	1	**-7.25**
scaffold_3:2486300-2486785(+)	143.91	1	0.95	1	**-7.24**
scaffold_5:2178757-2178957(-)	137.8	1	0.91	1	**-7.24**
scaffold_1:5569943-5571260(+)	274.1	1	1.82	1	**-7.23**
scaffold_3:4070523-4071493(-)	102.26	0.99	0.68	1	**-7.23**
scaffold_2:2620753-2621227(+)	110.49	1	0.74	1	**-7.22**
scaffold_5:1411977-1412363(+)	84.8	1	0.57	1	**-7.22**
scaffold_3:3643147-3643280(+)	67.59	1	0.46	1	**-7.20**
scaffold_2:4121528-4122164(+)	67.34	1	0.46	1	**-7.19**
scaffold_4:3942034-3943044(+)	367.21	1	2.51	1	**-7.19**
scaffold_8:1042654-1042976(+)	98.52	1	0.68	1	**-7.18**
scaffold_1:774771-775097(-)	73.35	1	0.51	1	**-7.17**
scaffold_2:3717796-3718369(+)	65.84	1	0.46	1	**-7.16**
scaffold_1:4337291-4337579(-)	65.59	1	0.46	1	**-7.16**
scaffold_1:5700058-5700673(-)	65.34	1	0.46	0	**-7.15**
scaffold_10:638811-638952(+)	136.05	1	0.96	1	**-7.15**
scaffold_3:3509220-3509371(+)	127.95	1	0.91	1	**-7.14**
scaffold_2:2413637-2413696(-)	64.35	1	0.46	1	**-7.13**
scaffold_12:574664-575417(-)	64.1	1	0.46	1	**-7.12**
scaffold_2:3833674-3834085(-)	94.28	1	0.68	1	**-7.12**
scaffold_1:4750110-4750958(+)	345.93	0.72	2.51	0.82	**-7.11**
scaffold_2:3347263-3347785(-)	78.06	1	0.57	1	**-7.10**
scaffold_11:560797-561626(+)	466.77	1	3.42	1	**-7.09**

Locus	WT abundance	WT strand bias	*r3b2*⁻ abundance	*r3b2*⁻ strand bias	*r3b2*⁻ $\log_2$ fold change vs WT
scaffold_2:1367350-1369052(+)	1762.23	1	12.94	0.67	**-7.09**
scaffold_6:1450184-1450905(-)	62.6	1	0.46	1	**-7.09**
scaffold_11:754068-754395(+)	62.35	1	0.46	1	**-7.08**
scaffold_3:2594031-2594257(+)	62.35	1	0.46	1	**-7.08**
scaffold_4:2867602-2867899(-)	137.29	1	1.02	1	**-7.07**
scaffold_9:689933-690281(-)	305.77	1	2.28	1	**-7.07**
scaffold_6:2756020-2756982(+)	580	1	4.33	0.89	**-7.07**
scaffold_3:26578-26755(+)	90.29	1	0.68	1	**-7.05**
scaffold_2:3188870-3189156(+)	120.71	1	0.91	1	**-7.05**
scaffold_1:1662389-1662662(-)	60.86	1	0.46	1	**-7.05**
scaffold_15:15802-16646(-)	239.68	1	1.82	0.75	**-7.04**
scaffold_3:4845995-4846174(-)	60.36	1	0.46	1	**-7.04**
scaffold_4:959858-960016(-)	59.86	1	0.46	1	**-7.02**
scaffold_6:1303485-1304195(-)	118.22	1	0.91	1	**-7.02**
scaffold_2:236117-236725(-)	82.89	1	0.64	1	**-7.02**
scaffold_14:20509-20975(-)	73.58	1	0.57	1	**-7.01**
scaffold_4:959539-959632(-)	59.19	1	0.46	0	**-7.01**
scaffold_9:782396-784795(-)	116.72	0.98	0.91	1	**-7.00**
scaffold_7:1510529-1511065(+)	58.86	1	0.46	1	**-7.00**
scaffold_7:2184841-2184989(+)	116.22	1	0.91	0	**-7.00**
scaffold_3:3754247-3754575(+)	86.79	1	0.68	1	**-7.00**
scaffold_4:776350-776959(+)	464.51	1	3.64	1	**-7.00**
scaffold_1:1755176-1755426(+)	782.39	1	6.15	1	**-6.99**
scaffold_3:1773072-1773274(-)	144.75	1	1.14	1	**-6.99**
scaffold_7:1973243-1973846(+)	86.17	1	0.68	1	**-6.99**
scaffold_2:681229-681354(+)	58.11	1	0.46	1	**-6.98**
scaffold_1:65744-65896(-)	200.02	1	1.59	1	**-6.97**
scaffold_2:4122355-4123327(+)	256.52	1	2.05	1	**-6.97**
scaffold_13:232044-232515(+)	57.11	1	0.46	1	**-6.96**
scaffold_2:377017-377372(-)	225.71	1	1.82	1	**-6.95**
scaffold_3:2263189-2263246(-)	392.82	1	3.19	1	**-6.94**
scaffold_5:8429-8672(-)	111.24	1	0.91	1	**-6.93**
scaffold_8:489133-490148(+)	911.33	1	7.53	1	**-6.92**
scaffold_1:2495909-2496730(+)	399.83	1	3.32	1	**-6.91**
scaffold_1:702120-702316(-)	55.12	0.99	0.46	1	**-6.90**
scaffold_2:530742-531435(+)	81.37	1	0.68	1	**-6.90**
scaffold_4:1476634-1477442(-)	774.91	1	6.49	0.72	**-6.90**
scaffold_3:4111869-4113210(-)	665.65	1	5.6	1	**-6.89**
scaffold_5:1192022-1192380(-)	162.61	1	1.37	1	**-6.89**
scaffold_3:3109712-3110169(-)	54.25	1	0.46	1	**-6.88**
scaffold_3:3438701-3440037(+)	132.68	1	1.14	1	**-6.86**
scaffold_7:1586757-1587815(+)	53.12	0.99	0.46	1	**-6.85**
scaffold_9:688843-689747(+)	314.75	1	2.73	1	**-6.85**
scaffold_2:4312080-4312156(-)	209.75	1	1.82	1	**-6.85**
scaffold_2:2053866-2053979(+)	4088.03	1	35.53	1	**-6.85**
scaffold_3:1550075-1550546(+)	130.44	1	1.14	1	**-6.84**
scaffold_2:1331754-1332210(-)	77.57	1	0.68	1	**-6.83**
scaffold_5:1281445-1281709(-)	207.01	1	1.82	0.89	**-6.83**
scaffold_4:12648-13905(-)	77.32	1	0.68	1	**-6.83**
scaffold_7:2001159-2002852(+)	77.19	1	0.68	1	**-6.83**
scaffold_7:1176028-1176141(-)	76.69	1	0.68	1	**-6.82**
scaffold_2:3604325-3604567(+)	102.26	1	0.91	1	**-6.81**
scaffold_6:926637-926769(-)	255.14	1	2.28	1	**-6.81**
scaffold_10:261904-262201(-)	101.76	1	0.91	1	**-6.81**
scaffold_13:545622-546572(-)	127.29	1	1.14	1	**-6.80**
scaffold_4:3278517-3278735(+)	427.48	1	3.87	1	**-6.79**
scaffold_1:5588398-5588692(+)	74.82	1	0.68	1	**-6.78**
scaffold_4:608730-609057(+)	83.6	0.95	0.76	0.6	**-6.78**
scaffold_2:3019244-3020118(+)	124.97	0.99	1.14	0.6	**-6.78**
scaffold_7:964433-964719(+)	99.51	1	0.91	1	**-6.77**
scaffold_7:1417893-1418109(+)	74.32	1	0.68	1	**-6.77**
scaffold_3:3805076-3805844(-)	52.4	0.65	0.48	0.75	**-6.77**
scaffold_2:208590-209374(+)	211.33	1	1.94	0.78	**-6.77**
scaffold_3:4171656-4172326(+)	296.79	1	2.73	1	**-6.76**
scaffold_1:3137322-3137925(+)	73.76	1	0.68	1	**-6.76**
scaffold_4:2592958-2594773(+)	73.58	1	0.68	1	**-6.76**
scaffold_3:1253777-1254409(-)	73.58	1	0.68	1	**-6.76**
scaffold_6:1945172-1945273(-)	98.07	1	0.91	1	**-6.75**
scaffold_4:3982859-3984071(+)	283.66	1	2.66	1	**-6.74**
scaffold_2:3443124-3443359(+)	238.93	1	2.28	1	**-6.71**
scaffold_9:1060892-1061455(+)	59.73	0.85	0.57	0.33	**-6.71**
scaffold_13:77920-78651(-)	95.27	1	0.91	1	**-6.71**
scaffold_7:1431408-1431601(+)	70.83	1	0.68	1	**-6.70**
scaffold_2:4251961-4252243(+)	94.03	1	0.91	1	**-6.69**
scaffold_7:1275720-1276037(-)	163.86	1	1.59	1	**-6.69**
scaffold_9:631999-632544(+)	1044.2	1	10.14	1	**-6.69**
scaffold_8:833978-835452(-)	186.43	0.96	1.82	0.78	**-6.68**
scaffold_10:1143848-1144495(-)	116.22	1	1.14	1	**-6.67**
scaffold_10:337625-337819(+)	155.71	1	1.56	1	**-6.64**
scaffold_2:14633-15441(-)	93.82	1	0.94	-0.6	**-6.64**
scaffold_4:1408199-1409208(+)	181.17	1	1.82	1	**-6.64**
scaffold_1:1738761-1739173(+)	67.34	1	0.68	1	**-6.63**
scaffold_2:2659109-2659629(+)	112.82	1	1.14	1	**-6.63**
scaffold_10:1187692-1188033(+)	89.94	0.96	0.91	1	**-6.63**
scaffold_4:1491930-1492491(-)	979.17	1	9.91	0.95	**-6.63**
scaffold_12:799451-799918(+)	156.88	0.99	1.59	1	**-6.62**
scaffold_1:439071-439208(+)	155.63	1	1.59	1	**-6.61**
scaffold_1:4533561-4533969(+)	208.13	1	2.13	1	**-6.61**
scaffold_5:2082657-2083167(+)	88.29	1	0.91	1	**-6.60**
scaffold_1:4767385-4767699(+)	65.84	1	0.68	1	**-6.60**
scaffold_5:2429021-2429410(+)	87.17	1	0.91	1	**-6.58**
scaffold_1:2712692-2712811(-)	65.1	1	0.68	1	**-6.58**
scaffold_12:321107-321306(+)	76.57	1	0.8	1	**-6.58**
scaffold_7:78959-79464(-)	87.04	1	0.91	1	**-6.58**
scaffold_2:4822715-4823166(-)	283.08	1	2.96	1	**-6.58**
scaffold_10:72449-73306(+)	135.15	1	1.42	1	**-6.57**
scaffold_4:3984137-3984626(+)	158.87	1	1.67	1	**-6.57**

Locus	WT abundance	WT strand bias	*r3b2*⁻ abundance	*r3b2*⁻ strand bias	*r3b2*⁻ log_2 fold change vs WT
scaffold_3:4633536-4633562(-)	64.6	1	0.68		**-6.57**
scaffold_5:78168-78305(-)	64.47	1	0.68	1	**-6.57**
scaffold_10:1000470-1000948(-)	85.8	1	0.91	1	**-6.56**
scaffold_1:3852654-3852837(+)	64.1	1	0.68	1	**-6.56**
scaffold_5:1295127-1295768(-)	363.14	1	3.87	1	**-6.55**
scaffold_1:33443-35056(+)	638.73	1	6.83	1	**-6.55**
scaffold_6:457856-458276(+)	63.1	1	0.68	1	**-6.54**
scaffold_6:2106019-2106480(-)	52.87	1	0.57	1	**-6.54**
scaffold_5:2237632-2239321(-)	79.61	1	0.86	1	**-6.53**
scaffold_1:632236-632425(+)	62.85	1	0.68	1	**-6.53**
scaffold_3:4485987-4486338(+)	62.73	1	0.68	1	**-6.53**
scaffold_4:1802624-1803151(+)	83.3	1	0.91	1	**-6.52**
scaffold_13:322463-322863(+)	311.01	1	3.42	1	**-6.51**
scaffold_6:1396599-1397275(+)	103.63	1	1.14	1	**-6.51**
scaffold_10:1263090-1263485(-)	82.3	0.99	0.91	1	**-6.50**
scaffold_3:2977869-2978451(-)	61.35	1	0.68	1	**-6.50**
scaffold_1:4746767-4749128(-)	451.05	1	5.01	1	**-6.49**
scaffold_9:630428-631003(+)	163.61	1	1.82	1	**-6.49**
scaffold_4:3794144-3795017(-)	61.1	0.97	0.68	1	**-6.49**
scaffold_4:1493957-1494440(+)	122.46	1	1.37	1	**-6.48**
scaffold_6:2161814-2161976(+)	101.51	1	1.14	1	**-6.48**
scaffold_13:162059-164587(+)	177.55	0.97	2	0.83	**-6.47**
scaffold_4:3525483-3526450(-)	139.67	0.99	1.59	1	**-6.46**
scaffold_3:4582396-4582609(-)	159.37	1	1.82	1	**-6.45**
scaffold_11:560082-560729(+)	139.17	1	1.59	1	**-6.45**
scaffold_3:2324837-2325895(+)	365.76	1	4.21	1	**-6.44**
scaffold_6:1200208-1200526(+)	140.35	1	1.62	1	**-6.44**
scaffold_5:221374-222216(-)	186.01	0.99	2.16	1	**-6.43**
scaffold_5:661949-662232(+)	185.14	1	2.16	1	**-6.42**
scaffold_3:3220687-3220836(-)	77.81	1	0.91	1	**-6.42**
scaffold_1:4749123-4750048(+)	135.93	1	1.59	1	**-6.42**
scaffold_12:667602-667939(+)	214.24	1	2.51	1	**-6.42**
scaffold_3:797557-798333(+)	77.32	1	0.91	1	**-6.41**
scaffold_8:776345-776511(-)	62.68	1	0.74	1	**-6.40**
scaffold_4:1225053-1225801(-)	134.43	1	1.59	1	**-6.40**
scaffold_2:4537782-4538024(-)	76.57	1	0.91	1	**-6.39**
scaffold_13:773883-774747(+)	121.13	1	1.44	1	**-6.39**
scaffold_6:2322068-2322643(+)	172.09	1	2.05	1	**-6.39**
scaffold_1:1965944-1966543(-)	95.61	1	1.14	1	**-6.39**
scaffold_11:216372-216560(-)	56.86	1	0.68	1	**-6.39**
scaffold_1:3582317-3582677(-)	76.07	1	0.91	1	**-6.39**
scaffold_10:410671-411404(+)	56.62	1	0.68	1	**-6.38**
scaffold_9:1358615-1358815(+)	56.62	1	0.68	1	**-6.38**
scaffold_4:4187742-4188623(+)	56.49	0.98	0.68	1	**-6.38**
scaffold_5:1765470-1765898(+)	74.57	1	0.91	1	**-6.36**
scaffold_3:2056273-2056847(-)	111.98	1	1.37	1	**-6.35**
scaffold_1:5448999-5449565(+)	148.65	1	1.82	1	**-6.35**
scaffold_1:1184425-1184976(+)	73.83	0.76	0.91	1	**-6.34**
scaffold_2:1326607-1326759(+)	294.8	1	3.64	1	**-6.34**
scaffold_8:1077167-1078909(-)	156.75	0.95	1.94	0.78	**-6.34**
scaffold_12:662506-663017(+)	73.33	1	0.91	1	**-6.33**
scaffold_2:975955-976278(+)	110.36	1	1.37	1	**-6.33**
scaffold_1:4823637-4823817(-)	54.74	1	0.68	1	**-6.33**
scaffold_4:3274398-3274692(-)	119.09	1	1.48	1	**-6.33**
scaffold_1:1253047-1253484(-)	54.62	1	0.68	1	**-6.33**
scaffold_2:4978028-4978487(-)	73.08	1	0.91	1	**-6.33**
scaffold_1:1526030-1526778(-)	109.99	1	1.37	1	**-6.33**
scaffold_3:3527238-3527551(-)	91.28	1	1.14	1	**-6.32**
scaffold_2:1329918-1329988(-)	91.28	1	1.14	1	**-6.32**
scaffold_6:140948-141311(-)	419	1	5.24	1.00	**-6.32**
scaffold_4:3749348-3749825(-)	163.11	1	2.05	1	**-6.31**
scaffold_1:3838489-3839674(+)	234.36	1	2.96	1	**-6.31**
scaffold_4:652566-652815(-)	62.98	1	0.8	1	**-6.30**
scaffold_1:2505423-2505555(-)	71.58	1	0.91	1	**-6.30**
scaffold_7:1533852-1534336(+)	89.66	1	1.14	1	**-6.30**
scaffold_3:1419383-1419523(-)	53.37	1	0.68	1	**-6.29**
scaffold_7:735959-736321(-)	53.12	1	0.68	0.50	**-6.29**
scaffold_11:257376-257712(-)	107	1	1.37	0.67	**-6.29**
scaffold_6:833419-833550(-)	55.22	1	0.71	1	**-6.28**
scaffold_2:3809503-3809874(-)	122.96	1	1.59	0.71	**-6.27**
scaffold_13:564669-565282(-)	61.6	1	0.8	0.50	**-6.27**
scaffold_4:2104350-2105816(+)	70.03	0.5	0.91	0.57	**-6.27**
scaffold_7:1944511-1945407(+)	69.96	1	0.91	1	**-6.26**
scaffold_3:4117118-4117354(+)	52.13	1	0.68	1	**-6.26**
scaffold_7:711990-712077(+)	104.63	1	1.37	1	**-6.25**
scaffold_5:2809722-2809862(+)	51.63	1	0.68	1	**-6.25**
scaffold_1:2142884-2143667(-)	138.84	1	1.83	1	**-6.25**
scaffold_5:1311393-1311576(+)	51.21	1	0.68	1	**-6.23**
scaffold_2:3262123-3263988(+)	275.47	1	3.67	1	**-6.23**
scaffold_3:414428-415607(+)	85.55	1	1.14	1	**-6.23**
scaffold_11:688678-689099(+)	383.34	1	5.12	0.91	**-6.23**
scaffold_5:437258-437668(+)	67.84	1	0.91	1	**-6.22**
scaffold_11:414364-414696(+)	59.61	1	0.8	1	**-6.22**
scaffold_2:1756491-1757010(-)	102.01	1	1.37	1	**-6.22**
scaffold_3:2529428-2529670(-)	168.85	1	2.28	1	**-6.21**
scaffold_7:1408230-1409229(-)	134.68	1	1.82	1	**-6.21**
scaffold_1:5560939-5562399(+)	67.34	1	0.91	1	**-6.21**
scaffold_8:389458-390181(+)	142.04	1	1.92	0.8	**-6.21**
scaffold_11:643299-643653(+)	83.55	1	1.14	1	**-6.20**
scaffold_10:260349-260793(-)	116.06	0.99	1.59	0.71	**-6.19**
scaffold_1:3940629-3940931(+)	66.34	1	0.91	1	**-6.19**
scaffold_8:278945-279467(+)	66.34	1	0.91	1	**-6.19**
scaffold_1:2883052-2884914(-)	163.68	0.99	2.25	0.91	**-6.18**
scaffold_6:763703-764469(+)	407.96	1	5.62	0.97	**-6.18**
scaffold_3:869087-869788(-)	314	1	4.33	1	**-6.18**
scaffold_7:2201014-2201227(-)	82.3	1	1.14	1	**-6.17**
scaffold_1:4254780-4255885(+)	65.39	0.99	0.91	1	**-6.17**

Locus	WT abundance	WT strand bias	*r3b2*⁻ abundance	*r3b2*⁻ strand bias	*r3b2*⁻ $\log_2$ fold change vs WT
scaffold_10:241612-241648(+)	384.34	1	5.35	1	**-6.17**
scaffold_5:2858301-2858848(+)	68.09	0.98	0.95	1	**-6.16**
scaffold_10:1074153-1074725(-)	264.21	1	3.76	1	**-6.13**
scaffold_7:1416581-1416786(-)	238.43	1	3.42	1	**-6.12**
scaffold_3:2231118-2233271(-)	225	0.99	3.23	1	**-6.12**
scaffold_2:1122878-1123126(-)	362.76	1	5.24	1	**-6.11**
scaffold_10:464606-464747(+)	62.85	1	0.91	1	**-6.11**
scaffold_3:4632773-4632868(-)	243.55	1	3.53	1	**-6.11**
scaffold_3:1415580-1416074(-)	62.73	1	0.91	1	**-6.11**
scaffold_10:979212-979720(-)	109.49	1	1.59	1	**-6.11**
scaffold_2:399223-399400(-)	507.42	1	7.4	1	**-6.10**
scaffold_2:2892168-2892293(-)	93.28	1	1.37	1	**-6.09**
scaffold_2:4302009-4302608(+)	185.62	1	2.73	1	**-6.09**
scaffold_1:5200397-5203203(+)	437.96	1	6.45	1	**-6.09**
scaffold_1:4913207-4914340(-)	123.04	1	1.82	1	**-6.08**
scaffold_1:3024226-3025229(-)	107.12	0.99	1.59	0.71	**-6.07**
scaffold_1:1779254-1779831(+)	153.01	1	2.28	0.8	**-6.07**
scaffold_10:639013-639622(+)	76.37	1	1.14	1	**-6.07**
scaffold_2:3562430-3564472(+)	155.51	0.97	2.33	0.58	**-6.06**
scaffold_1:5748823-5748960(-)	379.68	0.99	5.69	0.48	**-6.06**
scaffold_2:534825-535300(+)	110.75	0.85	1.66	-0.78	**-6.06**
scaffold_6:475586-475824(+)	60.61	1	0.91	1	**-6.06**
scaffold_3:4117638-4117778(+)	60.36	1	0.91	1	**-6.05**
scaffold_12:554093-555028(+)	105.13	1	1.59	1	**-6.05**
scaffold_7:1758409-1758893(+)	239.26	1	3.64	1	**-6.04**
scaffold_4:1674065-1674101(+)	336.45	1	5.12	1	**-6.04**
scaffold_1:1362112-1362993(-)	79.47	1	1.21	1	**-6.04**
scaffold_2:2144219-2144331(-)	237.19	1	3.64	1	**-6.03**
scaffold_1:4829391-4829862(+)	59.23	1	0.91	1	**-6.02**
scaffold_2:3973228-3973298(-)	58.86	1	0.91	1	**-6.02**
scaffold_1:2102947-2103239(-)	58.86	1	0.91	1	**-6.02**
scaffold_5:3051459-3052942(-)	131.94	1	2.05	1	**-6.01**
scaffold_10:337220-337351(+)	73.33	1	1.14	1	**-6.01**
scaffold_10:8772-9198(-)	88.04	1	1.37	1	**-6.01**
scaffold_3:3519451-3520227(+)	218.23	1	3.42	1	**-6.00**
scaffold_6:1868288-1868350(-)	101.13	1	1.59	1	**-5.99**
scaffold_3:2616087-2616539(+)	71.83	1	1.14	1	**-5.98**
scaffold_7:148386-148586(+)	158.12	1	2.51	1	**-5.98**
scaffold_4:1222832-1223099(+)	171.59	1	2.73	1	**-5.97**
scaffold_7:2149637-2150005(-)	468.93	0.96	7.48	0.97	**-5.97**
scaffold_2:623114-624681(-)	120.96	0.86	1.94	0.56	**-5.96**
scaffold_4:1235361-1235439(-)	141.91	1	2.28	1	**-5.96**
scaffold_2:3932152-3932336(-)	70.83	1	1.14	1	**-5.96**
scaffold_3:2882112-2882763(+)	190.24	1	3.07	0.87	**-5.95**
scaffold_4:3972605-3973147(+)	84.8	1	1.37	1	**-5.95**
scaffold_4:2008612-2008775(-)	70.33	1	1.14	1	**-5.95**
scaffold_2:3162275-3163368(-)	321.98	1	5.24	1	**-5.94**
scaffold_8:1235992-1237153(+)	55.91	0.98	0.91	1	**-5.94**
scaffold_1:2383382-2384348(+)	167.35	0.99	2.73	1	**-5.94**
scaffold_8:1850055-1853770(+)	460.82	0.99	7.55	1	**-5.93**
scaffold_7:644729-645944(+)	180.57	1	2.96	1	**-5.93**
scaffold_12:179691-180532(-)	215.11	1	3.53	1	**-5.93**
scaffold_1:4647395-4647753(+)	749.03	1	12.3	1	**-5.93**
scaffold_5:1978007-1978267(-)	57.05	1	0.94	1	**-5.92**
scaffold_3:3022112-3022683(+)	52.63	0.99	0.87	0.9	**-5.92**
scaffold_8:356330-357007(+)	68.96	1	1.14	1	**-5.92**
scaffold_5:410067-410504(+)	96.02	1	1.59	1	**-5.92**
scaffold_2:4259822-4260259(-)	151.39	1	2.51	1	**-5.91**
scaffold_3:3320717-3321708(-)	122.71	0.99	2.05	1	**-5.90**
scaffold_3:1130894-1131080(+)	95.02	1	1.59	1	**-5.90**
scaffold_9:856718-856883(-)	68.09	1	1.14	1	**-5.90**
scaffold_2:859088-859708(-)	285.32	1	4.78	0.90	**-5.90**
scaffold_13:462663-463556(-)	244.17	1	4.1	0.89	**-5.90**
scaffold_10:1074786-1075156(-)	203.52	1	3.42	1	**-5.90**
scaffold_1:1919751-1919919(-)	54.12	1	0.91	1	**-5.89**
scaffold_1:4823894-4824165(-)	54.12	1	0.91	1	**-5.89**
scaffold_9:801474-801796(-)	267.7	1	4.52	1	**-5.89**
scaffold_7:896012-897307(+)	121.31	1	2.05	1	**-5.89**
scaffold_3:4122213-4125134(+)	309.44	1	5.24	1	**-5.88**
scaffold_1:3137973-3139074(-)	53.62	1	0.91	1	**-5.88**
scaffold_8:22792-23352(+)	53.52	1	0.91	1	**-5.88**
scaffold_6:2065364-2067876(-)	188.58	0.99	3.23	1	**-5.87**
scaffold_2:4003522-4003770(+)	53	1	0.91	1	**-5.86**
scaffold_11:76156-77069(+)	92.53	0.91	1.59	1	**-5.86**
scaffold_2:2153525-2156071(+)	1064.32	1	18.3	1	**-5.86**
scaffold_3:4670515-4670911(-)	92.03	0.99	1.59	1	**-5.86**
scaffold_1:4885131-4886443(-)	118.59	1	2.05	1	**-5.85**
scaffold_4:2534266-2534337(+)	131.44	1	2.28	1	**-5.85**
scaffold_1:4132718-4133396(+)	156.88	1	2.73	1	**-5.84**
scaffold_13:446471-446902(-)	117.6	1	2.05	1	**-5.84**
scaffold_6:2870011-2870260(-)	212.99	1	3.72	1	**-5.84**
scaffold_1:4033967-4034606(-)	130.07	1	2.28	1	**-5.83**
scaffold_14:36463-36761(-)	3096.89	-0.98	54.32	-0.78	**-5.83**
scaffold_5:1207765-1208982(-)	51.88	1	0.91	1	**-5.83**
scaffold_6:605967-606475(-)	90.53	1	1.59	1	**-5.83**
scaffold_4:983106-985686(+)	97.29	-0.56	1.71	-0.25	**-5.83**
scaffold_1:5284550-5285097(+)	77.57	1	1.37	1	**-5.82**
scaffold_10:637481-638090(+)	102.63	1	1.82	1	**-5.82**
scaffold_11:534282-536030(-)	75.23	0.99	1.34	1	**-5.81**
scaffold_3:868466-869020(-)	166.11	1	2.96	1	**-5.81**
scaffold_2:2121841-2122220(+)	50.88	1	0.91	-0.33	**-5.81**
scaffold_1:1540203-1541290(+)	50.88	1	0.91	1	**-5.81**
scaffold_4:2389823-2390067(+)	387.52	1	6.94	0.99	**-5.80**
scaffold_1:3360756-3362486(+)	59.67	0.96	1.07	0.89	**-5.80**
scaffold_12:421944-422215(-)	76.32	0.99	1.37	0.67	**-5.80**
scaffold_7:344784-345415(-)	63.35	0.97	1.14	1	**-5.80**
scaffold_3:3585336-3585990(-)	50.56	1	0.91	0.50	**-5.80**

Locus	WT abundance	WT strand bias	*r3b2*⁻ abundance	*r3b2*⁻ strand bias	*r3b2*⁻ $\log_2$ fold change vs WT
scaffold_6:1359714-1360139(-)	63.27	1	1.14	1	**-5.79**
scaffold_4:2181662-2181994(+)	100.64	1	1.82	1	**-5.79**
scaffold_11:754905-755959(+)	62.6	1	1.14	1	**-5.78**
scaffold_8:1301699-1302454(-)	561.83	1	10.25	1	**-5.78**
scaffold_6:177828-177954(+)	106	-0.99	1.94	0.33	**-5.77**
scaffold_3:4413703-4414550(+)	62.01	0.99	1.14	1	**-5.77**
scaffold_13:730432-730797(+)	173.09	1	3.19	1	**-5.76**
scaffold_7:1394594-1395037(-)	90.53	1	1.67	0.75	**-5.76**
scaffold_7:1511126-1511899(+)	55.12	1	1.02	1	**-5.76**
scaffold_5:2584445-2584874(-)	73.82	1	1.37	1	**-5.75**
scaffold_6:2154405-2155591(+)	98.02	1	1.82	1	**-5.75**
scaffold_3:1159352-1159403(+)	61.35	0.99	1.14	1	**-5.75**
scaffold_1:1325958-1326394(+)	73.58	1	1.37	1	**-5.75**
scaffold_1:2975621-2976676(-)	526	1	9.91	1	**-5.73**
scaffold_4:3773598-3774483(+)	61.48	1	1.16	1	**-5.73**
scaffold_1:3435138-3435555(+)	60.31	1	1.14	1	**-5.73**
scaffold_13:136354-137239(+)	65.03	1	1.23	1	**-5.72**
scaffold_4:4162548-4163336(+)	65.99	0.98	1.25	1	**-5.72**
scaffold_13:120191-121221(-)	180.32	-0.98	3.42	-0.33	**-5.72**
scaffold_5:126745-127250(-)	138.05	1	2.62	1	**-5.72**
scaffold_3:948885-949462(-)	119.72	1	2.28	1	**-5.71**
scaffold_6:1148652-1148779(+)	59.86	1	1.14	1	**-5.71**
scaffold_4:2305042-2305725(-)	131.69	0.99	2.51	1	**-5.71**
scaffold_8:478384-478942(+)	119.51	1	2.28	1	**-5.71**
scaffold_3:3463016-3463204(+)	59.61	0.99	1.14	0.6	**-5.71**
scaffold_1:4368819-4369226(+)	59.48	1	1.14	1	**-5.71**
scaffold_9:424451-424559(-)	141.41	1	2.73	1	**-5.69**
scaffold_4:4088671-4089897(+)	165.19	1	3.19	1	**-5.69**
scaffold_3:2752800-2752936(+)	82.3	1	1.59	1	**-5.69**
scaffold_9:936397-937529(+)	400.42	1	7.74	1	**-5.69**
scaffold_2:786599-787306(+)	564.78	0.99	10.93	1	**-5.69**
scaffold_1:1698364-1698715(-)	58.61	1	1.14	1	**-5.68**
scaffold_6:2104282-2105951(-)	790.39	1	15.39	1	**-5.68**
scaffold_4:3569632-3570143(-)	93.45	1	1.82	1	**-5.68**
scaffold_3:3075208-3075708(-)	133.56	1	2.62	0.83	**-5.67**
scaffold_2:1123195-1123385(-)	161.99	1	3.19	1	**-5.67**
scaffold_3:1435889-1437913(-)	69.46	1	1.37	1	**-5.66**
scaffold_3:2559881-2560141(-)	68.84	0.99	1.37	1	**-5.65**
scaffold_2:469181-469276(-)	114.48	1	2.28	1	**-5.65**
scaffold_2:21533-23408(+)	468.14	1	9.34	1	**-5.65**
scaffold_2:4962853-4963880(-)	187.8	1	3.76	1	**-5.64**
scaffold_4:4142712-4143451(-)	50.88	1	1.02	1	**-5.64**
scaffold_6:1869154-1869393(+)	85.28	1	1.71	1	**-5.64**
scaffold_1:2876530-2877079(+)	135.93	1	2.73	0.83	**-5.64**
scaffold_6:2643643-2644017(+)	192.4	0.99	3.87	1	**-5.64**
scaffold_2:3044599-3047217(-)	113.98	1	2.31	1	**-5.62**
scaffold_1:4224677-4224718(+)	56.12	1	1.14	1	**-5.62**
scaffold_4:1181214-1181964(-)	100.85	0.94	2.05	1	**-5.62**
scaffold_3:223382-223677(+)	67.34	1	1.37	1	**-5.62**
scaffold_11:604159-604899(+)	88.54	1	1.82	1	**-5.60**
scaffold_4:3684022-3684981(-)	165.23	1	3.42	1	**-5.59**
scaffold_11:902332-902555(-)	121.21	-0.99	2.51	-0.45	**-5.59**
scaffold_2:4827793-4829940(+)	98.91	1	2.05	1	**-5.59**
scaffold_7:1538471-1538993(-)	246.66	0.98	5.12	0.91	**-5.59**
scaffold_6:1475930-1476175(+)	95.34	1	1.98	1	**-5.59**
scaffold_2:3868791-3868871(+)	372.12	1	7.74	0.94	**-5.59**
scaffold_3:2064022-2064394(-)	98.52	1	2.05	1	**-5.59**
scaffold_5:1161527-1163402(+)	109.49	0.97	2.28	1	**-5.59**
scaffold_10:510191-510899(+)	163.91	1	3.42	0.88	**-5.58**
scaffold_1:162560-163275(+)	76.05	1	1.59	1	**-5.58**
scaffold_9:1466049-1466356(-)	724.03	-0.99	15.15	-0.7	**-5.58**
scaffold_1:1725986-1726145(-)	271.44	1	5.69	1	**-5.58**
scaffold_1:4011622-4012723(+)	119.47	1	2.51	1	**-5.57**
scaffold_1:3874707-3876342(-)	95.56	1	2.01	1	**-5.57**
scaffold_7:1075861-1076961(+)	66.75	1	1.41	1	**-5.57**
scaffold_1:4687528-4688737(-)	387.95	1	8.2	1	**-5.56**
scaffold_3:1940826-1941423(-)	89.7	0.99	1.9	1	**-5.56**
scaffold_6:366503-366765(+)	85.8	1	1.82	1	**-5.56**
scaffold_10:1223846-1224472(+)	343.41	1	7.29	1	**-5.56**
scaffold_2:3556055-3556711(-)	53.44	0.97	1.14	1	**-5.55**
scaffold_15:7560-7922(-)	53.37	1	1.14	1	**-5.55**
scaffold_4:1747102-1747278(-)	64.1	1	1.37	1	**-5.55**
scaffold_6:70959-72680(-)	64.1	1	1.37	0.33	**-5.55**
scaffold_1:5952833-5953237(-)	95.77	1	2.05	1	**-5.55**
scaffold_11:12890-13011(-)	63.85	1	1.37	0.67	**-5.54**
scaffold_1:1756191-1756731(+)	180.32	0.99	3.87	1	**-5.54**
scaffold_4:1137440-1137915(+)	199.28	1	4.33	1	**-5.52**
scaffold_1:1280974-1281648(-)	62.85	1	1.37	1	**-5.52**
scaffold_10:396842-398112(+)	1017.21	1	22.21	1	**-5.52**
scaffold_10:739928-741494(-)	83.33	0.91	1.82	0.75	**-5.52**
scaffold_5:706062-706482(+)	83.3	1	1.82	1	**-5.52**
scaffold_11:75519-76097(+)	93.78	1	2.05	1	**-5.52**
scaffold_6:2597012-2597659(+)	93.78	0.99	2.05	1	**-5.52**
scaffold_8:1452151-1453354(-)	302.28	1	6.61	1	**-5.52**
scaffold_1:2548854-2549386(-)	52.13	1	1.14	1	**-5.52**
scaffold_8:1754974-1755905(+)	197.28	1	4.33	0.95	**-5.51**
scaffold_1:2015867-2016017(-)	103.75	1	2.28	1	**-5.51**
scaffold_6:1929117-1930362(-)	98.14	0.98	2.16	0.80	**-5.51**
scaffold_3:1264629-1266775(-)	92.58	0.99	2.05	0.60	**-5.50**
scaffold_7:2169683-2171031(-)	51.38	1	1.14	1	**-5.49**
scaffold_1:1590885-1592405(+)	220.73	1	4.9	0.91	**-5.49**
scaffold_7:1379681-1381386(-)	112.86	1	2.51	1	**-5.49**
scaffold_2:3976958-3977505(+)	460.41	1	10.25	1	**-5.49**
scaffold_4:270629-272112(-)	147.9	1	3.3	0.87	**-5.49**
scaffold_3:1624239-1624658(+)	111.98	1	2.51	1	**-5.48**
scaffold_1:4105832-4106415(+)	70.65	0.89	1.59	1	**-5.47**
scaffold_4:1965139-1967466(+)	293.55	1	6.61	0.79	**-5.47**

Locus	WT abundance	WT strand bias	*r3b2*⁻ abundance	*r3b2*⁻ strand bias	*r3b2*⁻ $\log_2$ fold change vs WT
scaffold_10:345326-346550(-)	55.47	1	1.25	1	**-5.47**
scaffold_4:110511-111201(+)	111.3	1	2.51	1	**-5.47**
scaffold_4:1660738-1661328(-)	312.17	0.99	7.05	1	**-5.47**
scaffold_1:5227260-5227835(-)	84.09	1	1.9	1	**-5.47**
scaffold_6:117553-120449(-)	85.69	-0.62	1.94	-0.19	**-5.46**
scaffold_1:2415013-2415157(+)	100.39	1	2.28	1	**-5.46**
scaffold_4:1057243-1057437(+)	89.79	1	2.05	1	**-5.45**
scaffold_4:3039875-3040903(+)	89.58	0.98	2.05	1	**-5.45**
scaffold_2:2429920-2433673(+)	347.8	1	7.97	1	**-5.45**
scaffold_1:2826286-2827106(+)	148.9	1	3.42	0.88	**-5.44**
scaffold_13:215342-216132(-)	59.03	0.99	1.37	0.67	**-5.43**
scaffold_6:1420710-1421741(-)	186.43	1	4.33	0.89	**-5.43**
scaffold_1:1210559-1211219(-)	58.61	1	1.37	1	**-5.42**
scaffold_7:1323702-1324598(-)	77.81	1	1.82	1	**-5.42**
scaffold_1:2027355-2027776(+)	58.4	1	1.37	1	**-5.41**
scaffold_6:2110855-2111066(+)	514.44	1	12.07	1	**-5.41**
scaffold_7:1556113-1556219(-)	125.95	1	2.96	0.92	**-5.41**
scaffold_10:830006-830844(-)	58.19	0.83	1.37	0.67	**-5.41**
scaffold_13:71517-72199(-)	161.81	0.89	3.81	0.52	**-5.41**
scaffold_9:1097516-1099557(+)	1407.65	1	33.22	0.96	**-5.41**
scaffold_2:493217-493942(-)	134.93	1	3.19	0.14	**-5.40**
scaffold_10:1075211-1076116(-)	192.67	1	4.56	1	**-5.40**
scaffold_1:2437785-2438299(+)	57.87	1	1.37	1	**-5.40**
scaffold_7:339718-340215(+)	57.86	1	1.37	1	**-5.40**
scaffold_1:5729563-5730269(-)	197.16	1	4.69	1	**-5.39**
scaffold_9:572250-572536(-)	66.59	1	1.59	1	**-5.39**
scaffold_1:1966918-1969467(-)	113.98	0.99	2.73	1	**-5.38**
scaffold_1:5222327-5223671(+)	56.99	0.97	1.37	1	**-5.38**
scaffold_1:5423519-5426132(-)	56.86	1	1.37	1	**-5.38**
scaffold_3:4254887-4255640(+)	56.86	0.99	1.37	1	**-5.38**
scaffold_4:771558-772868(+)	141.54	0.97	3.42	0.67	**-5.37**
scaffold_5:3135906-3137233(-)	199.03	1	4.81	0.90	**-5.37**
scaffold_1:4751022-4751379(+)	61.23	0.71	1.48	0.86	**-5.37**
scaffold_1:2936779-2938025(-)	273.35	1	6.61	0.93	**-5.37**
scaffold_8:1498238-1498546(+)	402.09	1	9.73	0.99	**-5.37**
scaffold_3:3545730-3546675(+)	56.47	1	1.37	1	**-5.37**
scaffold_3:136174-136288(-)	65.1	1	1.59	1	**-5.36**
scaffold_4:1011913-1012512(-)	65.05	1	1.59	1	**-5.35**
scaffold_7:2158415-2159329(-)	64.85	1	1.59	1	**-5.35**
scaffold_1:1450389-1450691(-)	55.87	1	1.37	1	**-5.35**
scaffold_3:433252-433732(-)	727.4	1	17.99	1	**-5.34**
scaffold_7:2167568-2168046(+)	82.68	1	2.05	1	**-5.33**
scaffold_9:668917-669731(-)	64.1	1	1.59	1	**-5.33**
scaffold_6:1817250-1817945(-)	109.57	1	2.73	1	**-5.33**
scaffold_7:1016001-1017115(-)	137.1	0.98	3.42	0.88	**-5.33**
scaffold_13:627618-627998(-)	200.77	1	5.01	1	**-5.32**
scaffold_12:718390-719111(-)	54.87	0.98	1.37	1	**-5.32**
scaffold_2:2645363-2648956(-)	396.68	1	9.91	1	**-5.32**
scaffold_3:2644858-2645311(-)	82.05	1	2.05	1	**-5.32**
scaffold_5:2023116-2023202(-)	85.92	1	2.16	1	**-5.31**
scaffold_9:1080002-1082299(-)	134.93	0.98	3.42	0.85	**-5.30**
scaffold_6:1802393-1802528(-)	150.93	1	3.83	1	**-5.30**
scaffold_9:1104031-1104899(+)	71.7	1	1.82	1	**-5.30**
scaffold_9:353024-353483(+)	71.58	1	1.82	1	**-5.30**
scaffold_7:2122197-2124124(+)	89.63	0.95	2.28	1	**-5.30**
scaffold_3:3803083-3805016(-)	67.06	1	1.71	0.50	**-5.29**
scaffold_12:909462-910266(+)	151.02	1	3.87	0.75	**-5.29**
scaffold_9:850125-851243(-)	53.38	1	1.37	1	**-5.28**
scaffold_8:1828040-1828341(+)	53.37	1	1.37	1	**-5.28**
scaffold_1:5869786-5870487(+)	70.83	0.99	1.82	1	**-5.28**
scaffold_1:3505405-3505981(+)	53.3	1	1.37	1	**-5.28**
scaffold_3:4670966-4671388(-)	150.39	1	3.87	0.88	**-5.28**
scaffold_1:3993900-3994141(-)	123.96	1	3.19	1	**-5.28**
scaffold_2:1214475-1214886(-)	70.71	0.99	1.82	1	**-5.28**
scaffold_1:1072749-1073120(+)	61.6	1	1.59	0.71	**-5.28**
scaffold_3:3725262-3726320(+)	211.75	1	5.47	0.92	**-5.27**
scaffold_3:862581-863654(-)	211.75	1	5.47	1	**-5.27**
scaffold_7:368149-369232(+)	63.37	0.86	1.64	1	**-5.27**
scaffold_3:3808160-3808595(-)	95.32	0.98	2.47	1	**-5.27**
scaffold_1:2216030-2218176(+)	93.72	0.95	2.43	0.86	**-5.27**
scaffold_4:1775757-1777563(-)	79.03	0.98	2.05	1	**-5.27**
scaffold_8:1255830-1257459(+)	109.74	1	2.85	1	**-5.27**
scaffold_1:2538606-2538884(-)	69.96	1	1.82	0.75	**-5.26**
scaffold_8:1349618-1351573(-)	107.8	1	2.81	1	**-5.26**
scaffold_10:1258449-1258667(+)	52.5	1	1.37	1	**-5.26**
scaffold_3:675400-675839(+)	78.36	1	2.05	1	**-5.26**
scaffold_1:749961-750198(+)	60.73	1	1.59	1	**-5.26**
scaffold_2:112376-113383(+)	60.61	1	1.59	0.71	**-5.25**
scaffold_2:984561-985454(-)	64.85	0.99	1.71	0.75	**-5.25**
scaffold_1:5594455-5595622(-)	99.26	1	2.62	1	**-5.24**
scaffold_6:2412133-2413021(+)	862.7	1	22.78	1	**-5.24**
scaffold_5:807706-807955(+)	51.88	1	1.37	1	**-5.24**
scaffold_11:911162-911463(-)	68.84	0.99	1.82	1	**-5.24**
scaffold_2:440765-440855(+)	60.11	1	1.59	1	**-5.24**
scaffold_4:2784603-2787764(+)	232.3	0.98	6.17	0.93	**-5.23**
scaffold_1:3591169-3591680(+)	64.22	1	1.71	1	**-5.23**
scaffold_10:193720-194832(+)	76.82	1	2.05	1	**-5.23**
scaffold_4:2792271-2793136(-)	94.03	1	2.51	1	**-5.23**
scaffold_5:73419-73995(-)	59.24	0.96	1.59	0.88	**-5.22**
scaffold_12:531502-532080(-)	143.85	1	3.87	1	**-5.22**
scaffold_3:2189599-2190325(-)	118.22	1	3.19	1	**-5.21**
scaffold_2:4991191-4991477(-)	58.86	1	1.59	1	**-5.21**
scaffold_5:2626372-2627244(-)	218.98	1	5.92	1	**-5.21**
scaffold_8:866523-866959(+)	179.07	1	4.89	1	**-5.19**
scaffold_7:671716-672527(-)	58.11	0.98	1.59	1	**-5.19**
scaffold_3:658259-658626(+)	66.34	1	1.82	1	**-5.19**
scaffold_5:1416124-1416928(+)	119.72	1	3.3	1	**-5.18**

Locus	WT abundance	WT strand bias	*r3b2*⁻ abundance	*r3b2*⁻ strand bias	*r3b2*⁻ $\log_2$ fold change vs WT
scaffold_4:2414137-2415705(-)	131.94	1	3.64	1	**-5.18**
scaffold_6:1084491-1085381(-)	65.97	1	1.82	1	**-5.18**
scaffold_8:161823-162315(+)	123.96	1	3.42	1	**-5.18**
scaffold_5:728348-729718(-)	57.36	0.98	1.59	1	**-5.17**
scaffold_1:1384778-1385476(-)	89.91	1	2.51	1	**-5.16**
scaffold_3:2863938-2866154(+)	312.88	1	8.77	1	**-5.16**
scaffold_12:825614-826150(+)	73.08	1	2.05	1	**-5.16**
scaffold_5:3202511-3203296(-)	81.06	1	2.28	1	**-5.15**
scaffold_1:127965-129926(-)	113.4	1	3.19	1	**-5.15**
scaffold_3:1568634-1569944(-)	72.83	1	2.05	1	**-5.15**
scaffold_1:3481250-3482894(-)	113.23	1	3.19	1	**-5.15**
scaffold_4:1573951-1574085(-)	96.77	1	2.73	1	**-5.15**
scaffold_7:70972-71808(+)	250.16	1	7.06	1	**-5.15**
scaffold_2:4536819-4537115(-)	128.69	1	3.64	1	**-5.14**
scaffold_6:2858471-2859364(-)	72.33	1	2.05	0.66	**-5.14**
scaffold_2:2765943-2767899(+)	88.54	1	2.51	1	**-5.14**
scaffold_4:1252257-1253194(-)	168.35	1	4.78	0.90	**-5.14**
scaffold_2:1293714-1294803(-)	96.12	0.85	2.73	1	**-5.14**
scaffold_1:712302-715279(+)	432.94	1	12.3	0.93	**-5.14**
scaffold_1:5921333-5923451(+)	240.3	1	6.83	1	**-5.14**
scaffold_10:680290-682206(+)	53.29	0.98	1.52	0.5	**-5.13**
scaffold_2:2094910-2094975(-)	76.93	1	2.2	1	**-5.13**
scaffold_11:119042-119988(-)	190.92	0.99	5.47	1	**-5.13**
scaffold_10:816041-816996(-)	71.08	0.93	2.05	1	**-5.12**
scaffold_10:84671-85342(+)	63.1	1	1.82	1	**-5.12**
scaffold_5:466020-468296(+)	185.18	0.99	5.35	0.92	**-5.11**
scaffold_1:1225644-1226735(+)	54.99	1	1.59	1	**-5.11**
scaffold_3:3094944-3095258(+)	59.11	1	1.71	1	**-5.11**
scaffold_4:2465005-2465363(-)	90.53	1	2.62	1	**-5.11**
scaffold_2:864367-865482(+)	90.82	0.99	2.63	1	**-5.11**
scaffold_12:369713-370797(+)	393.07	1	11.39	1	**-5.11**
scaffold_1:289354-290080(+)	78.56	1	2.28	1	**-5.11**
scaffold_13:346828-347026(+)	62.6	1	1.82	1	**-5.10**
scaffold_8:1307965-1312081(+)	78.05	0.87	2.28	0.6	**-5.10**
scaffold_4:1369296-1371086(-)	54.18	0.93	1.59	1	**-5.09**
scaffold_1:5178504-5179536(-)	69.71	0.78	2.05	1	**-5.09**
scaffold_3:2431322-2432125(-)	143.16	1	4.21	0.89	**-5.09**
scaffold_8:1824005-1825093(+)	73.28	1	2.16	1	**-5.08**
scaffold_11:719018-719200(+)	100.39	1	2.96	1	**-5.08**
scaffold_6:1151715-1153553(+)	99.76	1	2.96	1	**-5.07**
scaffold_5:2059541-2061161(+)	84.55	1	2.51	1	**-5.07**
scaffold_3:3485975-3486359(+)	115.14	1	3.42	1	**-5.07**
scaffold_6:1815915-1817186(-)	126.28	1	3.76	0.88	**-5.07**
scaffold_1:1755695-1756129(+)	129.94	1	3.87	1	**-5.07**
scaffold_3:669048-669580(+)	60.81	1	1.82	1	**-5.06**
scaffold_1:1449811-1450328(-)	53.12	1	1.59	1	**-5.06**
scaffold_4:1699681-1701208(+)	98.89	1	2.96	1	**-5.06**
scaffold_1:4576022-4576423(-)	53.65	1	1.61	1	**-5.06**
scaffold_1:5608076-5610572(-)	52.92	1	1.59	0.43	**-5.06**
scaffold_1:3960432-3960664(-)	90.78	1	2.73	1	**-5.06**
scaffold_4:1405688-1406055(-)	56.86	1	1.71	1	**-5.06**
scaffold_5:75642-75789(-)	78.94	1	2.39	1	**-5.05**
scaffold_2:3239692-3240969(+)	60.11	0.99	1.82	1	**-5.05**
scaffold_1:787802-789520(-)	330.19	1	10.01	0.96	**-5.04**
scaffold_2:4479725-4480705(+)	187.3	1	5.69	1	**-5.04**
scaffold_12:484523-485765(-)	105	1	3.19	1	**-5.04**
scaffold_10:241911-242584(+)	268.94	1	8.2	1	**-5.04**
scaffold_6:2459257-2459742(-)	59.36	1	1.82	1	**-5.03**
scaffold_9:1456202-1457993(-)	403.77	0.99	12.41	0.90	**-5.02**
scaffold_2:114505-114612(+)	155.26	1	4.78	1	**-5.02**
scaffold_1:1725800-1725921(-)	73.82	1	2.28	1	**-5.02**
scaffold_10:396360-396779(+)	250.3	1	7.74	1	**-5.02**
scaffold_3:4299662-4300662(+)	66.09	1	2.05	1	**-5.01**
scaffold_12:420980-421883(-)	95.4	1	2.96	1	**-5.01**
scaffold_6:894972-895055(+)	257.27	1	8	1	**-5.01**
scaffold_2:4092746-4092939(+)	124.45	1	3.87	1	**-5.01**
scaffold_8:352289-352807(+)	58.48	1	1.82	1	**-5.01**
scaffold_13:30759-31570(+)	89.81	0.95	2.8	0.47	**-5.00**
scaffold_2:4712269-4712561(+)	50.87	1	1.59	1	**-5.00**
scaffold_1:4025336-4028228(+)	58.11	0.96	1.82	0.75	**-5.00**
scaffold_10:657243-658632(+)	79.69	1	2.51	1	**-4.99**
scaffold_12:394540-395511(+)	93.91	0.71	2.96	0.87	**-4.99**
scaffold_2:3417472-3419196(+)	89.71	0.69	2.83	0.57	**-4.99**
scaffold_1:3153888-3154534(-)	72.08	1	2.28	1	**-4.98**
scaffold_11:627728-628542(-)	73.53	0.99	2.33	1	**-4.98**
scaffold_7:1173710-1174441(-)	53.87	1	1.71	1	**-4.98**
scaffold_4:2219129-2219407(-)	93.15	1	2.96	1	**-4.98**
scaffold_3:2558471-2559585(-)	116.35	1	3.7	1	**-4.97**
scaffold_12:79028-79903(+)	85.8	0.99	2.73	1	**-4.97**
scaffold_7:25500-25921(-)	57.11	1	1.82	1	**-4.97**
scaffold_8:115903-116365(+)	78.69	1	2.51	1	**-4.97**
scaffold_1:2179010-2179688(+)	85.55	1	2.73	1	**-4.97**
scaffold_3:467623-469766(-)	897.08	1	28.73	1	**-4.96**
scaffold_5:983807-984466(-)	111.98	1	3.59	1	**-4.96**
scaffold_2:1230866-1231293(-)	234.44	1	7.52	1	**-4.96**
scaffold_6:2459794-2461549(-)	85.05	0.99	2.73	1	**-4.96**
scaffold_3:4753679-4754341(-)	106.37	1	3.42	1	**-4.96**
scaffold_1:1838088-1840008(-)	91.41	1	2.96	1	**-4.95**
scaffold_1:2929472-2930390(-)	133.43	1	4.33	1	**-4.95**
scaffold_7:317319-317744(+)	98.27	1	3.19	1	**-4.95**
scaffold_4:2531623-2532565(+)	97.98	1	3.19	1	**-4.94**
scaffold_1:1087437-1088450(-)	66.34	1	2.16	1	**-4.94**
scaffold_7:2134560-2135772(+)	69.96	0.97	2.28	1	**-4.94**
scaffold_2:4385024-4385959(-)	60.75	0.99	1.98	1	**-4.94**
scaffold_12:298363-300291(-)	69.58	1	2.28	1	**-4.93**
scaffold_8:1224703-1226646(+)	96.93	1	3.2	1	**-4.92**
scaffold_4:1525421-1527277(+)	96.52	1	3.19	1	**-4.92**

Locus	WT abundance	WT strand bias	*r3b2*⁻ abundance	*r3b2*⁻ strand bias	*r3b2*⁻ $\log_2$ fold change vs WT
scaffold_3:2223334-2224725(-)	89.35	0.99	2.96	0.85	**-4.92**
scaffold_3:1122144-1122577(-)	152.41	1	5.05	1	**-4.92**
scaffold_4:1803454-1805685(+)	79.07	0.99	2.62	1	**-4.92**
scaffold_4:2286821-2288042(-)	364.28	0.99	12.08	1	**-4.91**
scaffold_4:1627203-1627372(-)	54.87	1	1.82	1	**-4.91**
scaffold_7:1884405-1885363(-)	123.52	1	4.1	1	**-4.91**
scaffold_2:3603797-3604033(+)	61.35	1	2.05	1	**-4.90**
scaffold_3:135831-135979(-)	75.07	1	2.51	1	**-4.90**
scaffold_8:1546091-1546647(+)	190.8	-0.46	6.38	0.21	**-4.90**
scaffold_3:2555530-2558409(-)	193.79	0.99	6.49	0.93	**-4.90**
scaffold_11:348354-348548(+)	93.15	1	3.14	1	**-4.89**
scaffold_8:1879758-1880878(-)	162.11	1	5.47	1	**-4.89**
scaffold_6:2021794-2022498(-)	67.34	1	2.28	1	**-4.88**
scaffold_6:2849379-2849519(+)	294.09	1	9.98	1	**-4.88**
scaffold_6:1683288-1684699(+)	63.6	1	2.16	0.8	**-4.88**
scaffold_12:278043-278980(+)	250.2	1	8.54	0.95	**-4.87**
scaffold_5:461882-462748(+)	120.09	0.98	4.1	0.89	**-4.87**
scaffold_9:1499460-1501045(+)	53.16	0.98	1.82	0.75	**-4.87**
scaffold_1:5617517-5618158(-)	66.47	0.95	2.28	1	**-4.87**
scaffold_4:60738-61170(+)	86.05	1	2.96	1	**-4.86**
scaffold_4:4165285-4165710(+)	52.87	1	1.82	1	**-4.86**
scaffold_1:4369294-4369919(+)	75.4	1	2.62	1	**-4.85**
scaffold_11:168181-170186(+)	104	0.97	3.64	1	**-4.84**
scaffold_8:797754-798155(+)	64.97	1	2.28	1	**-4.83**
scaffold_6:2684967-2686079(-)	58.36	-0.81	2.05	-0.33	**-4.83**
scaffold_1:5298244-5299125(+)	119.47	1	4.21	1	**-4.83**
scaffold_2:213900-214483(+)	80.81	1	2.85	1	**-4.83**
scaffold_3:3419861-3419978(+)	64.6	1	2.28	1	**-4.82**
scaffold_1:1589331-1590463(+)	122.86	1	4.34	1	**-4.82**
scaffold_5:1434587-1434895(+)	410.69	1	14.52	0.99	**-4.82**
scaffold_11:816332-818486(+)	71.48	0.99	2.53	0.83	**-4.82**
scaffold_4:473692-474056(+)	64.22	1	2.28	1	**-4.82**
scaffold_5:2791759-2792121(+)	337.36	-1	11.98	-0.73	**-4.82**
scaffold_3:2888769-2889680(-)	76.82	0.99	2.73	1	**-4.81**
scaffold_8:448713-448862(+)	70.58	1	2.51	1	**-4.81**
scaffold_1:494399-495133(-)	64.1	1	2.28	1	**-4.81**
scaffold_4:3279020-3279678(+)	108.74	1	3.87	1	**-4.81**
scaffold_3:893194-894998(-)	70.46	1	2.51	0.82	**-4.81**
scaffold_9:645572-647485(+)	169.26	1	6.04	0.93	**-4.81**
scaffold_2:752213-753458(-)	65.64	1	2.35	0.83	**-4.80**
scaffold_2:1774085-1774723(-)	164.98	1	5.92	1	**-4.80**
scaffold_6:2709454-2709847(-)	260.75	1	9.38	0.96	**-4.80**
scaffold_4:61557-62430(+)	125.08	1	4.5	1	**-4.80**
scaffold_4:3699832-3700715(-)	61.26	1	2.22	1	**-4.79**
scaffold_1:1288479-1290818(+)	94.28	0.97	3.42	1	**-4.78**
scaffold_10:883189-884435(+)	127.57	1	4.63	0.92	**-4.78**
scaffold_3:4685241-4685862(+)	360.52	1	13.1	1	**-4.78**
scaffold_1:3358480-3359745(+)	62.73	0.99	2.28	0.6	**-4.78**
scaffold_4:1155451-1155603(-)	56.37	1	2.05	1	**-4.78**
scaffold_8:36133-36441(-)	409.32	1	14.9	0.99	**-4.78**
scaffold_2:4709232-4709733(-)	506.38	1	18.45	1	**-4.78**
scaffold_4:404106-406025(-)	64.77	0.97	2.36	0.93	**-4.78**
scaffold_6:2221355-2224078(+)	76.5	0.92	2.79	0.83	**-4.78**
scaffold_7:388869-389957(+)	168.6	1	6.15	1	**-4.78**
scaffold_5:513884-514272(+)	74.82	1	2.73	1	**-4.78**
scaffold_1:3027839-3029206(+)	71.6	0.94	2.62	0.92	**-4.77**
scaffold_3:434035-434888(-)	515.57	0.99	18.9	1	**-4.77**
scaffold_7:761528-762070(-)	68.46	1	2.51	1	**-4.77**
scaffold_10:619110-619492(-)	93.28	1	3.42	1	**-4.77**
scaffold_7:1437954-1440451(+)	139.2	0.99	5.12	1	**-4.76**
scaffold_2:2608065-2609391(-)	86.21	0.99	3.19	1	**-4.76**
scaffold_3:1639096-1640480(-)	550.45	1	20.38	1	**-4.76**
scaffold_4:3190387-3191628(+)	73.58	-0.31	2.73	1	**-4.75**
scaffold_7:1755384-1756112(+)	351.95	1	13.06	0.89	**-4.75**
scaffold_4:3683796-3684000(-)	58.41	0.99	2.17	1	**-4.75**
scaffold_6:2555672-2556143(+)	61.09	0.99	2.27	0.96	**-4.75**
scaffold_7:320671-320861(+)	64.06	1	2.39	1	**-4.74**
scaffold_1:3394456-3394653(+)	79.06	0.13	2.96	0.21	**-4.74**
scaffold_9:14663-15566(+)	188.55	0.98	7.06	1	**-4.74**
scaffold_1:5145957-5147183(-)	61.62	0.58	2.31	0.69	**-4.74**
scaffold_7:893916-894909(-)	109.36	1	4.1	1	**-4.74**
scaffold_2:855383-856271(+)	85.05	1	3.19	1	**-4.74**
scaffold_3:2509060-2510039(+)	91.06	1	3.42	1	**-4.73**
scaffold_2:3732719-3733573(+)	51.65	1	1.94	1	**-4.73**
scaffold_1:504374-504867(+)	151.61	1	5.7	0.94	**-4.73**
scaffold_1:5033818-5034373(-)	63.35	1	2.39	0.82	**-4.73**
scaffold_13:678651-679453(+)	60.36	1	2.28	1	**-4.73**
scaffold_7:36168-37526(+)	90.53	1	3.42	1	**-4.73**
scaffold_1:2428098-2428419(-)	78.31	0.98	2.96	1	**-4.73**
scaffold_9:148190-148784(+)	143.16	1	5.47	1	**-4.71**
scaffold_2:362696-363280(-)	53.62	1	2.05	1	**-4.71**
scaffold_7:1225911-1227697(-)	81.31	0.99	3.11	1	**-4.71**
scaffold_8:804211-805902(+)	100.89	1	3.87	1	**-4.70**
scaffold_6:2422955-2423089(-)	151.39	1	5.81	1	**-4.70**
scaffold_13:227426-227923(+)	53.37	1	2.05	1	**-4.70**
scaffold_8:1830177-1830730(+)	70.83	0.99	2.73	1	**-4.70**
scaffold_6:2874319-2876414(-)	53.94	0.90	2.08	1	**-4.70**
scaffold_1:4421189-4422342(-)	52.87	1	2.05	1	**-4.69**
scaffold_2:579171-580090(+)	52.75	0.96	2.05	-0.33	**-4.69**
scaffold_5:1784832-1785233(+)	195.41	1	7.63	1	**-4.68**
scaffold_7:2056986-2057874(+)	75.57	1	2.96	1	**-4.67**
scaffold_5:1783703-1784287(+)	371.37	1	14.58	1	**-4.67**
scaffold_3:3770899-3771835(-)	63.85	1	2.51	1	**-4.67**
scaffold_6:296249-296987(+)	57.86	1	2.28	0.8	**-4.67**
scaffold_5:1405734-1408103(-)	55.8	0.98	2.2	1	**-4.66**
scaffold_5:1125937-1126251(-)	306.11	1	12.07	1	**-4.66**
scaffold_8:633189-633824(+)	97.98	1	3.87	1	**-4.66**

Locus	WT abundance	WT strand bias	*r3b2*⁻ abundance	*r3b2*⁻ strand bias	*r3b2*⁻ $\log_2$ fold change vs WT
scaffold_1:2171418-2171565(+)	86.54	1	3.42	1	**-4.66**
scaffold_1:297205-297801(+)	120.46	1	4.78	1	**-4.66**
scaffold_3:1448585-1449991(-)	69	0.98	2.74	1	**-4.65**
scaffold_1:558689-559773(+)	108.99	1	4.33	1	**-4.65**
scaffold_9:1511137-1511760(+)	63.1	1	2.51	1	**-4.65**
scaffold_1:3019892-3021925(-)	94.28	1	3.76	0.88	**-4.65**
scaffold_9:1176305-1176637(+)	98.02	1	3.91	0.7	**-4.65**
scaffold_1:4403622-4410176(-)	179.52	0.74	7.17	0.66	**-4.65**
scaffold_6:2315611-2320720(+)	342.48	0.99	13.69	1	**-4.64**
scaffold_11:882467-882536(-)	82.47	1	3.3	1	**-4.64**
scaffold_8:1927303-1927724(+)	99.17	0.99	3.98	1	**-4.64**
scaffold_12:532140-532733(-)	67.88	1	2.73	1	**-4.64**
scaffold_3:1417307-1418995(-)	396.31	1	15.94	1	**-4.64**
scaffold_3:4688054-4688222(-)	468.64	1	18.9	1	**-4.63**
scaffold_7:2057932-2059147(+)	81.81	1	3.3	1	**-4.63**
scaffold_2:859891-860437(-)	64.85	1	2.62	1	**-4.63**
scaffold_14:77562-77696(-)	233.69	1	9.45	1	**-4.63**
scaffold_9:1407850-1408411(+)	56.37	1	2.28	1	**-4.63**
scaffold_4:1674280-1674953(+)	253.4	1	10.25	1	**-4.63**
scaffold_3:2731941-2732809(+)	56.36	0.99	2.28	0.8	**-4.63**
scaffold_1:5143780-5145579(-)	56.46	0.95	2.29	1	**-4.62**
scaffold_5:1784359-1784758(+)	100.26	1	4.1	1	**-4.61**
scaffold_1:3913574-3914945(-)	56.04	1	2.3	1	**-4.61**
scaffold_2:1011977-1012132(+)	183.06	1	7.52	0.69	**-4.61**
scaffold_8:142686-143878(+)	83.18	1	3.42	1	**-4.60**
scaffold_2:2831799-2834387(-)	99.42	0.93	4.1	0.90	**-4.60**
scaffold_8:751816-753669(-)	110.24	1	4.56	1	**-4.60**
scaffold_1:4688802-4689134(-)	55.12	1	2.28	1	**-4.60**
scaffold_1:1742623-1743453(-)	54.96	1	2.28	1	**-4.59**
scaffold_1:2223317-2223881(+)	81.23	0.88	3.4	0.89	**-4.58**
scaffold_3:4117840-4119064(+)	125.08	1	5.24	1	**-4.58**
scaffold_7:914930-917036(-)	71.92	1	3.02	1	**-4.57**
scaffold_2:2228951-2230023(+)	81.43	0.99	3.42	0.87	**-4.57**
scaffold_4:489116-489933(-)	138.75	0.99	5.9	0.68	**-4.56**
scaffold_4:1371198-1371509(-)	69.58	1	2.96	1	**-4.56**
scaffold_10:395693-395964(+)	61.35	1	2.62	1	**-4.55**
scaffold_3:1530207-1530627(-)	62.02	1	2.66	1	**-4.54**
scaffold_5:2810574-2811012(+)	55.62	1	2.39	1	**-4.54**
scaffold_6:2289769-2290455(+)	79.06	0.98	3.42	0.87	**-4.53**
scaffold_4:2336563-2337988(+)	94.76	0.99	4.1	0.89	**-4.53**
scaffold_3:2299416-2301493(-)	68.4	0.91	2.96	0.85	**-4.53**
scaffold_1:2540235-2540572(-)	52.54	1	2.28	1	**-4.53**
scaffold_3:3283000-3283925(-)	70.58	0.95	3.07	1	**-4.52**
scaffold_2:991135-991540(+)	73.33	1	3.19	1	**-4.52**
scaffold_9:798779-799690(-)	79.91	1	3.48	0.70	**-4.52**
scaffold_5:2605783-2606079(+)	868.19	1	38.04	1	**-4.51**
scaffold_3:3824577-3824744(+)	62.1	1	2.73	1	**-4.51**
scaffold_4:3310858-3311846(-)	123.33	1	5.47	1	**-4.49**
scaffold_3:2797191-2797649(-)	52.87	1	2.35	1	**-4.49**
scaffold_10:1224545-1224806(+)	66.34	1	2.96	1	**-4.49**
scaffold_1:4024085-4024422(+)	382.34	1	17.08	1	**-4.48**
scaffold_8:1454252-1454893(-)	150.27	1	6.72	1	**-4.48**
scaffold_9:182746-184422(+)	169.64	0.98	7.63	1	**-4.47**
scaffold_6:196776-197697(+)	75.94	1	3.42	1	**-4.47**
scaffold_2:45015-45236(+)	66.05	1	2.98	1	**-4.47**
scaffold_4:2942169-2942519(-)	206.76	0.67	9.34	0.8	**-4.47**
scaffold_6:2411706-2411793(+)	60.11	1	2.73	1	**-4.46**
scaffold_1:556462-558623(+)	234.82	1	10.7	1	**-4.46**
scaffold_5:24806-26959(-)	174.67	1	7.97	0.94	**-4.45**
scaffold_7:1321754-1323622(-)	149.39	1	6.83	1	**-4.45**
scaffold_2:1398689-1400053(-)	81.07	1	3.72	0.95	**-4.45**
scaffold_2:4386119-4386471(-)	59.36	0.98	2.73	1	**-4.44**
scaffold_13:194318-196084(-)	103.58	1	4.78	1	**-4.44**
scaffold_1:1054791-1056179(-)	65.97	1	3.07	1	**-4.43**
scaffold_3:4402911-4403786(+)	63.54	1	2.96	1	**-4.42**
scaffold_3:1531214-1533081(-)	82.93	0.96	3.87	1	**-4.42**
scaffold_4:2405735-2408447(-)	58.24	0.97	2.73	1	**-4.42**
scaffold_11:104005-104745(-)	91.91	0.99	4.33	0.80	**-4.41**
scaffold_3:2278604-2279281(+)	53.12	0.93	2.51	1	**-4.40**
scaffold_6:1417485-1418241(-)	82.38	0.95	3.92	0.78	**-4.39**
scaffold_13:31722-32158(-)	130.68	0.98	6.23	0.90	**-4.39**
scaffold_1:5687016-5687606(+)	114.35	1	5.47	0.92	**-4.39**
scaffold_11:821793-823161(-)	122.96	1	5.92	1	**-4.38**
scaffold_2:4204539-4204851(+)	75.32	1	3.64	1	**-4.37**
scaffold_2:4971944-4974148(+)	56.37	1	2.73	1	**-4.37**
scaffold_10:309835-310002(-)	84.55	1	4.1	1	**-4.37**
scaffold_4:3792268-3792604(-)	84.3	1	4.1	1	**-4.36**
scaffold_6:2248488-2249454(+)	79.31	1	3.87	1	**-4.36**
scaffold_13:590151-591131(+)	55.74	1	2.73	1	**-4.35**
scaffold_2:3163869-3164078(-)	60.36	1	2.96	1	**-4.35**
scaffold_3:2636967-2638949(+)	88.29	0.99	4.33	1	**-4.35**
scaffold_6:1537992-1539437(-)	124.58	1	6.11	0.50	**-4.35**
scaffold_8:545577-546695(+)	185.56	1	9.11	1	**-4.35**
scaffold_1:1082753-1083250(+)	1470.54	-0.83	72.2	-0.74	**-4.35**
scaffold_1:710882-711514(+)	101.61	1	5.01	1	**-4.34**
scaffold_2:336820-338947(+)	69.21	1	3.42	0.87	**-4.34**
scaffold_6:2819648-2820290(+)	57.63	1	2.85	1	**-4.34**
scaffold_5:3072835-3073326(+)	82.8	0.99	4.1	1	**-4.34**
scaffold_5:462830-463557(+)	96.27	0.98	4.78	0.52	**-4.33**
scaffold_6:1123733-1124161(+)	321.26	0.91	15.99	0.78	**-4.33**
scaffold_2:4448804-4449032(-)	82.3	1	4.1	1	**-4.33**
scaffold_10:1259152-1260423(+)	168.85	1	8.43	1	**-4.32**
scaffold_4:2624510-2624908(+)	51.62	1	2.58	1	**-4.32**
scaffold_4:2012339-2012723(+)	54.37	1	2.72	1	**-4.32**
scaffold_5:1163466-1167005(+)	123.4	0.95	6.18	1	**-4.32**
scaffold_1:981248-981614(-)	72.58	1	3.64	1	**-4.32**
scaffold_5:2699501-2699929(+)	321.45	0.91	16.16	0.78	**-4.31**

Locus	WT abundance	WT strand bias	*r3b2*⁻ abundance	*r3b2*⁻ strand bias	*r3b2*⁻ $\log_2$ fold change vs WT
scaffold_10:1071266-1071937(-)	158.5	1	7.97	1	**-4.31**
scaffold_4:3871379-3871456(+)	77.27	1	3.9	1	**-4.31**
scaffold_2:3231367-3233251(-)	121.77	1	6.15	1	**-4.31**
scaffold_9:254086-254223(-)	53.87	1	2.73	1	**-4.30**
scaffold_4:2149776-2150200(+)	112.23	1	5.69	0.92	**-4.30**
scaffold_3:2064675-2064929(-)	76.32	1	3.87	1	**-4.30**
scaffold_2:3881819-3882814(-)	62.75	1	3.19	1	**-4.30**
scaffold_1:402250-402310(-)	174.21	1	8.88	1	**-4.29**
scaffold_8:425228-425893(-)	71.37	0.99	3.64	1	**-4.29**
scaffold_3:4039517-4040108(-)	55.87	1	2.85	1	**-4.29**
scaffold_7:342400-344087(-)	131.56	1	6.72	1	**-4.29**
scaffold_4:1958546-1961368(+)	64.6	1	3.3	0.87	**-4.29**
scaffold_5:2441673-2443394(-)	66.93	0.97	3.42	0.94	**-4.29**
scaffold_8:899612-900288(+)	84.42	1	4.33	1	**-4.29**
scaffold_4:2967422-2967528(+)	81.84	0.97	4.2	0.93	**-4.28**
scaffold_2:4773865-4774277(-)	75.32	1	3.87	1	**-4.28**
scaffold_1:5803824-5804735(-)	75.32	1	3.87	1	**-4.28**
scaffold_4:444358-446941(+)	223.34	0.99	11.5	1	**-4.28**
scaffold_11:133792-135504(+)	53.11	0.95	2.75	1	**-4.27**
scaffold_5:1783237-1783640(+)	65.34	1	3.42	1	**-4.26**
scaffold_1:4766612-4767327(+)	69.29	0.99	3.64	1	**-4.25**
scaffold_2:520771-522126(+)	71.37	1	3.76	0.88	**-4.25**
scaffold_2:3199302-3201003(+)	118.22	1	6.26	0.79	**-4.24**
scaffold_5:1777528-1778360(+)	55.74	1	2.96	1	**-4.24**
scaffold_3:416172-418829(+)	102.33	0.97	5.44	0.9	**-4.23**
scaffold_7:173394-173798(+)	68.54	0.95	3.65	0.41	**-4.23**
scaffold_13:113555-113838(+)	474.62	0.98	25.28	0.56	**-4.23**
scaffold_12:95735-97014(+)	68.09	1	3.64	1	**-4.23**
scaffold_1:5767181-5768436(-)	155.3	1	8.31	1	**-4.22**
scaffold_8:1545746-1546023(+)	55.27	1	2.96	1	**-4.22**
scaffold_5:2534522-2536342(-)	594.96	1	31.89	1	**-4.22**
scaffold_9:255698-256011(+)	50.88	1	2.73	1	**-4.22**
scaffold_1:4902882-4903496(+)	59.44	0.98	3.19	1	**-4.22**
scaffold_12:512679-513807(+)	236.22	0.96	12.75	1	**-4.21**
scaffold_5:1917184-1921545(+)	63.35	0.99	3.42	1	**-4.21**
scaffold_1:1424522-1424984(+)	92.65	1	5.01	1	**-4.21**
scaffold_4:3207902-3208330(+)	321.88	0.91	17.45	0.79	**-4.21**
scaffold_4:3731922-3732459(-)	100.76	1	5.47	0.83	**-4.20**
scaffold_6:893945-894915(+)	333.87	1	18.18	1	**-4.20**
scaffold_1:2333650-2335247(+)	54.25	0.98	2.96	0.85	**-4.20**
scaffold_3:2306261-2306978(+)	70.83	1	3.87	1	**-4.19**
scaffold_6:166615-167681(+)	59.86	1	3.28	0.62	**-4.19**
scaffold_2:2743053-2744298(+)	154.72	1	8.5	0.91	**-4.19**
scaffold_2:3444517-3445296(+)	86.88	0.97	4.78	1	**-4.18**
scaffold_7:13295-14565(+)	74.45	1	4.1	1	**-4.18**
scaffold_8:1190388-1192067(+)	51.67	0.98	2.85	1	**-4.18**
scaffold_1:5484922-5485968(-)	64.35	0.95	3.56	0.89	**-4.18**
scaffold_3:1522759-1523967(+)	139.79	1	7.74	1	**-4.17**
scaffold_3:955969-957624(+)	172.59	0.99	9.57	1	**-4.17**
scaffold_3:3787101-3790520(+)	235.24	0.99	13.06	0.97	**-4.17**
scaffold_5:75849-77009(-)	140.91	1	7.86	1	**-4.16**
scaffold_2:4214284-4214601(+)	85.67	1	4.78	1	**-4.16**
scaffold_1:4174132-4176419(-)	105.54	0.99	5.92	1	**-4.16**
scaffold_6:395860-397346(+)	89.29	0.96	5.01	1	**-4.16**
scaffold_12:734493-734750(+)	121.71	1	6.83	0.93	**-4.16**
scaffold_1:1060100-1061095(-)	64.6	1	3.64	1	**-4.15**
scaffold_19:3514-4305(-)	475.74	-0.11	26.88	-0.02	**-4.15**
scaffold_11:609659-611299(-)	58.11	1	3.3	1	**-4.14**
scaffold_4:4113654-4116718(+)	64.8	0.99	3.68	1	**-4.14**
scaffold_2:1731785-1733964(-)	124.04	0.99	7.06	1	**-4.13**
scaffold_9:730248-734885(+)	65.86	0.96	3.77	1	**-4.13**
scaffold_5:700051-700509(+)	107.37	1	6.15	1	**-4.13**
scaffold_9:1146635-1147813(+)	75.57	1	4.33	1	**-4.13**
scaffold_13:628209-629735(-)	190.55	1	10.93	1	**-4.12**
scaffold_2:3434545-3434865(-)	155.39	1	8.93	1	**-4.12**
scaffold_3:4270635-4271049(+)	67.34	0.99	3.87	1	**-4.12**
scaffold_3:454580-455144(-)	55.37	1	3.19	1	**-4.12**
scaffold_7:714548-715508(-)	53.87	0.98	3.11	0.71	**-4.11**
scaffold_8:177911-178402(+)	110.24	1	6.38	1	**-4.11**
scaffold_10:171393-172046(+)	409.03	0.79	23.69	0.06	**-4.11**
scaffold_2:457582-458407(-)	74.76	0.99	4.33	1	**-4.11**
scaffold_5:1680819-1681389(-)	805.33	1	46.65	1	**-4.11**
scaffold_4:1057715-1058368(+)	97.77	0.94	5.69	0.92	**-4.10**
scaffold_4:1780174-1782513(+)	113.48	0.99	6.61	1	**-4.10**
scaffold_1:705197-706768(-)	157.3	0.89	9.17	0.98	**-4.10**
scaffold_6:1333683-1336445(-)	52.18	0.95	3.05	0.94	**-4.10**
scaffold_3:282872-284146(-)	59.58	0.99	3.49	1	**-4.09**
scaffold_8:656612-657338(-)	353.74	1	20.76	0.92	**-4.09**
scaffold_2:155018-156445(-)	123.04	1	7.23	1	**-4.09**
scaffold_10:603983-604549(-)	267.27	-0.66	15.72	-0.16	**-4.09**
scaffold_4:1844292-1844784(-)	95.52	1	5.62	0.92	**-4.09**
scaffold_1:1977628-1979463(-)	58.11	0.99	3.42	0.87	**-4.09**
scaffold_3:2615187-2616028(+)	53.62	1	3.19	1	**-4.07**
scaffold_6:1332058-1332219(-)	64.85	1	3.87	1	**-4.07**
scaffold_2:115017-115596(+)	98.52	1	5.92	0.92	**-4.06**
scaffold_1:4225533-4225755(+)	91.03	0.95	5.47	1	**-4.06**
scaffold_4:1234990-1235303(-)	64.35	1	3.87	1	**-4.06**
scaffold_3:286729-286960(+)	54.87	1	3.3	1	**-4.06**
scaffold_2:4774327-4774621(-)	56.86	1	3.42	1	**-4.06**
scaffold_4:2177678-2178606(+)	79.44	0.99	4.78	1	**-4.05**
scaffold_3:455201-456693(-)	94.23	0.99	5.69	1	**-4.05**
scaffold_1:3768890-3769513(+)	505.36	-0.66	30.52	-0.82	**-4.05**
scaffold_2:3738720-3739617(+)	50.3	0.96	3.04	1	**-4.05**
scaffold_2:498678-499595(+)	99.51	1	6.04	1	**-4.04**
scaffold_2:2312215-2314321(-)	258.3	1	15.68	1	**-4.04**
scaffold_7:171315-171894(-)	146.28	-0.4	8.88	-0.09	**-4.04**
scaffold_3:855914-857835(+)	91.41	0.82	5.58	-0.12	**-4.03**

Locus	WT abundance	WT strand bias	*r3b2*⁻ abundance	*r3b2*⁻ strand bias	*r3b2*⁻ $\log_2$ fold change vs WT
scaffold_5:2912889-2914962(-)	52.13	0.97	3.19	1	**-4.03**
scaffold_4:1936389-1937152(+)	92.78	1	5.69	1	**-4.03**
scaffold_4:44011-44666(-)	1758.69	-0.77	108.42	-0.02	**-4.02**
scaffold_1:4982325-4984014(-)	169.97	0.99	10.51	0.98	**-4.02**
scaffold_1:4880683-4881111(-)	209.04	0.91	12.94	0.78	**-4.01**
scaffold_1:208254-208305(+)	73.45	1	4.56	1	**-4.01**
scaffold_6:168052-170728(+)	70.77	0.88	4.4	0.75	**-4.01**
scaffold_1:2104082-2104781(-)	57.86	1	3.64	1	**-3.99**
scaffold_1:1586340-1587030(-)	63.14	0.99	3.99	0.79	**-3.98**
scaffold_13:15170-16298(+)	54.12	0.97	3.42	1	**-3.98**
scaffold_7:447240-449148(-)	250.86	0.99	15.97	0.89	**-3.97**
scaffold_1:207646-208194(+)	167.1	0.99	10.7	0.96	**-3.97**
scaffold_2:4449444-4453088(-)	239.83	0.99	15.37	0.99	**-3.96**
scaffold_4:2166555-2166786(+)	75.57	1	4.86	1	**-3.96**
scaffold_4:298647-299377(-)	70.83	1	4.56	1	**-3.96**
scaffold_4:3802205-3804733(-)	148.56	0.98	9.57	0.90	**-3.96**
scaffold_5:3097306-3098996(-)	180.18	1	11.65	1	**-3.95**
scaffold_1:4795641-4797379(-)	77.48	0.94	5.01	0.82	**-3.95**
scaffold_6:1099853-1100191(-)	63.22	0.99	4.1	0.87	**-3.95**
scaffold_1:2429430-2431508(+)	52.39	0.93	3.42	0.94	**-3.94**
scaffold_6:2392894-2393027(-)	142.79	1	9.34	1	**-3.93**
scaffold_10:1229182-1231044(-)	56.68	0.97	3.71	0.67	**-3.93**
scaffold_4:3757918-3759619(-)	170.84	0.99	11.2	1	**-3.93**
scaffold_1:2560741-2562315(-)	55.49	1	3.64	1	**-3.93**
scaffold_12:343883-344588(+)	69.34	-0.99	4.56	-0.8	**-3.93**
scaffold_1:1902838-1904074(+)	62.89	-0.69	4.14	-0.18	**-3.93**
scaffold_6:1197122-1199976(+)	72.45	0.92	4.78	0.81	**-3.92**
scaffold_1:1253913-1256526(+)	108.39	1	7.17	0.94	**-3.92**
scaffold_3:2791626-2792390(+)	54.69	0.95	3.64	1	**-3.91**
scaffold_3:4155304-4155954(+)	107.24	1	7.17	1	**-3.90**
scaffold_4:2695491-2695745(-)	61.1	1	4.1	1	**-3.90**
scaffold_10:818159-820283(+)	71.09	0.87	4.78	0.9	**-3.89**
scaffold_4:3042743-3043742(-)	100.02	0.99	6.73	0.94	**-3.89**
scaffold_10:1311068-1312327(+)	57.49	1	3.87	1	**-3.89**
scaffold_3:2685864-2690433(-)	92.41	0.98	6.26	0.86	**-3.88**
scaffold_5:2511750-2512073(-)	285.74	-0.93	19.36	-0.71	**-3.88**
scaffold_7:64014-64932(-)	53.5	0.99	3.64	0.88	**-3.88**
scaffold_7:1557627-1557731(-)	291.06	-0.96	19.82	-0.49	**-3.88**
scaffold_8:1661654-1663057(+)	75.07	1	5.12	0.94	**-3.87**
scaffold_6:2729249-2730240(-)	60.11	0.98	4.1	1	**-3.87**
scaffold_6:2281288-2282353(-)	99.08	1	6.76	1	**-3.87**
scaffold_2:785581-786530(+)	321.61	1	22.09	1	**-3.86**
scaffold_1:2631996-2633691(+)	93.9	0.97	6.49	1	**-3.85**
scaffold_8:1602496-1603776(+)	98.77	1	6.83	0.93	**-3.85**
scaffold_1:3290086-3292070(-)	213.95	1	14.8	1	**-3.85**
scaffold_11:91274-92019(+)	75.57	1	5.24	1	**-3.85**
scaffold_2:3674313-3674662(+)	68.9	1	4.78	1	**-3.85**
scaffold_1:5236169-5237098(+)	86.75	0.99	6.04	0.76	**-3.84**
scaffold_6:2540656-2541633(+)	53.87	1	3.76	1	**-3.84**
scaffold_3:433787-433976(-)	88.04	1	6.15	1	**-3.84**
scaffold_3:712156-714765(-)	147.9	0.97	10.36	0.91	**-3.84**
scaffold_5:3049072-3050921(-)	85.92	0.99	6.04	1	**-3.83**
scaffold_7:826891-827671(-)	369.91	1	26.04	0.99	**-3.83**
scaffold_2:1841027-1841632(+)	83.96	0.92	5.92	0.86	**-3.83**
scaffold_8:1010034-1010456(-)	76.61	1	5.43	1	**-3.82**
scaffold_6:1959585-1960174(-)	67.36	0.88	4.78	1	**-3.82**
scaffold_2:4318833-4319390(-)	204.43	1	14.51	1	**-3.82**
scaffold_1:554849-556161(+)	73.82	1	5.24	1	**-3.82**
scaffold_4:2430874-2431477(+)	236.94	0.49	16.85	0.3	**-3.81**
scaffold_7:1349832-1350777(+)	151.49	0.99	10.82	0.96	**-3.81**
scaffold_1:1082263-1082508(+)	124.2	-0.92	8.88	-0.84	**-3.81**
scaffold_8:1862310-1862470(+)	104.75	0.94	7.52	-0.27	**-3.80**
scaffold_7:1096771-1099714(+)	72.83	0.99	5.24	0.91	**-3.80**
scaffold_3:4671448-4672147(-)	75.94	1	5.47	1	**-3.80**
scaffold_1:4576684-4578570(-)	56.72	0.64	4.1	0.89	**-3.79**
scaffold_2:2294153-2294860(-)	59.75	0.96	4.33	1	**-3.79**
scaffold_6:1541095-1542251(+)	64.35	1	4.67	1	**-3.78**
scaffold_8:400136-401142(-)	81.31	0.99	5.92	1	**-3.78**
scaffold_5:105628-110256(-)	53.13	1	3.87	1	**-3.78**
scaffold_3:1969491-1971552(+)	303.8	1	22.21	1	**-3.77**
scaffold_3:942512-942677(-)	411.02	0.4	30.06	0.37	**-3.77**
scaffold_4:4138016-4138756(+)	66.84	0.99	4.9	1	**-3.77**
scaffold_7:1692630-1694085(+)	62.1	1	4.56	1	**-3.77**
scaffold_2:3003673-3004803(-)	325.93	1	23.99	0.97	**-3.76**
scaffold_1:4393418-4396200(+)	84.77	0.99	6.26	0.93	**-3.76**
scaffold_1:3135174-3136588(-)	58.49	1	4.33	1	**-3.76**
scaffold_6:2850865-2851197(+)	273.35	1	20.27	1	**-3.75**
scaffold_2:3653547-3653688(-)	76.57	1	5.69	1	**-3.75**
scaffold_4:221727-222345(+)	62.73	-0.74	4.67	-0.88	**-3.75**
scaffold_7:1684586-1684938(+)	86.54	1	6.45	1	**-3.75**
scaffold_5:2328318-2330435(-)	64.26	1	4.79	0.74	**-3.75**
scaffold_4:1404506-1405623(-)	66.97	1	5.01	1	**-3.74**
scaffold_2:3257037-3258362(+)	102.52	0.83	7.74	1	**-3.73**
scaffold_4:1448262-1448551(-)	102.38	1	7.74	1	**-3.73**
scaffold_9:1007034-1009380(+)	56.99	1	4.33	1	**-3.72**
scaffold_4:3381827-3384115(+)	124.2	1	9.45	0.95	**-3.72**
scaffold_4:2512720-2516250(-)	75.08	0.96	5.83	0.82	**-3.69**
scaffold_9:703605-704208(-)	59.05	1	4.59	1	**-3.69**
scaffold_11:586459-587172(-)	404.04	-0.21	31.43	0.22	**-3.68**
scaffold_9:184491-185807(+)	163.61	1	12.75	1	**-3.68**
scaffold_1:947565-950812(-)	98.77	0.99	7.74	1	**-3.67**
scaffold_5:2755692-2759595(-)	75.32	0.89	5.92	1	**-3.67**
scaffold_1:1873782-1875243(-)	81.06	0.98	6.38	0.86	**-3.67**
scaffold_4:2695988-2696111(-)	60.61	1	4.78	1	**-3.66**
scaffold_4:222499-223296(+)	1012.26	-0.89	79.87	-0.82	**-3.66**
scaffold_3:4315981-4316956(+)	54.74	1	4.33	1	**-3.66**
scaffold_9:1409942-1412434(+)	160.45	0.98	12.75	1	**-3.65**

Locus	WT abundance	WT strand bias	*r3b2*⁻ abundance	*r3b2*⁻ strand bias	*r3b2*⁻ $\log_2$ fold change vs WT
scaffold_4:4241043-4243499(-)	111.5	1	8.88	1	**-3.65**
scaffold_1:2754607-2755344(+)	68.59	1	5.47	1	**-3.65**
scaffold_4:4226836-4228796(-)	103.76	0.97	8.31	1	**-3.64**
scaffold_5:1182047-1190371(-)	90.97	0.98	7.29	0.82	**-3.64**
scaffold_2:2517721-2517834(+)	204.64	-0.91	16.4	-0.77	**-3.64**
scaffold_8:1230761-1232908(+)	483.56	1	38.89	1	**-3.64**
scaffold_10:509253-509407(+)	83.55	1	6.72	1	**-3.64**
scaffold_4:2691550-2694653(-)	339.69	1	27.33	1	**-3.64**
scaffold_4:1481631-1482528(-)	67.59	1	5.47	1	**-3.63**
scaffold_4:3404947-3405505(-)	84.3	1	6.83	1	**-3.63**
scaffold_1:2167420-2167657(-)	117.6	1	9.53	1	**-3.63**
scaffold_8:344075-345596(-)	198.03	0.99	16.06	1	**-3.62**
scaffold_8:1104133-1104555(+)	151.64	-0.93	12.3	-0.98	**-3.62**
scaffold_1:3977229-3977974(+)	58.86	1	4.78	1	**-3.62**
scaffold_1:4028294-4033978(+)	75.44	0.91	6.13	0.8	**-3.62**
scaffold_5:1369251-1371236(+)	90.3	0.99	7.36	1	**-3.62**
scaffold_4:3653240-3654616(+)	139.67	1	11.39	1	**-3.62**
scaffold_2:4558669-4560014(-)	111.13	1	9.11	1	**-3.61**
scaffold_8:130841-131393(-)	715.92	1	58.76	1	**-3.61**
scaffold_3:432852-433193(-)	72.08	0.99	5.92	1	**-3.61**
scaffold_4:4062537-4063595(+)	75.53	0.91	6.23	0.53	**-3.60**
scaffold_8:1092492-1092909(-)	53	1	4.4	0.95	**-3.59**
scaffold_4:3774944-3776908(+)	65.84	1	5.47	0.92	**-3.59**
scaffold_4:1423928-1424666(+)	148.26	1	12.32	1	**-3.59**
scaffold_5:2322263-2323880(+)	105.72	0.86	8.81	0.98	**-3.58**
scaffold_7:1629917-1630344(+)	122.46	1	10.25	1	**-3.58**
scaffold_1:2894042-2900487(+)	85.55	0.99	7.17	1	**-3.58**
scaffold_9:1086464-1088286(-)	100.14	0.99	8.43	0.95	**-3.57**
scaffold_1:636350-639811(-)	94.23	0.98	7.99	1	**-3.56**
scaffold_1:141945-142387(+)	88.54	0.65	7.52	0.38	**-3.56**
scaffold_5:1477717-1477917(+)	53.12	1	4.56	1	**-3.54**
scaffold_1:860701-862188(-)	673.52	0.56	57.97	0.09	**-3.54**
scaffold_4:1399924-1400777(+)	91.41	1	7.87	1	**-3.54**
scaffold_7:160476-161239(-)	51.93	1	4.49	1	**-3.53**
scaffold_1:1218798-1220121(-)	55.37	1	4.79	1	**-3.53**
scaffold_1:5438029-5438439(+)	865.19	-0.98	75.16	-0.81	**-3.52**
scaffold_3:3176213-3177450(-)	259.51	1	22.55	1	**-3.52**
scaffold_1:4314124-4316394(-)	112.32	1	9.79	1	**-3.52**
scaffold_9:700453-701538(-)	93.9	1	8.2	1	**-3.52**
scaffold_1:3725858-3726466(-)	754.46	-0.98	66.05	-0.86	**-3.51**
scaffold_2:1982174-1982848(-)	75.37	-0.9	6.61	-0.14	**-3.51**
scaffold_7:168910-169627(-)	85.42	-0.21	7.52	-0.62	**-3.51**
scaffold_3:4312988-4313857(+)	225.33	0.99	19.95	0.96	**-3.50**
scaffold_5:2376245-2377235(-)	87.29	1	7.74	1	**-3.50**
scaffold_1:1628746-1629435(+)	89.87	1	7.97	0.94	**-3.50**
scaffold_9:1375534-1376025(+)	128.2	1	11.39	1	**-3.49**
scaffold_10:200208-200714(-)	142.24	0.98	12.64	1	**-3.49**
scaffold_4:2324646-2325269(+)	90.1	1	8.01	1	**-3.49**
scaffold_8:723873-724404(+)	1152.76	-0.84	102.49	-0.16	**-3.49**
scaffold_9:87317-90183(-)	84.26	0.99	7.52	1	**-3.49**
scaffold_2:4534264-4536759(-)	182.99	0.99	16.42	0.97	**-3.48**
scaffold_1:4079947-4085898(-)	78.3	0.97	7.06	0.97	**-3.47**
scaffold_5:1851915-1852735(-)	58.11	1	5.24	1	**-3.47**
scaffold_5:1345052-1347376(-)	63.75	0.98	5.75	1	**-3.47**
scaffold_11:865888-866326(+)	72.48	0.98	6.54	1	**-3.47**
scaffold_4:3870321-3871148(+)	175.08	1	15.83	0.97	**-3.47**
scaffold_6:706141-706275(+)	62.43	1	5.69	1	**-3.46**
scaffold_3:1783458-1784549(-)	300.54	-0.87	27.45	-0.34	**-3.45**
scaffold_3:2296890-2298200(-)	184.35	1	16.85	1	**-3.45**
scaffold_6:2411492-2411640(+)	52.13	1	4.78	1	**-3.45**
scaffold_8:1244913-1245597(-)	247.41	-0.18	22.78	-0.16	**-3.44**
scaffold_13:361267-363330(-)	60.35	0.96	5.56	0.85	**-3.44**
scaffold_9:1513577-1514464(+)	109.24	1	10.07	1	**-3.44**
scaffold_7:1149634-1150098(+)	60.5	1	5.58	1	**-3.44**
scaffold_1:3925913-3926224(-)	98.97	0.99	9.15	1	**-3.44**
scaffold_4:604970-605258(+)	140.17	1	12.98	1	**-3.43**
scaffold_8:1903325-1904469(+)	88.54	0.99	8.2	1	**-3.43**
scaffold_5:2593714-2593963(-)	61.5	0.99	5.7	1	**-3.43**
scaffold_13:505315-507633(+)	971.44	-0.99	90.57	-0.84	**-3.42**
scaffold_1:2435270-2436251(-)	56.19	0.68	5.24	1	**-3.42**
scaffold_12:371683-372727(+)	106.25	1	9.91	1	**-3.42**
scaffold_5:659756-661368(+)	193.29	1	18.07	0.95	**-3.42**
scaffold_6:226142-227628(-)	51	1	4.78	0.90	**-3.42**
scaffold_4:1159265-1161824(+)	111.69	0.94	10.48	1	**-3.41**
scaffold_7:1556364-1556890(-)	542.83	-0.65	51.02	-0.08	**-3.41**
scaffold_10:1160379-1161128(+)	203.39	-0.89	19.13	-0.48	**-3.41**
scaffold_1:5634968-5635532(-)	53.12	1	5.05	0.93	**-3.39**
scaffold_1:992134-992675(+)	88.66	1	8.43	1	**-3.39**
scaffold_8:1287081-1287384(-)	55.53	0.99	5.29	1	**-3.39**
scaffold_4:3843333-3844379(-)	506.79	-0.77	48.29	-0.06	**-3.39**
scaffold_4:1055148-1056016(+)	97.85	1	9.34	1	**-3.39**
scaffold_7:1413703-1414684(-)	52.38	1	5.01	1	**-3.39**
scaffold_8:1224126-1224337(-)	88.96	1	8.54	1	**-3.38**
scaffold_9:578931-587791(+)	81.63	0.99	7.9	0.93	**-3.37**
scaffold_2:3686810-3687921(-)	73.58	1	7.17	1	**-3.36**
scaffold_2:2648968-2652576(-)	53.77	0.94	5.24	1	**-3.36**
scaffold_6:327724-328089(-)	105.75	1	10.33	1	**-3.36**
scaffold_5:1737293-1737762(+)	129.69	1	12.68	0.95	**-3.35**
scaffold_3:3699141-3699808(-)	69.34	0.96	6.79	0.96	**-3.35**
scaffold_8:749479-751803(-)	113.85	1	11.16	1	**-3.35**
scaffold_3:1142121-1142864(+)	752.46	-0.68	73.8	-0.24	**-3.35**
scaffold_1:17628-19760(-)	92.78	1	9.11	1	**-3.35**
scaffold_9:1023704-1026733(+)	116.35	1	11.5	1	**-3.34**
scaffold_6:1800628-1800978(-)	364.97	1	36.44	1	**-3.32**
scaffold_4:918486-919696(+)	92.28	1	9.22	1	**-3.32**
scaffold_2:3986963-3987698(+)	312.01	-0.79	31.2	-0.45	**-3.32**
scaffold_9:1465434-1466006(-)	179.57	0.43	17.99	0.27	**-3.32**

Locus	WT abundance	WT strand bias	*r3b2*⁻ abundance	*r3b2*⁻ strand bias	*r3b2*⁻ $\log_2$ fold change vs WT
scaffold_9:423194-423655(-)	73.08	1	7.36	1	**-3.31**
scaffold_5:2716480-2717336(+)	163.74	1	16.51	1	**-3.31**
scaffold_12:485833-490031(-)	72.25	0.82	7.29	0.94	**-3.31**
scaffold_2:1230075-1230810(-)	81.18	1	8.2	0.89	**-3.31**
scaffold_8:1459880-1460164(-)	67.59	1	6.83	0.94	**-3.31**
scaffold_10:616757-619040(-)	249.78	0.99	25.28	1	**-3.30**
scaffold_4:2520728-2521067(-)	363.97	1	36.9	1	**-3.30**
scaffold_8:559478-559878(-)	65.84	-0.86	6.68	-0.29	**-3.30**
scaffold_11:829803-830513(+)	168.58	-0.94	17.14	-0.9	**-3.30**
scaffold_8:1056348-1056794(+)	263.87	-0.78	26.88	-0.73	**-3.30**
scaffold_1:4598192-4600977(-)	89.21	0.99	9.12	0.93	**-3.29**
scaffold_11:594283-595659(+)	791.12	-0.57	80.97	-0.51	**-3.29**
scaffold_5:1385520-1386187(-)	640.23	-0.85	65.6	-0.72	**-3.29**
scaffold_2:1582196-1583712(-)	116.72	0.99	12.01	1	**-3.28**
scaffold_3:3465413-3467378(+)	94.9	1	9.79	1	**-3.28**
scaffold_3:4192440-4193040(+)	70.46	1	7.29	1	**-3.27**
scaffold_2:798646-800374(+)	87.35	0.97	9.04	0.9	**-3.27**
scaffold_9:866120-866442(-)	178.08	-0.58	18.45	-0.3	**-3.27**
scaffold_2:1548336-1548833(-)	58.49	1	6.07	1	**-3.27**
scaffold_6:1695393-1695862(+)	2169.72	-0.79	225.94	-0.57	**-3.26**
scaffold_9:831021-832481(-)	87.29	1	9.11	1	**-3.26**
scaffold_6:653142-654827(+)	62.1	1	6.49	1	**-3.26**
scaffold_4:2713457-2714072(-)	73.58	1	7.74	0.94	**-3.25**
scaffold_11:623328-623852(-)	69.81	0.98	7.35	1	**-3.25**
scaffold_2:4021394-4021803(-)	87.35	1	9.22	1	**-3.24**
scaffold_1:1640877-1641371(-)	57.86	-0.82	6.15	-0.62	**-3.23**
scaffold_4:2534397-2534611(+)	59.73	1	6.38	1	**-3.23**
scaffold_4:3643422-3644263(-)	187.24	1	20.04	1	**-3.22**
scaffold_2:420283-421962(-)	213.82	0.99	22.89	1	**-3.22**
scaffold_8:1227171-1227521(+)	73.82	1	7.93	0.97	**-3.22**
scaffold_4:147565-151579(-)	85.74	0.97	9.35	1	**-3.20**
scaffold_3:4639585-4640377(+)	66.59	0.99	7.29	1	**-3.19**
scaffold_9:1299458-1300225(+)	113.11	1	12.41	1	**-3.19**
scaffold_2:4222329-4223694(+)	120.22	0.99	13.21	0.97	**-3.19**
scaffold_4:2977282-2978342(+)	55.85	-0.84	6.15	0.48	**-3.18**
scaffold_1:3355409-3355730(+)	74.41	0.94	8.2	1	**-3.18**
scaffold_3:1838134-1839573(-)	856.71	0.06	94.98	0.33	**-3.17**
scaffold_5:2240668-2241472(+)	110.74	1	12.3	1	**-3.17**
scaffold_1:2568331-2569500(+)	84.26	0.99	9.4	1	**-3.16**
scaffold_8:153294-153408(+)	63.1	-0.91	7.06	-0.16	**-3.16**
scaffold_1:5043128-5046511(+)	64.09	0.98	7.18	1	**-3.16**
scaffold_4:1506854-1509105(-)	60.69	0.98	6.83	1	**-3.15**
scaffold_4:1007522-1007758(-)	54.62	1	6.15	1	**-3.15**
scaffold_11:701954-702426(-)	380.47	0.59	43.05	0.09	**-3.14**
scaffold_3:46636-49297(-)	67	0.85	7.59	0.78	**-3.14**
scaffold_3:82488-83639(-)	245.17	1	27.79	0.99	**-3.14**
scaffold_2:2579478-2580562(-)	352.45	0.99	39.97	0.98	**-3.14**
scaffold_4:2423319-2424680(-)	54.63	0.97	6.2	1	**-3.14**
scaffold_8:1541417-1541864(+)	58.74	0.97	6.68	0.93	**-3.14**
scaffold_8:1106093-1106927(+)	458.41	-0.64	52.2	-0.54	**-3.13**
scaffold_7:1792947-1793777(+)	654.49	-0.32	74.54	-0.04	**-3.13**
scaffold_1:5571320-5573634(+)	78.73	0.99	9	0.95	**-3.13**
scaffold_6:621286-622581(+)	63.68	1	7.29	1	**-3.13**
scaffold_11:910486-910774(-)	71.46	1	8.2	1	**-3.12**
scaffold_1:2273087-2273423(-)	67.22	0.86	7.82	0.38	**-3.10**
scaffold_7:182602-185259(+)	70.42	0.99	8.2	0.94	**-3.10**
scaffold_5:3104083-3106722(+)	81.81	0.99	9.57	1	**-3.10**
scaffold_1:2639103-2641259(+)	140.49	1	16.44	1	**-3.10**
scaffold_4:773260-774591(-)	155.55	0.99	18.22	0.97	**-3.09**
scaffold_3:3257954-3258378(+)	359.64	0.79	42.14	0.15	**-3.09**
scaffold_4:3250007-3250888(+)	53.37	0.99	6.26	1	**-3.09**
scaffold_2:4447229-4448602(-)	75.32	1	8.88	1	**-3.08**
scaffold_7:541505-546575(-)	130.19	0.99	15.49	1	**-3.07**
scaffold_1:4626897-4628928(-)	95.15	1	11.39	0.88	**-3.06**
scaffold_9:181116-182237(+)	72.2	0.97	8.66	0.95	**-3.06**
scaffold_5:2982957-2983933(-)	83.3	0.99	10.02	1	**-3.06**
scaffold_2:4459833-4462073(+)	51.88	1	6.26	0.93	**-3.05**
scaffold_2:1918636-1919832(+)	178.82	1	21.64	1	**-3.05**
scaffold_1:2991850-2992305(+)	52.87	1	6.42	0.93	**-3.04**
scaffold_1:4522310-4523904(-)	72.08	0.99	8.77	1	**-3.04**
scaffold_1:3203752-3206322(+)	99.1	0.66	12.07	0.95	**-3.04**
scaffold_3:1208381-1209652(+)	52.92	1	6.49	1	**-3.03**
scaffold_3:4318394-4319297(-)	61.23	0.99	7.55	0.94	**-3.02**
scaffold_1:1396153-1396563(-)	97.21	0.95	12.07	0.75	**-3.01**
scaffold_5:3159770-3160231(-)	62.56	1	7.79	0.95	**-3.01**
scaffold_10:1159093-1160364(+)	168.1	-0.52	20.95	-0.17	**-3.00**
scaffold_3:3941319-3941570(-)	238.68	-0.53	29.84	0	**-3.00**
scaffold_13:5884-6047(+)	164.53	-0.92	20.73	-0.33	**-2.99**
scaffold_4:4001774-4002992(-)	428.44	1	54.51	0.98	**-2.97**
scaffold_6:1408981-1409119(+)	55.37	-0.95	7.06	-0.94	**-2.97**
scaffold_11:587613-587843(-)	82.05	-0.15	10.48	-0.11	**-2.97**
scaffold_3:43059-46570(-)	62.94	0.98	8.06	0.91	**-2.97**
scaffold_1:2306156-2308304(-)	69.21	0.99	8.88	0.90	**-2.96**
scaffold_1:2983392-2984651(+)	111.78	0.94	14.35	1	**-2.96**
scaffold_8:1929470-1931373(+)	107.58	1	13.85	0.99	**-2.96**
scaffold_2:1345771-1347165(-)	210.75	-0.91	27.41	-0.63	**-2.94**
scaffold_1:3570024-3571560(+)	98.89	0.97	12.89	1	**-2.94**
scaffold_1:5687850-5688568(+)	84.17	1	11.05	1	**-2.93**
scaffold_2:2063997-2064857(+)	851.48	-0.91	112.52	-0.69	**-2.92**
scaffold_1:5548437-5559059(+)	90.2	0.94	11.92	0.93	**-2.92**
scaffold_3:449851-451021(-)	80.28	1	10.63	1	**-2.92**
scaffold_9:423721-424269(-)	58.36	1	7.74	0.94	**-2.91**
scaffold_9:378459-378911(-)	404.29	-0.49	53.75	-0.18	**-2.91**
scaffold_3:4633281-4633373(-)	73.58	1	9.79	1	**-2.91**
scaffold_5:975873-976423(+)	69.68	0.3	9.28	0.23	**-2.91**
scaffold_6:2478523-2481195(-)	57.84	0.99	7.77	0.89	**-2.90**
scaffold_9:724950-726074(+)	485.35	-0.4	65.37	-0.51	**-2.89**

Locus	WT abundance	WT strand bias	*r3b2*⁻ abundance	*r3b2*⁻ strand bias	*r3b2*⁻ $\log_2$ fold change vs WT
scaffold_1:4736719-4737143(-)	135.14	-0.39	18.22	-0.12	**-2.89**
scaffold_4:1850045-1852765(+)	52.38	1	7.13	1	**-2.88**
scaffold_1:2337972-2342334(-)	236.69	1	32.23	0.97	**-2.88**
scaffold_2:3631872-3632998(-)	60.24	0.96	8.21	1	**-2.88**
scaffold_5:1219565-1220386(+)	178.2	1	24.37	1	**-2.87**
scaffold_4:2162743-2165211(+)	94.77	1	12.98	0.82	**-2.87**
scaffold_1:4306555-4307445(+)	325.73	-0.89	44.76	-0.46	**-2.86**
scaffold_6:60116-60413(-)	59.61	1	8.2	1	**-2.86**
scaffold_8:1390673-1391594(+)	139.67	1	19.23	0.97	**-2.86**
scaffold_2:2681154-2681873(+)	281	-0.4	38.72	-0.14	**-2.86**
scaffold_2:4709797-4710721(-)	97.52	1	13.44	0.97	**-2.86**
scaffold_2:3767660-3768858(+)	62.6	1	8.66	1	**-2.85**
scaffold_3:1574919-1575739(-)	728.52	-0.62	101.01	-0.06	**-2.85**
scaffold_9:185870-187021(+)	82.43	1	11.43	0.97	**-2.85**
scaffold_8:345649-346755(-)	101.51	1	14.12	1	**-2.85**
scaffold_1:181491-185927(-)	54.06	0.96	7.54	0.94	**-2.84**
scaffold_9:1396263-1396750(+)	205.26	-0.89	28.7	-0.32	**-2.84**
scaffold_4:713508-714012(+)	118.72	-0.98	16.63	-0.97	**-2.84**
scaffold_4:3786436-3786906(-)	90.01	1	12.64	1	**-2.83**
scaffold_4:2400108-2400739(-)	52.31	0.98	7.38	0.96	**-2.83**
scaffold_5:2588524-2588656(-)	61.1	1.0	8.66	1	**-2.82**
scaffold_8:1023557-1024216(+)	261.13	-0.86	37.13	-0.7	**-2.81**
scaffold_7:147657-148330(+)	144.03	1	20.61	1	**-2.80**
scaffold_10:480769-482154(-)	272.1	-0.77	39.06	-0.61	**-2.80**
scaffold_11:701013-701644(+)	144.41	0.82	20.84	0.39	**-2.79**
scaffold_1:3922848-3923562(-)	53.41	1.0	7.71	0.95	**-2.79**
scaffold_3:4687184-4687576(-)	187.3	1	27.1	1	**-2.79**
scaffold_10:478662-479450(-)	423.12	0.68	61.27	0.39	**-2.79**
scaffold_4:2281337-2286772(-)	192.63	0.98	28.01	1	**-2.78**
scaffold_4:1916113-1919709(+)	61.63	0.5	9.01	0.56	**-2.77**
scaffold_5:2112913-2113788(+)	190.67	1	27.92	1	**-2.77**
scaffold_2:3684514-3686157(+)	223.09	0.95	32.68	1	**-2.77**
scaffold_8:560127-560715(-)	290.02	0.09	42.59	0.26	**-2.77**
scaffold_4:2473055-2473493(+)	86.79	0.7	12.75	0.45	**-2.77**
scaffold_4:3690081-3690867(-)	66.59	1	9.79	1	**-2.77**
scaffold_14:22623-23243(-)	91.41	1	13.44	0.95	**-2.77**
scaffold_1:2810024-2810467(-)	52.58	0.99	7.74	1	**-2.76**
scaffold_7:170791-171256(-)	73.45	-0.62	10.82	-0.36	**-2.76**
scaffold_8:449302-451511(+)	155.25	0.99	22.95	1	**-2.76**
scaffold_6:2402004-2403779(+)	52.28	1	7.74	1	**-2.76**
scaffold_9:701595-702389(-)	60.65	0.96	9.07	1	**-2.74**
scaffold_5:1232933-1233287(-)	110.24	-0.98	16.51	-0.9	**-2.74**
scaffold_5:1616372-1617047(-)	50.16	1	7.52	1	**-2.74**
scaffold_3:4320427-4320621(+)	97.21	1	14.58	1	**-2.74**
scaffold_10:932817-935768(+)	118.47	1.0	17.77	1	**-2.74**
scaffold_8:1842895-1843293(-)	207.51	-0.8	31.43	-0.32	**-2.72**
scaffold_13:40568-41392(-)	59.36	1	9	1	**-2.72**
scaffold_8:774958-775909(-)	52.75	0.94	8.03	1	**-2.72**
scaffold_3:155187-155833(-)	146.65	-0.61	22.55	-0.25	**-2.70**
scaffold_6:1731700-1732521(-)	54.2	0.99	8.36	1	**-2.70**
scaffold_7:738548-739126(+)	523.51	1	80.78	1	**-2.70**
scaffold_4:3497941-3498484(-)	191.79	1	29.61	1	**-2.70**
scaffold_9:148918-150654(+)	51.25	0.97	7.97	1	**-2.68**
scaffold_13:570601-571472(-)	189.05	1	29.48	1	**-2.68**
scaffold_1:3077281-3078838(+)	54.64	1	8.54	0.95	**-2.68**
scaffold_4:98233-98744(-)	170.84	-0.8	26.72	-0.47	**-2.68**
scaffold_10:1244037-1244474(-)	88.29	-0.71	13.89	-0.52	**-2.67**
scaffold_5:2456671-2458408(-)	174.09	0.99	27.45	1	**-2.66**
scaffold_2:4375020-4375627(+)	90.78	1	14.35	1	**-2.66**
scaffold_2:3633352-3635082(-)	73.61	1	11.65	1	**-2.66**
scaffold_1:3062334-3062715(+)	299.79	-0.84	47.72	-0.48	**-2.65**
scaffold_8:1629931-1631423(+)	79.3	0.99	12.69	1	**-2.64**
scaffold_2:1972074-1973272(-)	93.65	-0.83	15.03	0.01	**-2.64**
scaffold_11:881536-882408(-)	215.4	1	34.58	1	**-2.64**
scaffold_7:1557907-1558038(-)	82.8	-0.68	13.44	-0.43	**-2.62**
scaffold_4:1028515-1030503(-)	70.08	0.98	11.39	1	**-2.62**
scaffold_7:1477381-1479765(+)	127.09	0.97	20.83	0.98	**-2.61**
scaffold_3:1728671-1730215(+)	67.41	1	11.19	1	**-2.59**
scaffold_4:3229337-3232499(+)	65.84	0.47	10.93	0.94	**-2.59**
scaffold_2:4841221-4842326(-)	67.09	0.99	11.16	1	**-2.59**
scaffold_2:1069947-1070945(-)	101.34	1	16.88	1	**-2.59**
scaffold_1:2569558-2572415(+)	169.8	0.93	28.32	1	**-2.58**
scaffold_3:4214525-4215423(-)	167.85	0.99	28.01	1	**-2.58**
scaffold_4:2396194-2396621(-)	101.43	1	16.97	1	**-2.58**
scaffold_13:717153-718560(+)	127.32	1	21.41	1	**-2.57**
scaffold_3:120686-121610(-)	90.66	1	15.26	0.97	**-2.57**
scaffold_8:328794-330292(+)	99.78	0.87	16.97	0.71	**-2.56**
scaffold_2:289903-298717(+)	145.28	0.97	24.79	1	**-2.55**
scaffold_3:1460128-1461305(+)	85.3	0.99	14.67	1	**-2.54**
scaffold_5:2519145-2520073(+)	54.23	0.99	9.34	0.96	**-2.54**
scaffold_1:1081086-1081463(+)	117.47	-0.98	20.27	-0.89	**-2.53**
scaffold_1:689628-690463(+)	100.26	-0.88	17.31	-0.5	**-2.53**
scaffold_3:887762-888202(-)	189.8	-0.51	32.8	-0.64	**-2.53**
scaffold_2:890221-894272(+)	102.21	0.67	17.67	0.97	**-2.53**
scaffold_1:5670602-5671677(+)	59.53	1	10.36	1	**-2.52**
scaffold_1:596743-597906(+)	974.47	-0.89	170.09	-0.82	**-2.52**
scaffold_6:2205016-2206013(+)	57.36	1	10.02	1	**-2.52**
scaffold_3:3463522-3464758(+)	51.88	1	9.11	0.95	**-2.51**
scaffold_9:103157-103529(+)	241.18	-0.68	42.36	-0.55	**-2.51**
scaffold_5:770918-771475(+)	493.7	-0.42	86.83	-0.41	**-2.51**
scaffold_4:2521265-2522689(-)	672.25	1	118.26	0.98	**-2.51**
scaffold_8:1158944-1159311(+)	187.06	-0.16	32.91	-0.26	**-2.51**
scaffold_6:262675-263007(+)	151.14	0.94	26.65	0.7	**-2.50**
scaffold_1:3484245-3485076(-)	176.21	1	31.26	1	**-2.49**
scaffold_5:46216-49639(+)	95.4	0.98	16.95	1	**-2.49**
scaffold_3:424751-425577(-)	82.05	1	14.6	0.98	**-2.49**
scaffold_2:2892353-2892761(-)	75.49	1	13.44	1	**-2.49**

Locus	WT abundance	WT strand bias	*r3b2*⁻ abundance	*r3b2*⁻ strand bias	*r3b2*⁻ log_2 fold change vs WT
scaffold_2:1326831-1327108(+)	70.33	1	12.53	0.89	**-2.49**
scaffold_4:871849-872545(+)	115.14	-0.69	20.65	-0.15	**-2.48**
scaffold_10:735666-736990(-)	57.11	0.97	10.25	1	**-2.48**
scaffold_2:4531013-4533625(-)	108.48	0.95	19.63	1	**-2.47**
scaffold_6:2169946-2170141(+)	72.91	0.21	13.21	-0.45	**-2.46**
scaffold_6:2170419-2171438(+)	224.97	0.89	40.77	0.51	**-2.46**
scaffold_2:1583776-1586459(-)	75.32	1	13.74	0.97	**-2.45**
scaffold_3:337134-339865(+)	70	1	12.81	1	**-2.45**
scaffold_13:317519-318332(+)	88.54	0.99	16.29	0.94	**-2.44**
scaffold_4:3179996-3180716(-)	131.44	0.99	24.37	0.98	**-2.43**
scaffold_2:459755-460440(-)	56.34	0.99	10.48	1	**-2.43**
scaffold_8:197621-198326(+)	102.92	-0.68	19.17	-0.16	**-2.42**
scaffold_1:1705990-1707652(-)	57.55	1	10.75	1	**-2.42**
scaffold_2:2171796-2173496(-)	98.72	1	18.45	1	**-2.42**
scaffold_2:1982995-1983659(-)	60.86	-0.81	11.39	0.2	**-2.42**
scaffold_2:4163531-4165176(+)	74.32	0.99	14.01	1	**-2.41**
scaffold_5:2464431-2465323(+)	80.14	0.99	15.22	0.99	**-2.40**
scaffold_7:1739400-1739807(+)	154.13	-0.34	29.38	0.1	**-2.39**
scaffold_6:2608182-2608596(+)	310.39	-0.44	59.67	-0.41	**-2.38**
scaffold_2:2139284-2140603(-)	605.84	-0.01	116.57	-0.18	**-2.38**
scaffold_8:1639081-1641308(-)	113.36	0.99	21.87	0.98	**-2.37**
scaffold_9:1064948-1065522(-)	248.53	0.1	48.51	0.24	**-2.36**
scaffold_3:2735555-2736112(+)	56.74	1	11.16	1	**-2.35**
scaffold_7:120965-121366(+)	54.62	-0.32	10.75	-0.08	**-2.35**
scaffold_4:3488671-3489699(-)	113.67	-0.93	22.57	-0.89	**-2.33**
scaffold_1:5748514-5748766(-)	250.28	-0.15	49.77	-0.04	**-2.33**
scaffold_4:3482338-3483366(+)	113.58	-0.93	22.64	-0.89	**-2.33**
scaffold_8:527049-528043(+)	182.07	-0.67	36.33	-0.42	**-2.33**
scaffold_3:2924575-2925190(-)	59.35	1	11.86	0.97	**-2.32**
scaffold_6:431301-432410(+)	70.33	-0.8	14.12	-0.59	**-2.32**
scaffold_11:268136-271793(-)	90.39	0.94	18.23	0.98	**-2.31**
scaffold_3:4533270-4533629(-)	89.04	-0.71	17.99	-0.34	**-2.31**
scaffold_3:2492054-2493758(-)	116.72	1	23.69	1	**-2.30**
scaffold_7:737712-738401(+)	649.16	1	131.88	1	**-2.30**
scaffold_1:5754391-5756292(+)	57.11	1	11.62	1	**-2.30**
scaffold_1:1004000-1005374(+)	57.99	1	11.84	1	**-2.29**
scaffold_2:2800703-2801268(+)	1196.16	-0.73	245.07	-0.43	**-2.29**
scaffold_1:4737163-4737339(-)	106.5	-0.61	21.87	-0.42	**-2.28**
scaffold_11:393184-394845(+)	60.86	1	12.53	1	**-2.28**
scaffold_8:891752-892285(+)	499.94	0.85	103.06	0.17	**-2.28**
scaffold_2:2580638-2581166(-)	66.09	1	13.67	1	**-2.27**
scaffold_8:1764869-1766142(-)	147.2	1	30.57	1	**-2.27**
scaffold_1:1173211-1175552(-)	84.46	0.98	17.65	0.95	**-2.26**
scaffold_1:4299268-4300776(+)	135.86	0.33	28.43	0.02	**-2.26**
scaffold_4:1939304-1943131(+)	74.45	0.96	15.6	0.97	**-2.25**
scaffold_3:213616-215193(-)	59.11	1	12.42	0.96	**-2.25**
scaffold_2:4089382-4090172(+)	109.99	1	23.12	1	**-2.25**
scaffold_7:1737557-1738078(-)	265.87	-0.86	55.92	-0.47	**-2.25**
scaffold_10:774479-774887(+)	78.98	1	16.63	1	**-2.25**
scaffold_1:4017089-4017916(-)	55.62	1	11.73	1	**-2.25**
scaffold_6:1241223-1241662(+)	138.17	-0.71	29.15	-0.58	**-2.24**
scaffold_4:2940973-2941407(-)	128.44	-0.52	27.1	-0.45	**-2.24**
scaffold_10:1118213-1119452(-)	94.65	1	20.04	1	**-2.24**
scaffold_7:202031-203362(+)	254.64	-0.16	53.93	-0.1	**-2.24**
scaffold_10:68830-69970(+)	70.32	0.95	15.06	0.9	**-2.22**
scaffold_3:1172143-1172877(+)	96.23	0.99	20.69	0.75	**-2.22**
scaffold_2:2090763-2094099(-)	71.21	0.99	15.37	1	**-2.21**
scaffold_3:1919119-1921582(-)	86.71	0.98	18.79	0.98	**-2.21**
scaffold_3:1704439-1705752(-)	205.89	-0.79	44.64	-0.66	**-2.21**
scaffold_4:2534665-2535907(+)	104.13	1	22.78	1	**-2.19**
scaffold_9:1397600-1398069(-)	231.95	-0.2	50.79	-0.66	**-2.19**
scaffold_2:3184881-3186517(+)	104.38	0.99	22.89	1	**-2.19**
scaffold_1:2757056-2759512(+)	78.94	1	17.63	0.65	**-2.16**
scaffold_1:1895258-1895508(-)	99.2	1	22.16	1	**-2.16**
scaffold_1:3395233-3395554(+)	171.84	-0.61	38.95	-0.28	**-2.14**
scaffold_6:2033515-2034074(+)	122.33	-0.57	27.79	-0.26	**-2.14**
scaffold_2:4054027-4054572(+)	205.61	-0.28	46.92	-0.18	**-2.13**
scaffold_5:814780-815286(-)	50.96	1	11.63	1	**-2.13**
scaffold_1:3486986-3489115(-)	72.33	1	16.51	0.95	**-2.13**
scaffold_4:1782578-1785816(+)	64.35	0.99	14.72	0.94	**-2.13**
scaffold_1:1132601-1133055(-)	66.3	1	15.26	1	**-2.12**
scaffold_3:124858-125136(-)	144.28	-0.95	33.25	-0.9	**-2.12**
scaffold_13:169909-170206(+)	146.15	-0.48	33.71	-0.35	**-2.12**
scaffold_6:694894-696192(+)	61.73	0.98	14.24	0.97	**-2.12**
scaffold_4:2385430-2386485(+)	86.31	1	19.99	1	**-2.11**
scaffold_1:1133855-1139780(+)	82.3	0.75	19.13	0.98	**-2.11**
scaffold_2:3987729-3988516(+)	261.09	-0.19	60.81	-0.47	**-2.10**
scaffold_11:894221-895944(+)	61.1	1	14.35	0.97	**-2.09**
scaffold_5:671457-672308(-)	71.37	-0.86	16.99	-0.62	**-2.07**
scaffold_8:16260-18921(-)	66.09	0.97	15.98	0.94	**-2.05**
scaffold_9:1210953-1212272(+)	174.33	1	42.34	0.97	**-2.04**
scaffold_5:851647-852081(+)	61.6	1	15.03	1	**-2.04**
scaffold_12:398016-401166(-)	54.37	0.98	13.44	1	**-2.02**
scaffold_4:574133-574320(-)	317.74	1	0		**N/A**
scaffold_10:502786-502979(-)	161.37	1	0		**N/A**
scaffold_3:3108420-3108834(-)	143.41	1	0		**N/A**
scaffold_1:752396-752498(+)	142.66	0.99	0		**N/A**
scaffold_3:4148254-4148444(+)	138.92	1	0		**N/A**
scaffold_4:3682880-3683403(+)	136.67	0.96	0		**N/A**
scaffold_3:1273720-1274159(-)	125.45	1	0		**N/A**
scaffold_1:1053113-1054103(+)	120.09	1	0		**N/A**
scaffold_5:729937-730268(-)	108.62	1	0		**N/A**
scaffold_3:4863904-4865026(-)	107.87	1	0		**N/A**
scaffold_7:1813357-1813723(-)	102.01	1	0		**N/A**
scaffold_6:1415878-1415959(+)	97.27	1	0		**N/A**
scaffold_1:2663169-2663518(+)	95.02	1	0		**N/A**
scaffold_3:2502239-2502569(+)	88.54	1	0		**N/A**

Locus	WT abundance	WT strand bias	*r3b2*⁻ abundance	*r3b2*⁻ strand bias	*r3b2*⁻ $\log_2$ fold change vs WT
scaffold_10:422839-423633(-)	88.31	0.98	0		N/A
scaffold_8:1509096-1509416(+)	84.05	1	0		N/A
scaffold_3:4629093-4629267(-)	82.8	1	0		N/A
scaffold_6:2503427-2503652(-)	79.81	1	0		N/A
scaffold_5:1952247-1953638(+)	75.82	1	0		N/A
scaffold_9:925939-926801(+)	71.58	0.99	0		N/A
scaffold_10:44700-44908(+)	70.83	1	0		N/A
scaffold_2:1686635-1686748(+)	69.58	1	0		N/A
scaffold_2:3148292-3148537(-)	68.59	1	0		N/A
scaffold_5:2129127-2129825(+)	67.53	1	0		N/A
scaffold_5:1007905-1008033(+)	64.1	1	0		N/A
scaffold_4:1112288-1112426(-)	61.73	1	0		N/A
scaffold_4:4101576-4101936(+)	60.52	1	0		N/A
scaffold_1:1872717-1872802(-)	60.36	1	0		N/A
scaffold_8:1620995-1621249(+)	59.11	1	0		N/A
scaffold_10:84138-84309(+)	58.36	1	0		N/A
scaffold_4:1961510-1962030(-)	58.34	0.96	0		N/A
scaffold_3:4850144-4850342(+)	56.12	1	0		N/A
scaffold_7:2200478-2200598(+)	55.24	0.99	0		N/A
scaffold_1:2647274-2647469(+)	54.12	0.99	0		N/A
scaffold_5:1644202-1644411(+)	54.12	1	0		N/A
scaffold_4:1816693-1816911(+)	53.12	1	0		N/A
scaffold_2:1793127-1793498(+)	52.13	1	0		N/A

Table S3. Log_2 fold change of the *rdrp*-dependent *dicer*-independent rdRNAs in the *r3b2*$^-$ mutant compared to wild type. The fold change of the *r3b2*$^-$ mutant relative to the wild type is shown for the different classes of rdRNAs produced by the non-canonical *rdrp*-dependent *dicer*-independent degradation pathway. Loci that are *rdrp-1* and *rdrp-2* dependent, only *rdrp-1* dependent and only *rdrp-2* dependent have yellow, white and blue background, respectively. Data are sorted as in Table S1. The log_2 fold change of rdRNAs in the *rdrp-1*$^-$ and *rdrp-2*$^-$ mutants compared to the wild type are shown for comparison. Values that represent a fourfold or larger change are in bold. N/A, not applicable.

ID	WT strand bias	*rdrp1*$^-$ log_2 fold change vs WT	*rdrp2*$^-$ log_2 fold change vs WT	*r3b2*$^-$ log_2 fold change vs WT
90984	1	***-4.93***	***-2.91***	**-5.34**
95912	0.99	***-4.87***	***-3.11***	**N/A**
90984	1	***-4.77***	***-2.38***	**-3.84**
33232	1	***-4.71***	***-3.29***	**-9.34**
94432	1	***-4.68***	***-2.85***	**-6.11**
26072	1	***-4.62***	***-2.27***	**-7.09**
33232	1	***-4.59***	***-3.46***	**-7.17**
80802	0.98	***-4.54***	***-3.86***	**-7.25**
91526	0.99	***-4.40***	***-2.04***	**-4.56**
92910	1	***-4.40***	***-2.61***	**-8.70**
95769	1	***-4.32***	***-3.67***	**-8.13**
90984	0.99	***-4.30***	***-2.40***	**-4.77**
85485	0.99	***-4.26***	***-2.92***	**N/A**
93701	1	***-4.18***	***-2.93***	**-5.02**
32935	1	***-4.18***	***-2.77***	**-7.58**
86723	1	***-4.16***	***-2.80***	**-8.03**
78876	1	***-4.14***	***-3.15***	**-7.12**
49491	1	***-4.13***	***-2.88***	**-6.89**
31063	1	***-4.09***	***-2.93***	**-6.27**
82069	1	***-4.06***	***-2.39***	**-5.22**
94060	1	***-4.06***	***-2.09***	**-4.96**
75718	1	***-4.00***	***-2.26***	**-6.05**
49570	1	***-3.96***	***-2.01***	**N/A**
95442	1	***-3.96***	***-2.77***	**N/A**
9772	1	***-3.94***	***-3.06***	**-7.79**
31113	1	***-3.91***	***-3.15***	**-7.04**
46819	1	***-3.89***	***-2.12***	**-5.69**
83076	0.99	***-3.88***	***-2.29***	**-8.46**
45935	1	***-3.85***	***-2.12***	**-5.07**
88809	1	***-3.84***	***-3.21***	**-6.01**
30744	1	***-3.82***	***-2.68***	**-9.13**
49230	1	***-3.81***	***-2.80***	**-6.57**
30003	0.95	***-3.74***	***-2.74***	**-8.78**
90984	1	***-3.73***	***-2.37***	**-3.61**
39013	1	***-3.73***	***-2.32***	**-5.95**
91672	1	***-3.72***	***-2.73***	**-6.52**
94795	1	***-3.68***	***-2.11***	**-6.90**
90840	1	***-3.68***	***-3.18***	**-8.03**
88521	1	***-3.67***	***-3.39***	**-5.59**
95916	1	***-3.67***	***-2.65***	**-5.58**
76286	1	***-3.66***	***-3.09***	**-6.33**
32205	1	***-3.61***	***-3.32***	**-8.53**
48786	1	***-3.60***	***-3.85***	**-7.44**
89824	0.89	***-3.57***	***-3.62***	**-7.48**
30895	1	***-3.57***	***-3.42***	**-6.33**
82643	1	***-3.56***	***-2.58***	**-7.77**
30682	1	***-3.56***	***-2.29***	**-7.61**
90216	1	***-3.55***	***-2.89***	**-5.57**
93377	1	***-3.55***	***-2.85***	**-7.09**
28312	1	***-3.52***	***-2.68***	**-6.31**
49864	1	***-3.52***	***-2.22***	**-4.19**
93704	1	***-3.50***	***-2.78***	**-7.31**
86459	1	***-3.50***	***-2.45***	**-6.58**
69078	1	***-3.48***	***-2.88***	**-5.90**
89415	1	***-3.48***	***-2.97***	**-6.85**
90050	1	***-3.47***	***-3.01***	**-6.91**
87875	1	***-3.47***	***-2.09***	**-6.18**
93667	1	***-3.47***	***-2.64***	**-5.52**
72589	1	***-3.46***	***-2.85***	**-8.98**
48894	1	***-3.44***	***-2.94***	**-8.41**
89958	1	***-3.43***	***-3.23***	**-6.63**
50847	1	***-3.43***	***-2.68***	**-7.53**
87389	1	***-3.40***	***-2.43***	**-7.15**
31161	1	***-3.40***	***-2.71***	**-5.58**
79772	1	***-3.39***	***-2.77***	**-6.99**
92569	1	***-3.38***	***-2.64***	**-7.07**
46783	1	***-3.38***	***-3.26***	**-7.83**
80695	1	***-3.36***	***-2.52***	**-4.96**
88703	1	***-3.35***	***-2.87***	**-6.36**
46104	1	***-3.34***	***-2.63***	**N/A**
83434	1	***-3.33***	***-3.23***	**-7.02**
73842	1	***-3.32***	***-2.78***	**-7.19**
51719	1	***-3.31***	***-2.54***	**-4.64**
43928	0.99	***-3.31***	***-2.96***	**-5.30**
44126	1	***-3.30***	***-2.77***	**-6.01**
33806	1	***-3.29***	***-2.11***	**-8.17**
90407	1	***-3.28***	***-2.57***	**-8.08**
36942	1	***-3.28***	***-2.65***	**-7.24**
93671	1	***-3.27***	***-2.10***	**-9.25**
50312	-0.83	***-3.27***	***-2.81***	**-4.83**
51948	1	***-3.26***	***-2.35***	**-5.90**

ID	WT strand bias	*rdrp1*⁻ $\log_2$ fold change vs WT	*rdrp2*⁻ $\log_2$ fold change vs WT	*r3b2*⁻ $\log_2$ fold change vs WT
48566	1	-3.26	-2.06	-6.78
85633	1	-3.26	-2.21	-9.40
79712	1	-3.26	-2.82	-5.15
27316	1	-3.26	-2.52	-6.88
48456	1	-3.25	-2.63	-9.17
75510	1	-3.23	-2.66	-6.67
77712	1	-3.23	-2.68	-6.64
84716	1	-3.22	-2.87	-6.21
85759	0.99	-3.21	-2.59	-6.19
40368	1	-3.21	-2.26	-7.33
94671	1	-3.21	-2.81	-7.32
90427	1	-3.21	-3.09	-6.77
92297	1	-3.21	-2.41	-5.15
23700	1	-3.21	-2.34	-6.54
41731	1	-3.20	-2.87	-6.39
88521	1	-3.20	-2.77	-4.75
93377	1	-3.18	-2.50	-6.45
92837	1	-3.14	-2.99	-5.18
81329	0.99	-3.14	-3.12	N/A
87875	1	-3.13	-2.63	-5.81
76389	1	-3.13	-2.39	-8.25
27189	1	-3.12	-2.69	-7.64
93112	1	-3.12	-2.08	-7.89
29038	1	-3.12	-2.11	-5.83
92909	0.99	-3.11	-2.50	-6.68
28312	1	-3.10	-2.06	-7.29
68839	1	-3.10	-2.32	-3.76
81601	1	-3.10	-2.94	-7.07
80729	1	-3.09	-2.14	N/A
72128	1	-3.09	-2.41	-6.98
76861	1	-3.08	-2.71	-6.76
78974	1	-3.07	-3.49	-7.19
26855	1	-3.07	-2.68	-5.71
85759	1	-3.07	-2.62	-6.81
90989	1	-3.07	-3.35	-4.96
22420	1	-3.07	-2.31	-8.13
95180	1	-3.07	-3.32	-6.60
84236	1	-3.05	-2.31	-6.77
83427	1	-3.05	-2.16	-8.00
90661	1	-3.03	-2.34	-7.13
39231	0.98	-3.03	-2.61	-5.37
80392	1	-3.03	-3.20	-7.00
84935	0.99	-3.02	-2.71	-6.34
37397	1	-3.01	-2.73	-4.90
36402	1	-3.01	-2.35	-5.95
71319	1	-3.01	-2.82	-6.61
78510	1	-3.01	-2.28	-5.32
88759	1	-3.00	-2.32	-6.58
35570	1	-3.00	-2.83	-7.61
86091	1	-3.00	-2.27	-7.51
84211	1	-3.00	-2.21	-5.89
26919	1	-3.00	-2.38	-7.34
33319	1	-2.99	-3.06	-4.81
78974	1	-2.99	-3.26	-6.97
84311	1	-2.99	-2.15	-4.71
93567	1	-2.98	-2.18	-7.01
89243	1	-2.98	-2.27	-5.01
94941	1	-2.98	-2.69	-6.79
12399	1	-2.98	-2.83	-5.18
76134	1	-2.97	-2.65	-5.04
75313	1	-2.96	-2.19	-7.96
33458	1	-2.96	-2.56	-6.61
84114	1	-2.95	-2.63	-7.63
90057	1	-2.95	-2.81	-3.16
89950	1	-2.95	-2.84	-7.05
34025	1	-2.95	-2.04	-6.27
29487	1	-2.94	-2.86	-7.48
70091	0.98	-2.93	-2.89	-6.38
91230	1	-2.93	-2.64	-6.21
50500	1	-2.92	-2.52	-4.74
45044	1	-2.92	-2.59	-5.80
93787	1	-2.92	-2.28	-5.64
48059	1	-2.91	-2.60	-5.65
95140	1	-2.91	-2.45	-4.11
82159	1	-2.90	-2.35	-5.92
90918	1	-2.89	-2.38	-4.28
82482	1	-2.88	-3.08	-5.18
48786	1	-2.88	-2.24	-5.55
93782	1	-2.88	-3.04	-7.78
80802	1	-2.86	-2.04	-7.45
20075	1	-2.86	-2.67	-6.83
92734	1	-2.85	-2.56	-6.21
51408	1	-2.84	-3.00	-4.37
50238	1	-2.84	-2.59	-4.46
91591	1	-2.84	-3.14	-4.10
41987	1	-2.83	-2.06	-7.87
94401	1	-2.83	-2.81	-5.90
93173	0.99	-2.83	-2.37	-5.02
89017	1	-2.82	-2.34	-5.64
95599	1	-2.82	-2.82	-4.75
29691	1	-2.81	-2.15	-6.77
82047	1	-2.81	-2.52	-6.93
86333	1	-2.81	-2.40	-4.38
13626	1	-2.80	-2.14	-6.49
92089	1	-2.80	-2.21	-9.01
44205	1	-2.79	-2.22	N/A
44640	1	-2.78	-2.17	-9.76

ID	WT strand bias	*rdrp1*⁻ log_2 fold change vs WT	*rdrp2*⁻ log_2 fold change vs WT	*r3b2*⁻ log_2 fold change vs WT
88605	1	-2.77	-2.59	-7.39
46623	1	-2.76	-2.29	-4.39
94991	1	-2.76	-2.45	-7.47
44594	1	-2.75	-2.45	-6.23
43913	1	-2.75	-2.93	-6.38
93857	1	-2.75	-2.23	-5.28
94013	0.92	-2.75	-2.16	-6.06
50834	1	-2.75	-2.16	-6.92
87231	1	-2.73	-2.17	-7.97
37057	1	-2.73	-2.08	-7.45
93155	1	-2.71	-2.50	-8.07
91714	1	-2.71	-2.49	-5.79
92731	1	-2.71	-2.42	-5.76
48484	1	-2.70	-2.79	-7.04
94942	1	-2.70	-2.20	-7.59
91077	1	-2.70	-2.48	-7.87
93008	0.99	-2.69	-2.16	-4.70
30046	1	-2.69	-2.27	-7.18
45044	1	-2.68	-2.47	-5.01
79972	1	-2.68	-2.79	-8.31
38120	1	-2.67	-2.30	-5.69
31124	1	-2.67	-2.43	-5.75
30744	1	-2.66	-2.36	-6.22
92017	1	-2.66	-2.20	-7.61
77001	1	-2.66	-2.45	-5.23
90832	1	-2.65	-2.03	-7.43
42284	1	-2.65	-3.29	-6.25
95682	1	-2.65	-2.77	-4.09
48444	1	-2.65	-2.25	-6.11
93193	1	-2.65	-2.35	-7.31
81743	1	-2.64	-2.63	-4.49
77450	0.74	-2.64	-2.27	-4.74
87683	1	-2.62	-2.25	-7.05
39200	1	-2.62	-2.23	-5.97
84536	1	-2.62	-2.56	-6.99
93264	0.92	-2.62	-2.11	-5.52
31320	1	-2.60	-2.00	-4.66
89322	1	-2.58	-2.11	-5.52
90112	1	-2.58	-2.43	-6.07
93252	1	-2.57	-2.35	-7.15
50168	1	-2.57	-2.77	-5.41
18759	1	-2.56	-2.48	-6.42
92731	1	-2.56	-2.17	-7.26
81408	1	-2.56	-2.34	-4.98
94112	1	-2.55	-2.24	-6.85
90782	1	-2.55	-2.01	-7.56
32834	1	-2.55	-2.05	-5.14
48455	1	-2.54	-2.64	-5.28
91279	1	-2.54	-2.42	-6.50
44822	1	-2.54	-2.12	-5.24
80586	1	-2.53	-2.49	-5.77
91915	1	-2.53	-2.08	-6.49
76793	1	-2.53	-2.14	-5.37
77377	1	-2.52	-2.09	-6.08
76244	1	-2.52	-2.08	-7.30
79571	1	-2.50	-2.52	-4.92
46783	1	-2.50	-2.24	-6.90
87333	1	-2.49	-2.26	-5.85
94072	1	-2.49	-2.53	-6.34
89721	1	-2.49	-2.35	-6.96
78799	1	-2.48	-2.11	-6.06
91374	1	-2.47	-2.13	-5.27
47690	1	-2.46	-2.21	-8.62
86793	1	-2.46	-2.37	-6.80
25723	1	-2.46	-2.12	-6.09
50382	1	-2.44	-2.28	-5.98
79616	1	-2.42	-2.15	-5.50
47807	1	-2.40	-2.43	-4.64
31788	1	-2.38	-2.04	-5.68
95473	1	-2.38	-2.28	-3.75
47676	1	-2.38	-2.29	-6.41
94003	1	-2.38	-2.61	-3.22
79227	1	-2.36	-2.25	-4.37
74888	1	-2.35	-2.26	N/A
91660	0.99	-2.35	-2.24	-5.47
95461	0.95	-2.35	-2.26	-3.87
88998	1	-2.34	-2.02	-5.03
90918	1	-2.33	-2.01	-4.06
43050	1	-2.30	-2.31	-7.49
86763	1	-2.30	-2.28	-5.84
89561	1	-2.29	-2.23	-5.90
95242	1	-2.29	-2.13	-6.16
29487	1	-2.28	-2.31	-5.15
44317	1	-2.27	-2.01	N/A
81551	1	-2.26	-2.15	-3.90
89517	1	-2.26	-2.12	-6.11
32912	1	-2.26	-2.60	N/A
78620	1	-2.25	-2.16	-3.76
43858	1	-2.23	-2.75	-3.69
9964	1	-2.22	-2.60	-5.13
81477	1	-2.21	-2.22	-4.42
87856	1	-2.20	-2.21	-5.19
50622	1	-2.19	-2.18	-3.75
93011	1	-2.19	-2.15	-5.93
25842	1	-2.18	-2.40	-5.55
43628	0.99	-2.18	-2.08	-7.72
93656	0.87	-2.17	-2.98	-6.34

ID	WT strand bias	*rdrp1*⁻ log_2 fold change vs WT	*rdrp2*⁻ log_2 fold change vs WT	*r3b2*⁻ log_2 fold change vs WT
90750	1	-2.16	-2.48	N/A
38927	1	-2.14	-2.04	-3.72
46895	1	-2.13	-2.05	-8.62
20135	1	-2.13	-2.13	-4.81
79055	1	-2.11	-2.15	-4.94
46410	1	-2.09	-2.06	-3.52
68633	1	-2.08	-2.00	-6.53
92598	1	-2.05	-2.18	-4.18
48729	1	-2.03	-2.23	-3.73
94535	1	-2.02	-2.26	-5.98
91622	1	-2.02	-2.12	-4.56
51186	1	-2.01	-2.19	-6.69
9831	1	-2.00	-2.54	-4.51
95318	1	-5.25	-1.97	-6.18
88145	0.99	-4.85	-1.65	-7.23
91412	1	-4.20	-1.01	-6.76
94060	1	-3.89	-1.74	-3.31
95037	1	-3.85	-1.49	-5.72
45935	1	-3.84	-1.98	-5.54
80539	1	-3.72	-1.31	-4.12
47616	1	-3.71	-1.63	-6.23
30682	0.97	-3.67	-1.65	-7.97
80406	1	-3.64	-1.98	-5.29
87857	1	-3.60	-1.49	-5.06
93776	1	-3.41	-1.31	-6.58
92625	0.97	-3.39	-1.92	-5.80
49344	0.98	-3.38	-0.56	-4.87
89960	1	-3.35	-1.68	-4.59
46568	1	-3.30	-0.81	-5.38
89569	1	-3.27	-0.61	-5.56
73863	1	-3.26	-1.80	N/A
91193	0.99	-3.24	-1.41	-4.92
88136	1	-3.18	-1.94	-7.43
48022	1	-3.17	-1.94	-9.19
90890	1	-3.15	-1.82	-6.39
85063	1	-3.08	-1.13	N/A
47076	0.98	-3.07	-0.32	-3.79
49444	1	-3.07	-1.99	-8.02
91403	1	-2.99	-1.39	-5.88
92884	1	-2.98	-1.83	-4.66
51816	1	-2.97	-1.74	-4.16
96091	0.98	-2.95	-1.74	-5.43
86952	0.99	-2.95	0.05	-3.97
49344	0.98	-2.95	0.11	-4.33
77956	1	-2.94	-1.74	-8.07
95369	1	-2.94	-1.39	N/A
71281	1	-2.94	-1.89	-6.97
94536	1	-2.93	-1.93	-5.32
30682	1	-2.91	-1.61	-5.13
93564	1	-2.91	-1.56	-6.39
47565	1	-2.87	-1.54	-7.66
91173	1	-2.86	-1.83	-5.59
11610	0.99	-2.85	0.03	-3.09
48950	1	-2.85	-1.80	-4.94
51849	1	-2.84	-1.85	-5.29
78965	1	-2.83	-1.33	-5.01
85005	0.94	-2.82	-1.73	-5.10
93002	1	-2.82	0.13	-5.51
30700	1	-2.81	-1.83	-6.39
92607	1	-2.80	-1.71	-6.58
91590	1	-2.78	-1.82	-7.62
94997	1	-2.78	-0.98	-5.95
76277	1	-2.77	-1.00	-5.11
93592	1	-2.77	-1.24	-4.66
25571	1	-2.76	-1.96	-7.16
86055	1	-2.75	-1.65	-6.50
73872	0.98	-2.75	-1.93	-8.47
76823	1	-2.75	-1.76	-4.65
77714	1	-2.74	-1.84	-5.65
77774	1	-2.73	-1.90	-7.02
49974	1	-2.72	-1.89	-7.84
87147	1	-2.71	-0.89	-5.26
90691	1	-2.70	-1.83	-6.63
91672	1	-2.70	-1.75	-4.92
92655	1	-2.69	-1.68	-5.93
87586	1	-2.68	-1.62	-6.03
37988	0.65	-2.67	-1.53	-6.27
26602	1	-2.67	-1.69	-6.85
75629	1	-2.66	-1.53	-5.08
82167	1	-2.66	-1.75	-6.22
90890	1	-2.65	-1.36	-5.14
28089	1	-2.65	-1.47	-5.85
89684	1	-2.65	-1.67	-6.42
82741	1	-2.64	-1.65	-6.53
69078	1	-2.63	-1.72	-4.63
87636	1	-2.63	-1.81	-7.22
49981	1	-2.62	-1.99	-6.81
84769	1	-2.62	-1.58	-4.35
48719	1	-2.62	-1.11	-8.85
89569	1	-2.61	0.27	-4.49
89707	0.89	-2.61	-1.69	-5.41
90924	1	-2.61	-1.94	-6.58
85096	1	-2.61	-1.84	N/A
49864	0.94	-2.60	-1.54	-4.01
93760	0.98	-2.59	-0.89	-4.73
17522	1	-2.58	-1.84	-6.70
94383	1	-2.58	-1.61	-4.81

ID	WT strand bias	*rdrp1*⁻ log_2 fold change vs WT	*rdrp2*⁻ log_2 fold change vs WT	*r3b2*⁻ log_2 fold change vs WT
46576	1	-2.54	-1.28	-5.82
10358	1	-2.54	-1.66	-5.11
83198	1	-2.54	-1.59	-6.06
90548	1	-2.54	-1.69	-6.32
82855	1	-2.53	-1.71	-5.75
34433	1	-2.53	-1.82	-6.78
95947	1	-2.53	-0.87	-6.11
81707	0.38	-2.51	-1.88	-4.75
91279	1	-2.51	-1.70	-8.09
92704	0.96	-2.51	-1.83	-7.33
84389	1	-2.51	-1.38	-5.76
81173	1	-2.50	-1.76	-6.64
80609	1	-2.50	-1.39	-6.53
45528	1	-2.49	-1.59	-5.72
74535	0.98	-2.47	-0.81	-5.51
94446	1	-2.45	-1.35	-6.84
25669	1	-2.44	-1.36	-5.89
82711	1	-2.44	-1.77	N/A
79080	1	-2.43	-1.90	-7.57
95521	0.98	-2.42	-1.82	-5.19
28514	1	-2.42	-1.74	-7.70
19077	1	-2.41	-1.55	-4.51
88300	1	-2.41	-1.89	-5.62
94101	0.99	-2.40	-1.34	-3.83
44832	1	-2.40	-1.79	-4.14
87442	1	-2.40	-1.69	-6.95
32471	1	-2.40	-1.27	-6.21
92041	0.98	-2.39	-1.45	-5.17
33534	0.88	-2.39	-1.32	-4.99
92436	1	-2.39	-1.88	-8.17
91641	1	-2.38	-1.80	-3.63
77082	1	-2.38	-0.75	-4.61
50181	1	-2.37	-1.24	-6.48
91611	1	-2.37	-1.61	-5.96
91330	1	-2.37	-1.91	-6.86
89689	1	-2.36	-1.40	-8.27
87510	0.99	-2.36	-1.53	-5.28
88612	1	-2.35	-1.91	-5.11
46819	1	-2.35	-0.54	-3.86
29806	1	-2.34	-1.77	-4.63
93704	1	-2.34	-1.78	-6.07
48438	1	-2.34	-1.68	-6.45
92587	1	-2.34	-1.72	-8.29
77340	1	-2.33	-1.89	-3.95
25669	1	-2.33	-0.84	-6.33
49444	1	-2.33	-1.50	N/A
26661	1	-2.32	-1.75	-4.78
93550	1	-2.32	-1.78	-5.32
89689	1	-2.31	-1.51	-5.32
84249	0.98	-2.31	-1.69	-5.33
48886	0.99	-2.31	-1.65	-5.71
77585	1	-2.30	-1.33	-5.06
83388	1	-2.30	-1.93	-5.07
34228	1	-2.30	0.64	-7.10
84572	0.97	-2.30	-1.96	-5.30
90661	1	-2.29	-1.78	-8.58
78707	1	-2.29	-1.75	-6.23
91410	1	-2.28	-0.92	N/A
35064	1	-2.28	-1.63	-5.62
77450	1	-2.28	-1.77	-4.62
81582	1	-2.27	-1.71	-5.23
9840	1	-2.26	-1.08	-4.54
46467	1	-2.25	-1.04	-3.06
90244	1	-2.24	-1.81	-6.17
89561	1	-2.24	-1.64	-6.13
30173	1	-2.24	-1.48	-3.43
82657	1	-2.24	-1.80	-5.92
92814	1	-2.23	-1.78	-5.33
78510	0.98	-2.22	-1.91	-3.36
51704	1	-2.22	-1.77	-5.78
88216	1	-2.22	-1.80	-4.86
80723	1	-2.22	-1.94	N/A
49230	1	-2.20	-1.46	-6.74
94430	1	-2.20	-1.91	-7.48
93342	1	-2.20	-1.94	-4.84
90052	1	-2.20	-1.97	-6.30
94169	1	-2.19	-1.86	-6.09
84708	1	-2.19	-1.85	-5.92
88585	1	-2.19	-1.21	-6.57
80329	1	-2.19	-1.38	-5.37
77832	1	-2.18	-1.93	-4.11
36097	1	-2.18	-1.26	-4.52
47757	1	-2.17	-1.98	-5.75
48221	0.99	-2.17	-1.84	-5.90
92625	1	-2.16	-0.68	-4.29
86682	0.99	-2.16	-1.14	-6.47
73640	1	-2.16	-1.53	-5.18
90418	1	-2.16	-1.17	-5.25
93252	1	-2.16	-1.91	-5.82
47858	1	-2.15	-1.99	-5.48
90087	1	-2.15	-1.59	-5.44
79230	1	-2.15	-1.78	-6.33
92548	0.99	-2.13	-1.53	-5.52
74934	1	-2.13	-1.59	-5.35
93865	0.97	-2.13	-1.90	-5.47
74489	1	-2.13	-1.93	-4.35
90593	1	-2.13	-1.36	-6.22

ID	WT strand bias	*rdrp1*⁻ log_2 fold change vs WT	*rdrp2*⁻ log_2 fold change vs WT	*r3b2*⁻ log_2 fold change vs WT
30389	1	***-2.12***	-1.94	**-4.65**
25671	1	***-2.11***	-1.75	**-6.02**
87442	0.99	***-2.11***	-1.85	**-7.65**
92956	1	***-2.11***	-1.54	**-5.78**
82256	1	***-2.11***	-1.64	**-5.52**
90517	1	***-2.11***	-1.55	**-5.67**
73075	1	***-2.10***	-1.08	**-5.16**
51832	1	***-2.10***	-1.79	**-6.62**
90350	1	***-2.10***	-1.49	**-5.38**
93247	1	***-2.10***	-1.91	**-4.77**
72331	1	***-2.09***	-1.81	**-4.57**
30862	1	***-2.09***	-1.19	**-4.87**
37276	1	***-2.08***	-1.76	**-5.11**
85247	1	***-2.08***	-0.96	**-3.68**
94219	1	***-2.08***	-1.25	**-7.36**
89581	0.99	***-2.08***	-1.95	**-4.41**
93112	1	***-2.08***	-1.65	**-5.90**
89911	1	***-2.08***	-1.99	**-6.04**
19729	1	***-2.08***	-1.65	**-4.32**
93798	1	***-2.08***	-1.91	**-5.73**
87336	0.98	***-2.07***	-0.77	**-4.22**
92251	1	***-2.07***	-1.54	**-7.78**
84389	1	***-2.07***	-1.44	**-7.00**
89441	0.92	***-2.06***	-1.35	**-6.71**
93904	1	***-2.05***	-1.92	**-6.60**
84219	1	***-2.05***	-1.84	**-4.57**
95393	1	***-2.05***	-1.81	**-5.30**
46668	1	***-2.05***	-1.39	**-5.28**
33583	1	***-2.04***	-1.29	**-6.69**
49010	0.99	***-2.04***	-1.60	**-5.23**
83708	0.99	***-2.04***	-1.07	**-4.78**
50610	1	***-2.03***	-1.33	**-3.58**
72170	1	***-2.03***	-1.91	**-4.52**
92495	1	***-2.03***	-1.99	**-5.68**
93496	1	***-2.03***	-1.20	**-6.71**
47337	1	***-2.03***	-1.35	**-3.75**
90047	0.99	***-2.03***	-1.94	**-7.74**
95147	1	***-2.03***	-1.91	**-4.24**
93861	1	***-2.02***	-1.97	**-4.48**
83547	1	***-2.02***	-1.64	**-4.88**
75695	1	***-2.01***	-1.94	**-4.93**
95936	1	***-2.01***	-1.48	**-5.12**
92273	1	-1.98	***-2.63***	-1.91
43525	0.99	-1.98	***-2.14***	**-7.00**
84270	0.99	-1.96	***-2.13***	**-3.80**
91591	1	-1.94	***-2.03***	**-5.45**
84706	1	-1.90	***-2.59***	**-2.85**
93812	1	-1.85	***-2.14***	**-4.98**
94340	1	-1.84	***-2.36***	**-5.62**
27020	1	-1.81	***-2.08***	**-4.76**
81551	1	-1.75	***-2.10***	**-3.64**
33097	1	-1.67	***-2.02***	**-3.67**
92352	0.99	-1.65	***-2.14***	**-2.12**
94066	0.9	-1.64	***-2.28***	**-5.14**
11398	1	-1.63	***-2.01***	**-3.01**
94691	1	-1.63	***-2.10***	**-2.79**
76715	1	-1.62	***-2.19***	**-3.10**
48630	1	-1.59	***-2.17***	**-3.32**
90057	0.95	-1.45	***-2.12***	**-2.58**
81169	1	-1.35	***-2.09***	**-3.54**
93824	0.95	-1.27	***-2.21***	**-3.18**
76247	0.96	-1.25	***-2.05***	**-2.11**

Table S4. Log_2 fold change of the *dicer*-dependent ex-siRNAs in the *r3b2*$^-$ mutant compared to wild type. Data from Supplementary Table S2 were taken to show the log_2 fold changes of the different classes of *dicer*-dependent ex-siRNAs in the *r3b2*$^-$ mutant. Log_2 of the fold changes in *dcl*$^-$ (*dcl-1*$^-$, *dcl-2*$^-$ and the double mutant *dcl-1*$^-$/*dcl-2*$^-$) and *rdrp*$^-$ (*rdrp-1*$^-$ and *rdrp-2*$^-$) mutants (Nicolás et al., 2010), as well as the log_2 fold change of Ago-1-bound siRNAs in the wild type compared with the *ago-1*$^-$ mutant (Cervantes et al., 2013) are also shown in this table. Data are sorted for the fold change in *dcl-2*$^-$ strain, which almost perfectly separated the four ex-siRNA classes from each other. Class I, II, III and IV exons have yellow, white, blue and grey background, respectively. Numbers in bold indicate values that represent a fourfold or larger change. Decrease in expression is shown in red and increase in expression is shown in green. n.d.: ex-siRNAs not detected among those specifically bound to Ago-1. N/A, not applicable.

ID	*dcl1*$^-$ log_2 fold change vs WT	*dcl2*$^-$ log_2 fold change vs WT	*dcl1/2*$^-$ log_2 fold change vs WT	*rdrp1*$^-$ log_2 fold change vs WT	*rdrp2*$^-$ log_2 fold change vs WT	Ago-1 bound WT log_2 fold change vs *ago-1*$^-$	*r3b2*$^-$ log_2 fold change
80452	0.34	**-29.71**	**-9.29**	**3.17**	-1.00	**9.34**	**4.74**
80794	0.33	**-29.12**	**-7.70**	**4.40**	-0.38	**7.31**	**-3.75**
80452	0.16	**-9.14**	**-7.02**	**3.98**	-1.53	**8.39**	**4.13**
80794	0.60	**-8.84**	**-9.88**	**3.78**	-1.30	**8.15**	**-3.66**
82197	-0.70	**-8.56**	**-7.53**	**6.51**	0.70	**7.69**	**4.24**
82372	1.54	**-8.31**	**-8.68**	**3.69**	**-2.71**	**8.27**	**-10.91**
80452	0.33	**-8.23**	**-10.32**	**2.13**	**-2.11**	**9.50**	**3.05**
80452	0.64	**-7.76**	**-10.86**	**3.87**	**-2.26**	**8.67**	1.49
85302	-0.14	**-5.89**	**-8.42**	**2.17**	-1.35	**7.47**	0.02
77442	0.12	**-7.74**	**-12.37**	**-8.99**	**-2.47**	**8.54**	**3.19**
83462	0.98	**-7.60**	**-6.91**	**-4.72**	1.40	**8.82**	**-2.97**
83987	0.19	**-7.45**	**-8.08**	**-5.35**	1.00	**n.d.**	**-4.23**
86881	0.05	**-6.93**	**-10.86**	**-6.53**	0.34	**8.45**	**-5.83**
77020	-0.30	**-6.64**	**-8.83**	**-6.47**	-0.50	**n.d.**	**n.d.**
82926	0.24	**-6.09**	**-9.52**	**-5.92**	0.97	**6.55**	**-4.82**
84406	-0.42	**-5.86**	**-8.07**	**-6.21**	-0.23	**6.15**	**-3.88**
80649	0.06	**-5.72**	**-8.95**	**-5.23**	1.54	**5.15**	-1.03
77050	0.15	**-5.66**	**-9.38**	**-5.88**	0.65	**6.73**	**-4.05**
86467	-0.00	**-5.65**	**-7.85**	**-6.07**	0.16	**n.d.**	**-3.93**
86354	0.66	**-5.60**	**-30.06**	**-4.66**	1.45	**n.d.**	**-5.59**
83611	0.49	**-5.58**	**-8.09**	**-4.95**	1.65	**7.46**	-1.64
84460	-0.17	**-5.52**	**-7.96**	**-6.20**	0.96	**6.55**	**-2.25**
86022	0.52	**-5.44**	**-8.27**	**-4.27**	1.94	**n.d.**	**-3.41**
82518	-0.11	**-5.43**	**-4.17**	**-3.57**	1.28	**5.18**	**n.d.**
83098	0.39	**-5.35**	**-5.71**	**-4.62**	0.51	**7.51**	**-5.46**
79776	0.56	**-5.34**	**-8.96**	**-6.26**	0.61	**6.79**	**-3.45**
76230	0.12	**-5.34**	**-9.53**	**-6.58**	0.23	**7.04**	**-3.81**
84929	0.96	**-5.32**	**-8.45**	**-5.83**	0.28	**5.23**	**-3.30**
77527	0.50	**-5.31**	**-9.88**	**-5.39**	1.17	**6.46**	**-3.52**
84406	0.83	**-5.30**	**-6.75**	**-4.58**	**2.30**	**6.99**	**-2.10**
81030	0.30	**-5.20**	**-5.38**	**-4.86**	0.52	**7.71**	**-5.83**
80938	0.75	**-5.17**	**-9.62**	**-5.04**	1.32	**7.15**	**-2.84**
79278	1.34	**-5.12**	**-6.57**	**-3.14**	**3.24**	**7.46**	**-2.12**
85623	-0.01	**-5.08**	**-8.41**	**-4.83**	1.27	**6.32**	**-2.84**
85642	-0.50	**-5.06**	**-10.56**	**-8.12**	-1.40	**7.09**	**-5.58**
84958	0.88	**-5.06**	**-8.51**	**-4.15**	1.71	**6.22**	-1.51
82471	0.17	**-5.05**	**-9.45**	**-5.59**	0.87	**6.51**	**-3.29**
84406	1.19	**-5.04**	**-8.22**	**-5.41**	1.08	**6.07**	**-3.41**
79493	0.30	**-4.96**	**-9.29**	**-5.27**	1.03	**7.18**	**-2.53**
83227	1.27	**-4.96**	**-30.49**	**-4.78**	1.57	**n.d.**	**n.d.**
86627	-0.21	**-4.93**	**-29.80**	**-5.61**	1.19	**5.85**	**-2.99**
76229	0.47	**-4.93**	**-8.61**	**-4.44**	**2.01**	**6.22**	**-2.53**
76403	1.37	**-4.91**	**-29.00**	**-5.64**	1.16	**n.d.**	**-3.23**
78466	-0.44	**-4.88**	**-7.79**	**-5.76**	0.78	**5.79**	**-3.64**
83695	0.91	**-4.87**	**-7.91**	**-4.18**	1.81	**5.61**	**-2.46**
81492	0.49	**-4.84**	**-7.58**	**-4.81**	1.19	**7.30**	**-2.77**
78304	0.16	**-4.79**	**-29.07**	**-7.88**	-0.55	**n.d.**	**-2.42**
12058	0.52	**-4.71**	**-8.28**	**-6.05**	0.25	**n.d.**	**n.d.**
78304	0.46	**-4.69**	**-5.99**	**-6.55**	-0.41	**n.d.**	**-3.51**
78325	1.15	**-4.66**	**-8.87**	**-3.19**	**3.75**	**7.34**	**-2.92**
83973	-0.17	**-4.64**	**-7.50**	**-5.26**	1.09	**5.14**	**-2.35**
83735	0.49	**-4.62**	**-8.66**	**-3.93**	**2.14**	**n.d.**	-1.31
76941	-0.11	**-4.62**	**-29.49**	**-6.29**	0.22	**n.d.**	**-4.74**
85423	0.78	**-4.60**	**-9.05**	**-5.69**	0.58	**6.85**	**-2.89**
79285	0.50	**-4.60**	**-9.93**	**-4.32**	1.56	**6.32**	**-2.70**
84944	0.22	**-4.57**	**-7.02**	**-5.18**	1.32	**6.28**	-1.99
86787	-0.06	**-4.55**	**-7.23**	**-4.70**	1.63	**6.53**	-1.46
12058	0.55	**-4.55**	**-8.29**	**-6.02**	0.29	**n.d.**	**n.d.**
84646	0.45	**-4.52**	**-29.13**	**-3.76**	**2.95**	**5.72**	**-3.16**
83826	0.02	**-4.49**	**-8.68**	**-5.74**	0.73	**5.42**	**-2.38**
85223	1.19	**-4.48**	**-7.46**	**-3.56**	**3.22**	**7.34**	**-2.51**
85857	0.41	**-4.48**	**-7.16**	**-5.34**	0.96	**6.99**	**-4.09**
84944	0.38	**-4.46**	**-8.97**	**-4.42**	1.87	**6.42**	**-3.62**
79511	-0.31	**-4.46**	**-9.39**	**-6.19**	0.45	**6.27**	**-3.77**
86335	0.28	**-4.43**	**-7.53**	**-4.61**	1.52	**7.26**	**-3.30**
82833	0.30	**-4.42**	**-9.38**	**-4.28**	1.78	**6.99**	**-3.88**
83411	0.92	**-4.42**	**-9.81**	**-4.95**	1.82	**6.61**	**-2.24**
81899	0.45	**-4.42**	**-9.39**	**-5.87**	0.68	**6.91**	**-3.39**
78926	1.33	**-4.42**	**-9.36**	**-5.19**	1.31	**6.67**	**-3.32**
84773	0.15	**-4.42**	**-6.70**	**-5.81**	0.33	**n.d.**	**-3.30**
83986	0.55	**-4.40**	**-6.30**	**-5.47**	0.75	**7.20**	**-4.04**
80992	0.53	**-4.40**	**-10.88**	**-5.55**	1.27	**5.92**	**-2.48**
77205	1.47	**-4.36**	**-7.99**	**-5.26**	1.12	**6.28**	**-2.86**
94382	0.20	**-4.35**	**-6.32**	**-5.34**	1.69	**5.97**	-1.01
86261	0.76	**-4.33**	**-9.10**	**-4.81**	1.93	**6.95**	**-3.29**
83353	1.11	**-4.32**	**-6.67**	**-4.18**	**2.05**	**6.85**	-1.60

ID	*dcl1*⁻ $\log_2$ fold change vs WT	*dcl2*⁻ $\log_2$ fold change vs WT	*dcl1*⁻/*2*⁻ $\log_2$ fold change vs WT	*rdrp1*⁻ $\log_2$ fold change vs WT	*rdrp2*⁻ $\log_2$ fold change vs WT	Ago-1 bound WT $\log_2$ fold change vs *ago-1*⁻	*r3b2*⁻ $\log_2$ fold change
84657	0.04	-4.29	-10.78	-5.64	0.99	5.50	-2.42
77020	0.68	-4.26	-10.91	-0.09	1.81	7.21	-0.43
78887	0.33	-4.25	-9.68	-6.63	-0.09	n.d.	-5.59
76982	0.37	-4.23	-7.14	-4.32	2.24	5.83	-0.49
85309	0.86	-4.22	-8.06	-4.30	2.30	7.57	-2.91
84773	0.36	-4.21	-7.09	-5.28	1.23	6.08	-2.77
81795	0.37	-4.20	-5.99	-4.36	2.32	6.22	-2.33
81796	0.37	-4.20	-5.99	-4.36	2.32	6.22	-2.33
76077	0.87	-4.19	-8.31	-4.79	1.48	7.02	-2.52
81619	0.33	-4.17	-7.69	-4.59	1.33	7.49	-2.24
84461	1.62	-4.15	-7.65	-4.70	1.66	5.90	-2.39
77036	0.67	-4.14	-6.99	-4.82	1.49	5.93	-1.34
83986	0.79	-4.13	-9.25	-4.61	1.93	6.93	-2.76
76488	0.17	-4.10	-6.73	-6.79	-1.36	7.92	-3.93
83187	0.50	-4.08	-8.31	-5.46	0.86	5.94	-2.32
84912	0.92	-4.07	-8.22	-3.81	2.84	5.38	-2.07
84406	0.50	-4.05	-8.09	-5.22	1.11	6.03	-2.62
76230	0.47	-4.05	-10.12	-5.55	1.06	6.83	-4.35
83986	-0.21	-4.04	-8.77	-5.29	1.04	7.66	-3.51
77325	0.84	-3.99	-8.45	-4.92	2.00	7.18	-2.28
77038	0.01	-3.98	-8.47	-5.57	0.83	5.18	-3.51
76158	-0.02	-3.98	-6.56	-5.74	0.40	6.25	-3.54
82415	-0.02	-3.98	-6.56	-5.74	0.40	6.25	-3.54
84406	-0.69	-3.97	-30.12	-6.46	-1.07	n.d.	-5.41
83549	-0.47	-3.96	-10.80	-6.69	0.16	6.75	-3.26
84826	1.48	-3.96	-9.56	-5.25	1.27	5.66	-3.49
86260	0.52	-3.95	-8.91	-5.23	1.68	7.02	-3.68
86330	1.01	-3.93	-8.50	-5.92	1.22	6.80	-1.86
78207	1.14	-3.93	-7.59	-3.09	3.29	5.98	-0.52
85624	0.45	-3.93	-7.54	-2.66	3.00	5.92	-2.19
80938	0.65	-3.92	-7.24	-4.87	1.46	7.03	-1.94
84919	0.63	-3.91	-8.15	-5.12	1.31	6.84	-2.81
77142	1.23	-3.91	-6.36	-3.74	2.35	5.12	-0.95
84945	1.01	-3.89	-7.96	-5.55	1.07	6.94	-3.13
95230	0.58	-3.87	-5.83	-3.86	2.44	5.68	-1.62
95350	0.58	-3.87	-5.83	-3.86	2.44	5.68	-1.62
94937	0.57	-3.87	-5.83	-3.86	2.44	5.66	-1.61
85309	1.23	-3.86	-7.98	-3.21	2.96	5.78	-1.82
76071	1.56	-3.86	-6.89	-4.42	2.39	7.55	-1.99
83115	0.49	-3.83	-29.87	-7.36	0.32	n.d.	-5.77
78520	0.25	-3.83	-6.85	-5.07	1.44	5.72	-2.86
80750	0.74	-3.83	-9.19	-4.83	1.43	7.03	-1.69
79511	0.35	-3.82	-5.88	-4.82	1.51	5.64	-1.69
77620	0.75	-3.81	-7.41	-4.64	1.69	6.77	-0.93
78345	0.21	-3.74	-8.67	-5.13	1.13	6.70	-2.38
77620	0.82	-3.73	-6.51	-5.19	1.09	7.08	-2.33
82247	2.00	-3.73	-6.07	-5.01	1.06	6.24	-2.07
86417	0.59	-3.73	-28.92	-4.82	1.69	7.25	-2.09
84880	0.10	-3.73	-7.29	-5.47	0.94	6.69	-2.28
79798	0.98	-3.70	-7.88	-5.27	1.57	6.28	-3.17
77325	0.46	-3.69	-8.77	-5.24	0.63	5.78	-2.89
80110	0.34	-3.69	-7.20	-4.85	1.48	6.78	-1.68
82337	-0.24	-3.68	-1.50	-3.52	2.83	4.37	-1.89
85526	0.10	-3.65	-8.07	-5.47	1.19	6.30	-2.36
77503	0.65	-3.64	-6.38	-4.22	2.03	5.89	-1.83
79713	0.67	-3.64	-8.70	-4.87	1.61	7.57	-2.85
13790	0.22	-3.63	-9.32	-4.07	1.33	5.71	-2.79
82579	1.06	-3.60	-5.52	-4.20	2.31	5.48	-1.30
82472	1.22	-3.59	-6.65	-4.05	2.38	6.92	-1.59
84478	0.21	-3.57	-7.72	-5.90	0.70	6.58	-3.13
78553	0.24	-3.57	-8.94	-6.11	1.44	6.17	-2.29
85021	0.78	-3.55	-7.46	-4.10	2.13	6.29	-1.85
93912	1.07	-3.53	-6.00	-4.02	2.24	5.96	-1.51
85822	0.68	-3.53	-7.55	-5.23	1.09	6.48	-2.79
80749	-0.41	-3.53	-7.50	-6.09	0.54	5.79	-4.02
85421	1.05	-3.49	-8.49	-5.02	1.07	7.60	-0.57
79753	0.57	-3.49	-7.58	-4.63	1.76	6.87	-2.21
81619	-0.39	-3.49	-30.84	-6.12	-0.09	5.83	-4.47
81974	0.69	-3.44	-7.86	-4.46	1.93	6.35	-1.08
92875	0.43	-3.44	-6.06	-6.46	0.65	7.33	-2.33
77039	0.66	-3.42	-6.45	-5.00	1.79	6.91	-1.06
75923	0.94	-3.40	-7.31	-4.38	1.87	6.74	-1.94
80762	0.70	-3.35	-7.55	-4.45	2.05	5.96	-2.68
84987	0.89	-3.33	-9.06	-5.55	0.23	7.31	-3.44
94937	0.86	-3.33	-5.22	-5.27	1.23	5.03	-4.21
93912	0.87	-3.32	-5.22	-5.25	1.22	5.00	-4.01
95230	0.87	-3.32	-5.22	-5.25	1.22	5.00	-4.31
95350	0.87	-3.32	-5.22	-5.32	1.19	4.99	-4.33
77620	0.26	-3.32	-10.06	-5.60	0.86	n.d.	-6.06
78952	-0.28	-3.28	-6.65	-5.47	0.60	5.62	-2.13
78302	-0.00	-3.24	-10.74	-6.47	0.17	5.80	-2.64
81974	0.69	-3.24	-8.11	-3.84	2.77	5.40	-0.98
82337	0.45	-3.21	-4.67	-4.69	1.41	5.00	-2.91
85972	1.16	-3.19	-5.72	-4.62	1.51	4.94	-2.14
82208	1.16	-3.19	-7.10	-3.91	2.48	6.41	-1.83
76601	0.86	-3.18	-7.59	-4.61	1.53	6.40	-3.10
85468	0.77	-3.15	-7.88	-6.10	0.35	6.06	-3.27
78011	-0.30	-3.13	-5.71	-5.83	0.87	n.d.	-4.61
77392	0.83	-3.12	-7.08	-4.43	1.61	6.88	-1.73
86665	0.34	-3.09	-8.61	-6.29	0.22	5.63	-4.23
85823	0.64	-3.09	-9.23	-5.09	1.33	6.49	-2.80
82026	-0.41	-3.09	-6.51	-4.91	1.27	5.88	-1.90
85066	0.75	-3.07	-6.70	-3.88	1.87	5.93	-1.76
86930	1.24	-3.06	-7.81	-5.57	0.83	6.55	-4.15
76838	0.15	-3.05	-8.13	-5.12	1.20	6.49	-2.65
78926	1.09	-3.04	-6.82	-4.38	2.32	5.37	-2.10

ID	*dcl1*⁻ log_2 fold change vs WT	*dcl2*⁻ log_2 fold change vs WT	*dcl1*⁻*/2*⁻ log_2 fold change vs WT	*rdrp1*⁻ log_2 fold change vs WT	*rdrp2*⁻ log_2 fold change vs WT	Ago-1 bound WT log_2 fold change vs *ago-1*⁻	*r3b2*⁻ log_2 fold change
86476	0.53	-3.04	-7.28	-4.93	1.67	5.78	-1.91
85556	0.75	-3.03	-6.38	-3.32	3.08	6.57	-0.83
77282	0.76	-2.99	-8.52	-5.13	1.23	6.02	-1.91
78743	1.35	-2.98	-6.19	-3.88	2.27	7.01	-1.19
75939	-0.12	-2.98	-6.60	-6.52	0.08	n.d.	-3.56
86485	0.64	-2.96	-6.90	-4.90	1.59	6.43	-1.31
85742	1.26	-2.95	-6.67	-4.31	2.19	6.52	-0.70
84203	0.38	-2.93	-7.43	-4.82	1.47	7.30	-1.82
85731	0.66	-2.92	-7.94	-6.52	0.10	7.28	-4.11
77203	0.11	-2.91	-8.84	-5.54	1.11	7.07	-2.26
83994	0.36	-2.85	-7.94	-5.38	1.26	6.48	-2.24
80623	0.25	-2.85	-7.59	-5.49	1.36	6.88	-2.31
86022	0.73	-2.84	-8.22	-5.13	1.13	n.d.	-3.00
76330	0.32	-2.83	-4.02	-4.67	1.22	n.d.	-3.01
82275	0.98	-2.83	-7.84	-4.69	2.03	6.18	-2.51
77171	0.43	-2.82	-7.46	-4.03	2.26	6.09	-1.54
84957	0.33	-2.82	-6.38	-5.56	1.09	6.09	-2.51
85642	0.52	-2.81	-6.89	-6.12	0.52	7.16	-3.32
77520	0.63	-2.78	-9.95	-4.89	1.43	6.45	-1.80
85164	1.37	-2.77	-6.23	-3.82	2.77	5.55	-2.72
86260	0.27	-2.73	-8.06	-5.20	0.86	n.d.	-2.97
82417	1.05	-2.72	-7.93	-3.69	2.72	6.11	-2.74
78167	0.43	-2.69	-8.17	-5.14	1.46	6.39	-2.11
78424	0.36	-2.68	-6.01	-5.06	1.89	7.40	-1.50
85892	0.67	-2.67	-6.38	-4.11	2.62	6.37	-1.23
85565	1.61	-2.64	-6.24	-4.94	1.80	6.90	-1.75
79577	0.67	-2.63	-8.58	-5.15	1.37	6.04	-3.35
82385	0.14	-2.61	-3.42	-4.10	1.01	5.06	-1.56
86685	1.09	-2.61	-7.03	-5.49	1.34	5.80	-2.12
83142	0.55	-2.56	-8.38	-4.47	1.90	6.32	-2.50
80443	0.96	-2.56	-8.09	-5.11	1.61	6.27	-3.00
78011	0.39	-2.56	-5.31	-3.36	2.94	5.82	-0.07
77331	0.57	-2.55	-6.30	-4.87	1.19	5.18	-1.61
80061	0.85	-2.52	-10.96	-4.56	1.64	6.72	-2.04
79134	1.11	-2.47	-7.17	-4.10	2.07	7.02	-0.66
85793	0.79	-2.35	-6.62	-3.77	2.64	6.06	-0.58
76105	0.82	-2.34	-5.94	-4.87	1.60	5.90	-2.53
79714	0.00	-2.33	-7.64	-5.78	0.57	5.32	-1.37
78120	0.74	-2.31	-7.39	-5.60	0.50	6.09	-2.94
79907	0.46	-2.30	-6.41	-4.60	2.09	4.86	-1.27
79959	0.61	-2.26	-8.26	-5.16	1.37	7.37	-1.48
85846	1.36	-2.25	-8.88	-3.89	2.67	5.82	-1.20
83695	0.69	-2.25	-7.21	-5.38	1.01	7.17	-2.46
83652	1.13	-2.22	-7.27	-3.56	2.51	6.99	-2.14
86294	-0.57	-2.19	-8.04	-6.36	-0.12	5.20	-3.14
79183	0.73	-2.18	-6.71	-3.82	2.53	7.31	-0.20
76941	0.96	-2.18	-6.68	-4.09	2.31	7.62	-2.14
94870	0.91	-2.16	-2.96	-4.49	0.57	7.07	-3.81
86048	0.64	-2.14	-7.61	-5.33	0.88	n.d.	-2.67
80244	0.08	-2.12	-6.82	-5.92	0.88	5.81	-3.09
80211	0.49	-2.07	-8.23	-4.93	1.39	5.67	-1.82
85168	0.06	-2.03	-7.12	-6.86	0.50	n.d.	-3.80
82578	0.63	-2.00	-4.89	-4.19	2.18	6.22	-1.12
79061	0.95	-1.93	-6.36	-3.92	2.13	5.95	-1.32
16281	0.51	-1.68	-7.60	-5.50	1.77	6.28	-1.60
85794	0.86	-1.65	-7.30	-4.39	1.74	7.18	-1.25
85973	0.52	-1.61	-6.42	-3.79	2.61	7.19	-0.46
85565	1.24	-1.60	-7.28	-5.18	1.63	4.94	-1.33
86602	0.99	-1.48	-8.26	-4.13	2.09	7.61	-1.28
92716	-1.95	-1.98	-5.49	-5.99	-6.90	n.d.	-6.69
51581	-1.06	-1.59	-2.47	-2.94	-3.41	n.d.	-3.85
51423	-1.91	-1.14	-3.60	-6.19	-4.92	n.d.	-10.43
74643	-1.69	-1.03	-3.80	-5.66	-4.31	n.d.	-8.01
48689	-1.26	-1.00	-4.12	-4.83	-4.62	n.d.	-5.14
92980	-1.29	-0.97	-2.73	-5.21	-4.36	n.d.	-8.71
72854	-1.60	-0.90	-3.60	-7.92	-5.94	n.d.	N/A
95577	-0.80	-0.89	-2.13	-4.30	-3.86	n.d.	-6.12
85223	0.82	-0.87	-7.18	-5.01	1.62	6.96	-0.90
89225	-1.03	-0.87	-3.30	-2.79	-4.50	n.d.	-3.61
22967	-0.49	-0.75	-2.52	-3.41	-3.45	n.d.	-7.20
51876	-1.10	-0.49	-3.35	-4.84	-3.08	n.d.	-5.72
85168	-1.37	-0.45	-35.14	-14.94	-8.25	n.d.	-12.13
88244	-1.10	-0.41	-2.07	-3.74	-3.18	n.d.	-9.12
91077	-0.84	-0.40	-2.41	-3.85	-4.00	n.d.	-8.37
95922	-1.32	-0.38	-3.34	-6.33	-4.01	n.d.	-10.67
94043	-0.44	-0.33	-4.35	-6.20	-4.20	n.d.	-8.37
90193	-0.85	-0.29	-3.05	-3.96	-3.94	n.d.	-6.31
93857	-0.95	-0.26	-2.82	-4.31	-3.64	n.d.	-7.44
93203	-0.45	-0.23	-2.46	-5.22	-3.79	n.d.	-8.08
24857	-1.00	-0.23	-2.10	-3.84	-3.38	n.d.	-6.90
46499	-0.40	-0.22	-2.61	-2.40	-1.96	n.d.	-6.42
93645	-0.80	-0.20	-4.87	-7.05	-4.87	n.d.	N/A
29038	-0.72	-0.19	-2.75	-4.19	-3.02	n.d.	-7.91
92041	-0.86	-0.18	-3.10	-5.02	-4.15	n.d.	N/A
33552	-1.29	-0.17	-2.95	-6.23	-4.17	n.d.	-9.15
48455	-0.70	-0.16	-2.74	-3.65	-3.38	n.d.	-5.86
91402	-0.44	-0.14	-2.67	-4.49	-3.63	n.d.	-6.05
92570	-0.09	-0.12	-2.08	-3.09	-2.68	n.d.	-7.33
36390	-0.44	-0.09	-2.42	-4.17	-3.58	n.d.	-7.93
94536	-0.38	-0.06	-2.00	-3.76	-3.65	n.d.	-7.35
77956	-0.69	-0.03	-2.92	-4.84	-4.07	n.d.	-9.25
80654	-0.79	-0.03	-2.43	-3.37	-2.80	n.d.	N/A
86368	0.58	-0.02	-4.80	-4.33	1.07	n.d.	n.d.
47807	-0.25	-0.02	-2.55	-4.31	-3.87	n.d.	-7.96
86166	-0.99	-0.01	-2.59	-4.20	-2.84	n.d.	-6.29
93062	0.28	-0.00	-2.97	-2.91	-3.67	n.d.	-5.69

ID	*dcl1*⁻ log_2 fold change vs WT	*dcl2*⁻ log_2 fold change vs WT	*dcl1*⁻*/2*⁻ log_2 fold change vs WT	*rdrp1*⁻ log_2 fold change vs WT	*rdrp2*⁻ log_2 fold change vs WT	Ago-1 bound WT log_2 fold change vs *ago-1*⁻	*r3b2*⁻ log_2 fold change
37397	-0.73	-0.00	-2.72	-3.95	-3.67	n.d.	-5.36
96051	-0.20	0.01	-3.47	-3.92	-3.26	n.d.	-5.11
31141	-0.92	0.01	-3.03	-5.85	-4.26	n.d.	N/A
85828	-0.54	0.01	-3.35	-6.83	-4.00	n.d.	N/A
90818	0.06	0.04	-3.17	-4.78	-4.57	n.d.	-9.86
32849	-1.49	0.09	-2.14	-3.33	-2.75	n.d.	-8.52
94604	-0.18	0.10	-3.58	-5.11	-3.89	n.d.	-6.00
68938	-0.32	0.10	-2.31	-2.72	-2.32	n.d.	-6.49
73988	-1.13	0.11	-2.10	-4.59	-3.03	n.d.	-7.33
84706	-0.31	0.12	-2.08	-2.27	-2.92	n.d.	-3.62
30166	-0.18	0.13	-4.09	-5.87	-4.97	n.d.	-7.87
95149	-0.98	0.16	-2.92	-3.11	-2.78	n.d.	-4.61
82648	-0.33	0.20	-2.21	-4.34	-3.56	n.d.	N/A
81516	-0.44	0.21	-2.56	-4.63	-3.76	n.d.	-8.34
77956	-0.26	0.27	-2.28	-4.54	-3.13	n.d.	-8.36
38503	-0.10	0.27	-2.17	-3.63	-3.03	n.d.	N/A
27316	-0.09	0.29	-2.30	-4.44	-2.77	n.d.	N/A
77956	-0.30	0.30	-2.80	-5.51	-4.71	n.d.	-7.49
71324	0.10	0.31	-2.94	-4.17	-3.97	n.d.	-8.34
47486	-0.02	0.32	-2.47	-2.72	-2.94	n.d.	-5.04
87857	-1.33	0.32	-2.00	-5.35	-3.31	n.d.	-10.21
81072	0.21	0.37	-2.60	-2.87	-3.19	n.d.	N/A
87086	-0.09	0.38	-2.24	-4.31	-3.69	n.d.	-8.96
46499	0.16	0.39	-2.70	-2.59	-2.18	8.57	-7.11
27973	-0.50	0.41	-3.45	-5.58	-4.34	n.d.	-7.81
78571	-0.56	0.42	-2.83	-4.80	-3.71	n.d.	-7.51
88271	-1.30	0.46	-2.55	-5.57	-2.84	n.d.	-7.00
83918	-0.34	0.47	-2.10	-3.70	-3.24	n.d.	-5.14
93062	0.62	0.49	-3.02	-2.65	-3.04	n.d.	-2.91
93062	0.33	0.51	-2.69	-3.11	-3.51	n.d.	-3.31
94953	-0.11	0.54	-2.22	-3.13	-3.03	n.d.	-3.63
88145	-0.29	0.55	-2.45	-6.71	-2.87	n.d.	-10.27
94043	0.02	0.58	-3.24	-4.81	-3.49	n.d.	-6.33
46975	-0.23	0.59	-2.45	-5.37	-3.64	n.d.	N/A
68860	-0.66	0.63	-2.84	-3.85	-3.60	n.d.	-7.35
95149	-0.09	0.67	-2.66	-2.98	-3.02	n.d.	-4.26
94247	-0.33	0.67	-2.65	-2.33	-2.83	n.d.	-5.49
95149	0.02	0.69	-3.31	-3.43	-3.21	n.d.	-4.68
79017	0.24	0.69	-2.10	-3.95	-3.76	n.d.	-5.91
83860	-0.61	0.92	-2.45	-4.63	-4.43	n.d.	-7.43
94525	0.23	0.97	-2.06	-3.14	-2.67	n.d.	N/A
95149	0.32	1.03	-2.27	-2.61	-2.45	n.d.	-4.67
90885	0.63	1.07	-2.31	-3.75	-3.13	n.d.	-9.10
45670	0.05	1.07	-2.54	-6.31	-2.96	n.d.	-7.80
73657	0.34	1.11	-2.45	-6.35	-2.98	n.d.	-6.76
91508	-0.39	1.14	-2.05	-4.40	-3.09	n.d.	-9.42
45935	-0.09	1.24	-2.61	-4.59	-3.41	n.d.	-6.99
93776	0.27	1.42	-2.16	-5.09	-2.37	n.d.	-9.30
13065	0.18	1.43	-2.69	-3.60	-3.12	n.d.	-5.21
77853	-0.42	1.51	-2.51	-5.29	-3.48	n.d.	-4.25
73807	0.38	1.76	-2.90	-5.46	-3.93	n.d.	N/A
45585	-3.12	1.18	2.16	1.20	0.81	1.25	1.06
27711	-2.13	-0.11	-1.00	-2.15	-2.06	n.d.	-6.30
76922	-2.06	-0.55	-1.52	-3.33	-2.87	n.d.	-8.13
90826	-2.10	-0.97	-1.39	-3.22	-3.17	n.d.	-6.02
29653	-2.85	-0.85	-3.34	-5.55	-4.83	n.d.	-6.82